

**Developing an Europium-based optical biosensor for
detection of protein biomarkers**

Eiman Ali Al-Enezi

Submitted in accordance with the requirements for the degree of
Doctor of Philosophy

The University of Leeds

School of Biomedical sciences

Faculty of Biological sciences

March 2020

Declaration

The candidate confirms that the work submitted is her own and that appropriate credit has been given where reference has been made to the work of others.

This copy has been supplied on the understanding that it is copyright material and that no quotation from the thesis may be published without proper acknowledgement.

The right of Eiman Ali Al-Enezi to be identified as Author of this work has been asserted by her in accordance with the Copyright, Designs and Patents Act 1988.

© 2020 The University of Leeds and Eiman Ali Al-Enezi

Acknowledgements

First, I would like to express my sincere gratitude to my supervisor Prof. Paul Millner for the continuous support, guidance and encouragement for the last four years. His motivation, enthusiasm and knowledge has helped throughout my research and writing of this thesis. I would like to thank my co-supervisors Prof. Jin Jose and Dr. Sikha Saha for their valuable input and support during my PhD.

My sincere thanks also go to the following people in Millner's lab: Dr. Alexandre Vakurov, Dr. Jack Joode, Dr. Arindam Pramanik, Dr. Hussaini Majiya, Dr. Tarun Kakkar, Dr. Billy Richards, Mr. Juan Leva, Ms. Amy Eades, Ms. Mingyu Ding and all members of Millner group. I would like to thank Dr. Darren Tomlinson and Dr. Iain Manfield for their kind assistance regarding Affimers and SPR. Also, I would like to thank Dr. Shazana Shamsuddin, Dr. Moza Al-Owais and my life-long friend Dr. Fatemah Alattar. They were true friends and colleagues who helped me out in difficult times during my PhD. I could not have asked for a better team to complete my research. I am grateful to the Kuwait Government and the Ministry of Defence in Kuwait for funding my PhD and providing me and my family with all the support needed in the UK. I would not have been able to complete my PhD without their support.

I am indebted to my father Ali who passed away before I completed my PhD. He dreamt about me finishing my PhD and strongly believed that I could do it. Today I pray that he is showered with mercy and happiness upon my completion of my PhD and I wish he was here to see what I have achieved. I am also gratefully to my mother (Sabriya Al-Marzooq) who kept me in her prayers and supported me with all possible means to help me reach this stage. I would like to thank my soul mate and precious husband Waleed and my children

Fatemah and Khaled for their patience and encouragement during my PhD. Also, I am grateful to my brothers (Talal, Abdul-Aziz, Ahmed and Mahmood) and sisters (Tahani, Rawan, Reem, Fajer and Dalal), Samiya, Noor and Aalia. I am very grateful to you all for your support and patience. Finally, I would like to thank my mentor Mr. Fouad Al-Ghanim and Mr. Abdullah Baqiri who continued to encourage and support me to achieve my goal.

I cannot describe my heart-felt gratitude in words but I sincerely thank you all for the good days that you brought into my life.

Abstract

Protein biomarker measurement has been well established using ELISA which offers good sensitivity and specificity but remains slow and expensive. Biosensors offer the prospect of reagent-less, processing-free measurements at the patient's bedside while recent developments in synthetic binding proteins have facilitated biosensor fabrication. The trivalent Europium ion (Eu^{3+}) is a lanthanide that is attractive for use in optical biosensors due to its bright fluorescence when chelated by organic ligands. The aim of this project was to develop a platform for biosensing based on chelated Eu^{3+} against a range of proteins biomarkers for muscle injury/ heart attack, ischemic stroke, inflammation and colorectal cancer. Affimers against the biomarkers (human myoglobin, glial fibrillary acidic protein (GFAP), C-reactive protein (CRP) and carcinoembryonic antigen (CEA)) were used as targeting bioreceptors. The Affimers were purified and checked for selective binding using ELISA and immunoprecipitation assays. The Eu^{3+} was then chelated by pyromellitic dianhydride (PMDA) modified Affimers to form Eu^{3+} -Affimer complexes. The fluorescence characteristics of the complexes against the protein biomarkers were measured in diluted human serum at $\lambda_{\text{ex}} = 395 \text{ nm}$ and $\lambda_{\text{em}} = 590 \text{ nm}$ and 615 nm . The Eu^{3+} -Affimer complexes allowed sensitive detection of myoglobin, GFAP, CRP and CEA proteins as low as 100 fM in 1% (v/v) human serum in 2 to 3 minutes. The Eu^{3+} complex was far more sensitive against CRP and CEA proteins as compared to GFAP and human myoglobin, and sandwich assays, using an Affimer against the biomarker plus a polyclonal antibody, suggested that the mass of the biomarker may have a substantial effect on quenching of the Eu^{3+} complex luminescence. These data are the first to demonstrate that

the Affimer based Eu^{3+} complexes can function as nano-biosensors with potential analytical and diagnostic applications.

Table of contents

Acknowledgements	ii
Abstract	iv
List of Figures	x
List of Tables	xiii
List of Equations	xiv
Abbreviations	xv
Chapter one: Introduction	1
1.1 Overview	2
1.2 Biosensors.....	4
1.3 Types of biosensors	7
1.3.1 Electrochemical biosensors	7
1.3.2 Electro-mechanical biosensors	12
1.3.3 Optical biosensors	14
1.4 Overview of Lanthanides	19
1.4.1 Lanthanide chemical properties	20
1.4.2 Lanthanide optical properties.....	23
1.4.3 Lanthanide luminescent properties	27
1.4.4 Europium ion-complex fluorescence characteristics	31
1.4.5 Examples of luminescent lanthanide complexes	35
1.4.5.1 β - diketonate chelates	35
1.4.5.2 Cyclen derivatives	36
1.4.5.3 Cryptates.....	37
1.4.5.4 EDTA derivatives.....	38
1.4.5.5 DTPA derivatives.....	39
1.4.6 Europium ion complexes Applications	41
1.4.6.1 Lanthanide pH probes	41
1.4.6.2 Metal ion probes.....	42
1.4.6.3 DNA/ RNA probes	44
1.5 Bioreceptors	46
1.5.1 Oligonucleotides	46
1.5.2 Antibodies	47
1.5.3 Synthetic Binding Protein.....	53
1.5.3.1 Affibodies	54
1.5.3.2 Designed ankyrin repeat proteins (DARPin)s	55

1.5.3.3 Monobodies.....	57
1.5.3.4 Affimers.....	58
1.6 Human protein biomarkers of disease.....	60
1.6.1 Myoglobin.....	61
1.6.2 Glial fibrillary acidic protein (GFAP).....	61
1.6.3 C-reactive protein (CRP).....	62
1.6.4 Carcinoembryonic antigen (CEA).....	62
1.7 Hypothesis.....	65
1.8 Aims.....	65
Chapter two: Materials and Methods.....	66
2.1 Materials.....	67
2.1.1 Chemicals.....	67
2.1.2 Solvents and buffers.....	68
2.1.3 Proteins.....	68
2.1.4 Affimer production, extraction and purification.....	69
2.1.5 Affimer characterisation.....	70
2.1.6 Affimer functionalisation.....	70
2.2 Methods.....	71
2.2.1 Affimer production.....	71
2.2.1.1 Subcloning of Affimer DNA from the phagemid vector (pBSTG125) into <i>pET11 (a)</i> plasmids.....	71
2.2.1.2 Minipreps and transformation of ligation mixture into XL1-Blue super competent cells.....	75
2.2.1.3 DNA Sequencing.....	77
2.2.1.4 Affimer expression.....	77
2.2.1.5 Affimer extraction and purification.....	78
2.2.1.6 Sodium dodecyl sulphate polyacrylamide gel electrophoresis (SDS-PAGE).....	79
2.2.1.7 Affimer dialysis.....	79
2.2.2 Affimer characterisation.....	80
2.2.2.1 Analyte Biotinylation.....	80
2.2.2.2 Enzyme-linked immunosorbent assay (ELISA) to confirm analyte biotinylation.....	80
2.2.2.3 Enzyme-linked sandwich ELISA for Affimer selective binding.....	81
2.2.2.4 Pull-down assay.....	82
2.2.2.5 Western blotting.....	83
2.2.2.6 Surface Plasmon Resonance (SPR).....	84
2.2.2.7 SPR data analysis.....	85

2.2.3 Affimer functionalisation.....	88
2.2.3.1 Conjugation of Affimer with four different chelators: PMDA, maleimido-mono-amide-DOTA, DOTA-NHS-ester and p-SCN-Bn-DTPA	88
2.2.3.2 Bicinchoninic acid solution (BCA) protein assay	88
2.2.3.3 Fluorescein isothiocyanate (FITC) assay for free amine groups	89
2.2.3.4 Chelating Eu^{3+} with the modified Affimer.....	89
2.2.3.5 Emission fluorescence measurement	89
2.2.3.6 Lifetime measurement	90
2.2.3.7 Time-resolved fluorescence of Eu^{3+} complex chelated by Affimer modified with PMDA (Affimer assay)	92
2.2.3.8 Time-resolved fluorescence of Eu^{3+} complex chelated by Affimer modified with PMDA and antibody (Sandwich assay)	92
2.2.3.9 Time-resolved fluorescence of Eu^{3+} complex chelated by Affimer modified with PMDA and chelating agents (EDTA and tri-sodium citrate).....	93
2.2.3.10 Fluorimetric plate reader measurement and data analysis.....	93
2.2.3.11 Isothermal titration calorimetry (ITC) assay of Eu^{3+} solution binding to PMDA modified Affimer	95
Chapter three: Affimer production and characterisation	96
3.1 Introduction.....	97
3.2 Aims	99
3.3 Affimer expression and purification	100
3.3.1 DNA sequencing.....	100
3.3.2 Subcloning of anti- human myoglobin Affimer DNA	102
3.3.3 Expression and purification of human myoglobin and GFAP binding Affimer	108
3.4 Affimer characterisation.....	111
3.4.1 ELISA for selective binding	111
3.4.2 Immunoprecipitation (pull down) assays	115
3.4.3 Surface Plasmon resonance (SPR)	120
3.5 Discussion	125
3.5.1 Affimer expression and purification	125
3.5.2 Affimer characterisation	126
Chapter four:Affimer functionalisation	128
4.1 Introduction.....	129
4.2 Affimer as chelating scaffold.....	131
4.3 Aims	134
4.4 Eu^{3+} ion complex optimisation.....	135
4.4.1 Eu^{3+} complex characterisation	135
4.4.2 Eu^{3+} concentration optimisation	138

4.4.3 The selection criteria of the buffer for the Eu^{3+} complex system.....	140
4.4.4 The selection criteria of the chelator ligand for the Eu^{3+} complex system	145
4.4.5 Fluorescence intensity of Eu^{3+} chelated PMDA modified anti- human myoglobin Affimer complex in human serum	155
4.4.6 Fluorescence intensity of Eu^{3+} chelated PMDA modified anti- GFAP Affimer complex in 1, 2.5 and 5 % (v/v) human serum	159
4.5 Discussion	163
4.5.1 The selection criteria of the chelator ligand for the Eu^{3+} complex system	165
Chapter five: Time resolved fluorescence assay using Affimer chelated Eu^{3+}	169
5.1 Introduction.....	169
5.2 Aims	170
5.3 Integration time optimisation of Eu^{3+} complex.....	171
5.4 Time resolved fluorescence assay of PMDA modified anti- GFAP Affimer and anti- human myoglobin Affimer chelated Eu^{3+}	174
5.5 Time resolved fluorescence of Eu^{3+} chelated by PMDA modified anti- CRP and CEA Affimers	180
5.6 Time resolved fluorescence assay with Eu^{3+} complex and monoclonal/ polyclonal antibody as sandwich assay	183
5.7 Effect of chelating agents on plate based time resolved fluorescence assay	186
5.8 Isothermal titration calorimetry of Eu^{3+} -Affimer complex.....	188
5.9 Discussion	191
Chapter six: Discussion	194
6.1 General discussion	195
6.2 Factors affecting Eu^{3+} -based biosensor performance	196
6.3 Detection range of anti- human myoglobin and anti- GFAP Affimer based biosensors in comparison to other assays	200
6.4 Future work and opportunities	202
References	205

List of Figures

Figure 1.1 Schematic of a biosensor.....	6
Figure 1.2 Schematic of SPR instrument principle.....	16
Figure 1.3 Schematic of electron configuration.....	19
Figure 1.4 Splitting of the energy levels of Eu^{+3} with 4F^6 configuration.....	24
Figure 1.5 Energy level diagram of selected lanthanide ions.....	26
Figure 1.6 Photophysical schematic pathway representation of the lanthanide complex fluorescence emission processes.....	28
Figure 1.7 Schematic representation of the Eu^{3+} complex fluorescence emission processes.....	32
Figure 1.8 Examples of Lanthanide- β -diketonate complexes.....	36
Figure 1.9 Examples of cyclen derivatives ligands chelated lanthanide complex.....	37
Figure 1.11 Examples of pyridine- based ligands.....	39
Figure 1.12 Examples of DTPA- based ligands.....	40
Figure 1.13 Antibody structure (IgG).....	50
Figure 1.14 Antibody derivatives.....	52
Figure 1.15 Affibody synthetic binding protein.....	55
Figure 1.16 DARPin synthetic binding protein.....	56
Figure 1.17 Monobody synthetic binding protein.....	57
Figure 1.18 Affimer scaffold.....	59
Figure 1.19 Molecular structure of biomarkers.....	63
Figure 2.1 A schematic representation of incorporating Affimer -encoding sequence into <i>pET11 (a)</i> expression vector.....	74
Figure 2.2 A schematic showing ELISA platform for biotinylated biomarker. ...	81
Figure 2.3 A schematic showing ELISA platform to check the selective binding of the Affimer and their targets biomarker.....	82
Figure 2.4 Schematic showing the fluorescence spectroscopy measurements set up.....	91
Figure 2.5 Schematic of the sandwich Eu^{3+} complex platform.....	92
Figure 3.1 Schematic representation of pBSTG1 phagemid and <i>pET11 (a)</i> vector.....	98
Figure 3.2 DNA sequencing results of anti- human myoglobin Affimer.....	100
Figure 3.3 Gel electrophoresis of purified anti- human myoglobin Affimer DNA in phagemid vector.....	103
Figure 3.4 PCR products before digested with <i>Not I</i> and <i>Nhe I</i> restriction enzymes.....	104
Figure 3.5 Gel electrophoresis of digested <i>pET11 (a)</i> and PCR products.. ...	106
Figure 3.6 Sequence alignment of anti- human myoglobin and anti- GFAP Affimers.....	107
Figure 3.7 Binding of the His ₆ - tag functional group with the Ni^{2+} -NTA groups.....	108

Figure 3.8 SDS-PAGE gel of purified anti- GFAP and anti- myoglobin Affimers.	109
Figure 3.9 Mass spectra of purified anti- human myoglobin 4 and 6 Affimers and anti- GFAP Affimer proteins.	110
Figure 3.10 ELISA of biotinylated human myoglobin and GFAP.....	113
Figure 3.11 ELISA result to check the selective binding of the anti- human myoglobin and anti- GFAP Affimers for their targets.	114
Figure 3.12 Pull down assay showing the binding of the Affimers to target protein.....	117
Figure 3.13 Immunoblotting assay of anti- human myoglobin/ anti- GFAP Affimers binding to their target proteins.	119
Figure 3.14 Real time SPR sensorgrams for anti- GFAP Affimer.....	122
Figure 3.15 Real time SPR sensorgrams data of anti- human myoglobin Affimer.	124
Figure 4.1 Photophysical schematic of the four types of lanthanide complexes.	130
Figure 4.2 Affimer structure.....	132
Figure 4.3 Excitation spectrum of Eu^{3+} complex.	135
Figure 4.4 Eu^{3+} complex emission spectra.	137
Figure 4.5 Fluorescence intensity spectra of Eu^{3+} chelated by PMDA modified anti- human myoglobin Affimer complexes.	139
Figure 4.6 Fluorescence intensity spectra of Eu^{3+} chelated by PMDA modified anti- human myoglobin Affimer in PBS.	142
Figure 4.7 Fluorescence intensity spectra of Eu^{3+} chelated by PMDA modified anti- human myoglobin Affimer in MOPS.	143
Figure 4.8 Fluorescence intensity spectra of Eu^{3+} chelated by PMDA modified anti- human myoglobin Affimer in Tris.....	144
Figure 4.9 Schematic showing the reaction steps for Eu^{3+} chelated by PMDA modified Affimer.	145
Figure 4.10 Schematic showing the reaction steps for Eu^{3+} chelated by maleimido-mono-amide-DOTA modified Affimer.....	146
Figure 4.11 Schematic showing the reaction steps for Eu^{3+} chelated by DOTA-NHS-ester modified Affimer.	147
Figure 4. 12 Schematic showing the reaction steps for Eu^{3+} chelated by p-SCN-Bn-DTPA modified Affimer.	148
Figure 4.13 Fluorescence intensity spectra of the chelated Eu^{3+} with anti-human myoglobin Affimer modified by four different chelators.	151
Figure 4.14 Fluorescence quenching of DOTA-NHS-ester modified anti- human myoglobin Affimer.	152
Figure 4.15 Fluorescence quenching of p-SCN-Bn-DTPA modified anti- human myoglobin Affimer.	153
Figure 4.16 Fluorescence quenching of maleimido-mono-amide-DOTA modified anti- human myoglobin Affimer.	154
Figure 4.17 Fluorescence intensity spectra of Eu^{3+} chelated by PMDA modified anti- human myoglobin Affimer complex in 1 % (v/v) human serum.	156
Figure 4.18 Fluorescence intensity spectra of Eu^{3+} chelated by PMDA modified anti- human myoglobin Affimer complex in 2.5 % (v/v) human serum.	157

Figure 4.19 Fluorescence intensity spectra of Eu^{3+} chelated by PMDA modified anti- human myoglobin Affimer complex in 5 % (v/v) human serum.	158
Figure 4.20 Fluorescence intensity spectra of Eu^{3+} chelated by PMDA modified GFAP Affimer complex in 1 % (v/v) human serum.....	160
Figure 4.21 Fluorescence intensity spectra of Eu^{3+} chelated by PMDA modified GFAP Affimer complex in 2.5 % (v/v) human serum.....	161
Figure 4.22 Fluorescence intensity spectra of Eu^{3+} chelated by PMDA modified GFAP Affimer complex in 5 % (v/v) human serum.....	162
Figure 5.1 The principle of time resolved fluorescence measurements of chelated Eu^{+3} by modified Affimer complex.	172
Figure 5.2 Integration times for PMDA modified anti- GFAP Affimer Eu^{+3} complex.	173
Figure 5.3 Time resolved fluorescence of Eu^{3+} complex in PBS.....	176
Figure 5.4 Time resolved fluorescence of Eu^{3+} complex in 1% (v/v) human serum.....	177
Figure 5.5 Time resolved fluorescence of Eu^{3+} complex in PBS.....	178
Figure 5.6 Time resolved fluorescence of Eu^{3+} complex in 1% (v/v) human serum.....	179
Figure 5.7 Time resolved fluorescence of Eu^{3+} complexes in 1% (v/v) human serum.....	181
Figure 5.8 Time resolved fluorescence of Eu^{3+} complexes in 1% (v/v) human serum.....	182
Figure 5.9 Time resolved fluorescence assay with Eu^{+3} complex and mAb/ pAb as sandwich assay in 1% (v/v) human serum.	184
Figure 5.10 Time resolved fluorescence assay with Eu^{+3} complex and EDTA/ citrate in 1% (v/v) human serum.	187
Figure 5.11 ITC data of the interaction between Eu^{3+} and PMDA modified anti-human myoglobin Affimer.	189
Figure 5.12 Affimer modified with PMDA chelated Eu^{3+} structure.....	190
Figure 6.1 Comparison between Eu^{3+} chelates biosensor and other biosensor assays.....	201
Figure 6.2 Schematic showing the reaction steps for Eu^{3+} chelated by PMDA modified Affimer onto amine-magnetic beads in human serum.	204

List of Tables

Table 1.1 Symbols, atomic numbers and electron configuration of lanthanide ions.	21
Table 1.2 Examples of ligand types.	30
Table 1.3 Energy transitions and their relative wavelength within Eu^{3+} -complex spectra	34
Table 1.4 Biosensors developed for detection of the protein biomarkers myoglobin, GFAP, CRP and CEA.	64
Table 2.1 Composition of bacterial growth media	69
Table 2.2 Miniprep kit buffer compositions.....	76
Table 2.3 Optima control settings	94
Table 3.1 Sequence of variable loops of anti- human myoglobin Affimers.....	101
Table 3.2 Kinetic parameters of anti- human myoglobin and anti- GFAP Affimers interactions.....	121
Table 5.1 Fluostar Optima control settings.	175
Table 5.2 Showing the percentage quench in fluorescence counts of the chelated Eu^{3+} to PMDA modified Affimers in PBS + 1 % (v/v) human serum.	185
Table 5.3 Showing the clinical cut-off range of the biomarker of myoglobin, GFAP, CRP and CEA and their limit of detection using Eu^{3+} -based biosensor.	191

List of Equations

Equation 1.1 Oxidation of glucose	4
Equation 1.2 Reduction of hydrogen peroxide	4
Equation 1.3 Arginine metabolism	4
Equation 1.4 Faraday's law.....	8
Equation 1.5 Nernst equation.....	9
Equation 1.6 Ohm's law	10
Equation 1.7 Sauerbrey equation.....	12
Equation 3.1 Equilibrium dissociation constant.....	120

Abbreviations

Ab	Antibody
AOX	Activities of oxidised species
ARED	Activities of reduced species
CDR	Complementarity determining region
Ce	Cerium
CEA	Carcinoembryonic antigen
CRP	C-reactive protein
CT-DNA	Calf thymus DNA
DARPinS	Designed ankyrin repeat proteins
DMSO	Dimethyl sulfoxide
DNA	Deoxyribonucleic acid
DOTA	1,4,7,10-tetra-azacyclododecane-1,4,7,10-tetraacetate
DTPA	Diethylenetriaminepentaacetic acid
Dy	Dysprosium
EIS	Electrochemical impedance spectroscopy
Er	Erbium
Eu	Europium
F	Faraday's constant
Fc	Constant region
FN3	Fibronectin type III
FRET	Förster Resonance Energy Transfer
Gd	Gadolinium
GFAP	Glial fibrillary acidic protein
GFP	Green fluorescent protein
HER2	Epidermal growth factor receptor 2
HFABP3	Anti- human fatty acid binding protein 3
Ho	Holmium
HPV16	Human papilloma virus 16
<i>i</i>	Current
Ig	Immunoglobulins
InP	Indium phosphide
IPTG	Isopropyl- β -D-thiogalactopyranoside
J	Total angular momentum
L	Total atomic orbital angular momentum
La	Lanthanum
La (β -dik) ₃	β -diketonate chelated lanthanide
Lu	Lutetium
mAb	Monoclonal antibody
Nd	Neodymium
OLED	Light emitting diodes
pAbs	Polyclonal antibody
PCR	Polymerase chain reaction
Pfl	Proflavin
PLIR	Photoluminescence intensity ratio
Pm	Promethium
POC	Point-of-care diagnostic
Pr	Praseodymium

PtCl ₂ NH ₃	Akynylpyridine chromophore
QCM	Quartz crystal microbalance
QDs	Quantum dots
REEs	Rare earth elements
RI	Refractive index
RNA	Ribonucleic acid
S	Total spin angular momentum
SAW	Surface acoustic wave
SELEX	Systematic evolution of ligands by exponential enrichment
Si	Silicon
Sm	Samarium
SPR	Surface plasmon resonance
T	Temperature
Tb	Terbium
Tb	Ytterbium
TIR	Total internal reflection
Tm	Thulium
V	Voltage
VEGFR2	Vascular endothelial growth factor receptor 2
<i>f</i>	Frequency
EDTA	Ethylenediaminetetraacetic acid
Ni ²⁺ -NTA	Nickel- nitrilotriacetic acid
ELISA	Enzyme-linked immunosorbent assay
k _d	Equilibrium dissociation constant
k _a	Association rate constant
k _D	Dissociation rate constant
BSA	Bovine serum albumin

Chapter one: Introduction

Chapter 1

Introduction

1.1 Overview

Recent advancements in biomedical technologies have revolutionised the design of biosensors in the last decade. Biosensors have attracted the attention of many scientists as an alternative solution to overcome many limitations associated with conventional analytical apparatus such as cost, complexity of the setup, low sensitivity and specificity and slowness. The existing limitations of conventional systems such as enzyme-based biosensors, tissue-based biosensors and immunosensors have made them inappropriate to be used for point-of-care diagnostic (POC) devices (Ahmed et al., 2014, Rushworth and Hirst, 2013, Thangsunan, 2018, Mahatnirunkul, 2017, Shamsuddin, 2018, Millner et al., 2012).

There have been many advances in the manufacture, design and applications of biosensors (Shuvaev et al., 2017, Ravindra et al., 2007). Biosensors consist of three essential components. The detector (bioreceptor) is the main component of a biosensor that identifies the target analyte which can range from a small molecule to proteins, nucleic acids and up to viruses and bacteria (Rushworth and Hirst, 2013, Ravalli et al., 2013, Mejri et al., 2010, Barton et al., 2009). The transducer then converts the bio-recognition event to a useful signal and output and involves amplification and displays of the signal in a readable format (Binnemans, 2015). The reaction between the bioreceptor and the analytes is translated to a product in the form of thermal, optical, acoustic or

chemical change, while the transducer is appropriate to this change, and maybe an electrode, photomultipliers or other physical device (Mehrvar and Abdi, 2004, Mehrvar et al., 2000).

Different applications of biosensors have been developed including those for clinical diagnostics, drug development, defence, environmental monitoring (air, water, and soil), agricultural, and food quality control (Shuvaev et al., 2017). During the past decade, antibodies have been used as bioreceptors for biosensing due to their specificity for antigen recognition. Despite their advantages, they have several limitations. Complicated isolation and cloning steps are required for the development of recombinant monoclonal antibodies and their manufacture is expensive and time-consuming. It also depends on use of living animals which is undesirable and leads to batch-to-batch variation. All of these disadvantages can affect the performance of the biosensor (Werner, 2004). As antibodies show a range of limitations, effort has been explored towards synthetic binding proteins as alternatives. A recent non-antibody scaffold has been developed and is known as the Affimer. Affimers can offer high specificity and affinity for the analyte, ease of production, small size and are thermostable which enables long-term storage at ambient temperature (Khaled et al., 2013, Tiede et al., 2014).

In this thesis, our aim is to develop optical nano-biosensors based on rare earth ions chelated to Affimers to detect specific protein biomarkers.

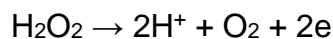
1.2 Biosensors

In the late 1970s, the term “biosensor” began to appear in the scientific literature. Clark and Lyons in 1962 demonstrated the first biosensor, known as the “enzyme electrode”(Clark Jr and Lyons, 1962). They fixed the enzyme glucose oxidase to an amperometric electrode for pO₂. Glucose oxidase catalyses the oxidation of β-D-glucose at working electrode which results in the formation of gluconic acid and hydrogen peroxide according to the following reaction:



Equation 1.1 Oxidation of glucose

Hydrogen peroxide then hydrolysed at platinum (Pt) electrode:



Equation 1.2 Reduction of hydrogen peroxide

The decrease in pO₂ is proportional to the glucose molecules presented in the test solution (Faulkner et al., 2005). Then, in 1977 a “bio-selective sensor” was established by Rechnitz et al. 2008 by immobilising living microorganisms (*Streptococcus faecium*) at the surface of an ammonia gas-sensing electrode (Resch-Genger, 2008). Arginine deiminase enzyme is produced by *Streptococcus faecium* and used to metabolise the arginine to citrulline and ammonia (NH₃) according to the following reaction:



Equation 1.3 Arginine metabolism

The NH_3 is detected by the gas-sensing electrode to create a selective electrode for the amino acid arginine. Later, the bio-selective sensor was shortened to “biosensor” and remains the common term.

Biosensors can be classified into several types depending on the transducing mechanism used with the most common being electrochemical and optical biosensors, although other transduction modes, including thermal, electromechanical and magnetic are also possible (Richardson et al., 2001). Electrochemical biosensors can be further classified as conductimetric, amperometric, and potentiometric. Mechanical biosensors include quartz crystal microbalance, microcantilevers and surface acoustic wave sensors. Optical biosensors can be further classified into labelled (fluorescent probes), label free (surface plasmon resonance, quantum dot) and reagentless (lanthanides) biosensors. The types of biosensor described are shown in **Figure 1.1**.

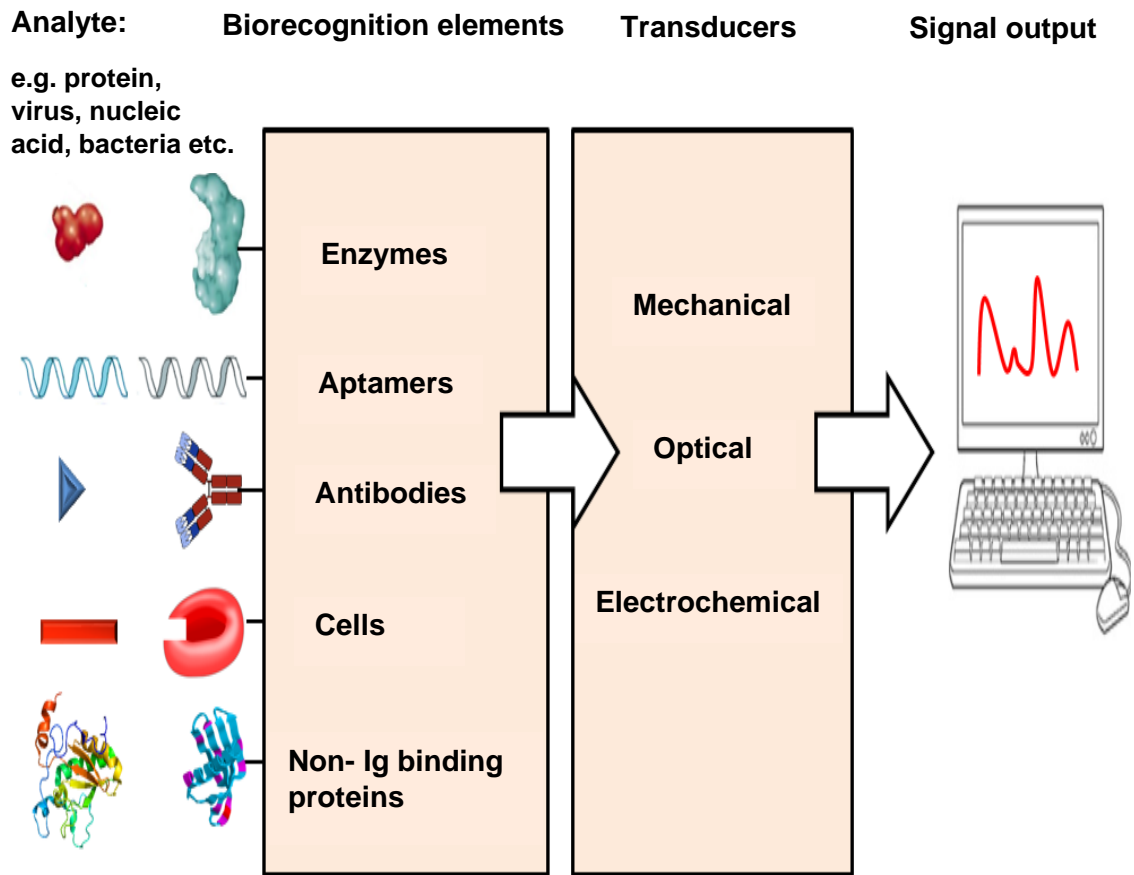


Figure 1.1 Schematic of a biosensor. Biosensors consist of a biorecognition elements, transducers that converts the bio-recognition events into an electrical signal and output device which is typically a PC.

1.3 Types of biosensors

1.3.1 Electrochemical biosensors

Electrochemical biosensors are the most developed biosensors at the present time which are commercially used in industrial, clinical and environmental fields due to their advantages. They are characterised by their high specificity and sensitivity, low cost, rapid response time and ease of use (Rushworth and Hirst, 2013). Although, electrochemical biosensors are the most commonly used in diagnostic tests, the selectivity, sensitivity and stability of the biosensors are affected by poor coupling between the biochemical recognition materials and transducers (Chaubey and Malhotra, 2002, Naessens et al., 2000). Electrochemical biosensors comprise two or three electrodes (Bekiari and Lianos, 1998). The first is the working electrode, which is commonly made from a conductive metal such as platinum, gold or from carbon. The second is a reference electrode; typically, a silver / silver chloride (Ag/ AgCl) electrode which maintains a fixed potential between reference electrode and working electrode. A third electrode, the counter, is often used to maintain the potential between the counter and the working electrode (Bünzli, 2006). Electrochemical biosensors detect the analyte by measuring the electrochemical changes in the form of current (amperometric), voltage (potentiometric) or impedance (impedimetric) signals (Bauer et al., 1964).

Amperometric biosensors measure the current resulting from the redox reactions (oxidation or reduction) at the surface of the electrode when a constant potential is applied between two electrodes (Ahmed et al., 2013, Ronkainen et al., 2010, Rushworth and Hirst, 2013). Redox enzymes are most commonly used in amperometric biosensors as biorecognition elements (Chaubey and Malhotra, 2002). Glucose oxidase is a major example of an enzyme used in commercialised amperometric biosensors used in a medical application (Wang, 2001). First, the enzyme is immobilised on the working electrode. The analyte then binds to the enzyme onto the surface of electrode and leads to redox reaction in which the electron is taken up or released and transferred across the surface of the electrode generating a flow of current. The generated current by the redox reaction can be described using Faraday's law (**Equation 1.4**). The concentration of the analyte can be measured from the calibration curve as the produced currents are proportional to the concentration of the target analyte.

$$i = n \cdot F \cdot A \cdot J$$

Equation 1.4 Faraday's law

Where,

i is current (nA-mA),

n is the number of transferred electrons,

F is the Faraday's constant (96,487 C mol⁻¹),

A is the electrode area (cm²) and

J is the flux coefficient (mol cm⁻² s⁻¹).

Potentiometric biosensors are based on a two-electrode system (indicator electrode and reference electrode) rather than three-electrode system in other electrochemical biosensors. The biosensors in contrast to amperometric biosensors, measure the potential change at zero current flow in the electrochemical cell (Mehrvar and Abdi, 2004, Ahmed et al., 2014, Ronkainen et al., 2010, Hirst, 2014). The binding of analyte molecules to the immobilised biological recognition layer on to a membrane, changes the ionic flux through the membrane which leads to a change in the transmembrane potential (Malon et al., 2006). The relationship between ion concentrations and potential can be calculated by the Nernst equation (**Equation 1.5**).

$$E_{\text{cell}} = (E^{\circ} - RT) / (nF) \log ([A_{\text{OX}}] / [A_{\text{RED}}])$$

Equation 1.5 Nernst equation

Where,

E_{cell} is the quantified cell potential at zero current,

E° is the constant potential for the reduction-oxidation reaction,

R is the general gas constant ($8.314 \text{ J K}^{-1}\text{mol}^{-1}$),

T is the temperature (298 degree Kelvin),

n is the charged number of electrode in the redox reaction,

F is the Faraday ($96,487 \text{ C mol}^{-1}$),

A_{OX} is the activities resulted from the oxidised species and

A_{RED} is the activities resulted from the reduced species.

Impedimetric biosensors, typically integrated by electrochemical impedance spectroscopy (EIS) were first described by Lorenz and Schulze in 1975 (Lorenz and Schulze, 1975). Impedimetric biosensors measure the change in resistive (real part) and capacitance (imaginary part) components of impedance with an excitation signal typically of 2–10 mV (Bartlett, 2008, Suni, 2008). Changes in the resistive (in-phase) or capacitive (out-of-phase) properties occur when the analyte binds to the bioreceptor molecules at the electrode surface. The bulk impedance (Z) is calculated as ratio of the voltage (V) and the detected change of current (I) as shown in **Equation 1.6**.

$$Z = \frac{V}{I} = \frac{V \sin(\omega t)}{I \sin(\omega t + \theta)}$$

Equation 1.6 Ohm's law

Where,

Z is bulk impedance,

V is maximum input voltage,

I is maximum output current,

t is time,

ω is the angular frequency = $2\pi f$,

θ is phase angle shift between the voltage and the current.

Impedimetric biosensors are characterised by wide applicability as they are capable of sensing electron transfer at both high and low frequencies although they are typically interrogated in the 0.1 – 100 Hz range where the maximum response is found. Therefore, they have the ability to measure the interaction between the analyte and a binding receptor including antibodies and synthetic binding proteins (Mehrvar et al., 2000). These features allowed impedimetric biosensors to be used as affinity biosensors (Van Emon et al., 2008). For example, a small change in impedance due to antibody- antigen immunological interaction can be monitored and is proportional to the concentration of the antigen. The surface of the electrode can be functionalised by a specific bioreceptor that can recognise a specific analyte. Usually the bioreceptor is immobilised onto the surface of a working electrode via a conductive polymer film using electrochemical deposition, although thin, insulating films are also used. Then the sampling process takes place when a known oscillating voltage is applied to the electrode followed by measurement of the resulting current. When the analyte binds to the bioreceptor on the electrode, changes in electron transfer resistance and capacitance occur at the interface between the electrode and the solution. Hence, impedimetric biosensors can offer label-free detection system with high signal-to-background ratio, ease of fabrication at low cost.

1.3.2 Electro-mechanical biosensors

Mechanical (piezoelectric) biosensors are based on detection of stress, force, wave and mass parameters that are transformed into an appropriate output signal. However, although mechanical biosensors provide label-free and real-time detection, their sensitivity is limited when detecting small molecules since essentially mass is measured. Mechanical biosensors have three main categories including quartz crystal microbalance (QCM), microcantilevers and surface acoustic wave sensors (SAW) (Mehrvar et al., 2000).

Quartz crystal microbalance (QCM) sensors are label-free piezoelectric biosensors. They detect the decrease in resonance frequency that results from increased mass of analyte when bound onto the immobilised bioreceptor on the sensor surface (Melby et al., 1964, Ranjan et al., 2017). The relationship between increased mass of analyte and frequency change is described by the Sauerbrey equation (**Equation 1.7**).

$$\Delta m = - C \cdot \Delta f$$

Equation 1.7 Sauerbrey equation

Where,

Δm = change in mass,

C= crystal constant (ng/cm²),

Δf = change in frequency.

QCM devices are sensitive to temperature and energy losses that results from the biomolecular interaction during oscillation. Therefore, it is valid for measurement of inelastic materials that do not generate energy during oscillation (Vashist and Vashist, 2011). In addition, Quartz Crystal Microbalance with Dissipation monitoring (QCM-D) offers a real-time analysis of surface phenomena such as thin film formation and reactions. QCM-D monitors the frequency and energy dissipation response as the sensor is repeatedly turned on and thereby generating more accurate and rapid results and allowing measurement of soft, viscoelastic components. QCM-Ds have been applied in the measurements of proteins, polymers and cells interacting with surfaces in liquid (Dixon, 2008).

Cantilever sensors operate in a similar way when a bioreceptor functionalised microcantilever fluctuates at a particular resonant frequency. The changes in the resonant frequency are due to induction of the mechanical bending upon an increase in mass on the sensor surface as a result of binding of analyte (Melby et al., 1964). Surface acoustic wave sensor (SAW) are based on acoustic waves which propagate across the sensor surface. Principally, when target molecules bind to immobilised biological recognition system located on the sensor surface, the acoustic wave changes due to the overall mass change. This shift in the acoustic wave can be detected and used to measure the analyte binding to the biological recognition layer (Greenbaum et al., 2003).

1.3.3 Optical biosensors

Optical biosensors can sense changes in the optical properties of their surroundings, and therefore can detect the binding of analytes to bioreceptors. Optical biosensors detect change in absorbance or fluorescence at the transducing surface (Hulko et al., 2011). Optical biosensors are considered as good alternatives to conventional analytical techniques to provide rapid, highly sensitive and real-time measurements. Analysis using optical biosensors has great potential in the field of environmental pollution control, food safety, drug development and biomedical diagnosis (Thibon and Pierre, 2009, Bünzli and Piguet, 2005). Optical biosensors are divided into two types e.g. chromophore tagged or label free detection (Thorson et al., 2015). Fluorescence based biosensing is one of the most widely used approaches for detection and quantification of biomolecules. Fluorescent probes can be naturally occurring or synthetic probes. Green fluorescent protein (GFP) is an example of a naturally occurring fluorophore obtained from the jellyfish *Aequorea Victoria* (Shimomura, 2008, Prasher et al., 1992, Ormö et al., 1996). It has been used as part of a fluorescent pair for Förster Resonance Energy Transfer (FRET) based biosensors (Pollok and Heim, 1999). When the donor and acceptor fluorophores are in range < 10 nm, excitation of the donor leads to non-radiative photon transfer to the acceptor molecule and thereby fluorescence from the acceptor is observed (Day and Davidson, 2012). The non-electrochemical glucose sensor is an example of a synthetic fluorophore designed by Marvin and Hellinga (1998) who incorporated cysteine residues at specific sites of *E. coli*-based glucose binding protein to covalently bind thiol groups of reactive fluorophores (Marvin and Hellinga, 1998). Although fluorescence based biosensors involving fluorescent tags have been widely used in sensing molecular interactions and provide

excellent sensitivity, there are a number of drawbacks. The requirement for sample labelling with fluorescent reagents increases the time and cost of the process. Moreover, fluorophores can photodegrade or photobleach which affects the sensitivity of the assays (Greenbaum et al., 2003).

In contrast to label-dependent biosensors, one of the first label free biosensors developed used surface plasmon resonance (SPR) for the detection of a range of analytes since the first device was produced by Biacore in 1990 (Wang et al., 2014). SPR occurs when polarised light arises from the higher refractive index which bends at a certain incident angle (critical angle) towards the plane of interface (**Figure 1.2**). All the incoming light is reflected within the glass prism and this phenomenon is called the total internal reflection (TIR). At TIR, the reflected incident light creates an electromagnetic field called evanescent wave in the lower refractive index surface (solution). The wavelength of the evanescent wave is similar to the incident light but the wave amplitude exponentially decreases with increasing distance from the interface. The prism on the reflection side is coated with a thin film of a metal like gold. When the energy of the incident light excites the electrons of the gold, surface plasmon resonance is generated causing reduction in the intensity of the reflected light at a specific angle, the resonance angle. This angle is very sensitive to changes in the refractive index (RI) at the metal surface and binding of a molecule at the surface will alter the surface plasmons and shift their associated evanescent wave. For the detection of ligand-analyte interaction, the bioreceptor is attached to gold surface sensor. Following by injection of the analyte, SPR detects the changes that happen in the refractive index as a result of the binding between the analytes to the bioreceptor. The binding of the molecules can be monitored

in real time in very low volumes and the association-dissociation kinetics can also be analysed (Deka et al., 1998).

Although SPR based biosensors are very sensitive, non-invasive and provide continuous real time measurements, they have some drawbacks. The equipment and SPR chips are expensive and expert operators are required for the assay measurement and the data analysis. Also limited detection of low molecular weight samples is seen (Ahmed et al., 2010, Damborský et al., 2016).

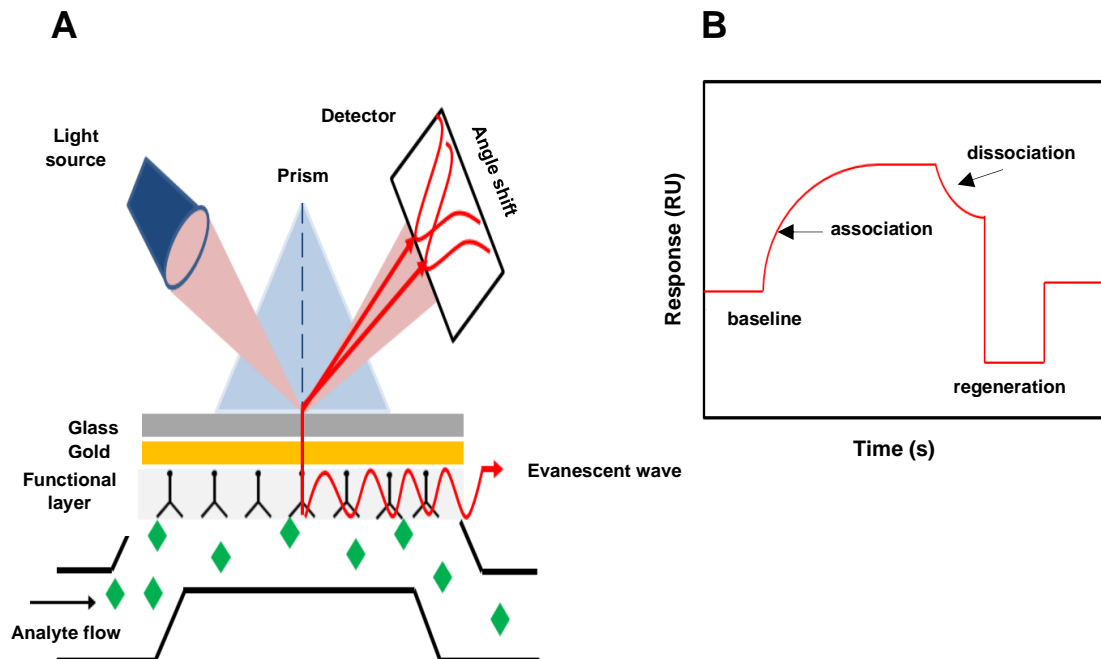


Figure 1.2 Schematic of SPR instrument principle. Bioreceptors (antibodies, Affimers, etc) are immobilised on the SPR surface, while the analyte is injected over the flow cell. (A), when the analyte-ligand interaction occurs, the surface plasmon is altered and subsequently the intensity of the reflected light reduced at the resonance angle. The intensity reduction is proportional to the mass on the surface. (B), a sensorgram is obtained by measuring the shift of the reflected light, wavelengths or angle against time.

Quantum dots (QDs) are fluorescent semiconductor nanocrystals that are characterised by a number of distinctive features when compared to other organic fluors (Michalet et al., 2005). The absorption and emission spectra of QDs is determined by their size which can be controlled or 'tuned' during their manufacture. QDs are 2-5 nm in size and consist of semiconductor materials such as silicon (Si), indium phosphide (InP) and cadmium selenide (CdSe). The extinction coefficients of QDs is claimed to be much larger and output fluorescence more stable than traditional fluorescent dyes (Watson et al., 2003, Ballou et al., 2003). A FRET approach is frequently used for QD- based biosensors. QDs are composed of 100 to 1000 atoms, in which a hole of electron pairs are created (Blasse et al., 1987). The excitation with a beam of light result in narrow and symmetric emission spectrum (Ludwig et al., 1995). Also, the surface of QDs can be coated with a chemical shell such as zinc sulphide, to reduce toxicity without compromising their optical properties (Cho et al., 2010, Darbandi et al., 2010) or modified to conjugate sensing elements such as antibodies to allow antigen-specific fluorescence detection (Gao et al., 2004, Wu et al., 2003, Ballou et al., 2003, Yang et al., 2009). QD-based fluorescent, bioluminescent, chemiluminescent or photoelectrochemical devices are considered as another example of label- free detection. QD-based fluorescent biosensors are most widely developed due to their high sensitivity and excellent capability for multiplex analysis (Wegner and Hildebrandt, 2015, Bedford et al., 2017). Although FRET methods are efficient for biosensing applications, they require external illumination to trigger the fluorescence transfer process and it can be compromised by high background noise (Yao et al., 2007, Berti et al., 2009).

The photochemical properties of QDs can potentially make them ideal for biosensing purposes. However, they are often highly toxic to humans as they are commonly constructed from cadmium and either tellurium or selenium, all of which are toxic to humans (Pelley et al., 2009). Despite early claims of huge advantages of QDs based biosensors robust supporting and conclusive data has not been forthcoming while QDs remain mostly cytotoxic and costly (Gonçalves e Silva et al., 2002, Wegner and Hildebrandt, 2015). The colour of the analyte matrix, such as blood, can be also a confounding factor in the sensitivity of QD biosensors whereas it is not known to affect electrochemical and electromechanical biosensors.

1.4 Overview of Lanthanides

The lanthanides comprise 15 elements found in the sixth period of the periodic table of elements. They include lanthanum to lutetium with atomic numbers from 57 to 71 respectively (Dong et al., 2015). The lanthanides are a branch of the transition metals family and are the only elements that partially fill the f-orbitals except for lanthanum that has empty f-shell while lutetium which has a completely filled f-shell (**Figure. 1.3**) (Eyring, 1979). They are called rare earth elements (REEs) because they are hard to extract from each other due to similarities in their chemical and physical properties but not in fact particularly rare (Adams and Ibball, 1949). The term lanthanides was proposed by the International Union of Pure and Applied Chemistry (IUPAC-IUB, 1971).

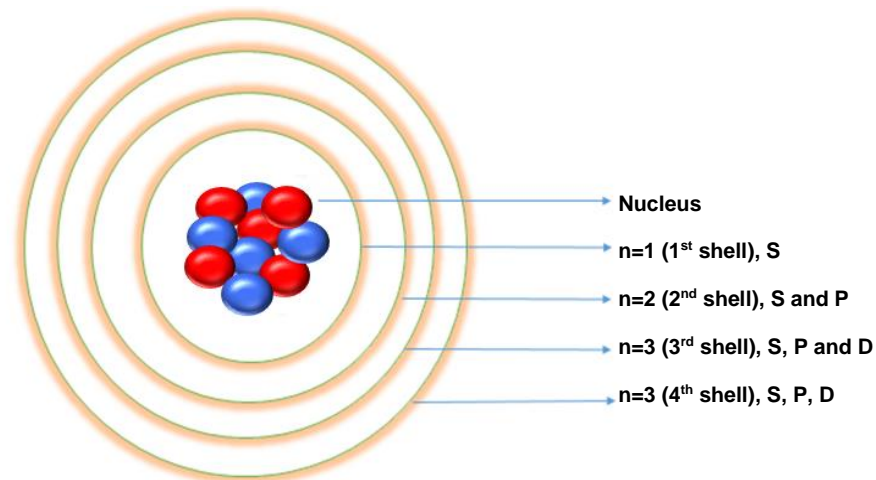


Figure 1.3 Schematic of electron configuration. A nucleus contains equal number of proton (blue) and neutron (red) and surrounding by electrons that exist in a several energy levels represented by $n= 1, 2, 3$ and 4 . The levels are divided into S, P, D, and F sub-levels. The first energy level has a S sub-level, the second energy level has S and P sub-levels, the third energy level has S, P, and D sub-levels and the fourth energy level has S, P, D and F sub-levels.

1.4.1 Lanthanide chemical properties

Lanthanide ions share similar chemical characteristics. All lanthanide ions are electropositive solid compounds with a valence of 3+. The solvated ions in numerous solvents form a stable oxidation state except for cerium, which also can occur in oxidation state 4+ (Ce^{4+}) and europium in oxidation state 2+ (Eu^{2+}) due to the electron configuration of the 4f shell. Lanthanides along with their chemical symbols and electron configurations are listed in **Table 1.1**.

Table 1.1 Symbols, atomic numbers and electron configuration of lanthanide ions.

Atomic number	Element	Symbol	Atom	Mr
57	Lanthanum	La	[Xe]5D ¹ 6S ²	138.90
58	Cerium	Ce	[Xe]4F ¹ 5D ¹ 6S ²	140.12
59	Praseodymium	Pr	[Xe]4F ³ 6S ²	140.90
60	Neodymium	Nd	[Xe]4F ⁴ 6S ²	144.24
61	Promethium	Pm	[Xe]4F ⁵ 6S ²	145.00
62	Samarium	Sm	[Xe]4F ⁶ 6S ²	150.40
63	Europium	Eu	[Xe]4F ⁷ 6S ²	151.96
64	Gadolinium	Gd	[Xe]4F ⁷ 5D ¹ 6S ²	157.25
65	Terbium	Tb	[Xe]4F ⁹ 6S ²	158.92
66	Dysprosium	Dy	[Xe]4F ¹⁰ 6S ²	162.50
67	Holmium	Ho	[Xe]4F ¹¹ 6S ²	164.93
68	Erbium	Er	[Xe]4F ¹² 6S ²	167.26
69	Thulium	Tm	[Xe]4F ¹³ 6S ²	168.93
70	Ytterbium	Tb	[Xe]4F ¹⁴ 6S ²	173.04
71	Lutetium	Lu	[Xe]4F ¹⁴ 5D ¹ 6S ²	174.97

Lanthanides are lithophilic, have a strong affinity for oxygen and are therefore concentrated in oxidic compounds such as silicates, carbonates and phosphates (Adams and Iberall, 1949, McGill, 2000). They differ from other metals in the Periodic Table due to the electron located in the inner 4F subshell orbital, shielded by 6S² and 5P⁶ outer closed subshells (Pihlasalo et al., 2017). This shielding results in non-blinking, sharp fluorescent emissions and photo-bleaching resistance (Slooff et al., 2001). Moreover, with their outer shell being stable and the atomic nucleus of the lanthanide being poorly shielded, the 4F shell electrons are pulled closer to the nucleus with increasing atomic number (Szkop et al., 2019). Lanthanide contraction occurs when an increase in atomic number of the element leads to a decrease in the ionic radius. Lanthanide ions have been commonly used as luminescent probes, specially terbium (Tb³⁺), Europium (Eu³⁺), samarium (Sm³⁺), and dysprosium (Dy³⁺), due to their properties. These include their long fluorescence lifetimes which can be up to milliseconds (Resch-Genger, 2008). They also show large Stokes and or anti-Stokes changes and sharp emission bands (De León-Rodríguez and Kovacs, 2007, Zhang et al., 2012b, Zhou et al., 1997).

Moreover, lanthanide ions are hard Lewis acids and have a binding preference for hard bases. The nature of bonding interactions is electrostatic among the commonly used donor atoms (oxygen > nitrogen > sulfur). The lanthanide ions in aqueous solution have a strong tendency to bind water molecules and hydroxide ions; therefore, only ligands containing negatively charged oxygen donor groups such as phosphonate, carboxylate, and sulfonate efficiently bind to the lanthanide ion.

Lanthanide ions share common coordination numbers ranging from 6 to 12 with the most common being 8 and 9. It is difficult to predict the coordination numbers of lanthanides in solutions. If the ligand's (chelator) donating little number of atoms or their electronic density is too low, the solvent or anions molecules such as water, chloride and hydroxide coordinate the lanthanide ions and complete its coordination sphere (Eyring et al., 2002). The term ligand in this context refers to the chelator.

1.4.2 Lanthanide optical properties

The 4F shell in the trivalent lanthanide ion series, (La^{3+} to Lu^{3+}), is filled with 0 to 14 electrons. Importantly, the outer 6S and 5P shells shield the 4F electrons resulting in little interaction with the chemical environment, leading to no role in chemical bonding of the lanthanide ion. The 4F^0 , 4F^7 and 4F^{14} shells are the most stable configurations in the lanthanide ions. The energy levels of the lanthanides are different due to the different interactions within the ion for the same configuration. Electron-electron repulsions, spin-orbit coupling and the ligand field are responsible for the energy levels within the 4F orbits. The strongest interaction is due to the electronic repulsion between the electrons yielding the largest energy separation in the order of 10^4 cm^{-1} . The interaction between the spin magnetic moment of the electron (spin angular momentum) and the movement of the electron around the nucleus (orbital angular momentum) is known as spin orbit coupling. The spin orbit coupling is therefore responsible for further splitting of the energy into several J-states level in order of 10^3 cm^{-1} (**Figure 1.4**). The spherical symmetry of the free ion is compromised when it is coordinated by the ligand due to the electrostatic bonding between the 4F

electrons and the ligand's electric field. This interaction leads to further energy splitting into sub-levels in the order of 10^2 cm^{-1} (Atkins and de Paula, 1998).

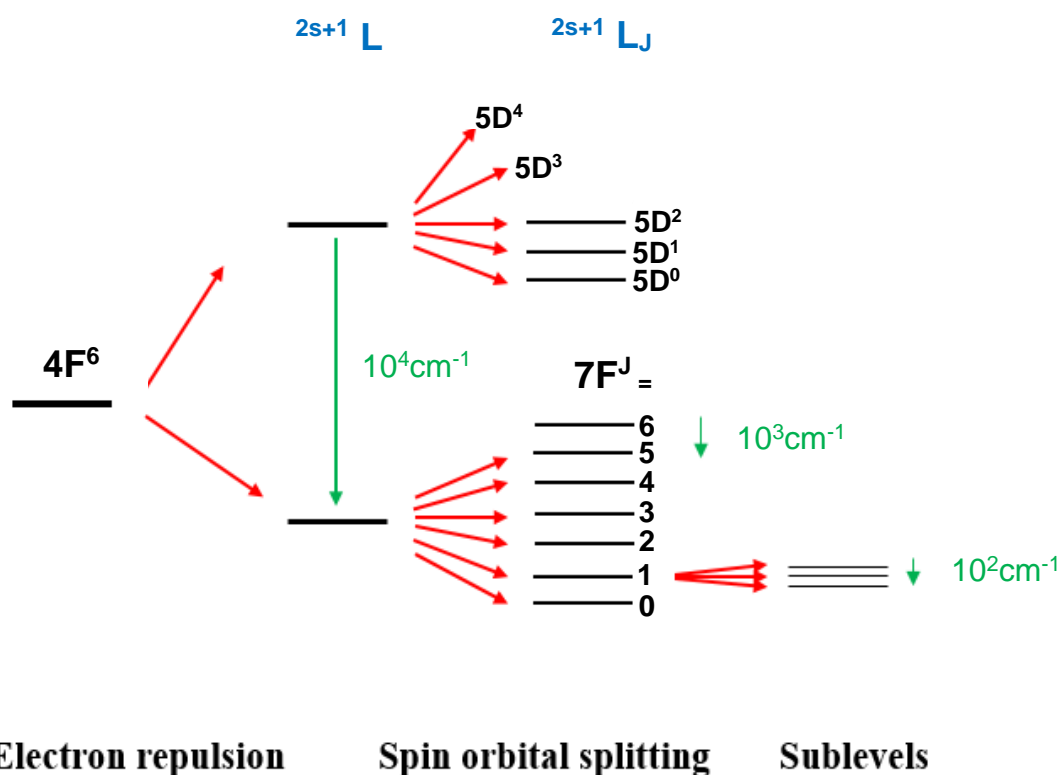


Figure 1.4 Splitting of the energy levels of Eu^{3+} with $4F^6$ configuration. The splitting of the Eu^{3+} energy levels ($4F^6$) due to electronic repulsion, spin orbit splitting and the ligand crystal field. The energy states are known by $(2S+1) L_J$ terms, where S refers to the total spin angular momentum, L refers to the total atomic orbital angular momentum and J refers to the total angular momentum.

The energy level diagram for the lanthanide ions can be used to classify the lanthanide ions into groups based on their luminescent properties as shown in **Figure 1.5**.

The first group includes holmium, praseodymium, neodymium, erbium, ytterbium and thulium. This group has small gaps between the energy level states (the lowest luminescent state and the highest non luminescent state) which allow weak fluorescence and short decay life time. The second group consists of samarium, dysprosium, europium and terbium. They have large gaps between their energy level states and therefore they exhibit strong luminescent intensities and have long decay life times. The third group of lanthanide ions are lanthanum, gadolinium and lutetium. They do not exhibit fluorescence due to completely empty or completely filled 4f subshells in La^{3+} and Lu^{3+} , respectively. Gd^{3+} fluorescence is rarely detected because of the large gap between the ground state and the first excited energy level.

It has been observed that some F-F transition intensities of the lanthanide ion complexes are very sensitive to small changes in the environment. These transitions have been termed hypersensitive transitions and obey the electric selection rules $|\Delta S| = 0$, $|\Delta L| \leq 2$ and $|\Delta J| \leq 2$. Hypersensitive transitions are useful tools in the spectroscopic data analysis of the lanthanide ion complexes.

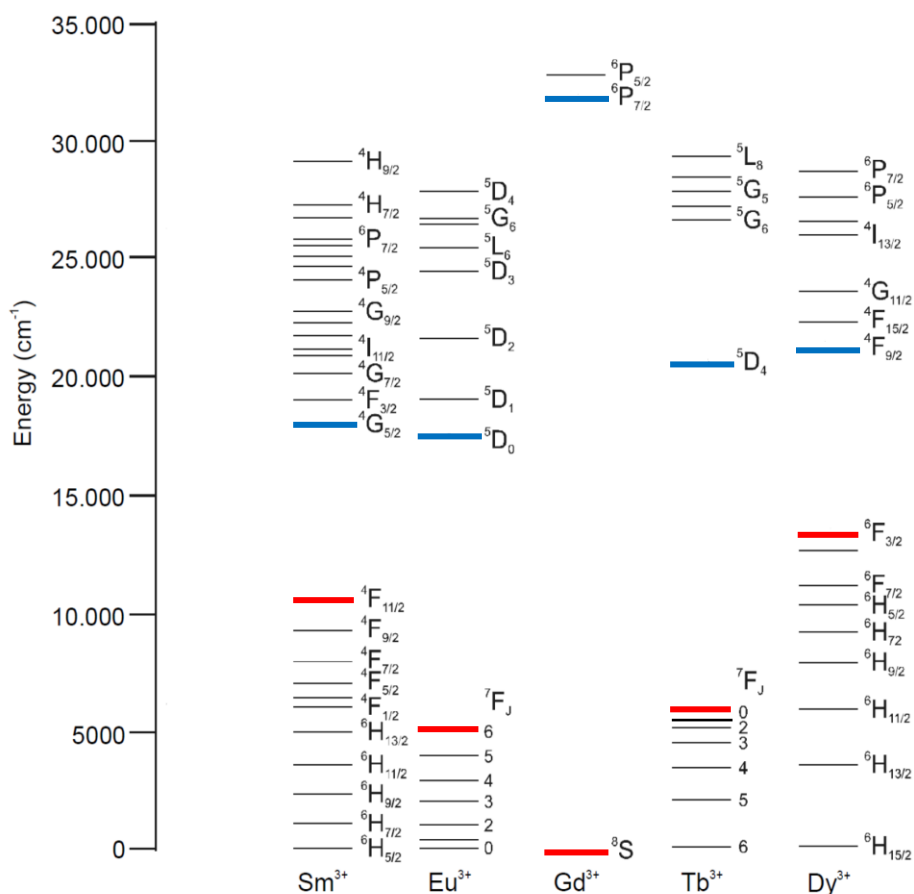


Figure 1.5 Energy level diagram of selected lanthanide ions. Energy level diagram of the 4F configuration levels that is responsible for the lanthanide ions luminescence. Blue bands represent the lowest luminescent (excited) state, and the red bands represent the highest non-luminescent (ground) state. The larger the energy gap between the lowest luminescent state and the highest non-luminescent state, the stronger the luminescent intensity of the lanthanide. The diagram is adapted from (Stein and Würzberg, 1975).

1.4.3 Lanthanide luminescent properties

Lanthanide ions have a weak optical absorbance, and they exhibit low fluorescence inherently, unless they are chelated with a suitable ligand with chromophore or antenna (Moore et al., 2009). The ligand absorbs energy in the UV region and transfers it to the lanthanide ions which reach an excited state and produce fluorescence in the visible region (**Figure 1.6**). There are three main factors that influence the fluorescence mechanism of lanthanide ions (Thibon and Pierre, 2009). First, the gap of the energy levels between the lowest fluorescence state of the lanthanide ion and the highest energy sublevel of its ground state. The larger the energy gap is, the stronger the fluorescence will be. Eu^{3+} and Tb^{3+} have appropriate gaps between their energy levels and therefore they are widely used as luminescent probes (Bünzli and Piguet, 2005). Second, the energy of the antenna triplet excited state has to be higher than the lanthanide 5D excited state to avoid energy back-transfer. Third, the transferred energy between the antenna and the lanthanide ions is strongly distance dependence (r), which follows either Dexter's or Förster's energy transfer mechanisms (Eliseeva and Bünzli, 2010, Thibon and Pierre, 2009).

- (i) Dexter's electron exchange theory is short range energy transfer of the excited electron from the antenna (donor) to the lanthanide ion (acceptor). This process requires spectral overlap between the phosphorescence spectrum of the donor and the absorption band of the acceptor.
- (ii) Förster resonance energy transfer (FRET) is mechanism of energy transferred between the excited antenna (donor) to the lanthanide ion (acceptor) within a distance range of r^{-6} .

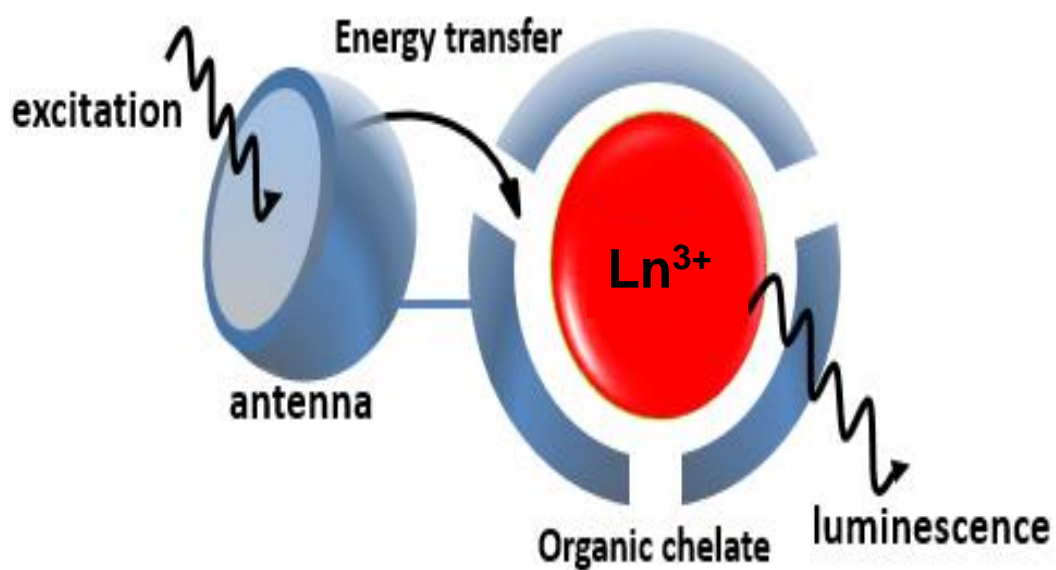


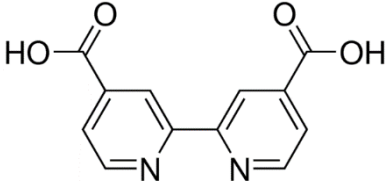
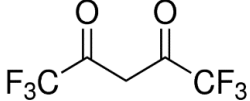
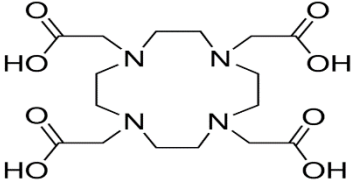
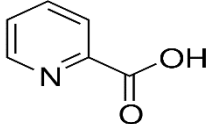
Figure 1.6 Photophysical schematic pathway representation of the lanthanide complex fluorescence emission processes. The antenna absorbs the UV light and then transfers the absorbed energy to the lanthanide ion. The lanthanide ion emits fluorescence as a result of intramolecular energy transfer from the excited level to the ground state level.

Lanthanide chelates have significant advantages in multiplex biological labelling applications due to several desirable features. The different excitation (less than 400 nm) and emission wavelengths (545-615 nm) of the lanthanides have shown that lanthanide chelates do not quench each other when they conjugate to other molecules. In addition, their photochemical characteristics in the form of high quantum yield, sharp emission peaks, long fluorescence lifetime from μs to ms and large shift Stokes's are all favourable features that are essential for biological applications (Zhang et al., 2012a). The Stokes shift is strongly associated with the energy emission that is dependent on the energy transition between the 4F levels of the central lanthanide ions and not the UV absorption which is dictated by the ligand absorption features.

Each lanthanide produces different emission wavelengths and intensity of luminescence. Eu^{3+} emits red light upon irradiation with UV light, whereas Sm^{3+} emits orange light, Tm^{3+} blue light and Tb^{3+} green light. Nd^{3+} , Er^{3+} and Yb^{3+} emit in the near-infrared region. The fascinating luminescent properties of the lanthanide ions make them significant for several applications including the construction of optical fibres used for telecommunications (Kido and Okamoto, 2002), lamp phosphors (Yen et al., 2007), light emitting diodes (OLED) (Reyes et al., 2004, Kido and Okamoto, 2002), contrast agents for resonance imaging (Faulkner et al., 2005), lasers and optical amplifiers (Bünzli et al., 2007, Kuriki et al., 2002), medical diagnosis and biosensors (Singh et al., 2015). The most popular rare earth elements for lanthanide chelate fluorescence used as labelling agents are europium followed by samarium, terbium and dysprosium (Terai et al., 2012b).

Many classes of ligand have been designed to chelate lanthanide ions including cryptands (Gonçalves e Silva et al., 2002, Blasse et al., 1987), 1, 3-diketonates (Ludwig et al., 1995, Lis, 2002, Tsaryuk et al., 2000) , macrocyclic ligands (Bünzli and Ihringer, 1996) and carboxylic acid derivatives (Parker et al., 1998). (Table 1.2).

Table 1.2 Examples of ligand types.

Ligand type	Example
Cryptands	<p>2,2'-Bipyridine-4,4'-dicarboxylic acid</p> 
1, 3-diketonates	<p>Hexafluoroacetylacetone</p> 
Macrocyclic ligand	<p>1,4,7,10-tetra-azacyclododecane-1,4,7,10-tetraacetate (DOTA)</p> 
Carboxylic acid derivatives	<p>Picolinic acid</p> 

1.4.4 Europium ion-complex fluorescence characteristics

Europium ion complexes have a unique advantage in biological applications over other lanthanide complexes. Eu^{3+} has three excited states (5D^2 , 5D^1 and 5D^0) that are lower in energy level than the triplet energy states of several types of ligands. Also, the biological tissues are transparent towards the red region of the visible light spectrum. Moreover, Eu^{3+} ions are fairly insensitive to quenching by oxygen. The presence of both magnetic dipole ($5\text{D}^0 - 7\text{F}^1$) and electric dipole ($5\text{D}^0 - 7\text{F}^2$) transitions in the Eu^{3+} complex fluorescence spectrum can provide further information about the nature of the coordination symmetry around the Eu^{3+} (Shuvaev et al., 2017).

Eu^{3+} complexes become significantly more luminescent when attached to appropriate ligands. The ideal ligand must be suitable for efficient ligand-to-metal energy transfer and ideally have aromatic group(s) with energy gaps that are suitable for UV light absorption (Hemmilá and Mikkala, 2001, Nishioka et al., 2007). The ligand absorbs the UV excitation light via ligand $\pi-\pi^*$ transition of the aromatic ring(s) and as a result the absorbed energy is transferred from S1 level in the ligand to the 5D^n level in the Eu^{3+} as shown in **Figure 1.7**. Hence, Eu^{3+} ion emits fluorescence when energy is transferred from 5D^0 to one of the 7F levels.

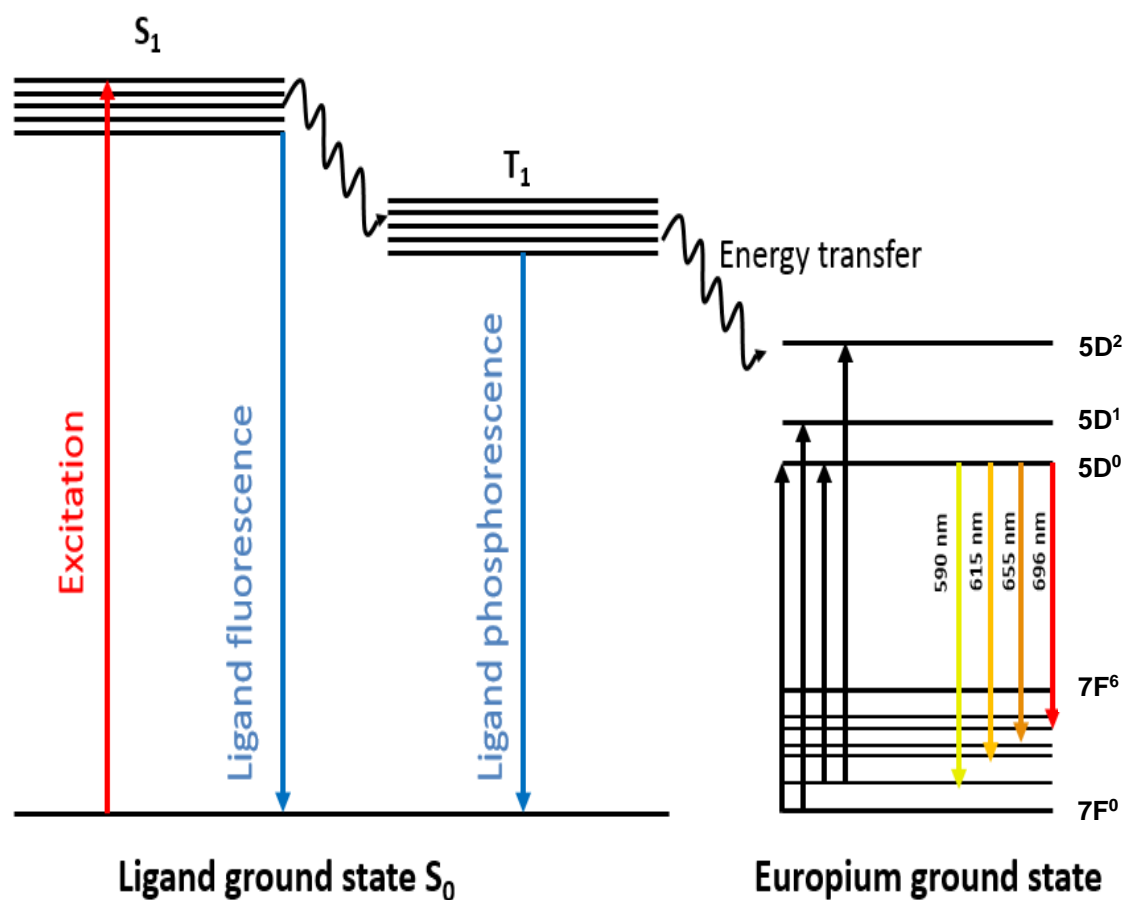


Figure 1.7 Schematic representation of the Eu^{3+} complex fluorescence emission processes. The ligand absorbs the UV light and is excited from ground singlet energy level S_0 to S_1 level; then the energy transferred to ligand's triplet energy state (T_1). The absorbed energy then transferred to the $5D^n$ level in the Eu^{3+} . Eu^{3+} ion emits fluorescence due to intramolecular energy transfer from $5D^0$ to one of the lower energy $7F$ levels, which illustrates the principle ligand-to-metal energy transfer.

The strongest emission peaks among several Eu^{3+} transition levels are between $5D^0 - 7F^n$ in the 590 nm to 700 nm range. The optical transitions of Eu^{3+} are shown in **Table 1.3**. The emission intensity of energy transitions from $5D^0$ to $7F^1$ levels are magnetic dipole transition which is relatively independent on the coordination sphere whereas the emission from the electric dipole transition from $5D^0$ to $7F^2$ is hypersensitive and strongly dependent on the symmetrical coordination surrounding the metal ion and hence the ligand type. Kirby and Richardson (1983) found that the ratio of the integrated intensity of electric dipole transition ($5D^0 \rightarrow 7F^2$) to magnetic dipole transition ($5D^0 \rightarrow 7F^1$) is a good measure to provide information about the symmetry of first coordination sphere of Eu^{3+} ions in the ligand complex (Kirby and Richardson, 1983). This ratio is termed the photoluminescence intensity ratio (PLIR). The final F-F transition is mainly responsible for the long lifetime of the luminescence, and it is fairly resistant to environmental factors. The Eu^{3+} complexes lifetimes are long, and range from several hundred μs to more than 1 ms (Matsumoto, 2010).

Table 1.3 Energy transitions and their relative wavelength within Eu^{3+} - complex spectra

Energy transition	Wavelength range	Dipole character	Intensity remarks
$5D^0 \rightarrow 7F^0$	570-585	Electric transition	Weak, rarely observed
$5D^0 \rightarrow 7F^1$	585-600	Magnetic transition (hypersensitive)	Strong, independent on the environment
$5D^0 \rightarrow 7F^2$	610-630	Electric transition	Very strong, dependent on the environment
$5D^0 \rightarrow 7F^3$	640-660	Electric transition	Weak, Forbidden transition
$5D^0 \rightarrow 7F^4$	680-710	Electric transition	Medium, dependent on the environment
$5D^0 \rightarrow 7F^5$	740-770	Electric transition	Weak, Forbidden transition
$5D^0 \rightarrow 7F^6$	810-840	Electric transition	Weak, rarely measured

1.4.5 Examples of luminescent lanthanide complexes

Lanthanide ions (Ln^{3+}) are spherical in shape and have triple charge cations, that bind to hard bases e.g nitrogen and oxygen atoms. Since the coordination number of lanthanide ions are eight to nine, the ligand of interest must have a strong coordinating groups such as charged oxygen atoms (carboxylates, phosphonates and phosphinates) to prevent solvent from binding to Ln^{3+} and to form stable complexes with Ln^{3+} .

There are many classes of ligand that have been designed to chelate the lanthanide ions including cryptands (Gonçalves e Silva et al., 2002, Blasse et al., 1987), 1, 3-diketonates (Ludwig et al., 1995, Lis, 2002, Tsaryuk et al., 2000) , macrocyclic ligands (Bünzli and Ihringer, 1996), polypyridyls (De Sa et al., 1993) and EDTA derivatives and DTPA derivatives.

1.4.5.1 β -diketonate chelates

β -diketonate chelated lanthanide complexes ($\text{La} (\beta\text{-dik})_3$) are the first designed luminescent lanthanide complexes. The two side chains (R-group) at the β -diketonate ligand's skeleton are attached to simple methyl groups or CF_3 groups as shown in **Figure 1.8**. These complexes are less stable in acidic environment as well as in water due to hydrolysis of the complexes (Melby and Rose, 1964). Thus, the stability of the complexes is depending on the nature of the solvents and the pK_a of the β -diketonate ligand. Some attention has been paid to the combined 1,10- phenantroline (Phen) and β -diketonates ($\text{La} (\beta\text{-dik})_3$ Phen) (**Figure 1.8**). The complexes show a substantial increase in the

fluorescence intensity of the Eu^{3+} and Tb^{3+} complexes (Melby and Rose, 1964, Frey and Gong, 1994).

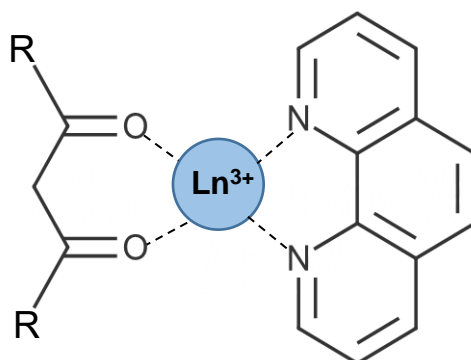


Figure 1.8 Examples of Lanthanide- β -diketonate complexes. Lanthanide- β -diketonate-phenanthroline complexes is a typical example of a Lanthanide- β -diketonate. The β -diketonate ligand's R groups can be either $-\text{CH}_3$ or $-\text{CF}_3$.

1.4.5.2 Cyclen derivatives

The cyclen derivatives family are water soluble ligands. Their structure is composed of 1,4,7,10-tetra-azacyclododecane skeleton functionalised with four coordinating pendant arms attached to additional donors which include amide, phosphate, phosphinate or carboxylate groups (Parker and Williams, 1996, Yilmaz et al., 1999). The resulting complexes can be anionic, cationic or neutral based on the donor group's charge. The most important chelated lanthanide complex reported are 1,4,7,10-tetra-azacyclododecane-1,4,7,10-tetraacetate (DOTA) and 1,4,7,10-tetraazacyclododecane-1,4,7,10-tetraphosphinate and others (**Figure 1.9**). These types of anionic ligands afford high stability due to an excellent f-orbital shielding of the lanthanide ion. The most important applications

of the cyclen based ligand chelated lanthanide ion complexes are the Tb^{3+} and Eu^{3+} complexes as luminescent probes in fluoroimmuno assays and Gd^{3+} complexes as a contrast reagent for MRI (Aime et al., 1996, Lehn, 1978).

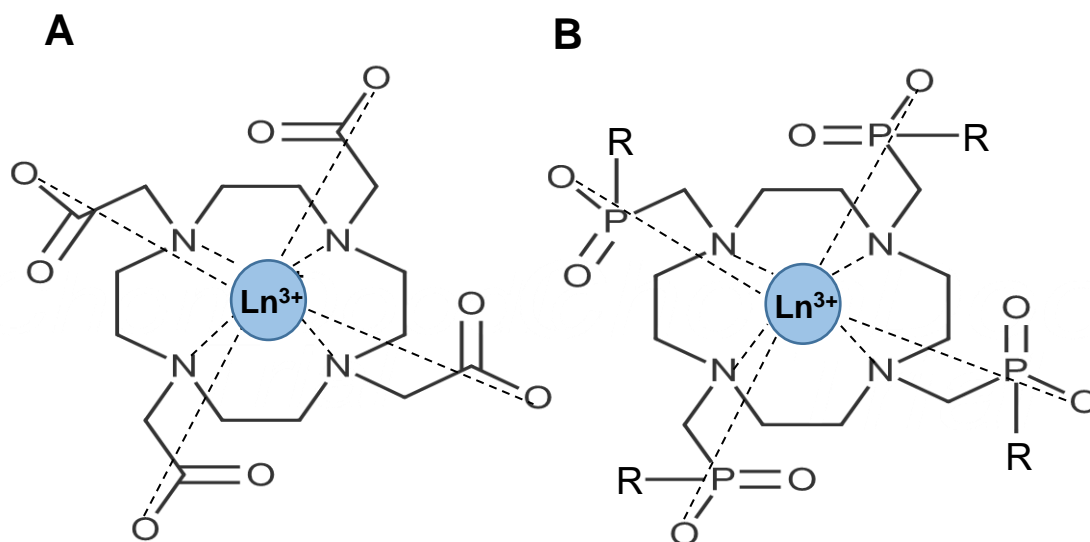


Figure 1.9 Examples of cyclen derivatives ligands chelated lanthanide complex. (A) 1,4,7,10-tetraazacyclododecane-1,4,7,10-tetraacetate (DOTA), (B) 1,4,7,10-tetraazacyclododecane-1,4,7,10-tetraphosphinate.

1.4.5.3 Cryptates

Cryptates are cage-type ligands in which the donor atoms are preorganised for complexation (**Figure 1.10**). The ligand alone has no absorption bands at 300 nm region but when it chelates lanthanide ion, a weak absorption band at 298 nm is observed due to a charge transfer transition relating to the amine nitrogens and La^{3+} (Lehn, 1978).

Tris (2,2'-bipyridine) cryptand ligand was synthesised by Alpha and coworkers (1987) that has absorption bands at 300 nm region because of the

bipyridine π - π^* transitions (Alpha et al., 1987). Although, the tris (2,2'-bipyridine) cryptand chelated Eu^{3+} complex is stable in water, its fluorescence suffer from energy back-transfer from the lanthanide excited level to the ligand triplet state.

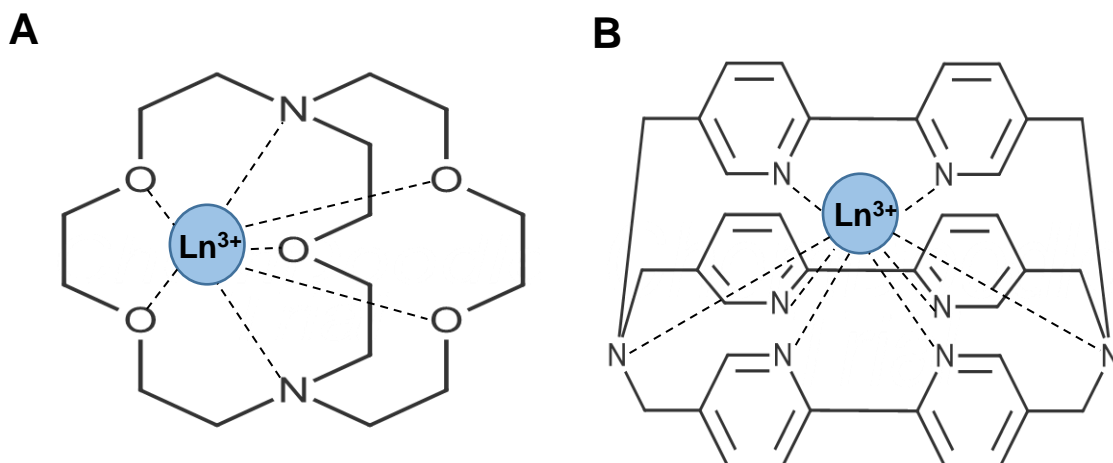


Figure 1.10 Examples of cryptates ligands chelated lanthanide complex. (A), Cage-type cryptates ligand; (B), Tris (2,2'-bipyridine) cryptand ligand.

1.4.5.4 EDTA derivatives

Takalo and coworkers (1996) synthesised a combined ligand consisting of EDTA (chelator) and pyridine (sensitizer) as shown in **Figure 1.11A** (Takalo et al., 1996a). The EDTA based- pyridine ligand showed strong fluorescence emission when chelated to lanthanide ions (**Figure 1.11B**). Also, the same group found that the integration of more than one sensitizer in the chelating EDTA ligand can improve the lanthanide complex fluorescence characteristics (Takalo et al., 1996b).

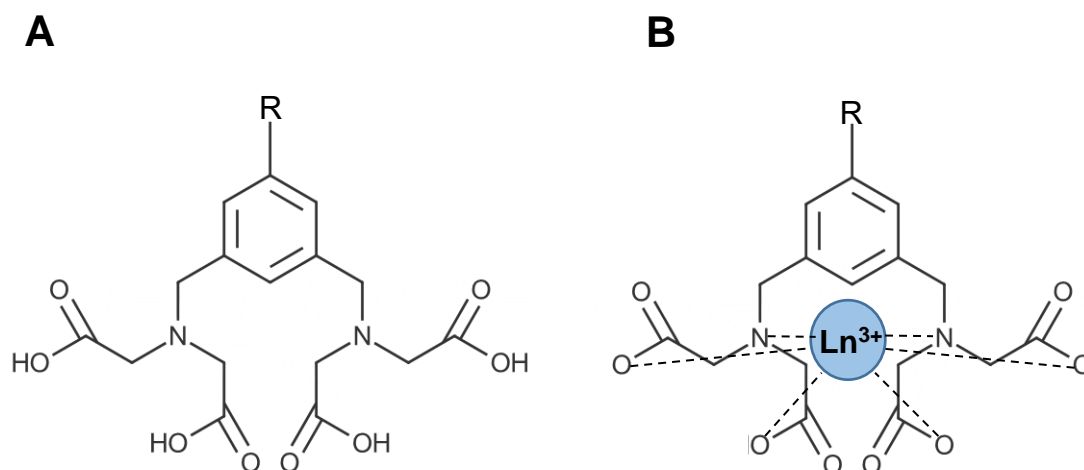


Figure 1.11 Examples of pyridine- based ligands. (A), Pyridine- based ligands can be functionalised with aminodiacetate; (B), Pyridine-based ligands chelated lanthanide complex.

1.4.5.5 DTPA derivatives

DTPA (diethylenetriaminepentaacetic acid) based ligands provide good f-orbital shielding of the lanthanide ion leaving only one coordination position free for the solvent molecule. Therefore, the stability of the DTPA chelates lanthanide complexes is very high in water. The sensitizers can be easily be incorporated into the DTPA-based ligand such as carbostyryl-124- DTPA for Eu^{3+} and fluorescein- DTPA ligand for the Nd^{3+} , Yb^{3+} , and Er^{3+} (**Figure 1.12**) (Werts et al., 1997).

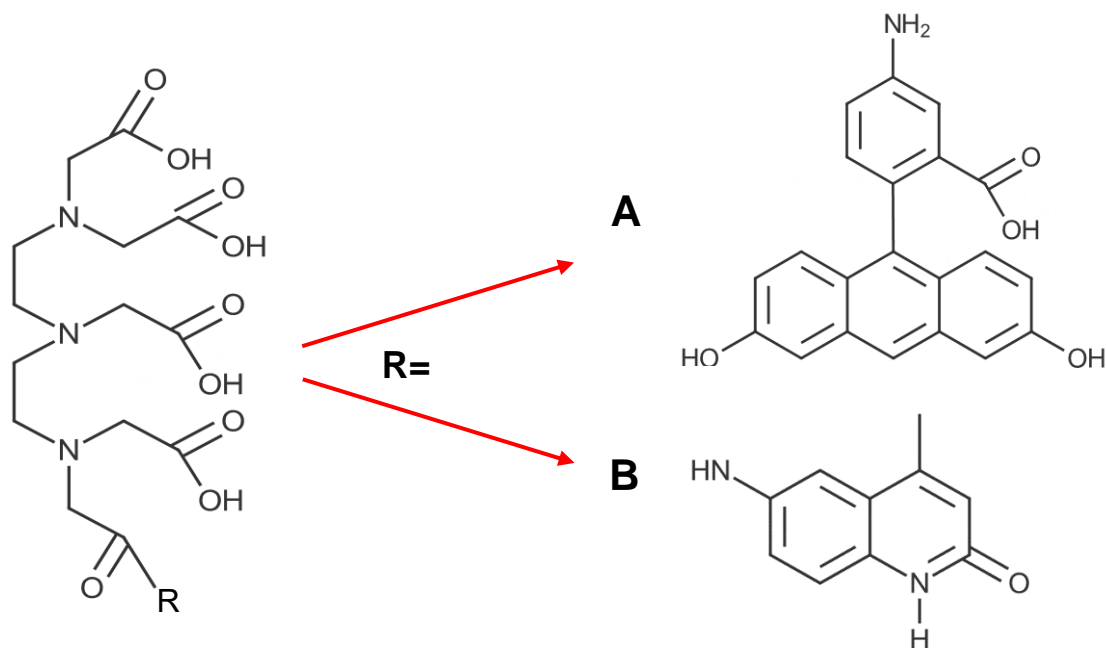


Figure 1.12 Examples of DTPA- based ligands. (A), DTPA- based ligands can be functionalised with fluorescein sensitizer; (B), carbostyryl-124 sensitizer. Adapted from (Klink, 2000).

1.4.6 Europium ion complexes Applications

1.4.6.1 Lanthanide pH probes

The physiological activity in various cellular environments is critically regulated by the pH value and as a result any deviation from the standard values can lead to a wide range of disease (Simon et al., 1994, Izumi et al., 2003). Accurate detection of the pH values would allow better understanding of the different biological processes and hence better intervention at cellular levels. The narrow window of normal pH value (7.35-7.45) in human serum necessitates a precise detection of any change. To date, a number of lanthanide-based luminescent complexes have been designed as pH sensitive probe (Bünzli, 2010, Gunnlaugsson et al., 2003, Li et al., 2004, Pal and Parker, 2007, Bonnet and Gunnlaugsson, 2009, Liu et al., 2013a). In order to achieve a bright and sensitive probe, a pH-sensitive group needs to be added to the ligand to perturb the coordination environment of the lanthanide by either changing the electron demand at the lanthanide ion or the coordination environment. As a result, the emission intensity of the probe would change with the different energy transfer efficiencies between protonated or deprotonated form of the ligand to lanthanide ions.

Smith et al (2012) have devised a series of probes that operated based on pH-selective dissociation of one ligand (Smith et al., 2012). In the Eu^{3+} based complex bearing a sulphonamide arm and an azaxanthone chromophore moiety as ligand, reversible protonation of the sulphonamide pendant arm took place at the nitrogen accounting for changing the coordination environment of Eu^{3+} . In another Tb^{3+} complex, the sulphonamide arm was replaced by the electron-rich p-MeOPh group that reversibly binds to the Tb^{3+} and changes the metal ion

coordination environment. It was reported that the emission intensity of the Tb^{3+} complex was quenched in an alkaline medium within the pH range of 3-9. When sulphonamide nitrogen binds with Tb^{3+} , the sulphonamide deprotonation process takes place leading to the change in fluorescence emission intensity. In addition, the hydration state of Tb^{3+} is changed from 1 in acidic to 0 in basic conditions. The high-frequency O-H vibrations was thought to be minimised by the loss of coordinated water molecule and neutralises the non-radiative quenching all of which may also induce the fluorescence enhancement of the Tb^{3+} complex (Law et al., 2009).

1.4.6.2 Metal ion probes

Undoubtedly, metal ions play an essential role in many biological processes, and hence metal ion probes that are sensitive and selective are highly indispensable. Several lanthanide complexes have been developed as probes for detection of metal ions including Au^{2+} , Cu^{2+} , K^+ and Hg^{2+} (Viguier and Hulme, 2006, Liu et al., 2010, Tan et al., 2011). Zn^{2+} is the second most abundant heavy metal ion in the human body and it is associated with gene expression, apoptosis, and neurodegenerative diseases (Berg and Shi, 1996, Burdette and Lippard, 2003). Hanaoka et al (2003) have designed Tb^{3+} and Eu^{3+} complexes as luminescent probes for Zn^{2+} detection (Hanaoka et al., 2003, Hanaoka et al., 2004). The high affinity of TPA-derivatives towards Cu^{2+} was used to create a Cu^{2+} - Eu^{3+} ion based complex sensitive probe where a DOTA platform with dipicolylamine moiety was utilised for selective binding of Cu^{2+} . Similarly, the macrocyclic N_2O_4 binding moiety (diaza-18-crown-6) was utilised for the design

of an Eu^{3+} complex based K^+ ion probe since it is known for its high affinity towards K^+ (Shuvaev et al., 2017).

The majority of the metal ion probes bear N, O, S- donor atoms as the coordination unit in their antenna as they possess a pyridyl, quinolyl, or macrocyclic moieties. When the antenna coordinates with the target metal ion, the energy transfer from antenna to lanthanide ion is modulated, and is reflected in the change in the fluorescence of the probe. The recognition of metal ions by lanthanide complexes has high sensitivity due to the strong binding capability of the coordination units in the antenna. The potential advantage of using lanthanide complex based metal ion probes is that they can offer a sensitive detection using time-resolved fluorescence measurement and eliminate short-lived auto-fluorescence in complexed environments. Nonetheless, many metal ions share similar chemical properties, and their local concentration varies considerably within the nature of the cell compartment and surrounding environment.

1.4.6.3 DNA/ RNA probes

Sensitive and selective recognition of nucleobases, nucleic acids, DNA and RNA are important for many cellular activities including gene expression, signal transduction, response to cancer therapy and gene therapy (White et al., 1998). To date, the application of Eu^{3+} based complexes for DNA/ RNA recognition remains challenging. The difficulty in creating a specific probe for nuclear DNA/ RNA arises from their charged nature which hinders their permeability to the nucleus in living cells. However, existing probes so far are designed based on two strategies. The first possess DNA/ RNA intercalation between the nucleotide bases via cisplatin-related moieties whilst the second use a synthetic DNA single strand that is matched to the target DNA/ RNA to form a triplex with DNA or duplex with RNA.

Ancel et al (2013) were able to design a Eu^{3+} complex based probe for sensing DNA using a proflavin (Pfl), a well-known intercalating agent which can sensitise Eu^{3+} - centred emission and give rise to an emissive Eu^{3+} complex (Ancel et al., 2013). When calf thymus DNA (CT-DNA) was added to solution containing Eu^{3+} complex, 45% quenching of Eu^{3+} was observed. Although the above probe demonstrated a photophysical response to DNA binding, the practical application of the system was not promising. The antennae used as intercalating moieties can quench the overall luminescent signal produced while the lack of internal reference signal renders the acquisition of the data difficult. In attempts to overcome these obstacles, Dasari et al (2015) suggested an introduction of “switch-on” system where a heterodinuclear lanthanide complex based probe was designed such that one of the metals were sensitised by an intercalating agent while the other had an antenna that remained intact upon

binding with DNA (Shuvaev et al., 2017, Dasari and Patra, 2015). The Eu^{3+} complexes bearing dipyridoquinoxaline or dipyridophenazine demonstrated an increased fluorescence intensity upon addition of CT-DNA due to intercalation of the antenna to the DNA. Nonetheless, due to the instability of the Eu^{3+} complexes in aqueous solution, ill-defined speciation of the emissive complex can be encountered. Another innovative system of a DO3A-based Eu^{3+} complex was designed by Li et al (2015). The complex, bearing akynylpyridine chromophore with a $[\text{PtCl}_2\text{NH}_3]$ unit, was used as a pro-drug that can be activated by UV (365 nm) or two-photon longer wavelength irradiation leading to controlled release of the cytotoxic drug $[\text{PtCl}_2\text{NH}_3\text{H}_2\text{O}]$. The release of the drug efficiently quenched the emission of the Eu^{3+} complex by quenching the singlet state of the chromophore only after the $[\text{PtCl}_2\text{NH}_3]$ unit was released and hence the quantum yield of the complex was increased by two folds (Li et al., 2015).

The use of pre-synthesised complementary sequences of nucleic acid with an attached lanthanide complex was designed to provide highly selective probe towards the target nucleic acid. For example, an Eu^{3+} complex-based probe comprising of a DTPA group was coupled to a peptide sequence bearing a phenanthroline moiety for sensing bovine immunodeficiency virus which is an RNA transactivation response element (Penas et al., 2016). To date, there remains no Eu^{3+} based complex that has been designed to be sensitive and highly selective for targeting specific proteins.

1.5 Bioreceptors

The crucial component of any biosensor is the receptor or the biorecognition element. It is responsible for specific analyte recognition, producing the physicochemical signal monitored on the transducer and finally, the sensitivity of the device (Matsumoto, 2010).

At the present time, several types of biorecognition elements in biosensors have been reported including oligonucleotide and proteins (antibodies and non-IgG binding proteins).

1.5.1 Oligonucleotides

Nucleic acid aptamers are single stranded DNA or RNAs that show strong affinity and specificity to their targets. Aptamer structures offer advantages over the traditional biorecognition elements (antibodies) including high stability, low immunogenicity (Song et al., 2012) and ease of production in large scale. Specific orientation can be easily established by incorporating reactive groups such as -SH and -NH₂.

The selection of the aptamers for the target of interest from oligonucleotide libraries can be achieved by using a Systematic Evolution of Ligands by Exponential enrichment (SELEX) (Ni et al., 2011, Santosh and Yadava, 2014). The process involves many rounds of negative and positive selection in order to obtain the highest affinity binding aptamers to the targets (Song et al., 2012, Darmostuk et al., 2015). The selected aptamers are screened against their target molecules, then the bound aptamers are separated and amplified using polymerase chain reaction (PCR). Different types of analytes have been

screened in addition to nucleic acids e.g. small molecules (Bala and Górski, 2018), cells (Park, 2018), viruses, bacteria and proteins (Ilkhani et al., 2015). The binding strategy of the aptamers is based on structural change (secondary and tertiary) due to their self-annealing properties (Chambers et al., 2008, Park, 2018).

1.5.2 Antibodies

Antibodies (immunoglobulins) are the most commonly used class of biological recognition molecules in biosensing. Antibodies are produced by the immune systems in vertebrates in response to the introduction of an antigen and/or a foreign molecule. An antigen can be any substance (toxin, virus and bacteria) that is recognised as a foreign which stimulates antibody production to react specifically with that antibody. Antibodies recognise specific regions called epitopes in the antigen and polyclonal antibodies, for example due to vaccination, will recognise many epitopes.

Each antibody is comprised of four polypeptides; two 25 KDa light chains and two 50 KDa heavy chains which are bound to each other by a disulphide bond and joined to form a "Y" shaped molecule (Chaplin, 2010) (**Figure 1.13**). Both heavy and light chains contain a variable region located at the amino terminus that consists of amino acids that are organised to produce a binding site for specific antigen through its complementarity-determining region (CDR). The heavy chains pair to form a constant region (Fc) located toward the carboxy terminus and it is responsible for binding to Fc receptors and activating the immune system. It is also used to differentiate the different classes of immunoglobulins. There are five isotypes of Immunoglobulins which are

classified as IgE, IgD, IgG (monomer), IgA (monomer and dimers) and IgM (pentamers).

Polyclonal and monoclonal forms of antibodies are widely used in different areas of research. The production of polyclonal (pAbs) and monoclonal (mAb) antibodies involve immunising an experimental animal such as mouse, goat, rabbit and others with the analyte of interest. Polyclonal Abs are derived from multiple B cells in serum resulting in the production of pool of polyclonal Abs that bind to multiple epitopes on the same antigen. Monoclonal Abs are produced by a technique called hybridoma technology. This technique involves fusion of myeloma cells (B cancer cells) with a single B cell extracted from the spleen tissue of the immunised animal yielding a hybridoma cell. The yielded monoclonal antibodies are identical and can bind specifically to a single epitope. Monoclonal Abs are widely used as a therapeutic agent in treatment of inflammatory or autoimmune disease, whilst polyclonal Abs are extensively used as a research agent in ELISA, western blot, immunochemical assay and flow cytometry applications (O'Kennedy et al., 2017). Despite the widespread applicability of antibodies as a research tool and therapeutic agents, they have several limitations. Antibodies are large molecules, which therefore limits their tissue penetration and may reduce targeted delivery or therapy. The complex structure of the antibodies light and heavy chains leads to unstable domain association in the production of small Fv fragments (Reisfeld, 2002). Complicated cloning steps are required for the development of recombinant antibodies and the manufacture of antibodies is expensive and time-consuming. It also depends on the use of live animals which is undesirable (Werner, 2004). In addition, batch to batch variability, lack in thermal stability, cross reactivity and costly production of pAbs limit their use in analytical devices (Baker, 2015, Bradbury and Plückthun, 2015,

Haurum, 2006). In the field of biosensor research, it is important to control the correct orientation of the biorecognition elements on the surface of the analytical platform. Antibodies scaffold consist of more than one lysine and cysteine amino acid residues; therefore, it is hard to modify these amino acids at specific sites in order to control the orientation. These drawbacks of antibodies encouraged researchers to find alternative binding protein.

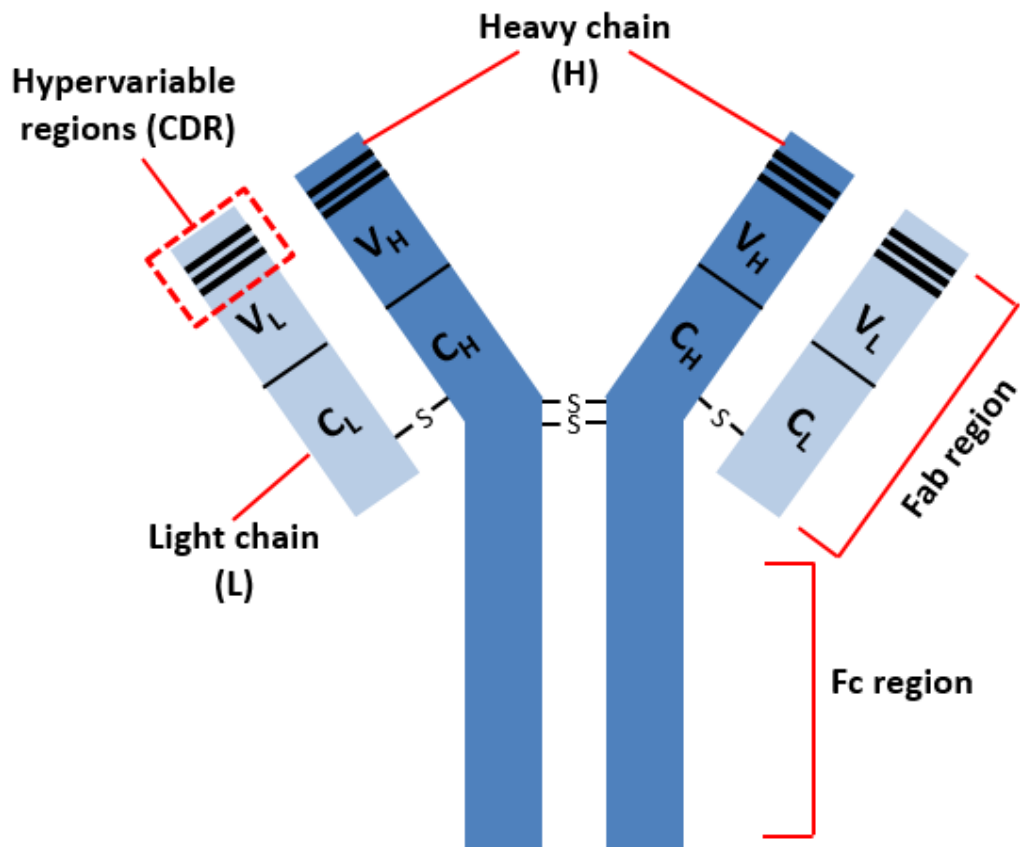


Figure 1.13 Antibody structure (IgG). IgG consists of four chains, two identical heavy chains (dark blue) and two identical light chains (light blue) are linked together by disulphide bonds. Both heavy and light chains form Fab domains, which contain the antigen-binding sites located at the CDR regions. The Fc and the Fab domains are linked by flexible linkers.

There are several alternative proteins derived from antibody structure that have been engineered with preferable properties such as small size and monoclonal (Hey et al., 2005, Ponsel et al., 2011, Chames et al., 2009, Richards et al., 2017). These fragments are composed of one or more than one part of antibody in addition to the antigen-binding sites located at the heavy and/or light chain variable domains. Single chain (Fv) ~25 KDa, diabodies ~50 KDa, nanobodies ~15 KDa and antigen-binding fragment (Fab) ~50 KDa are all examples of antibody derived fragments (Romer et al., 2011, Sharma et al., 2016b) (**Figure 1.14**).

Although antibody derived fragments technology become alternative to whole antibody in solving problems such as size and specificity, still most of them require immunising animals with the antigen of interest in order to generate Abs library. Also, some of them suffer from low stability as a result of the absence of Fc region which is responsible for the immobilisation processes in biosensors applications (Binz and Plückthun, 2005). In addition, the antibody fragments that consists of a single domain of recombinant heavy and/or light chain variable domain that contain hydrophobic amino acids on the surface are less soluble and susceptible to aggregation (Helma et al., 2015, Deffar et al., 2009). Antibody derived from *Camelidae* family (llamas, alpacas and camels) and sharks are composed of two heavy chains and lack the light chains. They are smaller than human antibodies and display a monomeric behaviour. Furthermore, they are highly soluble and thermostable. Nonetheless, their production and purification remain costly and involves animals.

Considering the above mentioned limitations of antibodies and their derivatives which have hindered their use in many clinical and biomedical fields,

there remains an immense need to redirect efforts to identify and develop an alternative solution that can overcome the obstacles seen with antibodies.

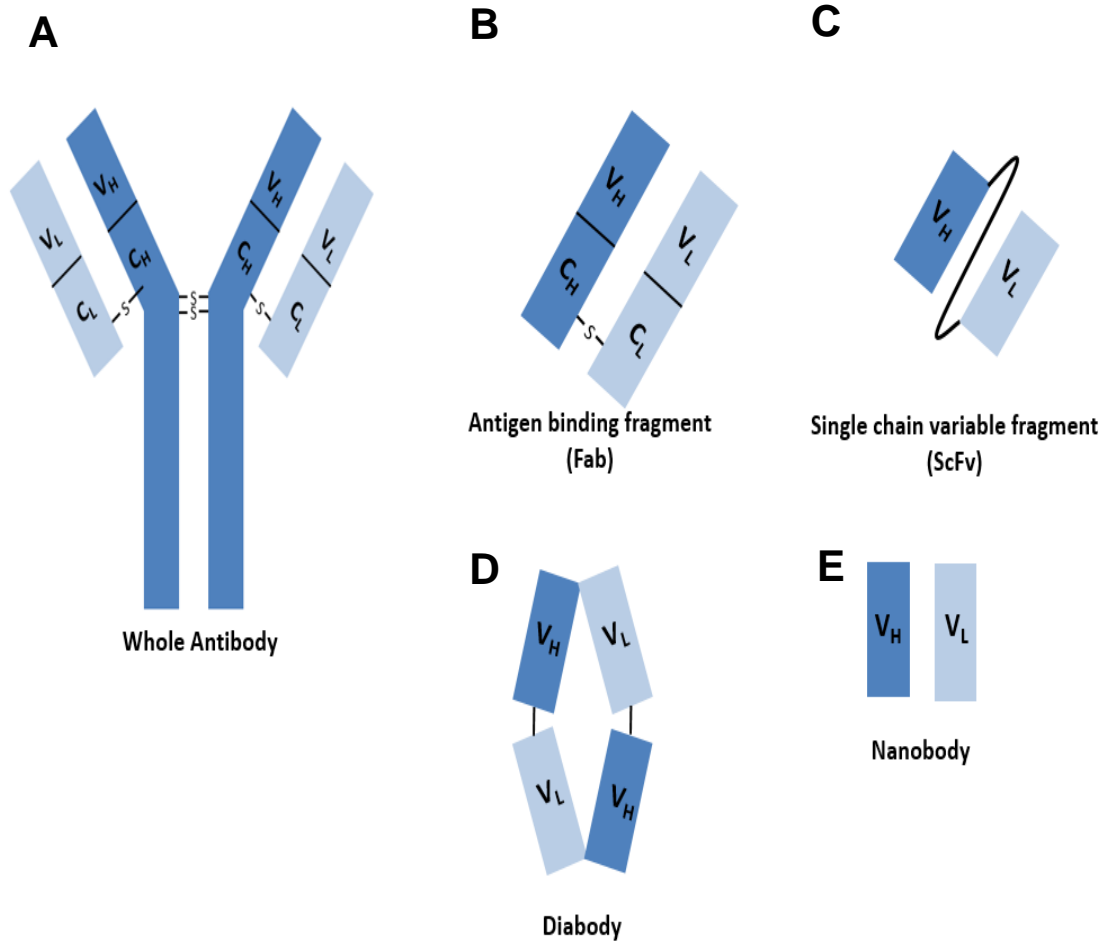


Figure 1.14 Antibody derivatives. Schematic showing some examples of antibody derivatives compared to (A), whole Ab; (B), Fab fragment is ~50 KDa and consists of VH-CH and VL-CL domains; (C), scFv is ~25 KDa and comprises of VH-VL domains; (D), Diabody is ~50 KDa and consists of two scFv domains connected by a disulphide bond; (E), Nanobody is ~15 KDa and comprises of a single antibody domain (VL or VH).

1.5.3 Synthetic Binding Protein

As antibodies and some of their derivatives show a range of limitations, effort has been explored towards synthetic binding proteins as alternatives. The ideal protein scaffold should exhibit some key characteristics in order to be successful as a binding protein. Protein scaffolds must have a compact and structurally rigid core with the ability to display surface loops of varying length or tolerate to side chain replacements in a contiguous surface region without changing the folding properties (Reisfeld, 2002). Protein scaffolds should be small in size (typically < 100 amino acid residues), highly soluble, allow tissue penetration and their binding sites should with high affinity and specificity to target protein (Reisfeld, 1990). Moreover, the desired binding protein should be stable and protease resistance (Reisfeld, 2002). Lack of cysteine residues in the native structure allows site specific conjugation to extra cysteine introduced later to couple florescent dyes or biotin (Khaled et al., 2013).

Three main processes are involved in the production of synthetic binding proteins. First, designing a library on particular protein scaffolds through site-directed/ random mutagenesis in order to create diversity. Second, display technique (e.g. yeast, bacteria, insect, mammalian cells, phage, mRNA and ribosome) is used to select the variants (Hamzeh-Mivehroud et al., 2013). Finally, the selection of the variants are based on their specificity and affinity binding to targets, also their stability at chemical, enzymatic and thermal conditions.

Up to now, there are more than 50 novel synthetic proteins which can be divided into two classes. The first is based on binding through amino acids exposed on the surface side chains of secondary structural elements of the scaffold. This type of synthetic protein scaffold binds conformationally to the

target epitope For example, Affibodies (Reisfeld, 1990), designed ankyrin repeat protein (DARPin) (Avnir et al., 1984) and Affilin (Ebersbach et al., 2007). The second class is based on binding through amino acids in exposed loops of the rigid scaffold protein structure which mimics the antibody binding site, e.g. Monobodies (Avnir et al., 1985), Anticalins (Korndörfer et al., 2003), Kunitz domain (Arnoux et al., 2002), Atrimer (Zelensky and Gready, 2005), Avimer (Silverman et al., 2005), Fynomer (Silacci et al., 2014) and Affimer (Tiede et al., 2014). Although, there are numerous synthetic binding proteins that have been produced, only a few of them are used in the biotechnological and biomedical fields. Commonly used non-antibody proteins in biosensor applications are Affibodies and DARPins (examples of the first class), monobodies and Affimer (examples of the second class).

1.5.3.1 Affibodies

This non-Immunoglobulin scaffold protein was designed based on the Z domain of *Staphylococcus aureus* protein-A which is made of three alpha helices with 58 amino residues, but lacking cysteines, and is approximately 6.5 KDa in (Reisfeld, 1990) (**Figure 1.15**). The Z domain was engineered from the B domain of the *Staphylococcus aureus* protein-A by a single mutation at helix 2. A combinatorial library of Affibody molecules was obtained by randomisation of 13 surface exposed amino acids located in two alpha-helices of the Z domain (Feilmeier et al., 2000). The Affibodies have been used as a drug delivery carrier (Ravindra et al., 2007) and for tumour targeted detection (Tiede et al., 2014). In the field of biosensing technology, Affibodies have been used in label-free SPR biosensors to detect a range of biomarkers include: human papilloma virus 16

(HPV16 E7), vascular endothelial growth factor receptor 2 (VEGFR2) and epidermal growth factor receptor 2 (HER2), (Xue et al., 2016, Fleetwood et al., 2014, Friedman et al., 2009).

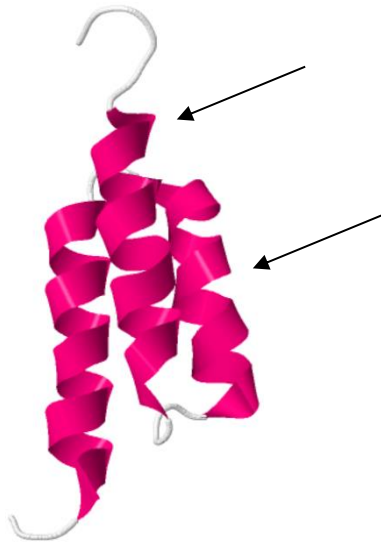


Figure 1.15 Affibody synthetic binding protein. Affibody structure consists of three alpha helices and randomisation of 13 surface exposed amino acids located in two alpha-helices (black arrows) (pdb ID: 2KZJ).

1.5.3.2 Designed ankyrin repeat proteins (DARPin)

Designed ankyrin repeat proteins, DARPins (< 14-18 kDa) are artificial scaffold proteins which are derived from naturally occurring ankyrin proteins. Typically, DARPins comprise of a 33 amino acid consensus ankyrin repeat (four or five repeats) of which the first repeat is the N-capping repeat (or N-cap) and last repeat is C-capping repeat (or C-cap) (**Figure 1.16**). Each repeat contains a β -sheet where the new amino acids are introduced followed by two alpha-helices (Ahmed et al., 2014). The N-cap and C-cap repeats provide a hydrophilic exposed surface (Naessens et al., 2000) which is thermally and denaturant resistant (Doi and Yanagawa, 1999). Applications of DARPins include for

diagnostics (Rushworth and Hirst, 2013), tumour targeting and drug delivery systems (Ravalli et al., 2013).

In biosensor applications, most DARPins based studies were limited to optical biosensors. Kummer et al. (2013) developed a fluorescence based biosensor for the detection of phosphorylated extracellular signal regulated kinase (pERK) in real time based on changes in DARPin conformation (Kummer et al., 2013). Also, DARPins based label-free fluorescent biosensors coupled to solvatochromic fluorophore were synthesised to detect maltose binding protein (Brient-Litzler et al., 2010, De Picciotto et al., 2016, Miranda et al., 2011).



Figure 1.16 DARPin synthetic binding protein. DARPin structure consists of repeated β - sheet and two α -helices with N-cap (first repeat) and C-cap (last repeat) (pdb ID: 4ZFH).

1.5.3.3 Monobodies

Monobodies are also known as Trinectins or Adnectins. Monobodies are derived from a human fibronectin type III domain (FN3) as a molecular scaffold (Mejri et al., 2010). They consist of seven β -sheets and three CDR-like loops and have been engineered to bind a wide variety of target proteins with high affinity (**Figure 1.17**). Monobodies have been shown to be effective compared to conventional antibodies as highly specific inhibitors due to the characteristics of the fibronectin type III scaffold that makes it thermodynamically stable, small in size (94 amino acid residues) and with no disulfide bonds. Monobodies are effective in treating rheumatoid arthritis, cancer, Crohn's disease (TNF α) and psoriasis (Hey et al., 2005).

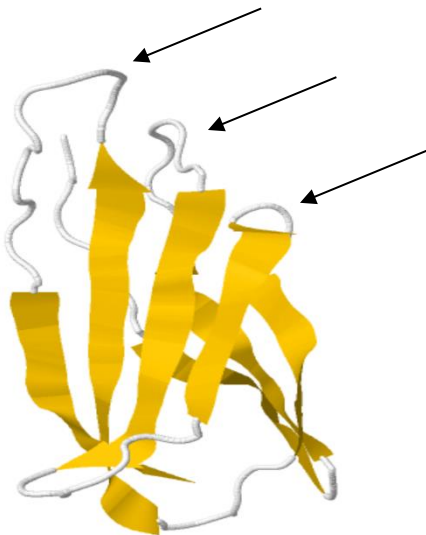


Figure 1.17 Monobody synthetic binding protein. Monobody structure consists of seven beta sheets and three CDR-like loops (black arrows) (pdb ID: 3QWQ).

1.5.3.4 Affimers

A recent scaffold is the Affimer, derived from a consensus of a large number of plant cystatins, which are small protein inhibitors, approximately 100 amino acids long, of cysteine proteases. Affimers were invented at the University of Leeds by the BSTG group initially called “Adhiron” (Tiede et al., 2014). The Adhiron has been commercialised by Avacta Life Sciences Ltd with the brand name “Affimer type II”. Affimer type I is another type of Adhiron derived from human stefin A protein scaffold (Stadler et al., 2011).

Affimers consist of a single α -helix and four antiparallel β -strands, lack cysteine and glycosylation sites and can be expressed in *E. coli* in large amounts (**Figure 1.18**). Affimers are small in size (12-13 KDa), monomeric structure, lack disulphide bonds and glycosylation site and have highly solubility. Affimers have two variable regions, each with nine randomised amino acids located between the first and second β strands (VR1) and between the third and fourth β strands (VR2)(Khaled et al., 2013). Affimers are thermostable, with melting temperature of up to 100 °C. This enables long-term storage at ambient temperature (Khaled et al., 2013). The variability of the Affimer libraries with $\sim 3 \times 10^{10}$ different clones enable large scale screening of target molecules including viruses (Jackson, 2017), small organic compound (e.g. methylene blue) (Koutsoumpeli et al., 2017), antibodies (Raina et al., 2015) and whole cells (Tiede et al., 2017). They have been used as an alternative binding protein in applications such as protein-protein interactions, ELISA and western blotting (Michel et al., 2017, Hughes et al., 2017, Kyle et al., 2015, Robinson et al., 2018). In recent studies, Affimers have been used as biorecognition elements for biosensing applications (Raina et al., 2015, Koutsoumpeli et al., 2017, Sharma et al., 2016a, Wang et al., 2017a).

Raina et al., (2015) developed an Affimer -based electrochemical biosensor for detection of the anti-myc tag antibody (Raina et al., 2015). Another Affimer- based electrochemical biosensor was developed by Johnson et al. (2012) for the detection of C-reactive protein (CRP). Quantum dot functionalised Affimer have been employed to develop label free ratiometric optical biosensors (Wang et al., 2017b).

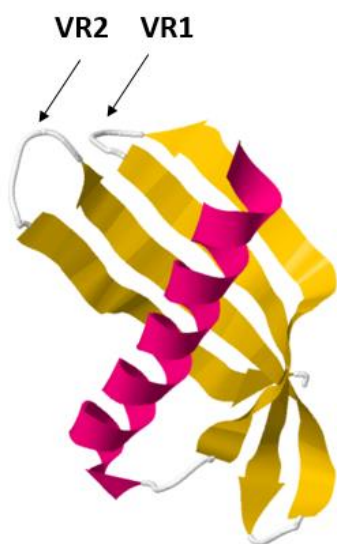


Figure 1.18 Affimer scaffold. Affimer structure consists of an alpha helix and four antiparallel β -strands and has two variable regions (VR1 and VR2) shown by black arrows (pdb ID: 4N6T).

1.6 Human protein biomarkers of disease

Serum biomarkers are not only important in making accurate diagnoses in critical conditions and disease but also play a substantial role in monitoring disease progression and response to treatments. Accurate and rapid diagnosis of certain clinical conditions is paramount for initiating the appropriate medical management. Biomarkers can be either highly sensitive but lack specificity such as CRP or highly sensitive and specific such as CEA.

ELISA is the gold standard test for the measurement of the majority of biomarkers in clinical laboratories. However, ELISA is not without limitations, which includes time and labour consumption and their high cost. An alternative solution would be to design a rapid, cheap and less time consuming probe that can offer desirable results when compared to ELISA. Optical biosensors appear to be a potential candidate that is worth investigating. Acute myocardial infarction and strokes are very common life threatening conditions that require rapid diagnosis and immediate medical management. A series of biomarkers have been investigated in the past for those two conditions and therefore, one biomarker for each will be selected to test the hypothesis of this project. Other biomarkers that are also commonly used in clinical practice such as CRP for inflammation and bacterial infection and CEA as a cancer biomarker can also be tested against the hypothesis of this project.

1.6.1 Myoglobin

Myoglobin is a monomeric globular small protein that facilitates oxygen storage in cardiac and peripheral muscle tissue. Myoglobin is a family member of the globin proteins and consists of eight alpha helices linked by loops, contains 154 amino acids and is around 17 KDa (Melanson et al., 2004) (**Figure 1.19A**). When myoglobin is found in the circulation, it is deemed pathological indicating either cardiac or skeletal muscle damage. Myoglobin is an ideal marker for cardiac injury because it can be detected in the circulation within one hour when compared to the gold standard serum troponin (for cardiac injury) which can take up to 6 hours before detection. Despite the high sensitivity of myoglobin, it is less specific for cardiac origin as it can be released following skeletal muscle injury. The optimal clinical diagnostic cut-off for myoglobin in circulation is 70-200 ng/ml (Melanson et al., 2004).

1.6.2 Glial fibrillary acidic protein (GFAP)

Glial fibrillary acidic protein (GFAP) is a homopolymeric type III intermediate filament protein that is expressed in the central nervous system (CNS) by different cell types including astrocytes and ependymal cells (Lei et al., 2015) (**Figure 1.19B**). GFAP is a 55 KDa protein and plays important roles in cell migration and signalling in astrocytes and glial cells. Any injury to the brain and/or spinal cord leads to release of GFAP into the circulation as an indication of astroglial cell damage, hence its use as a biomarker for damage to the central nervous system. A value > 1.5 ng/ml of GFAP in the circulation is diagnostic of brain injury (Ren et al., 2016).

1.6.3 C-reactive protein (CRP)

CRP is known as an acute-phase protein and it is a family member of the pentraxin group of proteins. CRP consists of five identical protomers (23 KDa) which are non-covalently associated symmetrically around a central pore. CRP is secreted mainly by the liver in response to inflammatory conditions (Sproston and Ashworth, 2018) (**Figure 1.19C**). CRP is used clinically as a biomarker for acute inflammatory conditions with a cut-off value of 5 µg/mL for tissue damage, including trauma and infection (Ciubotaru et al., 2005).

1.6.4 Carcinoembryonic antigen (CEA)

Carcinoembryonic antigen (CEA) is a member of the CEACAM family of immunoglobulin superfamily genes (Hatakeyama et al., 2013). CEA has been extensively used as a diagnostic and prognostic biomarker primarily for colorectal cancer, although it is present in many other solid cancers (**Figure 1.19D**). CEA consists of an N-terminal sequence with three conserved repeat domains (178 amino acids each) and an anchored hydrophobic C-terminal domain (Bjerner et al., 2002). The cut-off value for CEA in serum is 5 ng/ml (Kim et al., 2009). To date there are several studies that have designed biosensors for the detection of the above mentioned biomarkers. The characteristic features of those biosensors are summarised in **Table 1.4**.

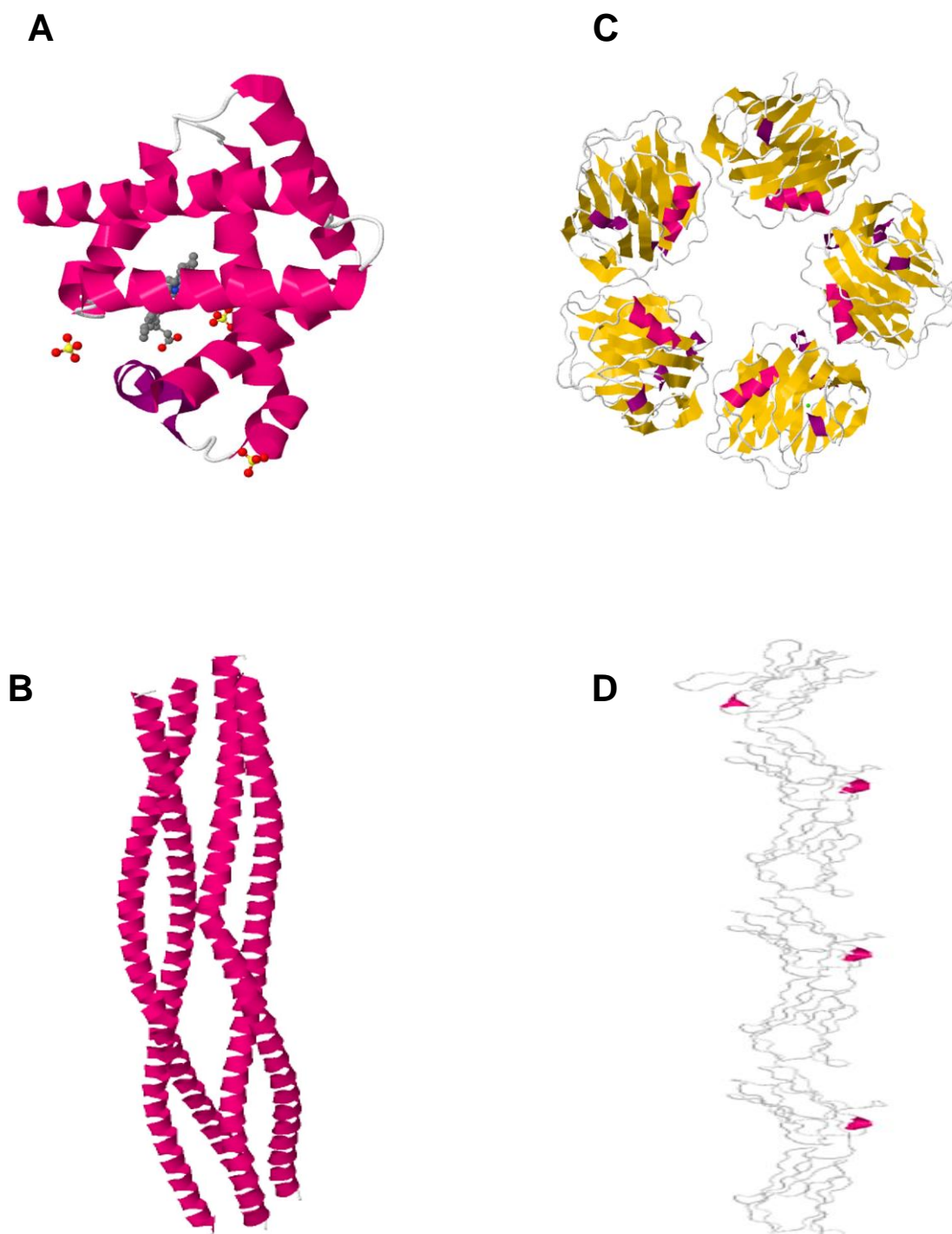


Figure 1.19 Molecular structure of biomarkers. A range of biomarkers have been used in this project to develop Eu^{3+} based optical biosensor. (A), protein biomarkers of cardiac injury (myoglobin, Pdb ID: 3RGK); (B), stroke (GFAP, Pdb ID: 6A9P); (C), inflammation (CRP, Pdb ID: 1GNH); (D), colorectal cancer (CEA, Pdb ID: 1E07).

Table 1.4 Biosensors developed for detection of the protein biomarkers myoglobin, GFAP, CRP and CEA.

Biosensor	Biomarker	Bioreceptor	Range of detection	Reference
Optical biosensors				
SPR	Myoglobin	Anti-myoglobin antibody	< 1 ng ml ⁻¹	(Liu et al., 2011)
SPR	CRP	Anti-CRP antibody	1–10 mg l ⁻¹	(CASA et al., 2006)
SPR	CRP	Aptamer	10 pM–100 nM	(Wu et al., 2016)
Electrochemical biosensors				
Impedimetric	Myoglobin	Anti-myoglobin antibody	100 ng ml ⁻¹	(Tweedie et al., 2006)
Impedimetric	CRP	Anti-CRP antibody	1.15x10 ⁻¹³ -1.15 ng ml ⁻¹	(Hennessey et al., 2009)
Impedimetric	GFAP	anti-GFAP antibody	1 pg ml ⁻¹ - 100 ng ml ⁻¹	(Arya et al., 2013)
Impedimetric	CEA	Anti-CEA antibody	1 ng ml ⁻¹	(Yeh et al., 2016)
Voltammetric	CEA	DNA Aptamer	1.5 pg ml ⁻¹	(Wen et al., 2016)
Mechanical biosensors				
QCM	CRP	Anti-CRP antibody	170–667 µg l ⁻¹	(Aizawa et al., 2001)

1.7 Hypothesis

The hypothesis for this study is that Eu^{3+} based optical biosensor using novel synthetic binding protein (the Affimer) would allow rapid detection and quantitation of a wide range of protein biomarkers in human serum.

1.8 Aims

- I. Express and purify anti- human myoglobin/ GFAP Affimers as bioreceptor for Affimer- based optical biosensor.
- II. Characterise Eu^{3+} -complex spectra including excitation and emission wavelengths.
- III. Modify anti- human myoglobin/ GFAP and control (anti- human fatty acid binding protein 3 (HFABP3)) Affimers with different chelators.
- IV. Assess the sensitivity of the optimised Eu^{3+} complex in human serum.
- V. Optimise the fluorescence measurements of the Eu^{3+} complex with different analytes using steady state and time-resolved fluorescence assay.

Chapter two: Materials and Methods

Chapter 2

Materials and Methods

2.1 Materials

2.1.1 Chemicals

Sodium chloride (NaCl), Isopropyl- β -D-thiogalactopyranoside (IPTG), Halt protease inhibitor cocktail, tris (2-carboxyethyl) phosphine (TCEP) disulphide reducing gel, Pierce ECL western blotting substrate and fluorescein isothiocyanate isomer (FITC) were purchased from ThermoFisher Scientific. Sodium phosphate (NaH_2PO_4), imidazole, biotin-maleimide, copper (II) sulfate pentahydrate, bicinchoninic acid, dimethyl sulfoxide (DMSO), sodium hydroxide (NaOH), D-glucose, glycine, ethylenediaminetetraacetic acid (EDTA) and magnesium sulfate (MgSO_4) were purchased from Sigma Aldrich. Glycerol, magnesium chloride (MgCl_2) and Tween-20 were purchased from Fisher Scientific. SYBRTM safe DNA gel stain, high sensitivity streptavidin-HRP and EZ-Link[®] NHS-SS-Biotin were purchased from Thermo Scientific. Nickel-nitrilotriacetic acid (Ni^{2+} -NTA) slurry was purchased from IBA Solutions for Life Sciences. 3,3',5,5'-tetramethylbenzidine (TMB) substrate was purchased from Seramun. 2-Log DNA ladder (100 bp /0.1-10 Kb) was purchased from New England BioLabs Inc.

2.1.2 Solvents and buffers

Casein blocking buffer (10X) and phosphate buffered saline solution (10X PBS) were obtained from Sigma-Aldrich. Methanol was purchased from Fisher Scientific. Tris-glycine SDS-PAGE (10X TGS) buffer was purchased from Bio-rad. 3- (N-morpholino) propanesulfonic acid (MOPS) was purchased from Sigma life science and tris were purchased from ThermoFisher Scientific.

2.1.3 Proteins

Glial fibrillary acidic protein (GFAP) was purchased from EnCor Biotechnology Inc. Anti-GFAP (mouse anti-human) monoclonal antibody was obtained from Proteintech, whilst Anti-GFAP (mouse anti-human) polyclonal antibody was purchased from Biomatic. Human myoglobin protein was purchased from EnCor Biotechnology Inc. Anti-human myoglobin (mouse anti-human) monoclonal antibody was purchased from Bio-Rad. Heart fatty acid binding protein (HFABP3) was purchased from Sino biological. Anti-HFABP3 (rabbit anti-human) polyclonal antibody was purchased from Aviva System Biology. C-reactive protein, bovine serum albumin (BSA) and horse myoglobin were purchased from Sigma Aldrich. CEA protein was purchased from 2B scientific. Anti- 6X His tag HRP was purchased from Abcam.

2.1.4 Affimer production, extraction and purification

The *pET11* (a) plasmids containing the coding sequence for anti-myoglobin, GFAP, CRP and CEA Affimers were obtained from the BioScreening Technology Group (BSTG), University of Leeds. BL21 Gold (DE3) *E.coli* cells and XL1-blue *E.coli* supercompetent cells were purchased from Agilent Technologies. *Nhe I*-HF, *Not I*-HF, Antarctic phosphatase, T4 DNA ligase and DpnI were supplied by New England BioLabs (NEB). Halt Protease Inhibitor Cocktail was purchased from Thermo Scientific. Lysozyme was purchased from Sigma. Benzonase nuclease was purchased from Novagen. Phusion DNA polymerase was purchased from ThermoFisher Scientific. NucleoSpin® gel and PCR clean-up kits were supplied by Macherey-Nigel. QIAprep Spin Miniprep kit was obtained from QIAGEN. Triton-X-100, Tryptone, yeast extract and agar were used to prepare super optimal broth (SOB), super optimal broth with catabolite repression (SOC), Luria-Burtani (LB) and 2YT media were purchased from Sigma-Aldrich. Details of media composition are listed in **Table 2.1**.

Table 2.1 Composition of bacterial growth media

Media	Composition (1 Litre)
Super optimal broth, SOB	20 g tryptone, 5 g yeast extract, 0.5 g NaCl , 1 M MgCl ₂ (10 ml), 1 M MgSO ₄ (10 ml)
Super optimal broth with catabolite repression, SOC	SOB media + 20% (w/v) glucose
Luria-Burtani, LB	10 g tryptone, 5 g yeast extract, 10 g NaCl
2YT	16 g tryptone, 10 g yeast extract, 5 g NaCl

2.1.5 Affimer characterisation

Mini-protean TGX 4-15% (w/v) precast polyacrylamide gels, 2-mercaptoethanol and 2X Laemmli sample buffer were purchased from Bio-rad. Quick Coomassie stain was obtained from Generon. Pur-A-Lyzer™ Midi dialysis kits were purchased from Sigma-Aldrich. Polyvinylidene difluoride (PVDF) membrane was obtained from GE Healthcare Life Sciences. 96 Maxisorp Nunc-immuno plates and Zeba spin desalting columns (7K MWCO) were purchased from ThermoFisher Scientific.

2.1.6 Affimer functionalisation

Europium (III) nitrate penta hydrate and pyromellitic dianhydride (PMDA) were purchased from Sigma-Aldrich. Maleimido-mono-amide-DOTA, DOTA-NHS-ester and p-SCN-Bn-DTPA were purchased from Macrocyclics™. Sephadex G-25 DNA grade desalting columns were purchased from GE Healthcare Life Sciences.

2.2 Methods

2.2.1 Affimer production

Affimers against GFAP and human myoglobin were selected and cloned by BSTG at University of Leeds. Also, phage display screening for human myoglobin binding Affimer was done by BSTG group. They kindly provided the plasmids for each of these Affimers for my PhD studies. Anti- CEA Affimer was purified by Dr. Shazana Shamsuddin and anti- CRP Affimer was obtained from Dr. Hope Adamson.

2.2.1.1 Subcloning of Affimer DNA from the phagemid vector (pBSTG125) into pET11 (a) plasmids

Polymerase chain reaction (PCR) amplification of the Affimer DNA sequences: Affimer- encoding DNA sequences from phage ELISA were amplified via PCR. A master mix reaction containing 5 µl Phusion HF Buffer (5x), 0.2 µl dNTP mix (25 mM), 0.75 µl of 3% (v/v) DMSO, 2 µl forward primer (5' – ATGGCTAGCAACTCCCTGGAAATCGAAG - 3'), 2 µl reverse primer pDHIS-C-rev (5' – TTACTAATGCGGCCGCACAAGCGTCACCA ACCGGTTTG – 3'), 0.25 µl of Phusion DNA polymerase and 1 µl of DNA template was prepared in a 0.2 ml PCR tube. The PCR tubes were transferred to the PCR machine and the thermocycling conditions were programmed as follows. Initial denaturation cycle at 98 °C for 30 s, followed by 30 cycles of amplification starting with denaturation cycle at 98 °C for 20 s, then annealing cycle at 54 °C for 20 s and ending with extension cycle at 72 °C for 20 s. Finally, a final extension cycle was run at 72 °C for 10 min. A Macherey-Nagel Nucleospin® gel and PCR cleanup kit were used

to purify the PCR products according to the manufacturer's instructions. The purified PCR products were eluted in 50 µl of sterile deionised water.

Digestion of the amplified Affimer DNA sequences using Nhe I and Not I restriction sites: A mixture reaction of CutSmart™ Buffer (10 µl), *Nhe I*-HF™ (167 units/ml) and *Not I*-HF™ (167 units/ml) were added to the 50 µl of purified PCR products and incubated overnight at 37 °C. Then, 0.5 µl of DpnI enzyme was added to remove *dam* methylated template DNA. The reactions were incubated at 37 °C for 1 h and then were purified using a Nucleospin® gel and PCR clean-up kit as the per manufacturer's instructions. A nanodrop lite spectrophotometer (Thermo Scientific) was used to measure the concentration of the Affimer-encoded DNA.

Digestion of the pET11 (a) vector with Nhe I and Not I restriction enzymes: A reaction of 5 µg of *pET11 (a)* plasmid, 20 µl of CutSmart™ buffer, 5 µl of *Nhe I* and 5 µl of *Not I* was prepared and incubated for 2h at 37 °C. Followed by adding of 20 µl of Antarctic phosphatase buffer (10X) and 1 µl of Antarctic phosphatase (5,000 units/ml) and incubation for 15 min at 37 °C. Then, inactivation of the Antarctic phosphatase was done by heating the reaction up to 65 °C for 5 min. After that, 20 µl of orange G loading (6X) dye was added to the digested vector and separated on 0.7 % (w/v) agarose gel electrophoresis. The gel was run at 90 V for 70 min. NucleoSpin® gel and PCR clean-up kit were used to extract the digested *pET11 (a)* plasmid from the gel according to the manufacturer's instructions. A nanodrop spectrometer was used to measure the concentration of digested *pET11 (a)* plasmid. The digested products were stored at -20 °C for the next ligation process.

Ligation of the digested Affimer DNA sequences into the digested pET11

(a) *vector*: A mixture reaction of 30 fmol of digested *pET11 (a)* plasmid, 90 fmol of digested Affimer DNA sequence insert, 2 μ l T4 DNA ligase buffer (10X) and 1 μ l T4 DNA ligase (20,000 units/ml) was prepared. The mixture was incubated at 16 °C overnight prior to transformation of the ligation products into *E.coli* cells. The schematic of subcloning Affimer-encoding PCR fragments into *pET11 (a)* vector is shown in **Figure 2.1**.

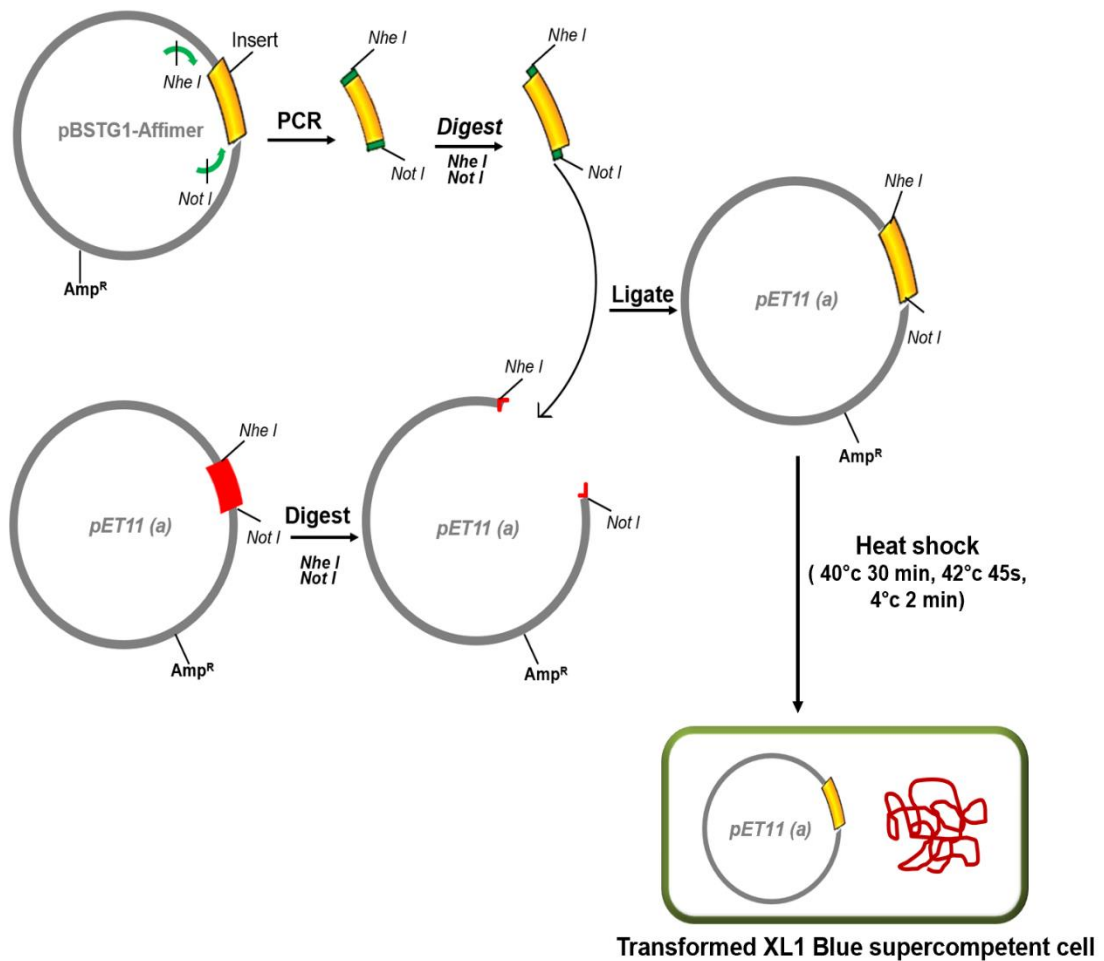


Figure 2.1 A schematic representation of incorporating Affimer -encoding sequence into *pET11 (a)* expression vector. Both *pET11 (a)* vector and PCR amplified fragment were digested with *Nhe I* and *Not I* restriction enzymes. The ligation between the vector and the Affimer fragment was carried out using T7 ligase. The subcloned vector was transformed into an XL1 Blue super competent *E.coli* cell via heat-shock process.

2.2.1.2 Minipreps and transformation of ligation mixture into XL1-Blue super competent cells

In order to multiply the sub-cloned plasmid DNA, 10 μ l of XL1-Blue super competent cells were mixed with 1 μ l of the *pET11* (a) vector containing Affimer-encoding sequences in a 1.5 ml microcentrifuge tube and incubated on ice for 30 min. Heat and shock protocol was applied for 45 seconds in a 42 °C water bath, followed by 2 min incubation on ice (Binnemans, 2015). SOB medium (180 μ l) was added to the above mixture and incubated at 37 °C for 1 hr with shaking at 230 rpm. The transformation mixture was then inoculated onto the LB carbenicillin plates with a total volume of 100 μ l and incubated at 37 °C overnight. A single colony of the overnight bacterial culture was inoculated into 5 ml of LB carbenicillin broth and incubated at 37 °C, 230 rpm overnight. QIAprep ® Spin Miniprep Kit (50) was used to purify the plasmid DNA using a mixture of buffers provided within the kit. The characteristic features of these buffers are shown in the **Table 2.2**. A nanodrop spectrophotometer was used to measure the concentration of the purified DNA plasmids.

Table 2.2 Miniprep kit buffer compositions.

Buffer	Contents
P1 (Alkaline lysis buffers)	50 mM Tris hydrochloride (Tris-HCl) (pH 8.0), 10 mM EDTA and 100 µg/ml RNaseA
P2 (Alkaline lysis buffers)	200 mM Sodium hydroxide (NaOH) and 1 % Sodium dodecyl sulfate (SDS)
N3 (Neutralization buffer)	4.2 M guanidinium hydrochloride (Gu-HCl) and 0.9 M potassium acetate (pH 4.8)
PB (Wash/binding buffer)	5 M Gu-HCl, 30 % and isopropanol
PE (Wash buffer)	10 mM Tris-HCl (pH 7.5) and 80 % (v/v) ethanol
EB (Elution buffer)	10 mM Tris chloride (Tris-Cl) (pH 8.5)

2.2.1.3 DNA Sequencing

The samples were collected and prepared at 100 µg/ml in PBS solution within 1.5 mL microcentrifuge tubes. DNA sequencing was performed by GENEWIZ UK, LTD, UK. DNA sequencing data were provided by the company in PDF format. Expasy Translate Tools were used through an online portal to translate the sequencing data into amino acid sequence.

2.2.1.4 Affimer expression

The optimised plasmid from the previously described experiments was used to express and purify the targeted Affimer. The *pET11 (a)* vector containing the Affimer coding sequence was transformed into BL21 Star™ (DE3) *E.coli* using a heat shock protocol. SOC medium at volume 180 µl was added to the transformed cells and incubated for 1 h at 37 °C, while shaking at 230 rpm. The transformed cells were then plated on LB agar supplemented with 100 µg/ml carbenicillin and allowed to grow at 37 °C with 230 rpm shaking overnight. Cells, from a randomly picked single colony, were grown into 3 ml of 2YT medium with 100 µg/ml carbenicillin and 1% (w/v) glucose overnight at 37 °C, 230 rpm. The overnight culture (1 ml) was added into 50 ml of pre-warmed LB media supplemented with 100 µl of 50 mg/ml carbenicillin and incubated for 2.5 to 3 h at 37 °C, 230 rpm until the OD₆₀₀ of the culture reached 0.8. The outgrown cultures in LB medium were induced with 0.1 mM IPTG and incubated at 25 °C for 16-18 h at 150 rpm. Cells were then harvested by centrifugation for 15 minutes at 3,220 xg. The supernatant was discarded and the cell pellets were stored at -20 °C prior to protein extraction and purification.

2.2.1.5 Affimer extraction and purification

Cell pellets were lysed in a mixture of 0.4 μ l benzonase nuclease (10 units/ml), 10 μ l Halt Protease Inhibitor Cocktail, 10 μ l Triton-X-100, 10 μ l lysozyme (10 mg/ml) and 969.6 μ l of lysis buffer (300 mM NaCl, 50 mM NaH₂PO₄, 30 mM imidazole, 10 % (v/v) glycerol, pH 7.4). The mixture was incubated for 40 min at room temperature on a rotator (Stuart SB2) and then centrifuged for 15 min at 14,000 xg to separate the soluble proteins from insoluble components and cell debris.

Chelated nickel affinity chromatography was used to purify the Affimer as follows; 300 μ l of Ni²⁺-NTA resin slurry was washed with 1 ml lysis buffer and centrifuged for 1 min at 1,000 xg to remove the buffer (supernatant). Ni²⁺-NTA slurry was mixed with the soluble Affimer (supernatant) and incubated on a rotator for 2 h at room temperature. After 2 h incubation, the mixture were centrifuged at 1,000 xg for 1 min to sediment the resin- bounded Affimer. The resin was resuspended in 1 ml wash buffer (500 mM NaCl, 50 mM NaH₂PO₄ and 20 mM imidazole at pH 7.4) and moved to a 2 ml polystyrene equilibrated column (ThermoFisher Scientific); followed by 3 washes using washing buffer to remove any unbound protein then eluted in 500 μ l of elution buffer (500 mM NaCl, 50 mM NaH₂PO₄, 300 mM imidazole and 20 % (v/v) glycerol at pH 7.4). A nanodrop spectrophotometer was used to measure the concentration of the purified Affimer.

2.2.1.6 Sodium dodecyl sulphate polyacrylamide gel electrophoresis (SDS-PAGE)

Size analysis of the purified protein was performed using SDS-PAGE. Equal volume of protein samples (10 μ l) were mixed with 10 μ l of 2X Laemmli sample buffer (95 % v/v) and 2-mercaptoethanol (5 % v/v) and heated immediately at 95 °C for 10 min. Protein markers (Spectra™ multicolour protein ladder, ThermoFisher Scientific) were used as a molecular weight standards. After running electrophoresis at 100 V for 65 min, SDS Mini-protean TGX gels were stained with Coomassie stain for 1h followed by washing overnight with deionized water to destain the gels. Images were captured using a Syngene G-box imager.

2.2.1.7 Affimer dialysis

A Pur-A-Lyzer™ Midi 6000 dialysis kit was equilibrated in PBS buffer then filled with 500 μ l of the eluted Affimer. The tube was placed into the floating rack in a stirred beaker containing a large volume of the dialysis buffer PBS, pH 7.4). The dialysis buffer was changed every hour for three times. Then the sample was pipetted carefully from the Pur-A-Lyzer tube to a clean Eppendorf tube and stored at -20 °C for further use.

2.2.2 Affimer characterisation

2.2.2.1 Analyte Biotinylation

EZ-Link® NHS-SS-Biotin (5 mg/ml) solution was prepared in DMSO, then 0.8 µl were mixed with 14 and 45 of 1 mg/ml of myoglobin or GFAP in a total volume of 100 µl PBS respectively. The reaction solutions were incubated for 1 h at room temperature. The mixtures were desalted to remove any remaining biotin using Zeba Spin desalting columns. The biotinylated analytes were mixed with an equal volume (100 µl) of 80 % (v/v) glycerol.

2.2.2.2 Enzyme-linked immunosorbent assay (ELISA) to confirm analyte biotinylation

Nunc-Immuno™ MaxiSorp™ strips were coated with 50 µl of PBS per well overnight then added 1, 0.1 and 0.01 µl of biotinylated analyte. The plate was incubated at 4 °C overnight then washed 3 times with 300 µl per well of phosphate-buffered saline/tween (PBST) using a Tecan Hydroflex plate washer. Blocking buffer (300 µl) at 2X concentration was added to the wells and incubated at 37 °C for 3 h. Blocking buffer was removed by tapping the strip on tissue paper. Diluted high sensitivity streptavidin-HRP (1:1000 in 10x blocking buffer) was added at 50 µl per well then incubated for 1 h at room temperature on a vibrating platform shaker (Heidolph vibramax 100; speed setting 3). Six washes with 300 µl per well of PBST was performed using the plate washer (**Figure 2.2**). TMB stock solution at volume 50 µl was added to each well for 2 min until the blue colour developed. The absorbance was measured at 620 nm using a Varioscan Flash plate reader.

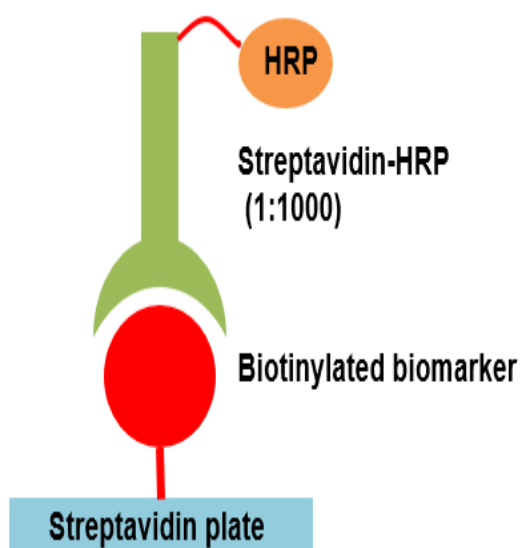


Figure 2.2 A schematic showing ELISA platform for biotinylated biomarker. The biotinylated biomarker is used as a primary reagent immobilised on the plate and streptavidin- HRP conjugate as detection reagent.

2.2.2.3 Enzyme-linked sandwich ELISA for Affimer selective binding

Casein blocking buffer (2X) in PBST (200 μ l) was added to streptavidin-coated 96 well plate and incubated over night at 37 $^{\circ}$ C followed by one wash using 300 μ l PBST. The diluted biotinylated analytes as 1mg/ml stocks diluted 1:1000 in 2X blocking buffer in volume 50 μ l aliquots were added into each well and incubated at room temperature for 1 h on a plate shaker at 450 rpm. Ten μ l of 10X blocking buffer was added into each well followed by 40 μ l of Affimer at 100 μ g/ml and incubated at room temperature for one h on a plate shaker (450 rpm). Three washes with 300 μ l per well of PBST were performed using plate washer. Fifty μ l of diluted anti-his₆ tag HRP conjugate at 1:1000 in 2x blocking buffer, was added to each well and incubated at room temperature for one hour on a plate shaker at 450 rpm, followed by 3 washes in PBST (**Figure 2.3**). TMB

stock solution (50 μ l) was added to each well for 2 min until the blue colour developed. The absorbance was measured at 620 nm using Varioscan Flash plate reader.

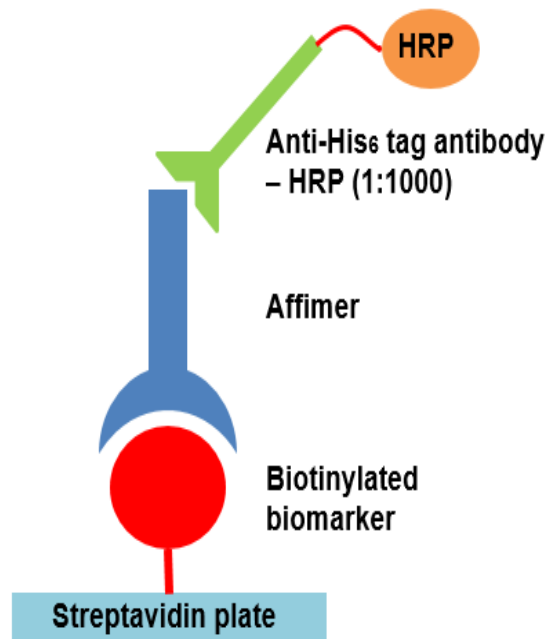


Figure 2.3 A schematic showing ELISA platform to check the selective binding of the Affimer and their targets biomarker. The biotinylated biomarker is immobilised on a Strept Avidin- coated plate. Affimer is used as primary detection agent, followed by diluted anti- His₆ – HRP at 1:1000 dilution in PBS, acting as secondary antibody and detection agent.

2.2.2.4 Pull-down assay

All selected Affimers were dialysed in PBS before pull-down assay as mentioned in section 2.1.7. Sixty μ l of Ni²⁺NTA resin was washed three times with washing PBS buffer and then resuspended in 30 μ l of washing buffer. Affimer (20 μ g) was added to the washed resin and incubated on rotator for 90 min at 4

°C. The Affimer loaded resin was centrifuged at 1000 xg for 1 min to remove unbound Affimer followed by a single wash in washing buffer. Similarly, 50 µg of the analyte protein was added to loaded resin and incubated overnight at 4 °C then centrifuged at 1000 xg for 1 min to remove the unbound analyte. The resin was washed three times using washing buffer and then was resuspended in 30 µl of washing buffer. SDS-PAGE was run with all fractions collected from the pull down including unbound Affimer, washed Affimer, unbound analyte, washes to remove free analyte. Ten µl of each fraction was mixed with 10 µl of reducing dye and heated for 10 min at 95 °C. 10 µl of the supernatants were loaded into the precast gel (4-15 % (w/v)) along with 5 µl of protein ladder. The gel was then run at 100 V for 75 min with tris-glycine running buffer and developed using quick Coomassie stain dye for 1 h at room temperature. Images were captured using a Syngene G-Box.

2.2.2.5 Western blotting

The pull-down products were separated by SDS-PAGE (**section 2.1.6**). Purified Affimer and analyte were used as positive controls. To start with, PVDF membranes were incubated in methanol for 1 min and then equilibrated in transfer buffer (20 % (v/v) methanol, 190 mM glycine, 25 mM Tris, pH 8.3) for 15 min. SDS gel containing protein samples were placed carefully in a transfer cassette as follows (black side down): sponge, double layer of filter paper, SDS gel, PVDF membrane, double layer of filter paper and sponge. The cassettes were tightly closed and placed into the electrophoresis tank. Transfer buffer was added to the cassettes and subjected to 115 V for 75 min. An ice block was used to keep the temperature steady through the transfer. Then the membranes were blocked using 5 % (w/v) milk in PBST at room temp for 1 h. Respective primary

antibodies were diluted 1:10,000 in 2 % (w/v) BSA in PBST. The first membrane was incubated with the primary antibody for 2 h at room temp on a shaker and followed by four changes of PBST wash buffer. HRP-substrate diluted 1:1000 in PBST was added to the membrane and incubated for 1 h at room temp on a rotator. The membrane was then rinsed with PBST and a Syngene G-Box system was used for imaging. A second membrane was incubated with anti-His tag₆ HRP diluted 1:1000 in 2 % (w/v) BSA in PBST for 1 h at room temp, followed by 4 washes in PBST and 3 washes in PBS. The blot were developed by adding Pierce ECL western blotting substrate solution and images captured on a Syngene G-box system.

2.2.2.6 Surface Plasmon Resonance (SPR)

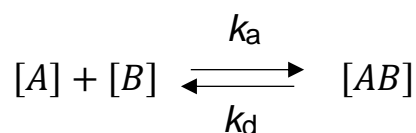
Kinetic binding analysis on the Affimers was carried out using BIAcore 3000 instrument (GE Healthcare, Sweden), amine sensor chip and 0.1 M sodium acetate buffer as running buffer for the experiment. The temperature of the instrument was set at 25 °C. Affimers and analyte were diluted into the running buffer before use to eliminate buffer mismatch. First, the dextran matrix on the amine sensor chip surface was activated by treatment with 100 µl of both 1-ethyl-3-(3-dimethylaminopropyl) carbodiimide (EDC) plus N-hydroxysuccinimide (NHS) to provide reactive succinimide esters. Then 5 µl/ml of the analyte was passed over the sensor surface at a flow rate of 5 µl/min on flow cell 2-4 until the surface density reached ~200 response units (RU). Flow cell 1 was used as a reference. Then, ethanolamine (35 µl over 7 min) was added to the sensor surface to deactivate free active esters. Before injection of Affimer, 0.1 M acetate buffer was flowed over to equilibrate the cell surface. Kinetic binding data was

collected by injecting 20 μl of the Affimer at the concentration of 0-100 nM into flow cell with a flow rate of 5 $\mu\text{l}/\text{min}$ for 15 min, followed by regeneration of the surface by using 0.1 M Na_2CO_3 at a flow rate of 35 $\mu\text{l}/\text{min}$ after each cycle of association and dissociation.

2.2.2.7 SPR data analysis

Label free optical biosensor based- SPR was used to investigate the affinity of biomolecular interaction in real time. The data provided by SPR are based on changes in refractive index near the sensor surface resulting from ligand- analyte interaction. These changes are measured during the association and dissociation phases of the binding proteins in real time and plotted as resonance units (RUs) versus time.

The binding kinetics of analyte (Affimer) to its target (ligand) were calculated using simple 1:1 binding interaction model as shown in **Equation 2.1** below:



Equation 2.1 Binding interaction model

Where,

[A] is the ligand (target) concentration (M),

[B] is the analyte (Affimer) concentration (M),

[AB] is the analyte- ligand complex concentration (M),

k_a is the association rate constant ($\text{M}^{-1} \text{s}^{-1}$), whereas

k_d is the dissociation rate constant (s^{-1})

Equation 2.2 was used in order to determine the binding kinetics parameters association (k_a), and dissociation (k_d) rate constants as shown below.

$$\frac{d[A]}{dt} = 0$$

$$\frac{d[B]}{dt} = -k_a [A][B] + k_d [AB]$$

$$\frac{d[AB]}{dt} = k_a [A][B] + k_d [AB]$$

$$R = [AB] + RI$$

Equation 2.2 Numerical integration

Where,

[A] is the immobilised ligand (constant during the association phase),

[B] is the injected Affimer on the surface (M),

[AB] is the ligand- analyte complex (M),

R is the SPR response (RU),

RI is the refractive index response (RU).

The equilibrium dissociation constant (k_D) indicates the steady-state affinity of the ligand for its target analyte. k_D represents the concentration of analyte that occupies 50 % of the ligand binding sites. Thus, the higher the k_D is, the weaker the binding between ligand and analyte is. The equilibrium dissociation constant (k_D) can be calculated using **Equation 2.3**.

$$k_D = k_a / k_d$$

Equation 2.3 Equilibrium dissociation constant

Where,

k_D is the equilibrium dissociation constant (M),

k_a is the association rate constant ($M^{-1} s^{-1}$),

k_d is the dissociation rate constant (s^{-1}).

2.2.3 Affimer functionalisation

2.2.3.1 Conjugation of Affimer with four different chelators: PMDA, maleimido-mono-amide-DOTA, DOTA-NHS-ester and p-SCN-Bn-DTPA

Chelator at 1 M was dissolved in 1 ml of DMSO and then diluted to a final concentration of 100 mM in DMSO. Then, 100 μ l of 100 mM chelator was mixed with 1 ml of Affimer (1 mg/ml) and incubated for 2 h at room temp. A sephadex G-25 DNA grade desalting column was used to desalt the mixture according to the manufacturer's instructions. The products were collected into Eppendorf tubes and stored at -20 °C for further use. A standard curve using 15 mM to 1.5 μ M of BSA protein was used to produce a calibration curve in a bovine serum albumin assay (**Section 2.2.3.3**) was developed and the curve was used to calculate the final concentration of the modified Affimer.

2.2.3.2 Bicinchoninic acid solution (BCA) protein assay

Bicinchoninic acid solution (BCA, 98 % v/v) was mixed with 2 % (v/v) copper (II) sulphate solution until the mixture colour turned bright green. The mixture solution was added into 96-well plate at 200 μ L/ well. A BSA concentration ladder was established (1mg/ml to 0.1 mg/ml) in PBS buffer, then 25 μ L of each was added into each well followed by another 25 μ L of the sample. The 96-well plate was incubated at 37 °C for 30 minutes. The absorbance was measured at 562 nm using a plate reader (BMG labtech).

2.2.3.3 Fluorescein isothiocyanate (FITC) assay for free amine groups

Fluorescein isothiocyanate stock solution at 1mM was prepared and diluted to 0.1 mM in 1 ml DMSO. The solution was wrapped in aluminium foil for protection from light. Then, 10 μ l of 0.1 mM solution was mixed with 100 μ l of Affimer (unmodified) and another 10 μ l with Affimer modified by chelator and incubated for 8 h at 4 °C in a dark room. A Sephadex G-25 DNA grade desalting column was used to remove any unbound FITC. The desalted samples were added into 96-well plate at 150 μ l. Absorbance was measured at 498 nm wavelengths using plate reader (BMG labtech).

2.2.3.4 Chelating Eu^{3+} with the modified Affimer

Europium (III) nitrate penta hydrate ($\text{Eu}(\text{NO}_3)_3 \cdot 5\text{H}_2\text{O}$) was prepared in PBS at 100 μ M. Then, 1 ml of the solution was mixed with 1 μ M of functionalised Affimer. The mixture was vortexed followed by immediate measurement of emission using QEPro high performance spectrometer (Ocean Optics) at 395 nm excitation wavelength.

2.2.3.5 Emission fluorescence measurement

Fluorescence emission spectra at room temperature with different concentrations of analyte were measured and recorded using a QEPro spectrometer as shown in **Figure 2.4**. A class 3B laser diode with fluorescence excitation at 395 ± 5 nm (395LM-120-FC-1V 080114416, KVANT) was used. The current power was run at 100 mA. The diameter of the laser spot was 0.5 mm. A laser power-meter (M200 with S302C head, Thorlabs) was used to set the wavelength to 395 nm. Also, a digital thermometer (Hanna) was used to measure

the surrounding temperature and ensure minimal variability of temp. The fluorescence emission spectral data were recorded by the QEPro using Ocean optics software through a USB spectrometer (Ocean Optics) connected to the laptop. Prior to measurement, the dark background current of the laser was subtracted and all measurements were made for 120 s for each sample (30 measurements/ 120 s). A specific interference filter (FEL0500, Thorlabs) was placed in the laser system to cut off the auto fluorescence at wavelength < 500 nm. To ensure excellent optical transmission properties, a 2 mL quartz fluorescence cuvette (QG High precision cell, Hellma analytics) was used. Data were exported into GraphPad Prism 7 for analysis and standard curve production.

2.2.3.6 Lifetime measurement

Life time measurements for the chelated Eu^{3+} (100 μM) by PMDA modified anti- human myoglobin Affimer complex at volume of 1 ml were performed using a fluorescence spectrophotometer (FS920; Edinburgh Instruments, UK) equipped with a laser diode 395 nm excitation source. The time range of the laser source was 4 ms with a pulse width of 500 μs . All measurements were repeated 2000 times and the average was taken every 1 ms. Life time measurements were done at room temp.

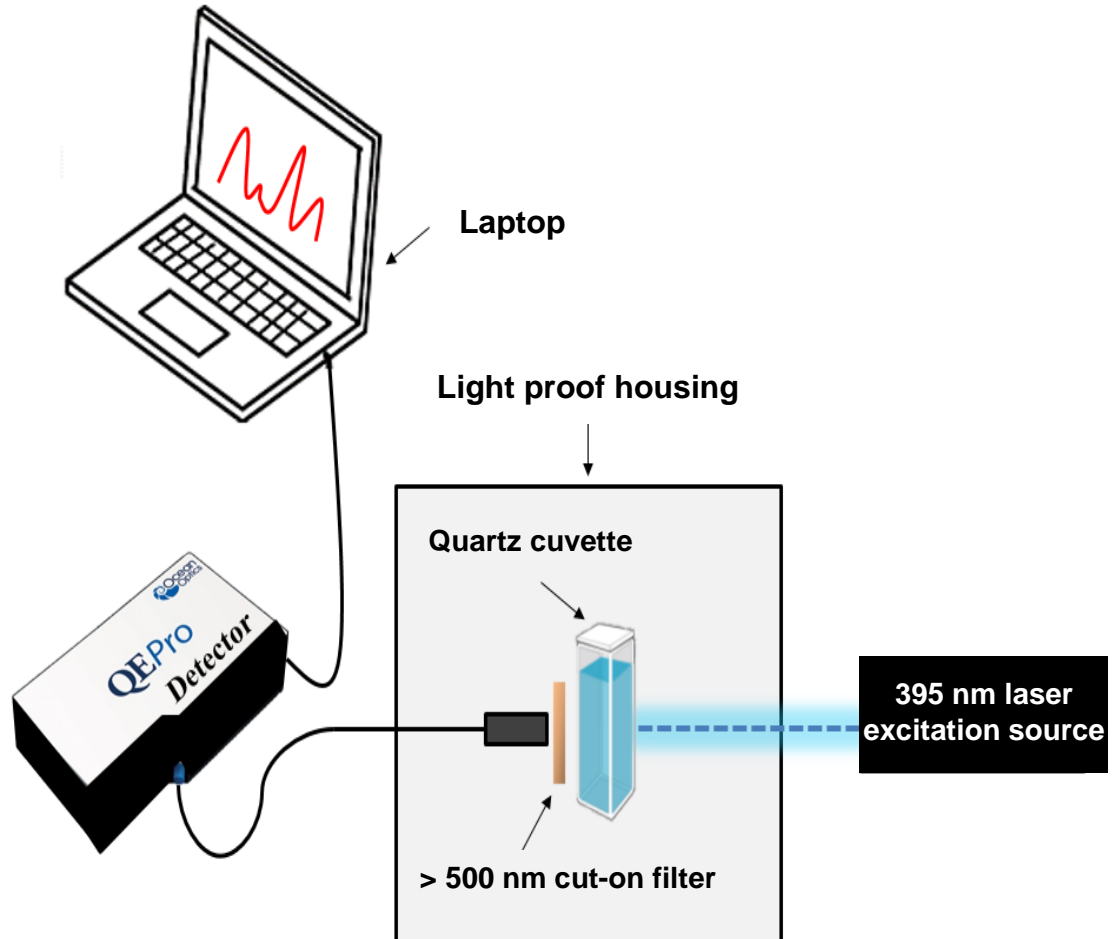


Figure 2.4 Schematic showing the fluorescence spectroscopy measurements set up.

2.2.3.7 Time-resolved fluorescence of Eu^{3+} complex chelated by Affimer modified with PMDA (Affimer assay)

Eu^{3+} was prepared in PBS at a concentration of 110 μM , then 180 μl of the prepared solution was added into each well of a glass 96 well- plate (Zinsser Analytic). The analyte (20 μl of 1 μM) was added to the first well and followed by serial dilution range from 100 fM to 100 nM. Modified Affimer was added at a concentration of 1 μM per well and incubated for 5 min at room temp; followed by measurement of emission using Fluostar Optima microplate reader.

2.2.3.8 Time-resolved fluorescence of Eu^{3+} complex chelated by Affimer modified with PMDA and antibody (Sandwich assay)

After preparing Affimer assay as mentioned in **Section 2.2.3.7**, sandwich assays were conducted using monoclonal and polyclonal antibodies (**Figure 2.5**). Antibody at concentration of 100 nM was added to each well (containing Eu^{3+} chelated by modified Affimer with PMDA and its target analyte complex) and incubated for 5 min at room temp; followed by measurement of emission using Fluostar Optima microplate reader.

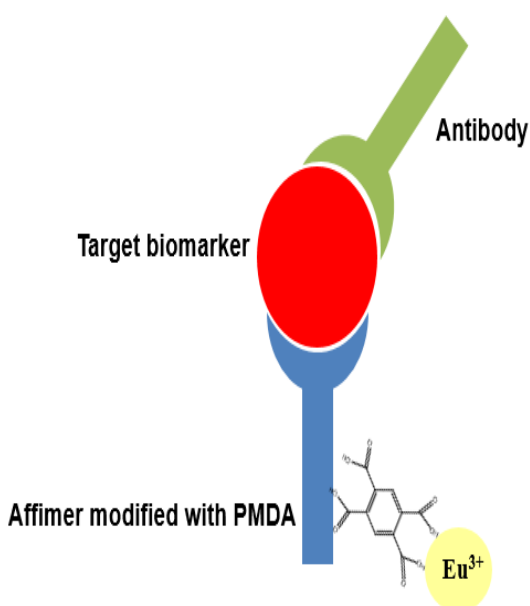


Figure 2.5 Schematic of the sandwich Eu^{3+} complex platform. The target biomarker is sandwiched between Eu^{3+} chelated by PMDA modified Affimer complex and antibody on the other side.

2.2.3.9 Time-resolved fluorescence of Eu^{3+} complex chelated by Affimer modified with PMDA and chelating agents (EDTA and trisodium citrate)

EDTA and $\text{Na}_3\text{C}_6\text{H}_5\text{O}_7$ stock solution were prepared in PBS at 100 μM . After preparing the sandwich assay, EDTA and $\text{Na}_3\text{C}_6\text{H}_5\text{O}_7$ were diluted to a final concentration of 10 μM and 1 μM , respectively into each well (containing Eu^{3+} chelated by Affimer modified with PMDA and its target analyte- antibody complex). Immediate measurement of emission was performed using a Fluostar Optima.

2.2.3.10 Fluorimetric plate reader measurement and data analysis

A Fluostar Optima plate reader was used to detect the intensity of the Eu^{3+} complex time-resolved fluorescence. The plate reader was integrated with a 395 nm excitation laser source, (KVANT). A specific filter was used to block undesired wavelengths with range of 520- 640 nm emission. BMG optima Windows™ based software was used to read the signals from the 96- well plates in time-resolved fluorescence measurement mode. The software allows control of different parameters as shown in the **Table 2.3**. Real time data was observed and recorded.

Table 2.3 Optima control settings

Sample	Plate mode settings	Optical settings
No. of replicate: 3	No. of cycles: 8	Excitation: 395 nm
Replicate reads/ well: 8	No. of flashes per well: 200 (maximum)	Emission: 520- 640 nm Gain: 2000 (maximum) Integration start: 20 μ s Integration time: 50 μ s

2.2.3.11 Isothermal titration calorimetry (ITC) assay of Eu^{3+} solution binding to PMDA modified Affimer

The ITC measurements were carried out using a MicroCal iTC200 calorimeter (GE Healthcare) at 25°C. All solutions including proteins and Eu^{3+} complex were prepared in 1 mM PBS buffer at pH 7.4. Each ITC titration consisted of 19 injections, the first injection volume was 0.5 μL and following injections were of 2 μL with 120 s intervals and constant stirring at 350 rpm. The titrations were performed by adding 20 injections of 2 μL of 300 μM Eu^{3+} solution into calorimeter sample cell containing 500 μL of 3 μM modified Affimer with PMDA, whereas the reference cell was loaded with PBS buffer. The resultant ITC data were analysed using Origin 8.0 software. The parameters of the association constant (K_a), the stoichiometry (n), and the changes in the enthalpy and entropy (ΔH and ΔS) during the reaction were determined. The Gibbs free energy (ΔG) was calculated using **Equation 2.4**.

$$\Delta G = \Delta H - T \Delta S$$

Equation 2.4 Gibbs free energy

Where,

ΔG is the Gibbs free energy (cal/mol),

ΔH is the changes in the enthalpy (cal/mol),

T is the Temperature (298 K)

ΔS is the changes in the entropy (cal/mol K).

**Chapter three:
Affimer production and
characterisation**

Chapter 3

Affimer production and characterisation

3.1 Introduction

Two types of vectors were used in the project to produce the Affimer proteins, *pBSTG1* phagemid and *pET11 (a)* vectors. The *pBSTG1* phagemid vector contains the coding region for Affimer clone (**Figure 3.1A**). It consists of a *pBR322* origin of replication and unique restriction sites (*Nhe I* and *Not I*) for sub-cloning of the inserted DNA. The plasmid also contains antibiotic resistant genes (*Amp^R*) to allow the selective culture. In addition, the plasmid possesses the *DsbA* gene which codes for a periplasmic disulphide bond oxidoreductase signal sequence to export the *E. coli* expressed protein to the periplasmic space of the bacterial cell. A C-terminal fusion of a truncated pIII coat gene to allow the expression of pIII coat fusion protein and His₆ tag coding gene at the C-terminus before the TAG amber stop codon gene of the Affimer for Affimer purification.

The *pET11 (a)* expression vector was used to express Affimer protein inside the *E. coli* cell (**Figure 3.1B**). It comprises a *pBR322* origin of replication, *Nhe I* and *Not I* restriction site, ampicillin resistant gene, *Lac I* repressor coding sequence and T7 promoter and terminator site for the transcription and translation of the Affimer gene. The expression of genes coding for Affimer proteins are inhibited by the binding of the *lac* repressor to the *Lac* operator involved in the vector. In order to induce expression of the Affimer, IPTG is used to inactivate the repressor at the bacterial exponential growth phase. In the present study, anti- GFAP or anti- human myoglobin Affimers were screened

through a phage display library of 1.3×10^{10} clones by the BioScreening Technology Group (BSTG). All phagemid plasmids containing anti- GFAP or anti-human myoglobin Affimer were obtained from BSTG.

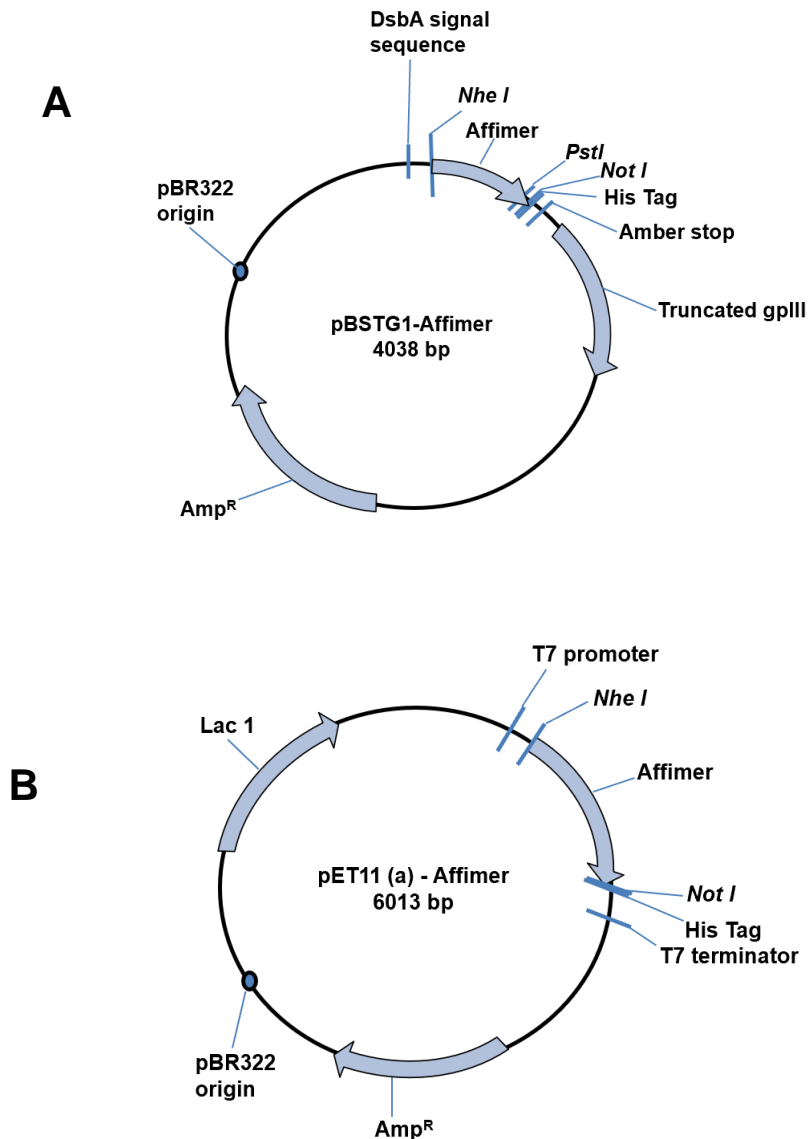


Figure 3.1 Schematic representation of pBSTG1 phagemid and pET11 (a) vector. (A), *PBSTG1* cloning vector consist of pBR322 origin of replication, a DsbA signal sequence, Affimer coding sequence flanked by *Nhe I* and *Not I* restriction sites, 6x histidine residue region, Amber stop codon, truncated pIII gene and ampicillin resistance gene. (B), *pET11 (a)* expression vector is comprises of the same origin of replication pBR322 and ampicillin resistance gene, T7 promoter and terminator flanking the coding sequence of the Affimer and *Nhe I* and *Not I* restriction sites.

3.2 Aims

The aims for this chapter were to:

- I. Express and purify anti- GFAP or anti- human myoglobin Affimers as bioreceptor for Affimer- based optical biosensors.

- II. Assess the selectivity and the affinity of the selected anti- GFAP or anti- human myoglobin Affimers to their target analytes by using biochemical and biophysical techniques including: ELISA, immunoprecipitation pull down assays and SPR.

Table 3.1 Sequence of variable loops of anti- human myoglobin Affimers.

Affimer	Variable region 1	Variable region 2	pI
<i>Human myoglobin 1</i>	YGDW K NPVE	VFPIIQMFW	6.75
<i>Human myoglobin 2</i>	HTMPD K WTN	DVPWFEMFW	6.54
<i>Human myoglobin 3</i>	MWHDLM L M K	K PALDMWFE	6.79
<i>Human myoglobin 4</i>	VHFQAWQFV	YIMQSETLS	7.94
<i>Human myoglobin 5</i>	QSSGHYFYS	T K NVII F R K	7.95
<i>Human myoglobin 6</i>	TSSHPQEWA	AYVWLSLEQ	6.79

Affimers anti- human myoglobin 1 to anti- human myoglobin 6 were selected for further study; pI is reported for each Affimer. The presence of lysine within the binding loops is highlighted; (**K**)

3.3.2 Subcloning of anti- human myoglobin Affimer DNA

Subcloning of Affimer DNA from the phagemid vector (pBSTG125) into pET11 (a) vector: In order to increase the expression of the anti- human myoglobin Affimer, the coding sequences were subcloned into the *pET11 (a)* vector according to the BSTG group's started protocol (**Chapter 2, Section 2.2.1.1**). The plasmids containing anti- human myoglobin Affimer were amplified, purified and stored following the mini-prep protocol. The final volume of the purified plasmid for each Affimer was 50 μ l. The expression across all binders was satisfactory with good yield of plasmids.

The same volume of six plasmids were loaded onto a 0.7 % (w/v) agarose gel to investigate their degree of purity. **Figure 3.3** shows that two distinct bands of DNA (linearized ~ 6 kb and supercoiled ~ 3 kb) were observed across all the anti- human myoglobin Affimer clones. These observations are in keeping with the features of undigested plasmid DNA.

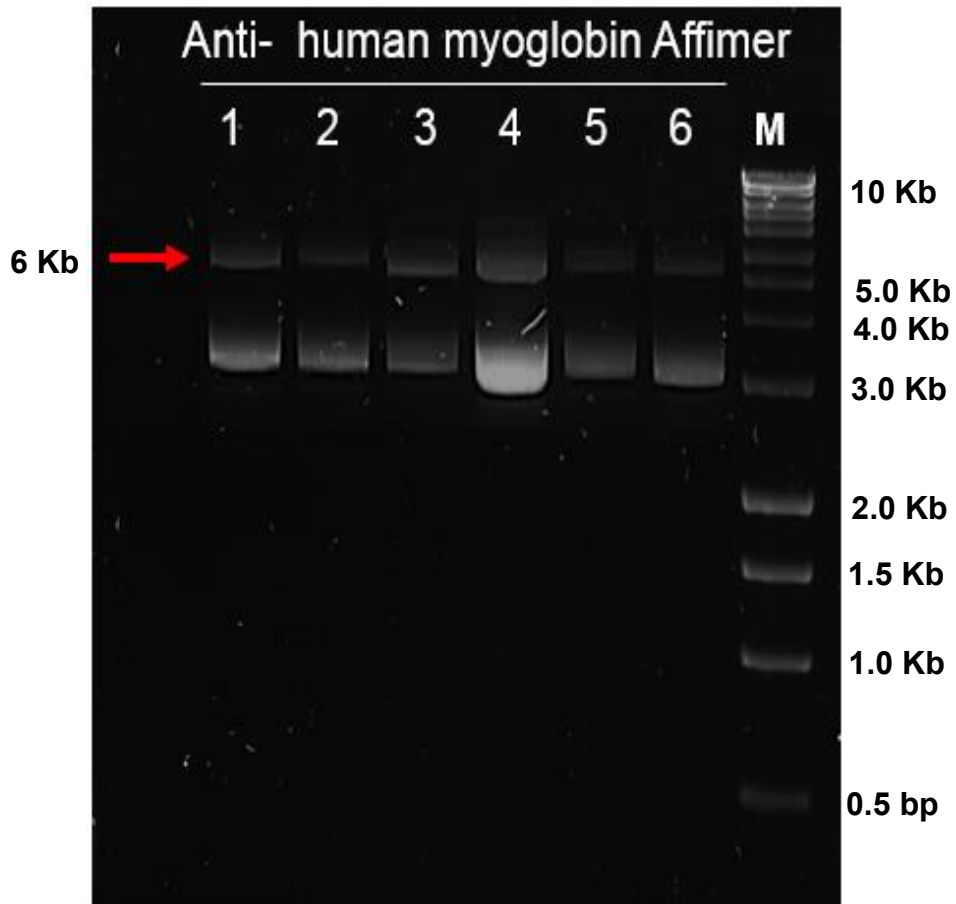


Figure 3.3 Gel electrophoresis of purified anti- human myoglobin Affimer DNA in phagemid vector. The phagemids were separated by 0.7 % (w/v) agarose gel in TAE buffer and stained with SYBR™ Safe. (M), a 2-log DNA ladder is used as a marker. Lanes 1- 6 indicate: anti- human myoglobin Affimers 1- 6.

PCR amplification of the Affimer DNA sequences: PCR was used to amplify the anti- human myoglobin Affimer encoding DNA sequence. During the PCR, a cysteine codon, *Not I* restriction site and histidine tag residue were incorporated into the reverse primer at the C-terminal region whilst *Nhe I* restriction site sequence was inserted into the forward primer. The PCR products prior to digestion with *Nhe I* and *Not I* restriction enzymes were examined by electrophoresis on 1.5 % (w/v) agarose gel as shown in **Figure 3.4**. A single band was observed at around 300 bp which corresponds to the theoretical Affimer size.

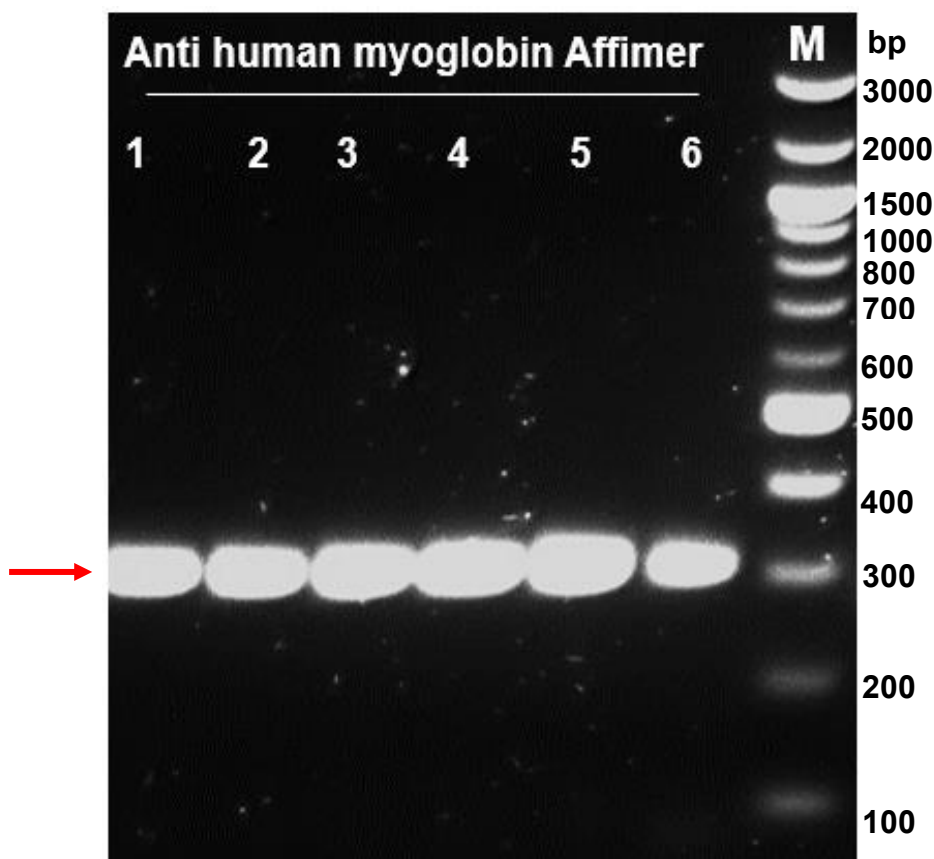


Figure 3.4 PCR products before digested with *Not I* and *Nhe I* restriction enzymes. The PCR products of anti- human myoglobin 1- 6 Affimer coding sequences were electrophoresed in 0.7% (w/v) agarose gel in TAE buffer and stained with SYBR™ Safe. (M), a 2-log DNA ladder is used as a marker. Lanes 1-6 indicate: anti- human myoglobin Affimers 1-6. Red arrow denotes the bands observed at 300 bp for the PCR products from each Affimer DNA.

Prior to subcloning of the amplified Affimer-encoding PCR fragments and *pET11 (a)* vector were digested with *Not I* and *Nhe I* restriction enzymes in order to ensure the binding of both ends of PCR fragments and the sticky ends of the *pET11 (a)* vector. The digested *pET11 (a)* vector with *Not I* and *Nhe I* restriction enzymes was separated in 0.7% (w/v) agarose gel electrophoresis (**Figure 3.5 A**). The data showed two bands of plasmid on the gel which reflected open circular (~ 10 kb) and supercoiled (~ 6 kb) DNA forms. The digested band of *pET11 (a)* vector was excised from the gel and purified for ligation.

Ligation of the digested *pET11 (a)* vector and the PCR fragments was carried out using T4 DNA ligase. The resulting products were electrophoresed on a 1.5 % (w/v) agarose gel as shown in **Figure 3.5 B**. It showed a single band with a molecular size of ~ 300 bp which corresponded to the Affimer sequence fragments. The ligation products were transformed into XL1 Blue competent cells. The positive subclones were mini-prepped to extract the plasmid DNA. Plasmids were sent out for sequencing to confirm the ligation process. Readymade plasmid containing anti- GFAP Affimer sequences and self-prepared anti- human myoglobin coding plasmid were mini-prepped and sent for sequencing. The sequencing results are shown in **Figure 3.6**.

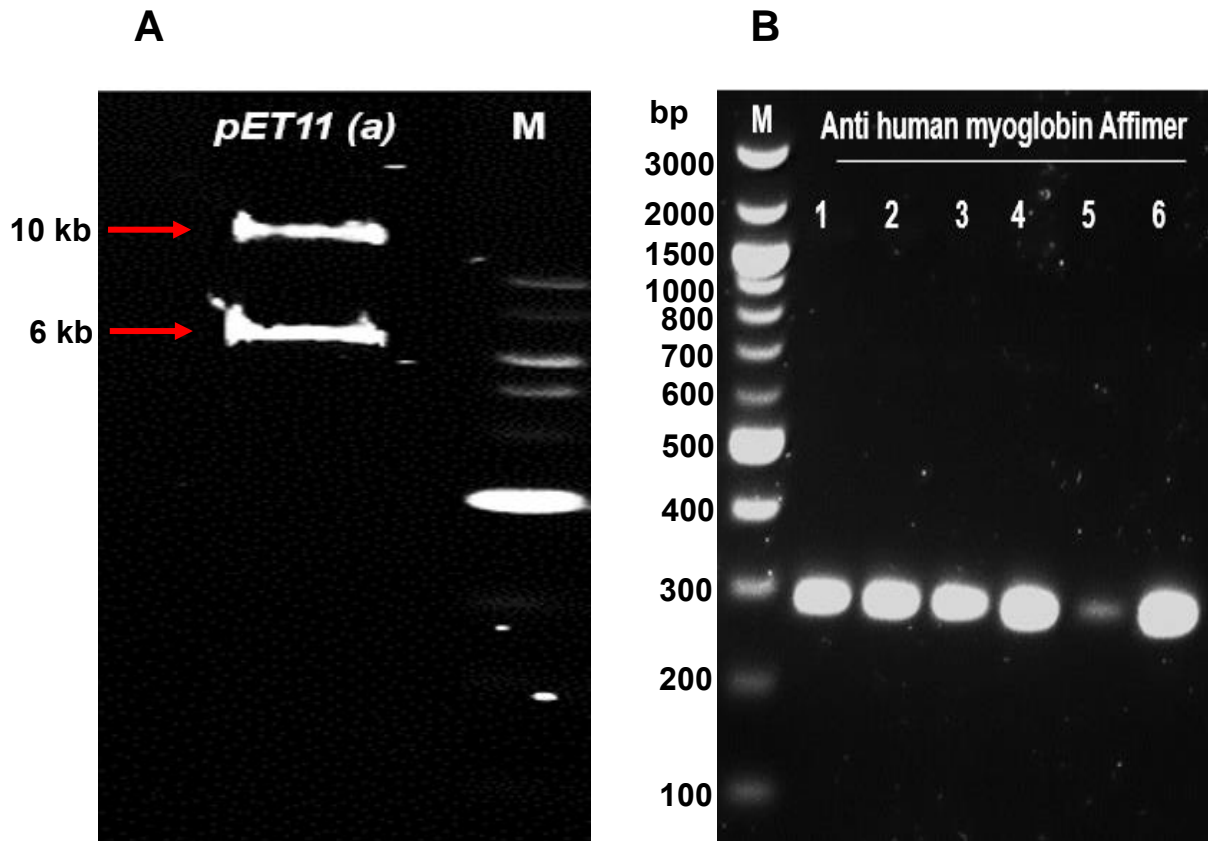


Figure 3.5 Gel electrophoresis of digested *pET11 (a)* and PCR products. (A), digested *pET11 (a)* vector with *Not I* and *Nhe I* restriction enzymes. The digested vector was separated in 0.7% (w/v) agarose gel electrophoresis and the DNA marker lane (M) is a 2-log ladder. (B), PCR products of anti- human myoglobin Affimers subcloned into *pET11 (a)* vector. The subcloning vectors were electrophoresed on a 1.5% (w/v) agarose gel in TAE buffer and stained with SYBR™ Safe. The DNA marker lane (M) is a 0.1- 3000 bp ladder.

Affimer	Variable region 1	Variable region 2	Cys	His-8 tag
Hu-myo 1				
Hu-myo 2				
Hu-myo 3				
Hu-myo 4				
Hu-myo 5				
Hu-myo 6				
GFAP 1				
GFAP 2				
GFAP 3				

Figure 3.6 Sequence alignment of anti- human myoglobin and anti- GFAP Affimers. All Affimers were successfully subcloned into the *pET11 (a)* vector. The blue highlight indicates the variable region 1 (loop 1) whereas the red highlight indicates the variable region 2 (loop 2). The green highlight refers to the position of cysteine residue at the C-terminal.

3.3.3 Expression and purification of human myoglobin and GFAP binding Affimer

After protein expression, Ni²⁺-NTA affinity chromatography is commonly used to purify the proteins containing His₆-tag, usually added as an N or C-terminal sequence. This is due to the high affinity binding of His₆ to Ni²⁺-NTA as shown in **Figure 3.7** and ability to elute the bound protein under gentle conditions using imidazole. According to the Affimer purification protocol (**Chapter 2, Section 2.2.1.5 and 2.2.1.6**) that has been optimised by the BSTG group, the washed Ni²⁺-NTA resin was first packed into the column and equilibrated with the lysis buffer. Affimer proteins containing His₆-tag were pipetted on to the column followed by several washing steps with washing buffer containing 20 mM imidazole. Affimers were consequently eluted from the Ni²⁺-NTA resin using elution buffer containing high concentration of imidazole, up to 300 mM.

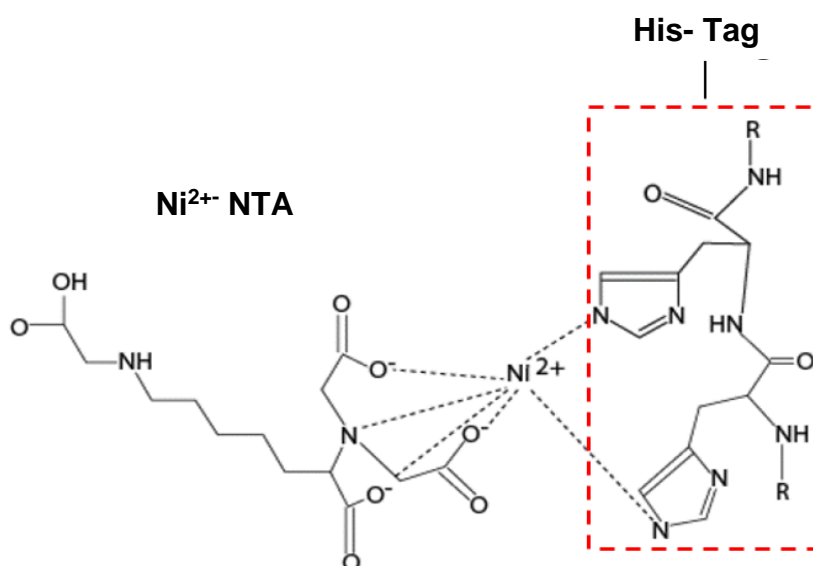


Figure 3.7 Binding of the His₆-tag functional group with the Ni²⁺-NTA groups. The histidine residues (His₆-tagged) of the Affimer bind to the nickel ions with high specificity and selectivity.

Affimers containing lysines in their binding site (anti- human myoglobin 1, 2, 3, 5 and anti- GFAP 2, 3) were excluded from this project because lysine-NH₂ would be modified to form negative oxygen rich groups and thereby chelate Eu³⁺. Hence, anti- human myoglobin 4 and 6 and anti- GFAP 1 Affimer were used for all future experiments.

Following expression and purification of the Affimers, the size of each Affimer was confirmed using SDS-PAGE (**Figure 3.8**) and mass spectrometry (**Figure 3.9**). **Figure 3.8** shows the Affimers of anti- GFAP 1 and anti- human myoglobin 4 and 6 were highly expressed; the molecular mass of the obtained bands were ranged between 12.5-13 KDa, while **Figure 3.9** shows that the molecular masses of anti- GFAP Affimer and anti- human myoglobin 4 and 6 were 12,351, 12,571 and 12,414 Da, respectively. These findings are in keeping with the theoretical molecular mass of the Affimers (12 – 13 KDa) (Khaled et al., 2013).

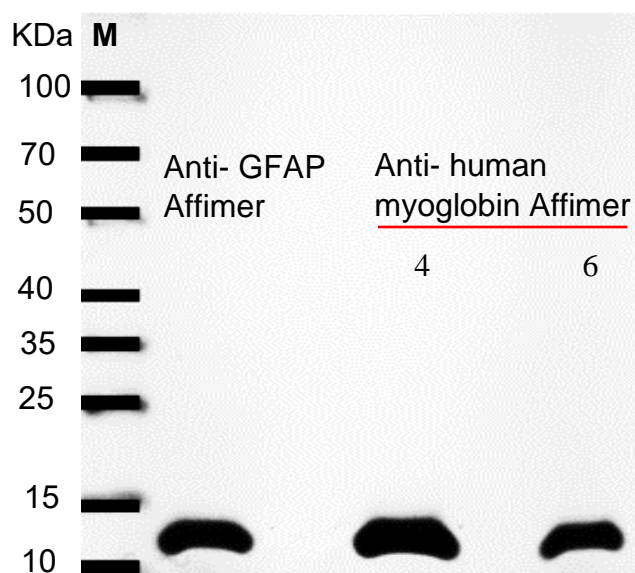


Figure 3.8 SDS-PAGE gel of purified anti- GFAP and anti- myoglobin Affimers. The gel shows purified Affimers by Ni²⁺-NTA affinity chromatography. The lanes show: (M), protein marker in KDa; anti-GFAP Affimer and anti-human myoglobin Affimer 4 and 6.

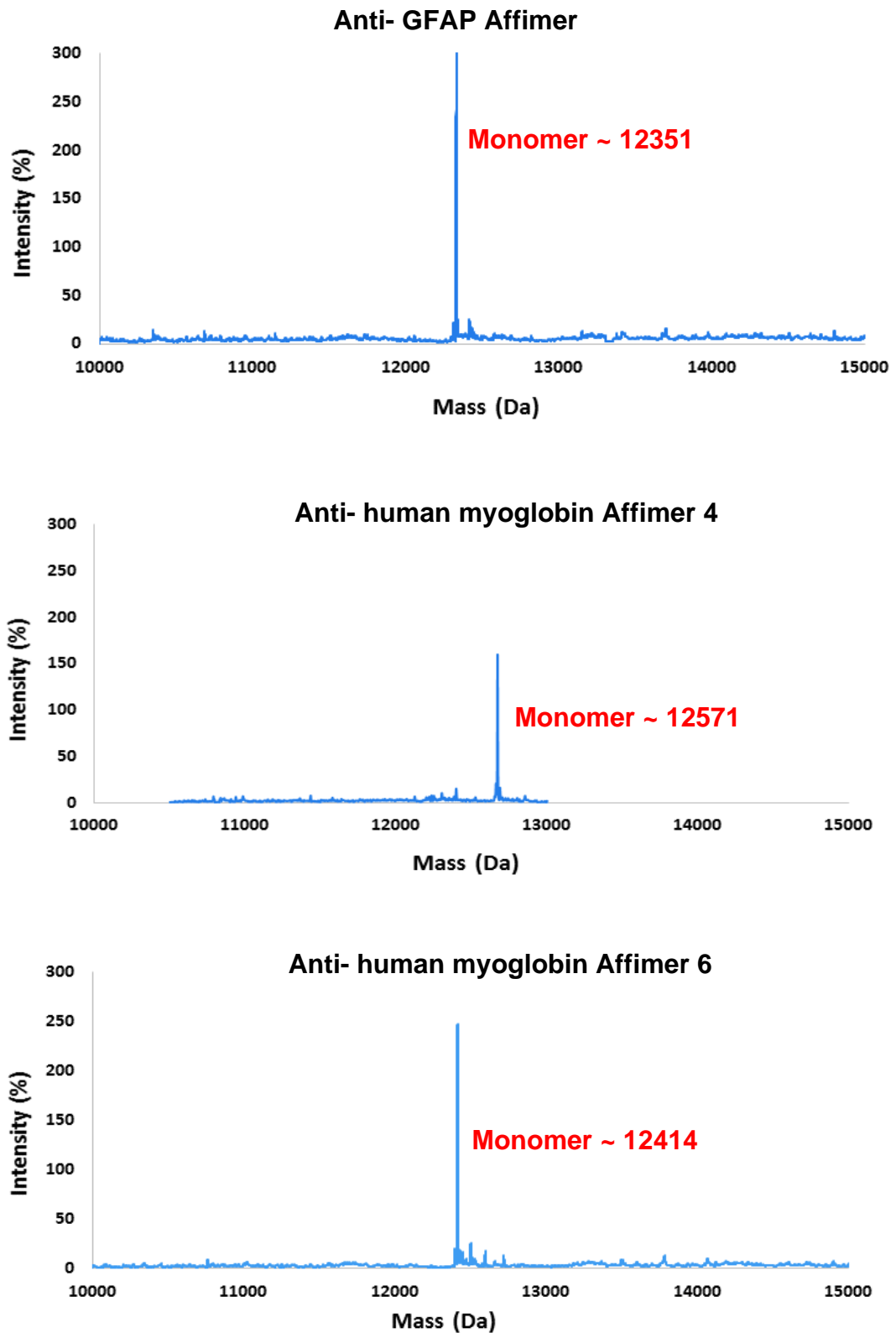


Figure 3.9 Mass spectra of purified anti- human myoglobin 4 and 6 Affimers and anti- GFAP Affimer proteins. All peaks showing the monomer (~ 12.3- 12.5 KDa) form of anti- GFAP Affimer and anti- human myoglobin 4 and 6 Affimers.

3.4 Affimer characterisation

Affimer binding specificity of all selected anti- human myoglobin and anti- GFAP Affimers was checked prior to use in the project to ensure the successful outcome of the assay. Several approaches were used to confirm the selective binding between the bioreceptors (Affimer) and the protein of interest including ELISA, immunoprecipitation assays and SPR.

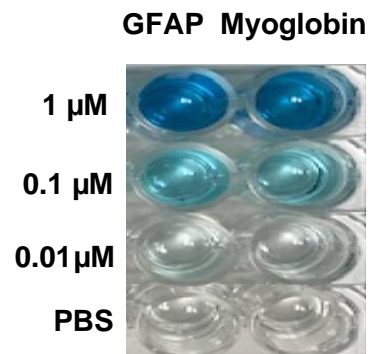
3.4.1 ELISA for selective binding

The ELISA immunoassay is often used to study the specificity of the interaction between the bioreceptors and the target analyte. GFAP and human myoglobin were biotinylated as previously described in **Section 2.2.2.2**. The biotinylated analytes were captured on a Strept Avidin- coated Nunc-immuno™ Maxisorp™ 96- well plate, followed by diluted streptavidin-HRP (1:1000 dilution) as detection agent. The plate image (**Figure 3.10 A**) shows the signal intensity following the ELISA while the histogram (**Figure 3.10 B**) presents the absorbance measurement at 620 (A_{620}) nm for both proteins and a control (PBS). The ELISA data confirmed the efficiency of analyte biotinylation.

Following on from biomarkers biotinylation, selective binding of Affimers was then checked using ELISA as described in **Section 2.2.2.3**. Biotinylated GFAP and human myoglobin were initially immobilised on a Strept Avidin- coated Nunc-immuno™ Maxisorp™ 96- well plate. Each Affimer was used as primary detection agent, followed by diluted anti- His₆ – HRP at 1:1000 dilution in PBS, acting as secondary antibody and detection agent. The histogram (**Figure 3.11**

A and B) shows the absorbance measurements at 620 nm. The ELISA data suggested strong binding of each Affimer to the biotinylated analyte.

A



B

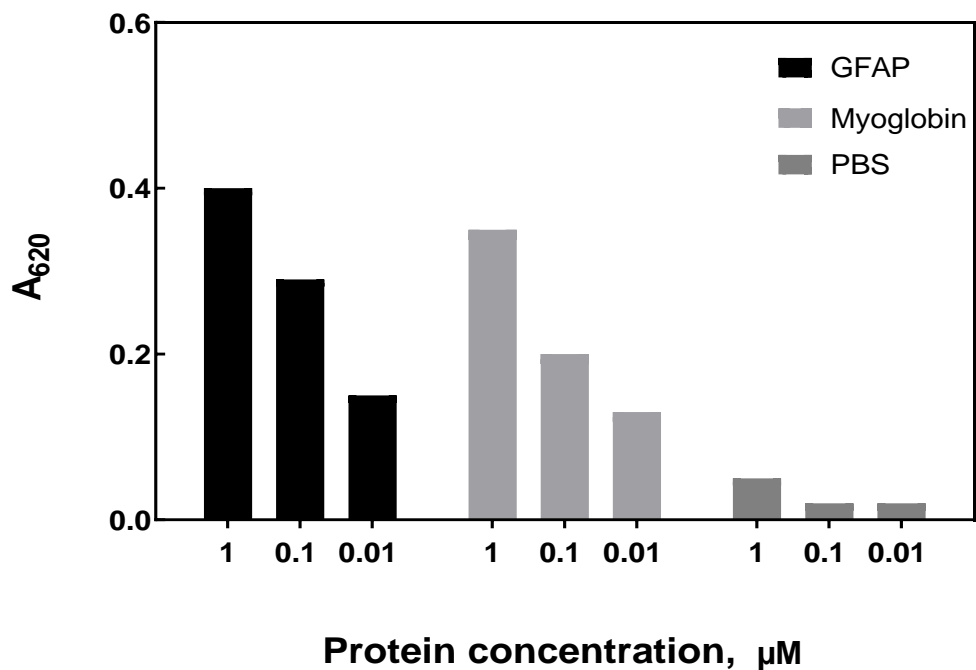
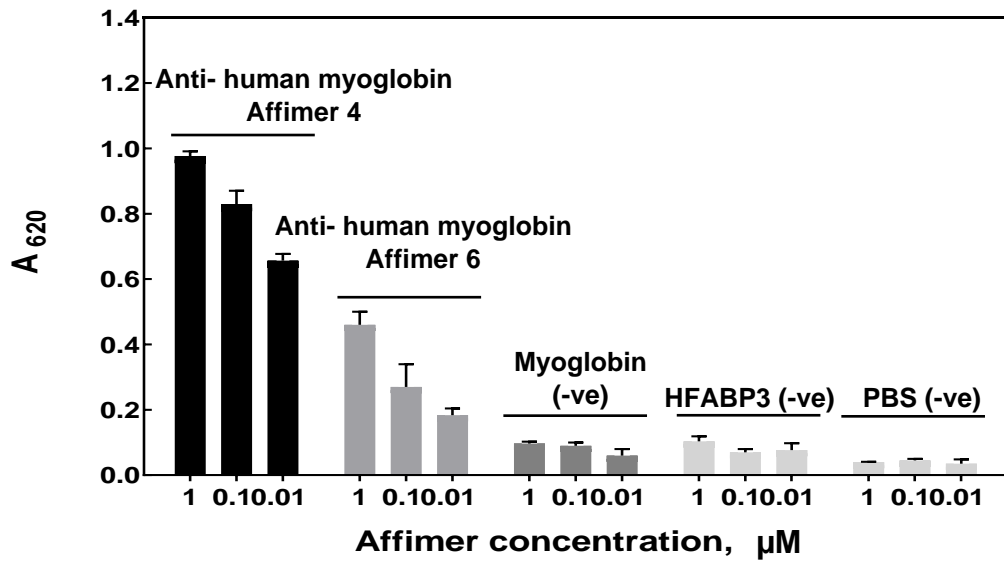


Figure 3.10 ELISA of biotinylated human myoglobin and GFAP. The biotinylated biomarkers were used as primary reagent immobilised on the plate and streptavidin- HRP conjugate as detection reagent; (A), biotinylated protein at 1 μM to 10 nM plus control (PBS); (B), data show A_{620} for each biomarker at 1, 0.1 and 0.01 μM concentrations.

A



B

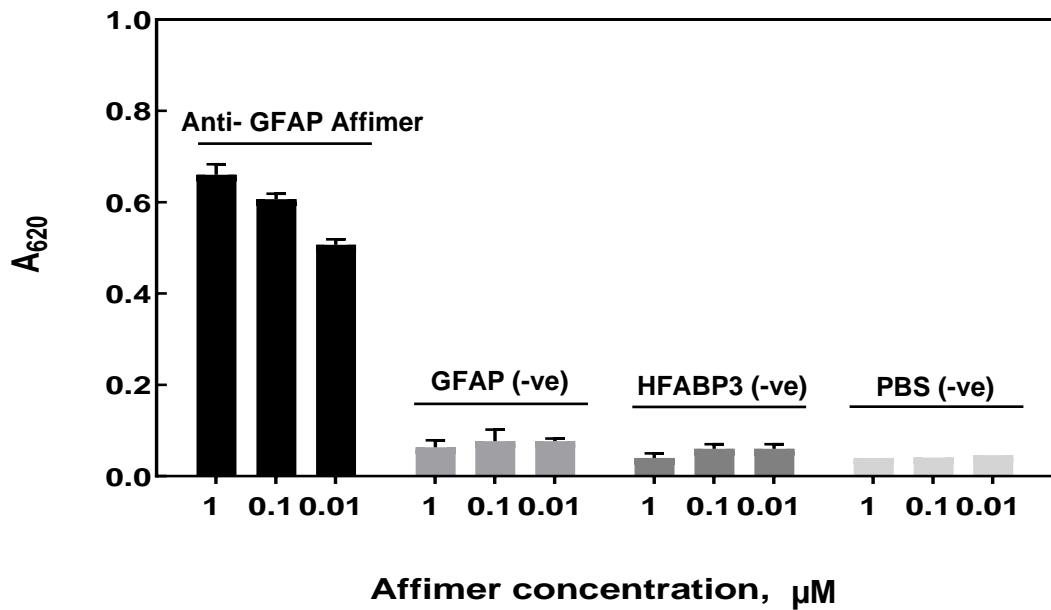


Figure 3.11 ELISA result to check the selective binding of the anti- human myoglobin and anti- GFAP Affimers for their targets. (A and B), showing the absorbance at 620 nm. In (A), columns are: anti- human myoglobin Affimer 4; anti- human myoglobin Affimer 6; myoglobin (-ve control); anti-HFABP3 Affimer (-ve control) and PBS (-ve control). In (B), columns are: anti- GFAP Affimer; GFAP (-ve control); anti- HFABP3 Affimer (-ve control) and PBS (-ve control).

3.4.2 Immunoprecipitation (pull down) assays

Immunoprecipitation or pull-down assays are widely used to isolate a protein of interest or target analyte out of solution depending on the interaction between bioreceptor (e.g. antibody) and antigen. In this project, Affimers against human myoglobin and GFAP were used as antibody replacements to pull down their targets. The affinity-precipitation assay was set up as shown in **Figure 3.12**. The purified Affimers anti- human myoglobin or anti- GFAP were immobilised onto Ni²⁺-NTA resin. The resin bound Affimer was then used to pull down the target protein from the solution as illustrated in **Figure 3.12 A**. Unbound Affimer was removed by washing in PBS buffer. The Ni²⁺-NTA- Affimer resin was incubated with human myoglobin or GFAP analyte overnight before removal of the unbound analyte by multiple washing. SDS-PAGE was used to separate all fractions collected from the pull down including unbound Affimer, washed Affimer, unbound analyte, washed analyte and Affimer bound analyte. Anti- HFABP3 Affimer was used as a negative control. SDS-PAGE results from anti- GFAP Affimer 1 is shown in **Figure 3.13 B**. In the unbound Affimer lane, there were bands detected at ~ 12 KDa, indicating that the Ni²⁺-NTA resin was saturated with the Affimers. Two bands were seen in the lane of Affimer plus analyte of anti- GFAP Affimer 1 at around ~ 12 and 55 KDa which are the sizes of the Affimer and GFAP protein respectively. The same results were obtained from anti- human myoglobin Affimer 4 and 6 as shown in **Figure 3.12 (C, D)**, respectively. Two bands were observed in the Affimer plus analyte lane at around 12 and 17 KDa of Affimer and human myoglobin respectively. A single band of ~ 12 KDa was detected in the negative control lane which had the anti- HFABP3 Affimer as pull down receptor. The SDS-PAGE data of all anti- GFAP or anti- human myoglobin

Affimers showed that Affimers selectively bound to their target proteins and pulled them down from solution.

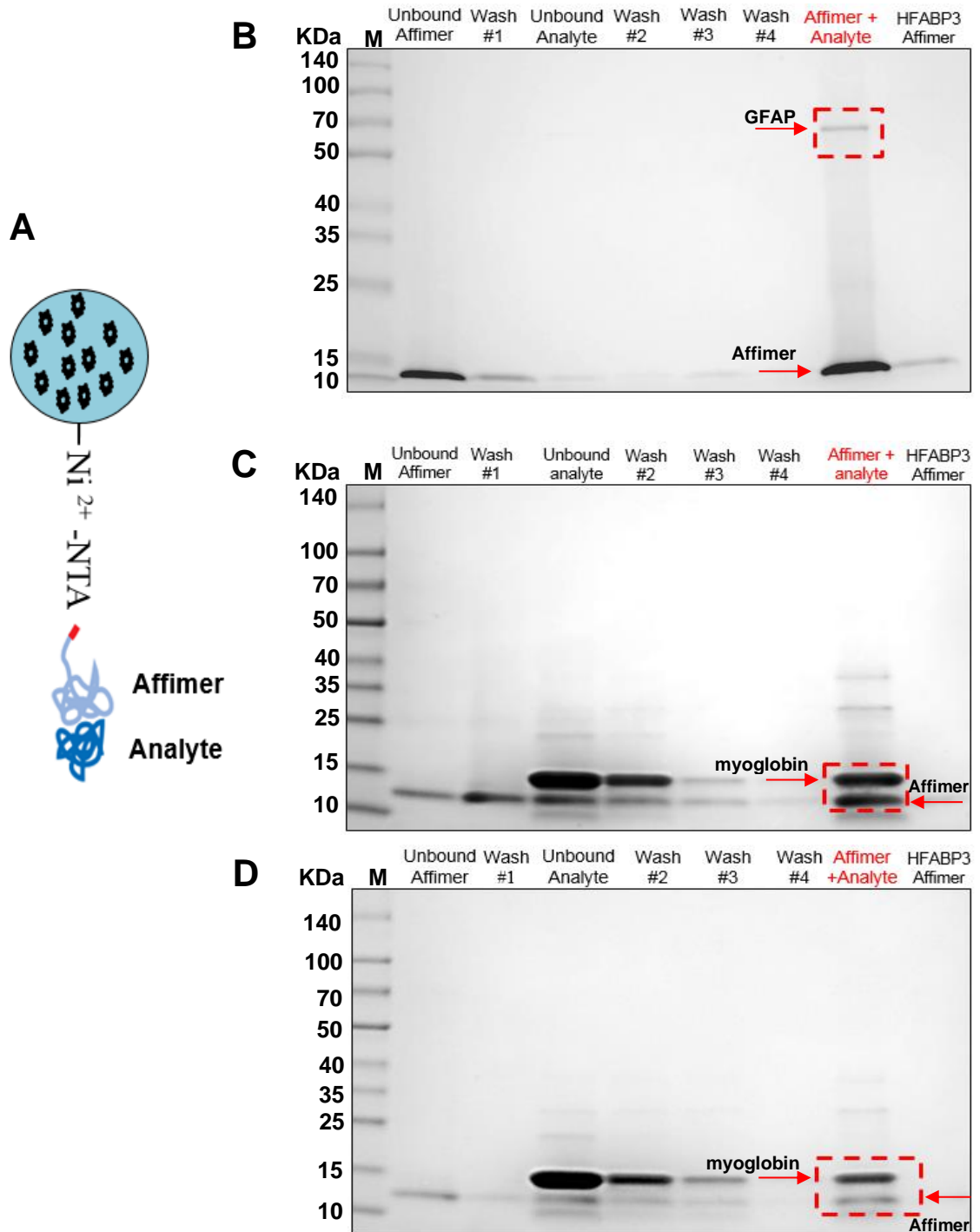
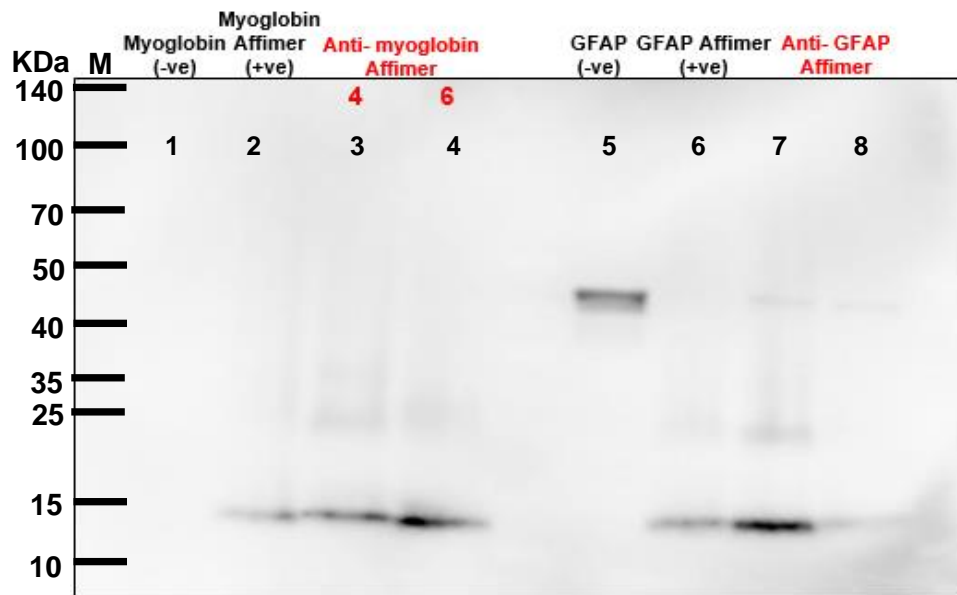


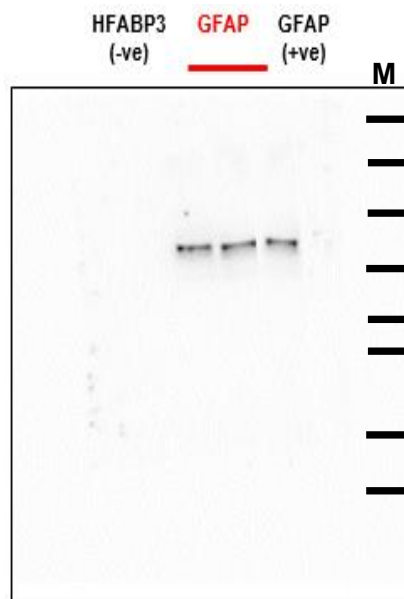
Figure 3.12 Pull down assay showing the binding of the Affimers to target protein. (A), schematic showing the pull down complex uses in the assay. (B-D), SDS- PAGE Gels showing the collected fractions during the pull-down assay using; (B), anti- GFAP Affimer 1; (C- D), anti- human myoglobin Affimer 4 and 6. Anti- HFABP3 Affimer was used as a negative control for both Affimers; (M), Protein markers. Red box denotes: protein band pull down.

For further confirmation of the selective binding between Affimer and target analyte, pull-down complex on SDS-PAGE gels were transferred to PVDF membrane to perform western blots. In **Figure 3.13 A**, the membrane was probed with anti- His₆- tag antibody to detect anti- human myoglobin or anti- GFAP Affimers. All Affimers were detected at ~ 12 KDa. A dimer form of anti- GFAP 1 and anti- human myoglobin 4 and 6 Affimer were also observed at around 25 KDa due to a disulphide bond formation between cysteine- SH group at the C-terminus. Anti- human myoglobin or anti- GFAP Affimers (positive controls) were detected in the first and fifth lanes respectively. The other two membranes were probed with primary anti-GFAP and anti- human myoglobin antibodies to detect GFAP and human myoglobin protein correspondingly. GFAP and human myoglobin protein bands were detected on the membrane as shown in **Figure 3.13 (B, C)**. GFAP and human myoglobin protein were used as a positive control as shown in **Figure 3.13 (B, C)** respectively. Both pull down and western findings confirmed that all of the Affimers were capable of selective binding to their target analyte. Based on the ELISA, pull down and western bolt results, SPR was done on anti- human myoglobin Affimers 4 and 6 and anti- GFAP Affimer 1 to obtain their affinity to their target protein.

A



B



C

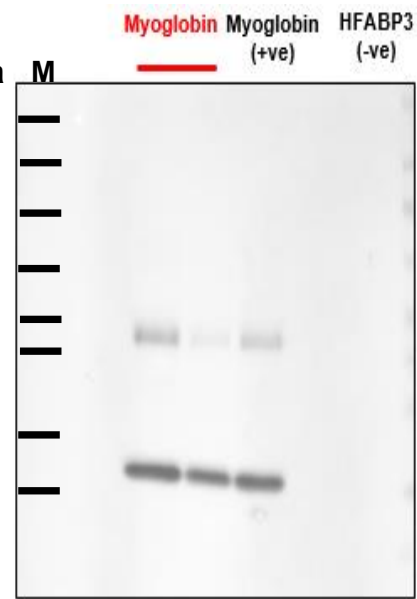


Figure 3.13 Immunoblotting assay of anti- human myoglobin/ anti- GFAP Affimers binding to their target proteins. (A), western blotting gel showing anti-human myoglobin 4 and 6 and anti- GFAP 1 Affimers after probing with anti- His₆-tag antibody. Human myoglobin and GFAP proteins were used as a negative control in lane 2 and 6 respectively whereas anti- human myoglobin and GFAP Affimers were used as a positive control in lane 3 and 7 respectively. Western blot showing (B), GFAP protein and (C), human myoglobin protein after probing with monoclonal anti- GFAP and anti- human myoglobin antibodies correspondingly. HFABP3 protein was used as a negative control; (M), Protein markers.

3.4.3 Surface Plasmon resonance (SPR)

The binding kinetics between the anti- human myoglobin/ anti- GFAP Affimers and their targeted analyte were investigated using SPR. The data provided by SPR are based on changes in refractive index resulting from Affimer-analyte interaction. These changes are measured in real time during the association and dissociation phases of the binding between Affimer and analyte proteins and plotted as resonance units (RUs) versus time. The SPR data were analysed using BIA evaluation software and GraphPad Prism 7 software. The first step of tidying up SPR data was to normalise the baseline by setting the start injection time to zero. The second step was to subtract the signal from the reference flow cell 1 (left empty) which is the first control. Then a second subtraction was done by subtracting a second control of signal, the buffer injection. This was carried out to eliminate any buffer mismatch effects and noise from the machine during the injection and regeneration steps. Hence, the signals we obtained were only binding data. The final step was to carry out fitting for affinity and kinetics (on rate and off rate constants). The binding affinity (k_D) was calculated using **Equation 3.1**.

$$k_D = k_a / k_d$$

Equation 3.1 Equilibrium dissociation constant

Where,

k_D is the equilibrium dissociation constant (M),

k_a is the association rate constant ($M^{-1} s^{-1}$),

k_d is the dissociation rate constant (s^{-1}).

In **Table 3.2**, χ^2 values were generated and calculated by the SPR software and were used as indicators of the appropriateness of the fitted curves. The smaller the χ^2 value, the better overlay between the data and the fitted curve. All data fits of Affimer binding data are shown and χ^2 values were ranged between 0.304- 0.57, suggesting excellent overlay between the data and the fitted curves. The SPR data showed that anti- GFAP (**Figure 3.14 A**) and anti- human myoglobin 4 Affimer (**Figure 3.15 A**) had high binding affinity to GFAP and human myoglobin protein respectively. The k_D value of anti- GFAP Affimer was 3.68 ± 0.023 nM; whereas, anti- human myoglobin 4 Affimer k_D value was 57.8 ± 0.001 nM. These findings are in keeping with the affinity binding values (k_D) of antibody-antigen complex, which ranged from pM to nM in general (Kim et al., 1990, Landry et al., 2015). In contrast, anti- human myoglobin 6 Affimer showed very low binding affinity to human myoglobin protein (**Figure 3.15 C**).

Table 3.2 Kinetic parameters of anti- human myoglobin and anti- GFAP Affimers interactions.

Affimer target	$k_a \pm SE$ ($M^{-1}s^{-1}$)	$k_d \pm SE$ (s^{-1})	$k_D \pm SE$ (nM)	χ^2
Human myoglobin 4	$9.76 (\pm 1.55) \times 10^6$	$5.64 (\pm 0.0041) \times 10^{-3}$	57.8 ± 0.001	0.30
GFAP 1	$6.60 (\pm 1.45) \times 10^5$	$2.43 (\pm 0.0001) \times 10^{-3}$	3.68 ± 0.023	0.57

SPR data is fit to one binding site model; data are means \pm SEM (n=3).

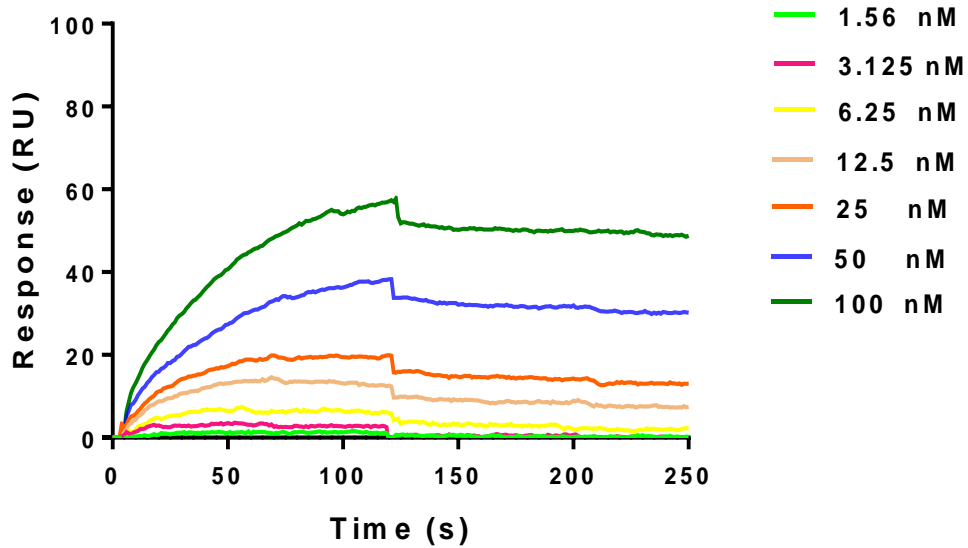
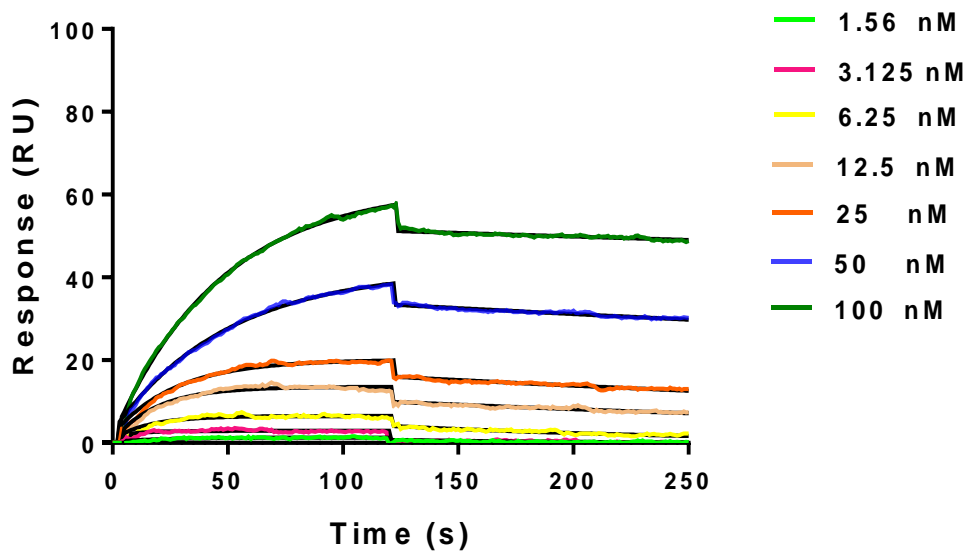
A**B**

Figure 3.14 Real time SPR sensorgrams for anti- GFAP Affimer. Changes of refractive index are showing in response units (RU). (A), GFAP protein was immobilised on a coated SPR amine chip and tested with 2-fold dilutions of anti-GFAP Affimer concentrations from 1.56- 100 nM; (B), the global fit analysis with one site interaction model of anti- GFAP Affimer binding to GFAP protein are shown as black line which overlay the coloured tracer.

C

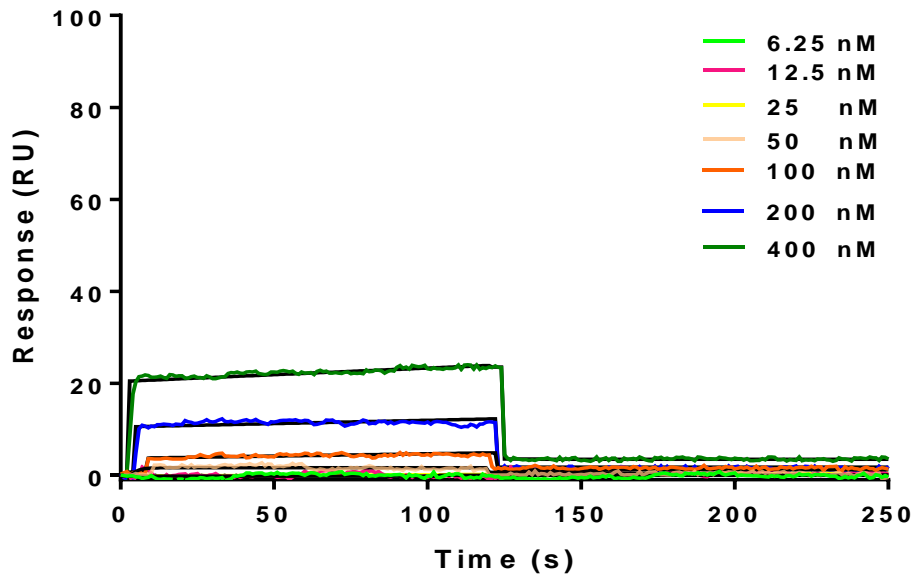


Figure 3.15 Real time SPR sensorgrams data of anti- human myoglobin Affimer. (A), human myoglobin protein was immobilised on a coated SPR amine chip and tested with 2-fold dilutions of (A), anti- human myoglobin 4 Affimer and (C), anti- human myoglobin 6 Affimer concentrations from 1.56- 100 nM; (B), the global fit analysis with one site interaction model of anti- human myoglobin 4 Affimer binding to human myoglobin protein are shown as black line black line which overlay the coloured tracer.

3.5 Discussion

The primary aim of this project was to develop a biosensor platform using rare earth ions chelated by modified Affimers and to test their feasibility on a series of human biomarkers e.g. stroke/heart attack markers (GFAP and myoglobin) and others, such as CRP and CEA which are inflammation and cancer biomarkers respectively. Our choice of targets was mainly dictated by ready availability of Affimer/ biomarkers protein pairs and the technology can be adapted to target any specific analyte of clinical interest. Additional novelty to this project is the use of synthetic binding protein (Affimers), which offer an excellent alternative targeting strategy to the existing antibodies.

3.5.1 Affimer expression and purification

In the present study, Affimers against human myoglobin and GFAP were subcloned, expressed and purified successfully using plasmids that were provided by BioScreening Technology Group (BSTG), University of Leeds. The Affimer expression was performed using a modified protocol that our group has adapted following previous extensive optimisation. Therefore, it was possible to express and purify the 2 clones of anti- human myoglobin and GFAP Affimers accordingly. The data presented indicate that the Affimers were 12.5-13 KDa in keeping with the previously published data (Khaled et al., 2013) and SDS-PAGE gels (**Figure 3.8**) confirmed the presence of Affimers as monomers. The DNA sequence confirmed that the amino acid sequence of the Affimers was identical to the original plasmid sequence and so no mutations have been introduced. This is significant, as changes in the amino acid sequence would impact the binding/ recognition specificity of the Affimer. The data showed that anti- human

myoglobin 4 and 6 Affimers and anti- GFAP 1 Affimer have no lysine in their binding loops and so they were selected for further characterisation.

3.5.2 Affimer characterisation

Several qualitative methods including ELISA, immunoprecipitation or pull down assays, western blotting and quantitative methods (SPR) were used to investigate the selectivity and affinity of binding of selected Affimers to human myoglobin and GFAP. In ELISA, anti- human myoglobin 4 Affimer showed the maximum response followed by anti- human myoglobin 6 Affimer, which is in keeping with the results obtained from the pull-down assay. Anti- GFAP Affimer showed strong binding to GFAP protein according to ELISA and pull down results.

Surface plasmon resonance (SPR) is widely used as an optical sensing platform to study binding kinetics and obtain k_a , k_d and k_D . The strength of affinity between the receptor and ligand was provided as a dissociation constant (k_D). The k_D values obtained from a one site binding fitting model were nM (anti- human myoglobin 4 (57.8 ± 0.001 nM) and anti- GFAP Affimer (3.68 ± 0.023)), which confirmed the high affinity interaction between the Affimer and the targeted analyte. Anti- human myoglobin 6 failed to bind to human myoglobin. This also supported the ELISA data which revealed that anti- human myoglobin 6 Affimer had a lower response than anti- human myoglobin 4 Affimer. However, the pull down data showed that anti- human myoglobin 6 Affimer was able to bind its target analyte. This discrepancy in anti- human myoglobin 6 Affimer data between ELISA and pull down and SPR may be explained by the fact that the Affimer loses its binding affinity to its target analyte when immobilised on solid surfaces.

Based on the results obtained from ELISA, pull down experiments and SPR, anti- human myoglobin 4 and anti- GFAP Affimers were selected as the bioreceptors to develop the Eu³⁺ chelate nano- biosensors.

Chapter four: Affimer functionalisation

Chapter 4

Affimer functionalisation

4.1 Introduction

The most popular rare earth elements for chelated lanthanide used as labelling agents are Europium and Terbium (Yuan et al., 2001). Eu^{3+} complexes become significantly more fluorescent when attached to appropriate chelating ligands such as β -diketonates, carboxylates and heteroaromatics (Pires et al., 2016). The ideal ligand must be suitable for efficient ligand-to-metal energy transfer and should have an aromatic group(s) with energy gaps that are suitable for UV light absorption (Hemmilá and Mukkala, 2001, Nishioka et al., 2007). The ligand absorbs UV excitation light through ligand π - π^* transitions of the aromatic ring(s) and then absorbed energy is transferred from the S1 energy level in the ligand to the $5D^n$ energy level in the Eu^{3+} . Subsequently, Eu^{3+} ions emit fluorescence when energy is transferred from the $5D^0$ level to one of the 7F energy levels. The strongest emission peaks of Eu^{3+} complexes are between $5D^0 - 7F^2$ at 590 nm to 700 nm. However, the emission intensity ratios of energy transitions from $5D^0$ to different $7F^n$ levels are strongly dependent on the symmetrical coordination surrounding the metal ion and the ligand type (Binnemans, 2015).

Fluorescent lanthanide complexes can be classified into main four groups based on their overall design (Armelaio et al., 2010, Bünzli et al., 2010, Lis et al., 2002). (**Figure 4.1**). Type 1 carries a pendant antenna linked to the chelating

ligand of lanthanide complex that can modulate the fluorescence via the energy transfer between the antenna and analyte. In Type 2 complexes, a chromophoric chelator with an incorporated antenna is involved in the coordination of the lanthanide ions. The modulation of the functional groups in the ligand accounts for the fluorescence change in this type. In sharp contrast, Type 3 antenna is not linked to a chelating ligand but directly coordinates the lanthanide. Type 1-3 are coordinatively saturated types whereas Type 4 complexes are coordinatively unsaturated. In type 4 complexes the unsaturated coordination site is occupied by solvent molecules such as H₂O which can be replaced by target protein leading to fluorescence changes in the lanthanide.

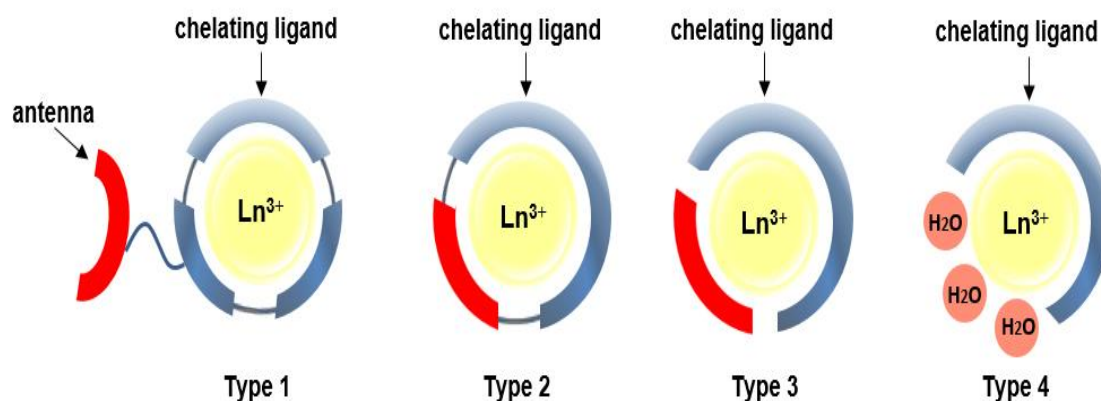


Figure 4.1 Photophysical schematic of the four types of lanthanide complexes. Fluorescent lanthanide complexes are classified into four types (1, 2, 3 and 4) based on the chelating ligand and antenna design. Type 1, a pendant antenna linked to the chelating ligand of lanthanide; Type 2, antenna incorporated into the chelator within the lanthanide complex; Type 3, antenna directly coordinates the lanthanide without being linked to the chelator and Type 4, part of the coordination site is occupied by solvent which is prone to replacement by proteins. Symbols indicate antenna (red arcs); chelating ligand, (blue shell) and lanthanide ion, (yellow blob).

Configuration alterations, and energy transfer mechanisms play important roles in modulating the fluorescence of the lanthanide complex in each type. In Type 1 and 2 the reaction between the antenna and analyte can eliminate or induce intramolecular charge transfer (ICT) (Liu et al., 2013b) and intramolecular photo induced electron transfer (PET) (Zhao et al., 2010) acting as switches in lanthanide complexes. In the resonance energy transfer (LRET) (Rajapakse et al., 2010) fluorescence mechanism, the complex's reaction with an analyte regulates energy transfer from the complex to the ligand chromophore (Zwier et al., 2014). In theory, LRET can be used in all types of lanthanide complexes.

4.2 Affimer as chelating scaffold

The Affimer scaffolds offer a range of linkage chemistries that can be utilised to allow stable and efficient chelation of Eu^{3+} . The wide spread amine groups from lysine- NH_2 on the scaffold and the cysteine-SH residues at the C-terminus of the Affimer (**Figure 4.2**) facilitate different strategic linkage chemistries for Eu^{3+} . Lysine- NH_2 and cysteine-SH functional groups can be modified to form negative oxygen rich groups and thereby chelate Eu^{3+} .

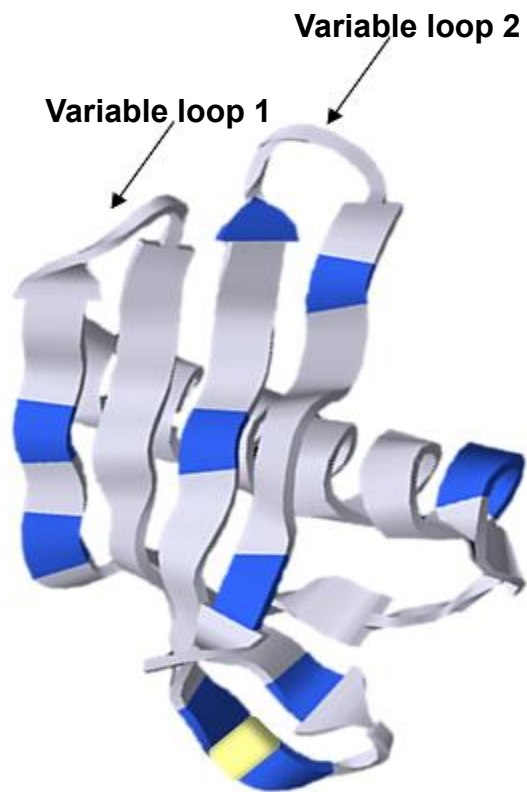


Figure 4.2 Affimer structure. The structure of a typical Affimer is shown. The blue colour shows lysines, whereas yellow shows the cysteine residues at the C-terminus of the Affimer scaffold (pdp. 4N6T).

There are many considerations that should be taken into account for the design principles of a fluorescent Eu^{3+} complex system:

- I. The choice of chelator: a sensitive chromophore or “antenna” is required to allow indirect excitation of the Eu^{3+} . The lanthanides are known to be difficult to be directly excite due to the weak F-F transition absorption and hence a chelator can be used to overcome this problem (Moore et al., 2009).

- II. The choice of bioreceptor: a bioreceptor characterised by high affinity to the targeted analyte, cost effective in production and small in size. Affimers appear to satisfy all the criteria for such a bioreceptor.

4.3 Aims

The aims for this chapter were to:

- I. Characterise Eu^{3+} complex spectra including their excitation and emission wavelength.
- II. Investigate the optimum conditions for the Eu^{3+} complex to be tested.
- III. Modify anti- human myoglobin and anti- GFAP Affimers and control HFABP3 Affimers to chelates.
- IV. Assess the performance of the optimised Eu^{3+} complex in human serum.

4.4 Eu³⁺ complex optimisation

4.4.1 Eu³⁺ complex characterisation

The aim of this part was to assess the excitation wavelengths of the Eu³⁺ chelated by PMDA modified-Affimer. The excitation spectrum of Eu³⁺ chelated by PMDA modified- anti-human myoglobin Affimer (1 ml in PBS) was measured by using a fluorescence spectrophotometer at 615 nm emission wavelength then quantified as shown in **Figure 4.3**. A low concentration of 100 μ M of Eu³⁺ was selected for the measurement to ensure a significant response was obtained whilst still being economical with Affimers and their target proteins. The striking finding is that the excitation spectrum of Eu³⁺ complex consisted of two bands. The first band at 290 nm was due to the UV light absorption of the ligands while the second bands at 395 nm and 405 nm were from the direct F–F electron transitions of Eu³⁺. The most prominent excitation peak of the Eu³⁺ was at 395 nm and 405 nm and was thought to be caused by direct excitation of the 5L² level of Eu³⁺. Therefore, 395 nm peak was selected for efficient excitation of complexes.

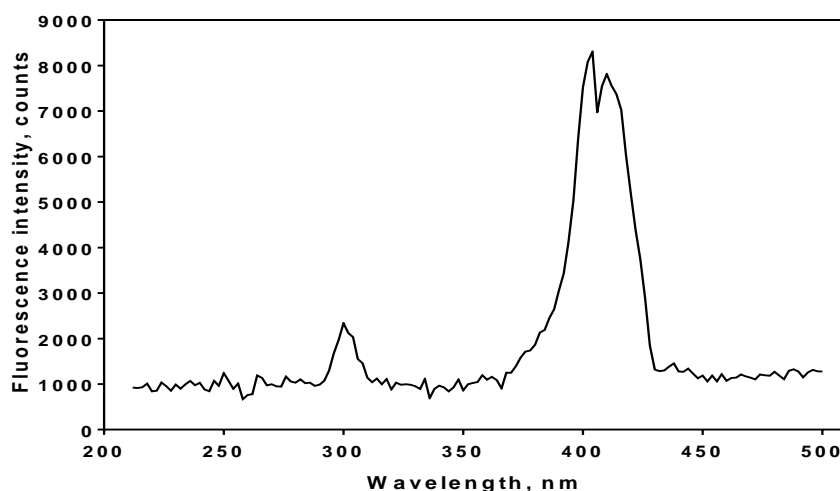


Figure 4.3 Excitation spectrum of Eu³⁺ complex. Peak excitation wavelengths for Eu³⁺ complex were measured and using $\lambda_{em}= 615$ nm.

After we established the excitation of Eu^{3+} at 395 nm, the emission spectrum of Eu^{3+} chelated with PMDA modified- anti- human myoglobin Affimers complex was measured as shown in **Figure 4.4**. The typical peaks related to the electronic transitions from the $5D^0$ excited state to the fundamental state $7F^J$ ($J = 1, 2, 3,$ and 4) of the Eu^{3+} ion were visible, while the $5D^0 \rightarrow 7F^0$ transition appeared to be absent. The strongest emission peaks were observed around 590 nm, 615 nm, and 696 nm, attributed to the $5D^0 \rightarrow 7F^1$, $5D^0 \rightarrow 7F^2$ and $5D^0 \rightarrow 7F^4$ transitions, respectively. Furthermore, an additional peak was found in the $5D^0 \rightarrow 7F^3$ transition at 650 nm. For the Eu^{3+} , the $5D^0 \rightarrow 7F^J$ transitions are predominantly electric dipoles for j even and completely magnetic dipoles for j odd. The emission intensities of electric dipole transitions, for $J = 0$ and for $J = 2$, are strongly sensitive to the lanthanide's surrounding environment where they are absent ($J = 0$) or small ($J = 2$) in high symmetry sites. In sharp contrast, the intensities of magnetic dipole transitions are almost independent of their environment all of which is in keeping with published data from other groups (Binnemans, 2015).

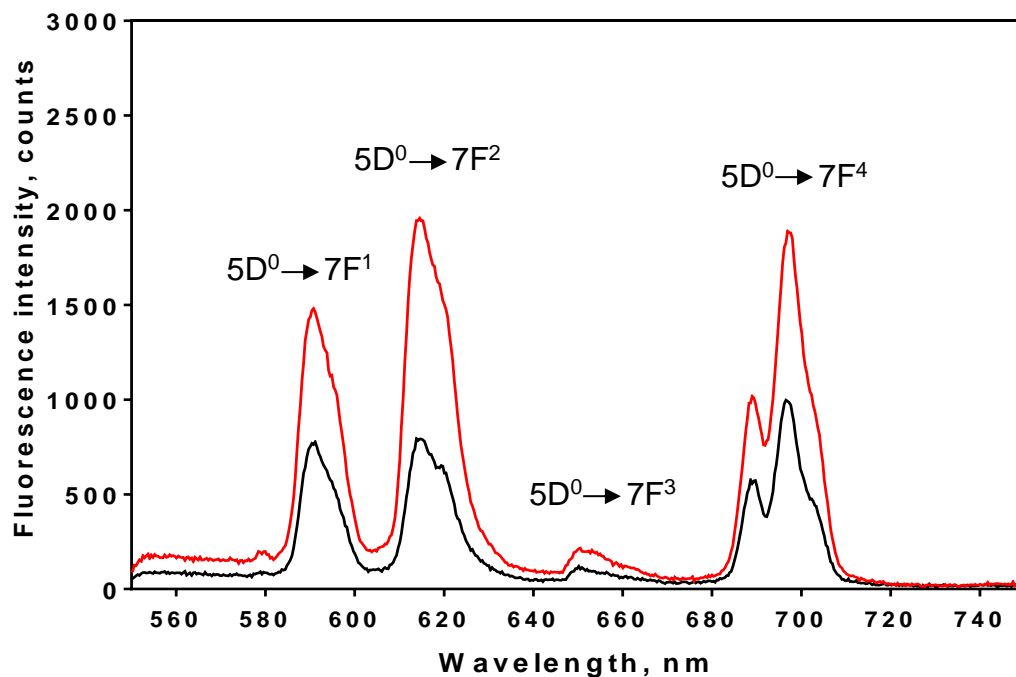


Figure 4.4 Eu³⁺ complex emission spectra. Peak emission wavelengths for Eu³⁺ complexes were measured for free Eu³⁺ (black line peaks) and Eu³⁺ chelated by PMDA modified anti-human myoglobin Affimer complex (red line peaks). The electronic transition corresponding to the emission peaks are indicated. λ_{ex} = 395 nm.

4.4.2 Eu³⁺ concentration optimisation

Having established the excitation and emission spectra of the PMDA-modified Eu³⁺ complex, the next step was to optimise and select the optimum Eu³⁺ concentration for complex chelation in the proposed assay. Three low concentration values of Eu³⁺ were selected (20, 50 and 100 μ M) to prevent precipitation in PBS buffer and for the purpose of cost effectiveness. The fluorescence intensity was measured accordingly as shown in **Figure 4.5**. At 20 μ M Eu³⁺ concentration, fluorescence quenching of the anti-human myoglobin Affimer: Eu³⁺ complex was directly proportional with increasing dose of the human myoglobin from 100 pM to 100 nM. The same fluorescence quenching was also observed at 50 μ M and 100 μ M concentrations of Eu³⁺. However, when comparing the three concentration values, it is evident that 100 μ M of Eu³⁺ allowed the most substantial fluorescence quenching (1.2 fold ($1625 \pm 0.22 - 1375 \pm 0.10$) at the 615 nm peak and 1.17 fold ($2130 \pm 0.19 - 1735 \pm 0.38$) at the 590 nm peak) when compared to the other two concentrations. Based on these results, 100 μ M was used as the optimised concentration of Eu³⁺ for the assay complex.

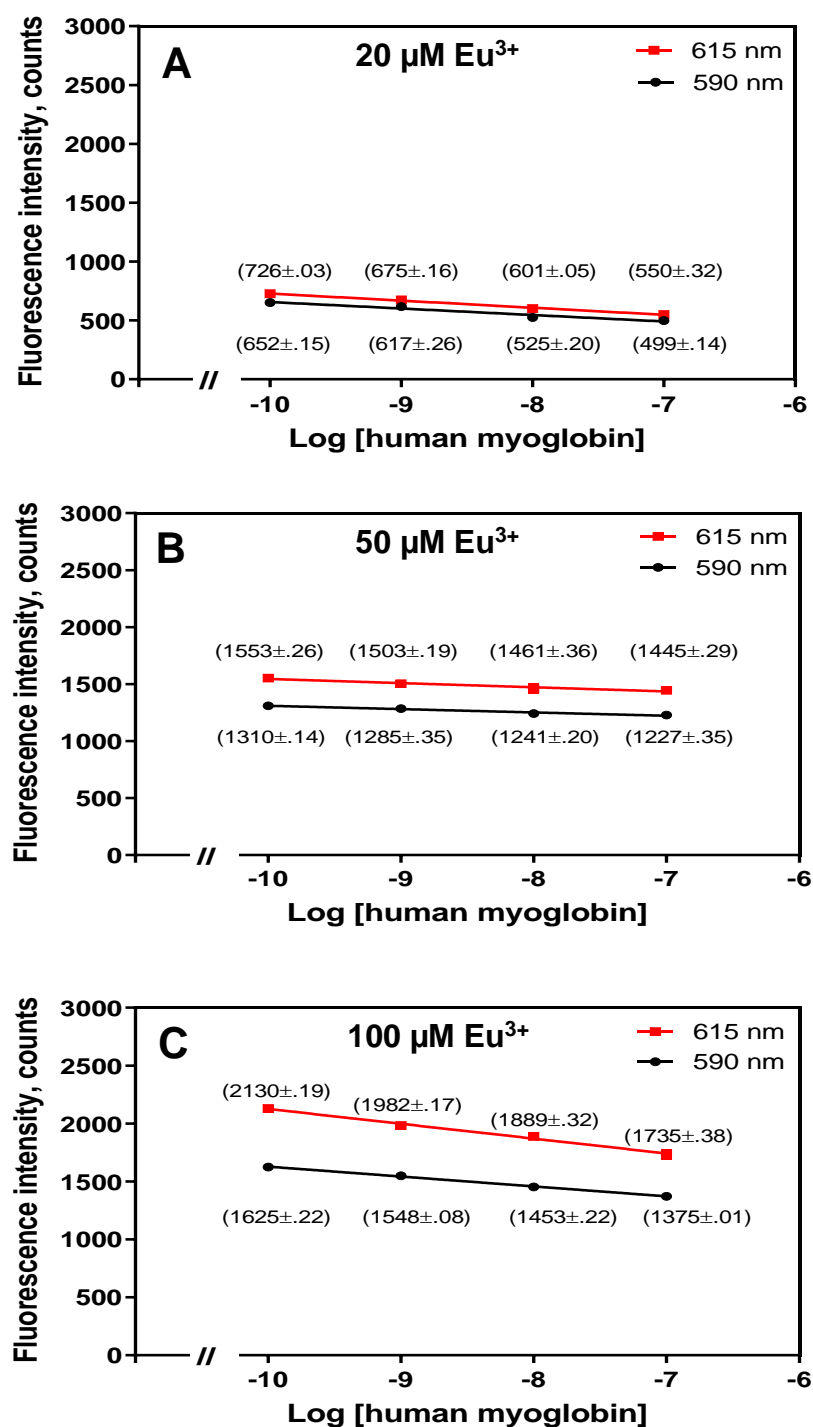


Figure 4.5 Fluorescence intensity spectra of Eu^{3+} chelated by PMDA modified anti-human myoglobin Affimer complexes. After adding the human myoglobin target, fluorescence was measured in an Ocean Optics QE Pro spectrometer with $\lambda_{\text{ex}} = 395$ nm. (A), 20 μM Eu^{3+} ; (B), 50 μM Eu^{3+} ; (C), 100 μM Eu^{3+} . Data are means \pm SEM ($n = 4$); in most data points SEM < size of data point.

4.4.3 The selection criteria of the buffer for the Eu^{3+} complex system

Having established the optimum concentration of Eu^{3+} to be used in the complex, we explored the options for the ideal buffer to test the system. Three potential buffers were selected to test the Eu^{3+} complex fluorescence quenching based on evidence from the literature that are most frequently used in biological experiments to maintain the pH (Sambrook and Russell, 2001). These buffers are: PBS, MOPS and Tris.

Fluorescence quenching of anti- human myoglobin Affimers bearing Eu^{3+} ions was tested in PBS, MOPS and Tris as shown in **Figure 4.6 to 4.8** respectively. The control analyte HFABP3 was also tested. The overall emission spectra of Eu^{3+} complex showed significant quenching with increased concentration of human myoglobin across all buffers. The fluorescence intensity peaks for the Eu^{3+} complex and their respective fluorescence quenching plots at different concentrations of human myoglobin are shown in **Figure 4.6 to 4.8 A**. These findings suggest that when the Eu^{3+} complex binds to the target protein, via the anti- human myoglobin Affimer, the fluorescence intensity decreases indicating that the Eu^{3+} complex was specific to the target antigen. This was further confirmed when HFABP3 protein was used as a control against the same Eu^{3+} complex as shown in **Figure 4.6 to 4.8 B**. Here, the increased concentration of HFABP3 resulted in no detectable change in the fluorescence intensity of the Eu^{3+} complex. The percentage change in the fluorescence intensity comparing the targeted Eu^{3+} - Affimer complex against myoglobin versus the control protein, HFABP3, was quantified in a normalised data plot (**Figure 4.6 to 4.8 C**) and the photoluminescence intensity ratio (PLIR) of the transitions $5\text{D}^0 \rightarrow 7\text{F}^2$ and $5\text{D}^0 \rightarrow 7\text{F}^1$ (**Figure 4.6 to 4.8 D**) are shown. PLIR is essentially the integrated area

under the emission peaks and defined by the ratio of integrated intensity of electric dipole transition to magnetic dipole transition $I(604-640 \text{ nm})/I(570-604 \text{ nm})$. PLIR provides information about the distortion from local sites inversion symmetry of the Eu^{3+} in the ligand complex. The normalised data showed a statistically significant percentage change in fluorescence intensity of the targeted Eu^{3+} complex over all the three buffers. The percentage change in fluorescence intensity of the Eu^{3+} complex modified with human myoglobin Affimer in PBS showed a $\sim 5.5 \pm 1.09 \%$ difference at a concentration of 100 fM of the analyte ($P < .001$) and $\sim 15.6 \pm 1.09 \%$ difference at 100 nM ($P < .001$); whereas, in MOPS, the percentage change in fluorescence intensity showed a $\sim 5.8 \pm 1.14 \%$ difference at a concentration of 100 fM of the analyte ($P < .01$) and $\sim 15.4 \pm 0.24 \%$ difference at 100 nM ($P < .001$). In Tris buffer, the percentage change in fluorescence intensity of the same Eu^{3+} complex showed a $\sim 6.09 \pm 0.96 \%$ difference at a concentration of 100 fM of the analyte ($P < .01$) and $\sim 13.69 \pm 1.17 \%$ difference at 100 nM ($P < .001$).

Figure 4.6 to 4.8 C showed that the PLIR value, ranged from 1.4 to 1.3 in PBS; 1.9-1.8 in MOPS and 1.7-1.6 in Tris with increasing concentration of the human myoglobin. These findings indicate a strong deformation of the symmetry around the Eu^{3+} ion and that Eu^{3+} ion fluorescence changes are induced by changes within the ligand complex and not the surrounding environment. Considering the comparable results observed between the three different buffers, we decided to use PBS as the working buffer for all subsequent experiments, the reason being is that PBS is much cheaper and appears to be the closest match to human serum environment.

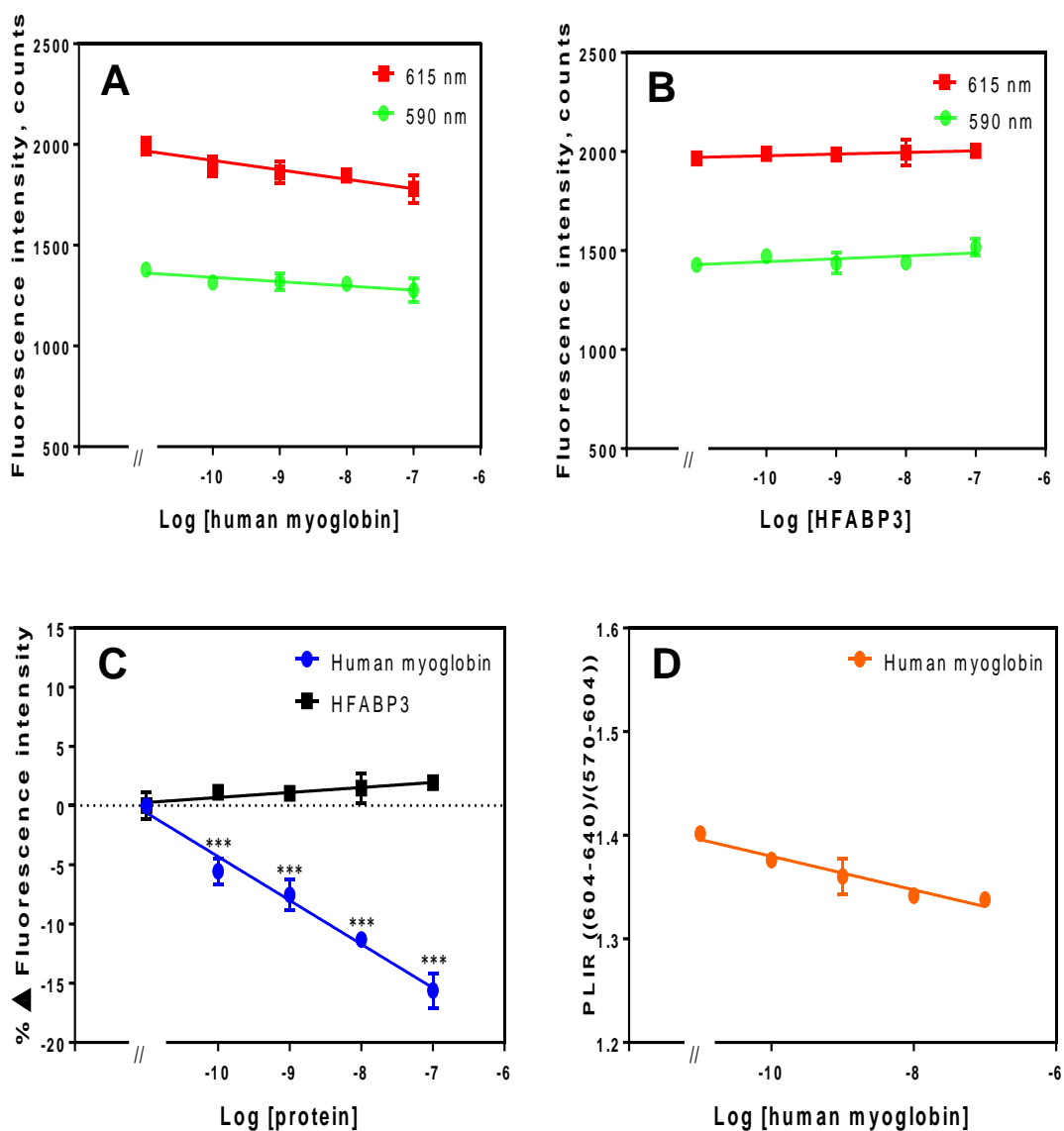


Figure 4.6 Fluorescence intensity spectra of Eu^{3+} chelated by PMDA modified anti- human myoglobin Affimer in PBS. Measurements were carried out in PBS, pH 7.4. (A), fluorescence intensity spectra of Eu^{3+} chelated by PMDA modified anti- human myoglobin Affimer; (B), fluorescence intensity spectra of same complex with HFABP3 added; (C), percentage change in fluorescence intensity; (D), photoluminescence intensity ratio ($\lambda_{\text{ex}} = 395 \text{ nm}$). Some error bars are smaller than data points (*, ** and *** with p -value < .05, .01, and .001 respectively indicate significance of the specific analyte (human myoglobin) compared to the control (HFAPB3) data). Data are means \pm SEM ($n = 4$).

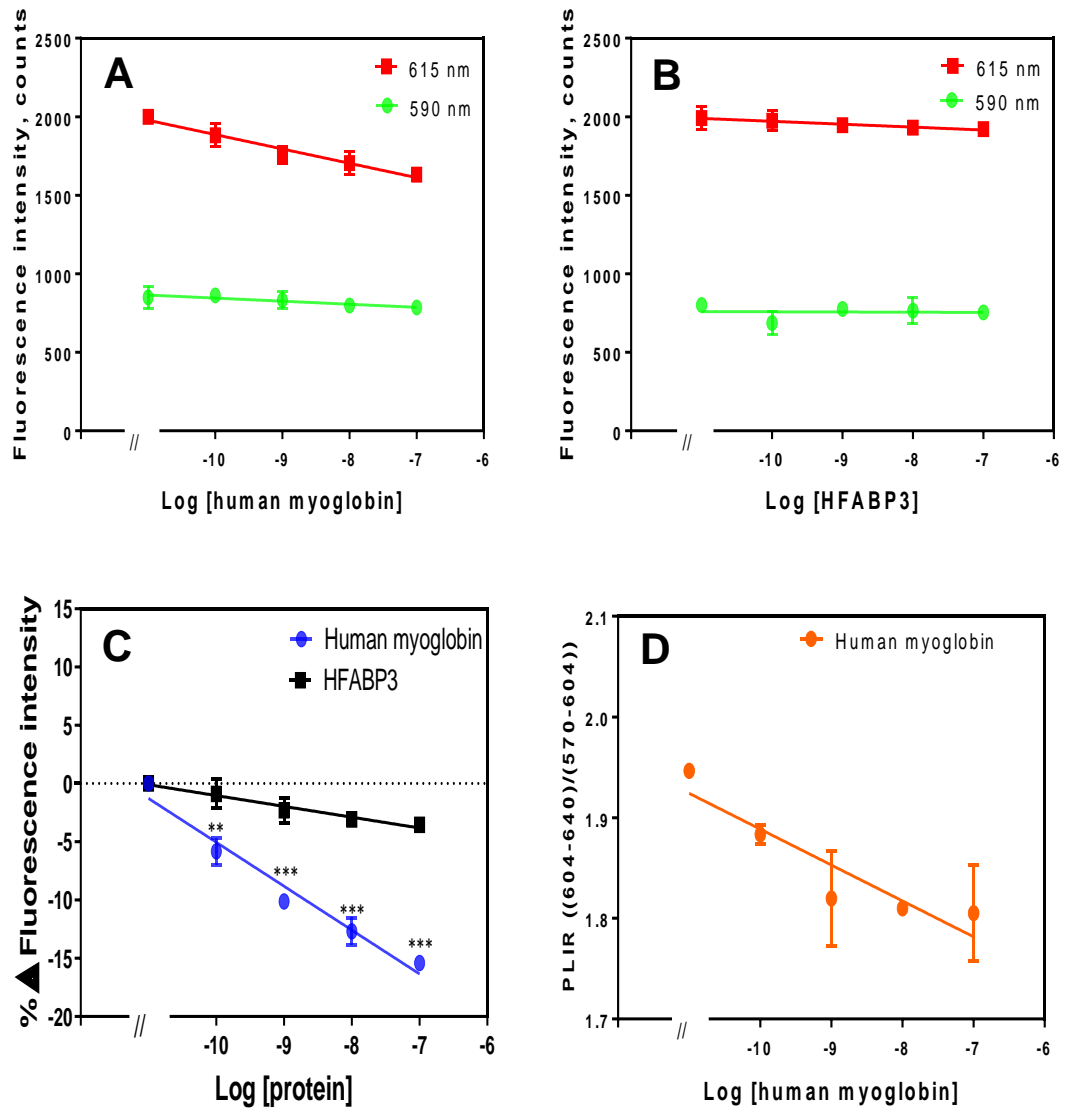


Figure 4.7 Fluorescence intensity spectra of Eu^{3+} chelated by PMDA modified anti-human myoglobin Affimer in MOPS. Measurements were performed in 50 mM MOPS, pH 7.4. (A), fluorescence intensity spectra of Eu^{3+} chelated by PMDA modified anti-human myoglobin Affimer; (B), fluorescence intensity spectra of same complex with HFABP3 added; (C), percentage change in fluorescence intensity; (D), photoluminescence intensity ratio ($\lambda_{\text{ex}} = 395 \text{ nm}$). Some error bars are smaller than data points (*, ** and *** indicate significance with p -value < .05, .01, and .001 respectively of the specific analyte (human myoglobin) compared to the control (HFABP3) data). Data are means \pm SEM ($n = 4$).

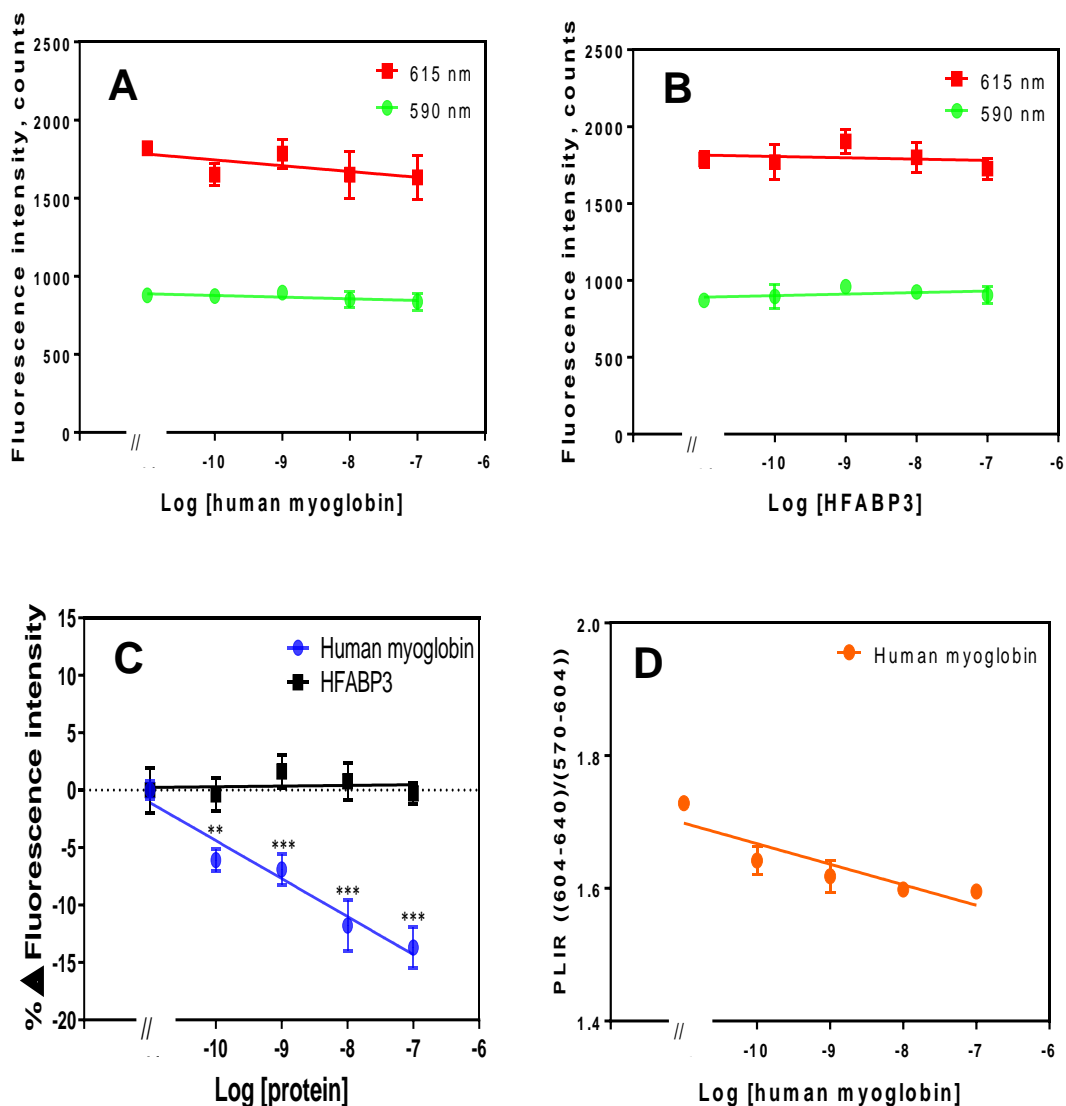


Figure 4.8 Fluorescence intensity spectra of Eu^{3+} chelated by PMDA modified anti-human myoglobin Affimer in Tris. Measurements were performed in 50 mM tris, pH 7.4. (A), fluorescence intensity spectra of Eu^{3+} chelated by PMDA modified anti-human myoglobin Affimer; (B), fluorescence intensity spectra of same complex with HFABP3 added; (C), percentage change in fluorescence intensity; (D), photoluminescence intensity ratio ($\lambda_{\text{ex}} = 395$ nm). Some error bars are smaller than data points (*, ** and *** indicate significance with p -value < .05, .01, and .001 respectively of the specific analyte (human myoglobin) compared to the control (HFABP3) data). Data are means \pm SEM (n= 4).

4.4.4 The selection criteria of the chelator ligand for the Eu^{3+} complex system

The optimised Eu^{3+} complex, thus far, was modified with PMDA to create a 3x carboxy chelating structure (**Figure 4.9**) and this has aided the selection of PBS as the appropriate buffer. However, we wanted to investigate a number of other chelators to ascertain whether changing the chelator could enhance the fluorescence quenching and hence the diagnostic accuracy of the biosensor. Three commonly used chelators; maleimido-monoamide-DOTA, DOTA-NHS-ester and p-SCN-Bn-DTPA (**Figure 4.10- 4.12**) were selected and tested in identical experimental settings.

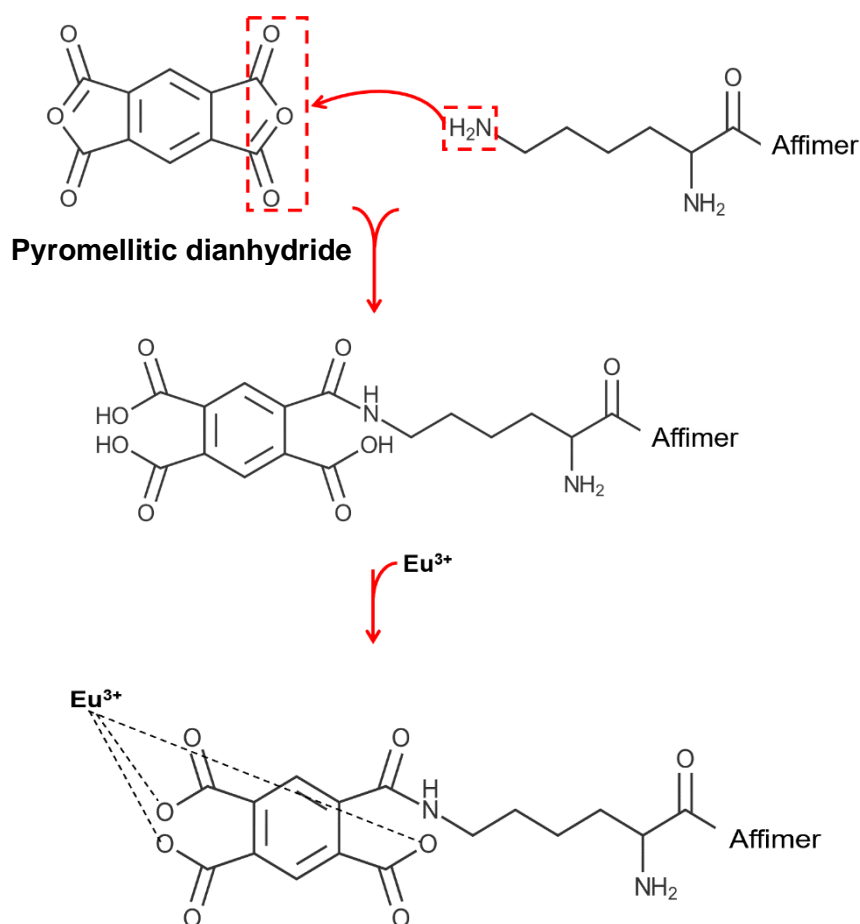


Figure 4.9 Schematic showing the reaction steps for Eu^{3+} chelated by PMDA modified Affimer. The lysine- NH_2 groups on Affimer scaffold react with anhydride group of PMDA creating one peptide bond and generating 3x $-\text{COO}^-$ carboxylic groups for Eu^{3+} chelation.

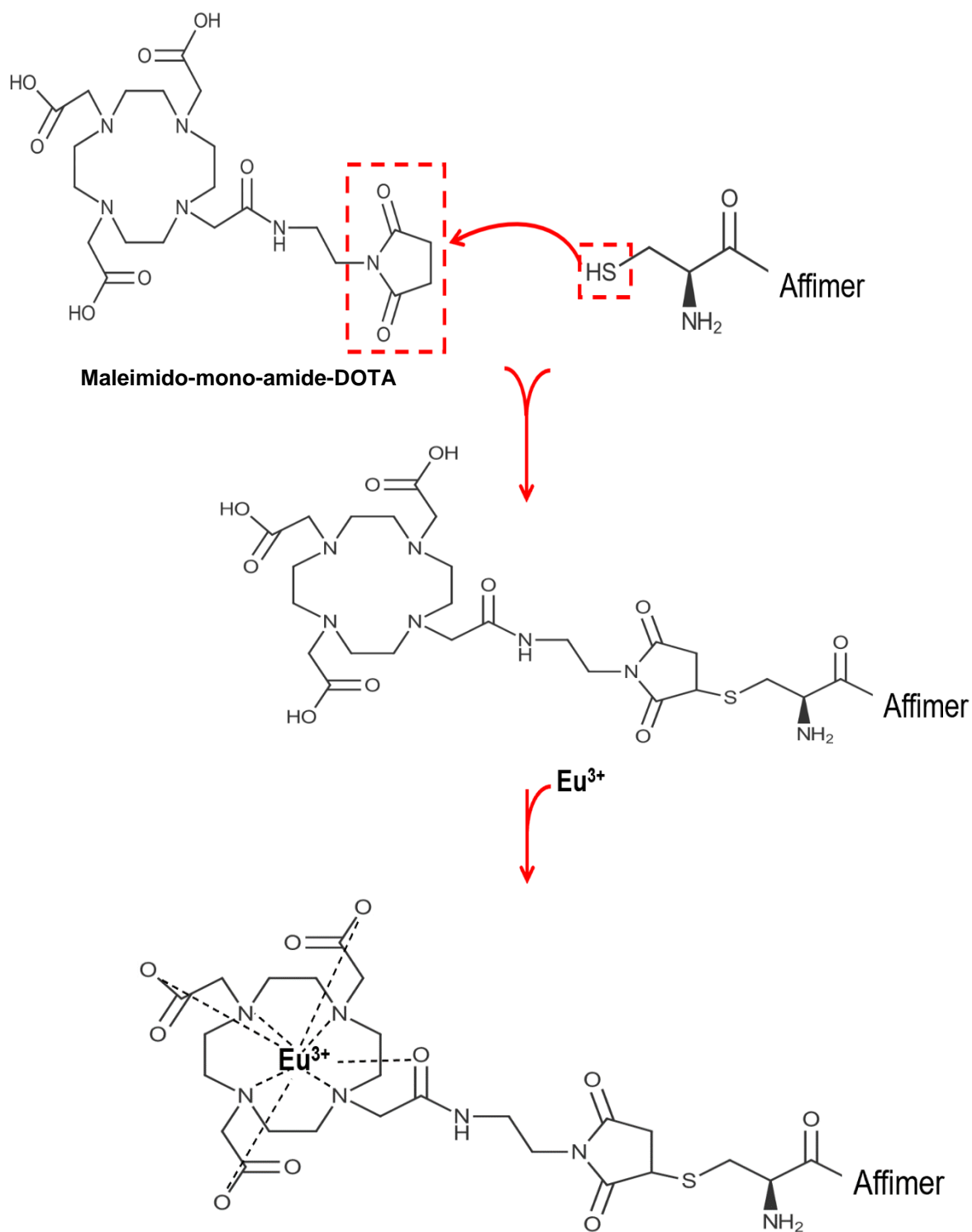


Figure 4.10 Schematic showing the reaction steps for Eu^{3+} chelated by maleimido-mono-amide-DOTA modified Affimer. The cysteine-SH on the Affimer scaffold reacts covalently with maleimido-mono-amide-DOTA through the maleimide moiety generating 3x $-\text{COO}^-$ carboxylic group and one amide carboxyl group for Eu^{3+} chelation.

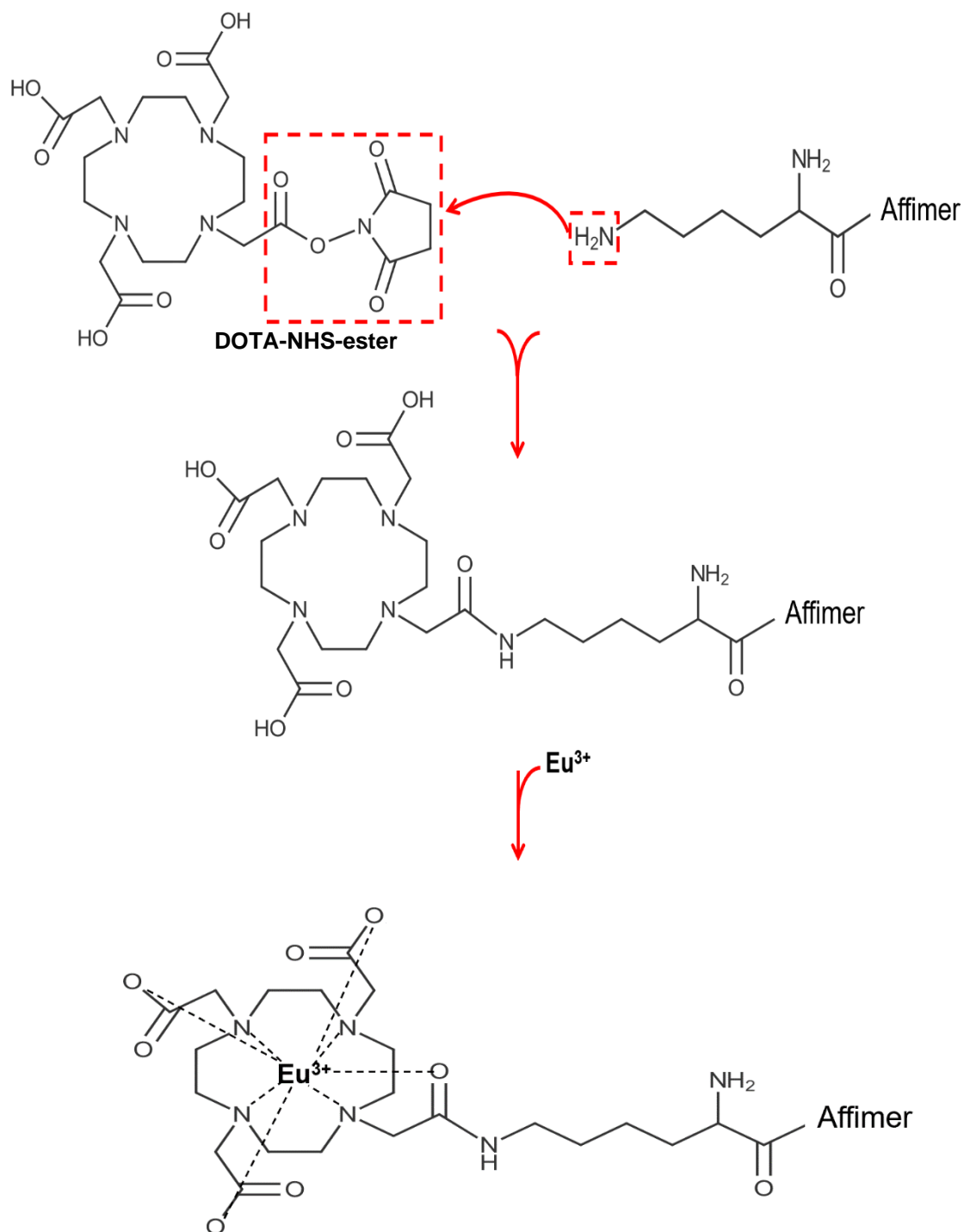


Figure 4.11 Schematic showing the reaction steps for Eu^{3+} chelated by DOTA-NHS-ester modified Affimer. The lysine-NH₂ group on the Affimer scaffold reacts with NHS-ester group of DOTA-NHS-ester creating one peptide bond and generating 3x -COO⁻ carboxylic groups one amide carboxyl group for Eu^{3+} chelation.

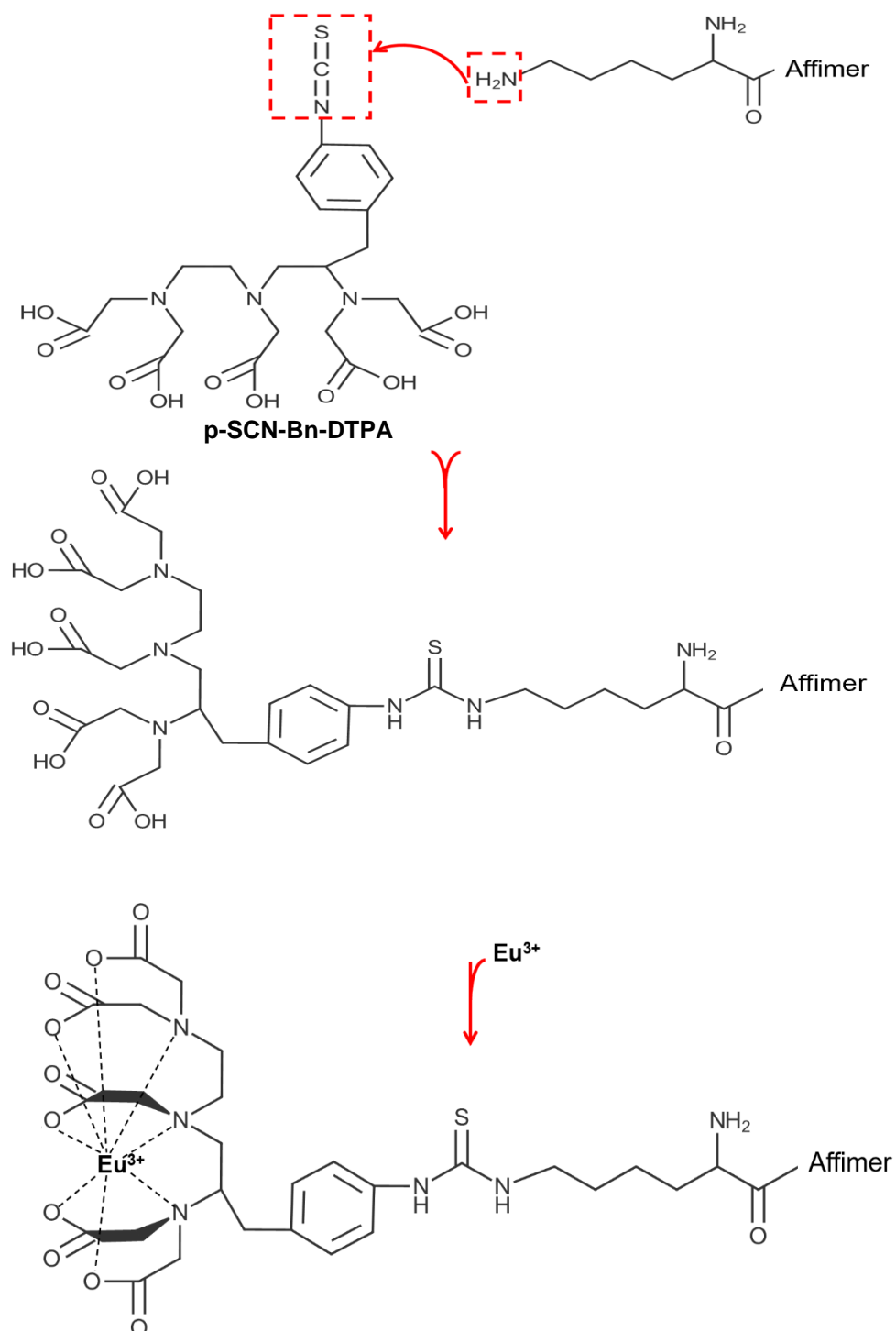


Figure 4. 12 Schematic showing the reaction steps for Eu³⁺ chelated by p-SCN-Bn-DTPA modified Affimer. The lysine-NH₂ on Affimer scaffold reacts with isothiocyanate of p-SCN-Bn-DTPA generating 5x -COO⁻ carboxylic groups for Eu³⁺ chelation.

The fluorescence intensity of the Eu^{3+} when incubated with Affimer modified chelators is shown in **Figure 4.13**. Theoretically, the fluorescence intensity should be enhanced due to the intramolecular energy transfer from the antenna on the ligand (chelator) to the Eu^{3+} . The data in **Figure 4.13** showed an increase in the fluorescence intensity spectra of the chelated Eu^{3+} with anti-human myoglobin Affimer modified by four different chelators (pyromellitic dianhydride, maleimido-monoamide-DOTA, DOTA-NHS-ester and p-SCN-Bn-DTPA) with no analyte added which are in keeping with the intramolecular energy transfer theory as fluorescence enhancement was observed across all chelator modified Affimers when compared to the base line of Eu^{3+} alone.

Eu^{3+} chelated by DOTA-NHS-ester modified anti-human myoglobin Affimer complex in PBS was tested against human myoglobin as shown in **Figure 4.14**. The percentage change in fluorescence intensity of the Eu^{3+} complex showed a $\sim 1.3 \pm 1.11$ % difference at a concentration of 100 fM of the analyte and $\sim 9.38 \pm 1.29$ % difference at 100 nM. Although, the data representing the DOTA-NHS-ester modified Affimer mediated Eu^{3+} complex showed a substantial fluorescence quenching, there was significant non-specific binding to the control protein HFAPB3. It is unclear as to what has led to the high non-specific binding but further optimisation and investigation into the experimental design may reduce the non-specific binding. P-SCN-Bn-DTPA is the longest chelator and interestingly there was no significant fluorescence quenching observed as shown in **Figure 4.15**. Equally the PLIR plot showed negligible change from 1.2-1.19 which is in sharp contrast to data from PMDA and DOTA-NHS-ester chelated complexes. It is worth mentioning that three chelators were conjugated to the Affimer via lysine. Conjugation via cysteine on the Affimer is another potential site for linking the chelator to the Affimer and therefore, maleimido-monoamide-

DOTA was tested as another chelator for producing the Eu^{3+} complex (**Figure 4.16**). The percentage change in fluorescence intensity of the Eu^{3+} complex showed a $\sim 4.86 \pm 1.06$ % difference at a concentration of 100 fM of the analyte ($P < .05$) and showed a significant fluorescence quenching at around $\sim 17.08 \pm 0.58$ % difference at 100 nM when compared to control $\sim 2.7 \pm 0.99$ % ($P < .001$). Similarly, The PLIR plot showed a 1.38-1.24 change in keeping with the results in **Figure 4.6** where PMDA modified lysine was the chelator.

Collectively, PMDA and maleimido-monoamide-DOTA chelators allow specific and substantial fluorescence quenching in the Eu^{3+} complex. PMDA was selected to be the chelator of choice for the complex as it is widely used, readily available, small so can position the Affimer next to Eu^{3+} and significantly less expensive than maleimido-monoamide-DOTA.

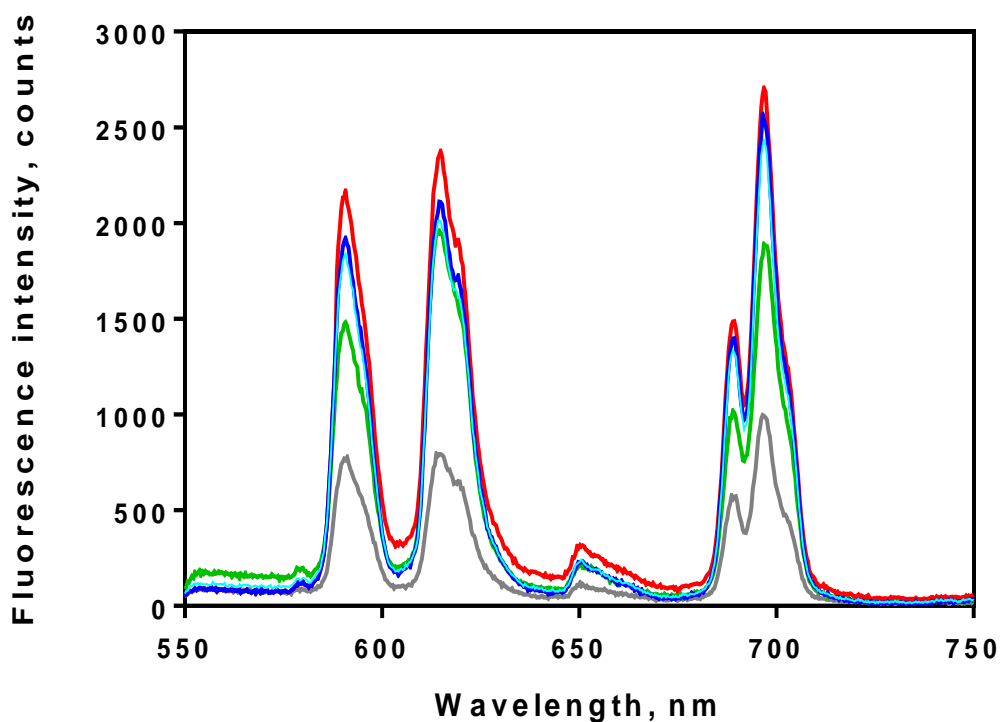


Figure 4.13 Fluorescence intensity spectra of the chelated Eu^{3+} with anti-human myoglobin Affimer modified by four different chelators. Emission wavelengths for Eu^{3+} complexes were measured and plotted for Eu^{3+} , (—); Eu^{3+} chelated by PMDA modified human myoglobin, (—); Eu^{3+} chelated by DOTA-NHS-ester modified human myoglobin, (—); Eu^{3+} chelated by maleimido-monoamide-DOTA modified human myoglobin (—) and Eu^{3+} chelated by p-SCN-Bn-DTPA modified human myoglobin, (—) $\lambda_{\text{ex}} = 395 \text{ nm}$.

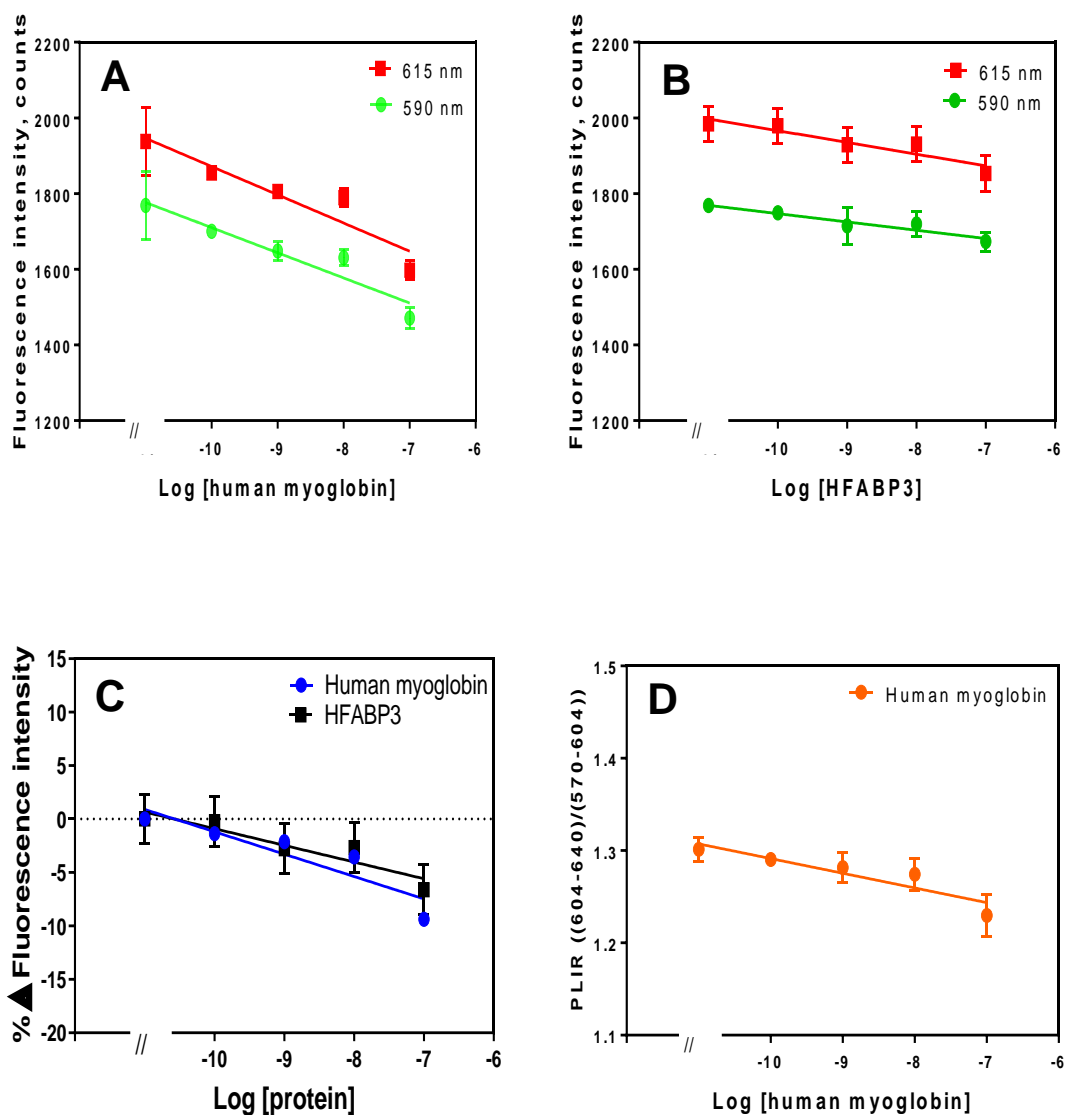


Figure 4.14 Fluorescence quenching of DOTA-NHS-ester modified anti-human myoglobin Affimer. (A), fluorescence intensity spectra of Eu^{3+} chelated by DOTA-NHS-ester modified anti- human myoglobin Affimer; (B), fluorescence intensity spectra of the same complex after HFABP3 added; (C), percentage change in fluorescence intensity; (D), photoluminescence intensity ratio, $\lambda_{\text{ex}}= 395$ nm. Data are means \pm SEM ($n= 6$). Some error bars are smaller than data points.

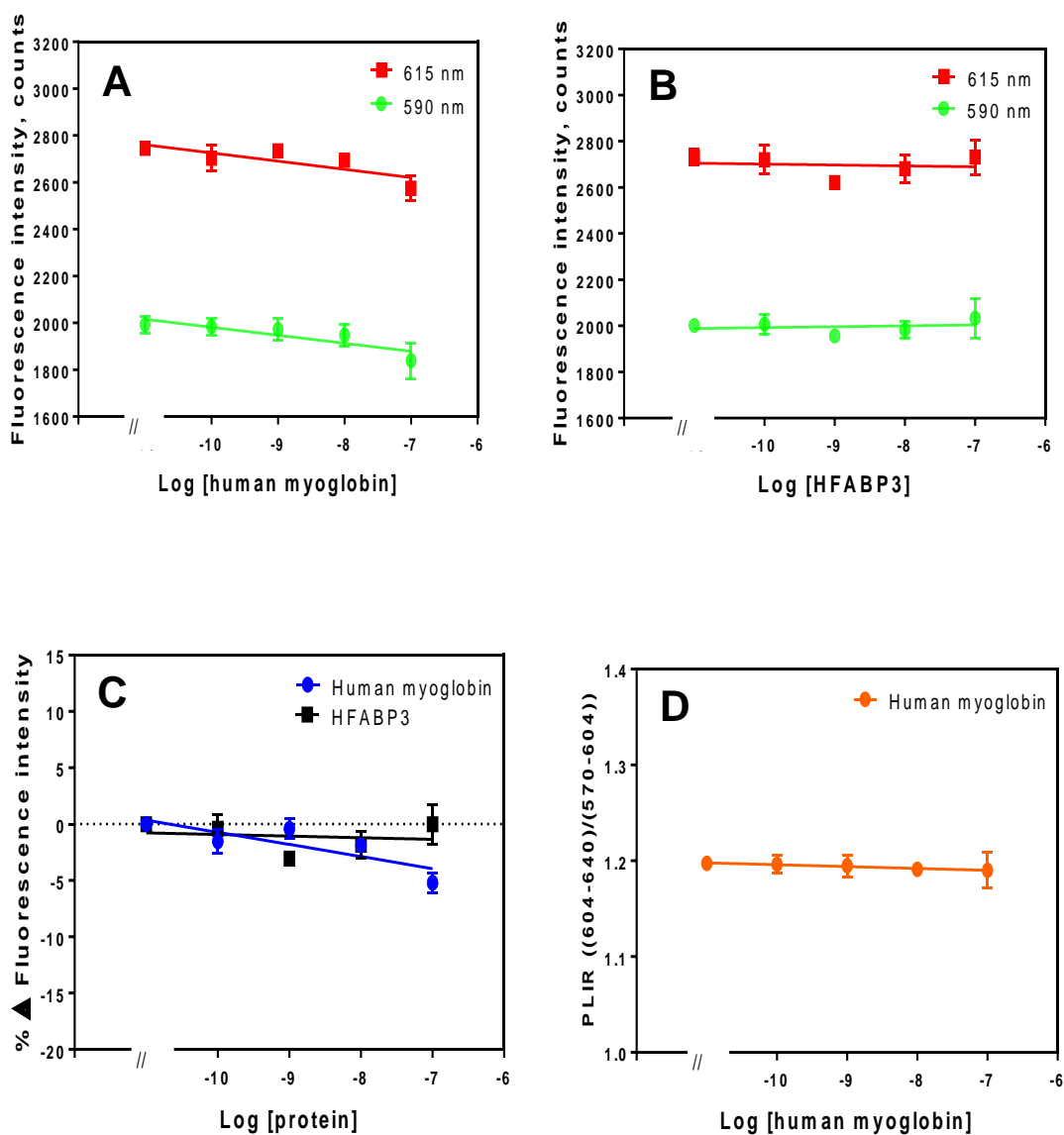


Figure 4.15 Fluorescence quenching of p-SCN-Bn-DTPA modified anti-human myoglobin Affimer. (A), fluorescence intensity spectra of Eu^{3+} chelated by p-SCN-Bn-DTPA modified anti-human myoglobin Affimer; (B), fluorescence intensity spectra of the same complex after HFABP3 added; (C), percentage change in fluorescence intensity; (D), photoluminescence intensity ratio, $\lambda_{\text{ex}}=395$ nm. Data are means \pm SEM ($n=6$). Some error bars are smaller than data points.

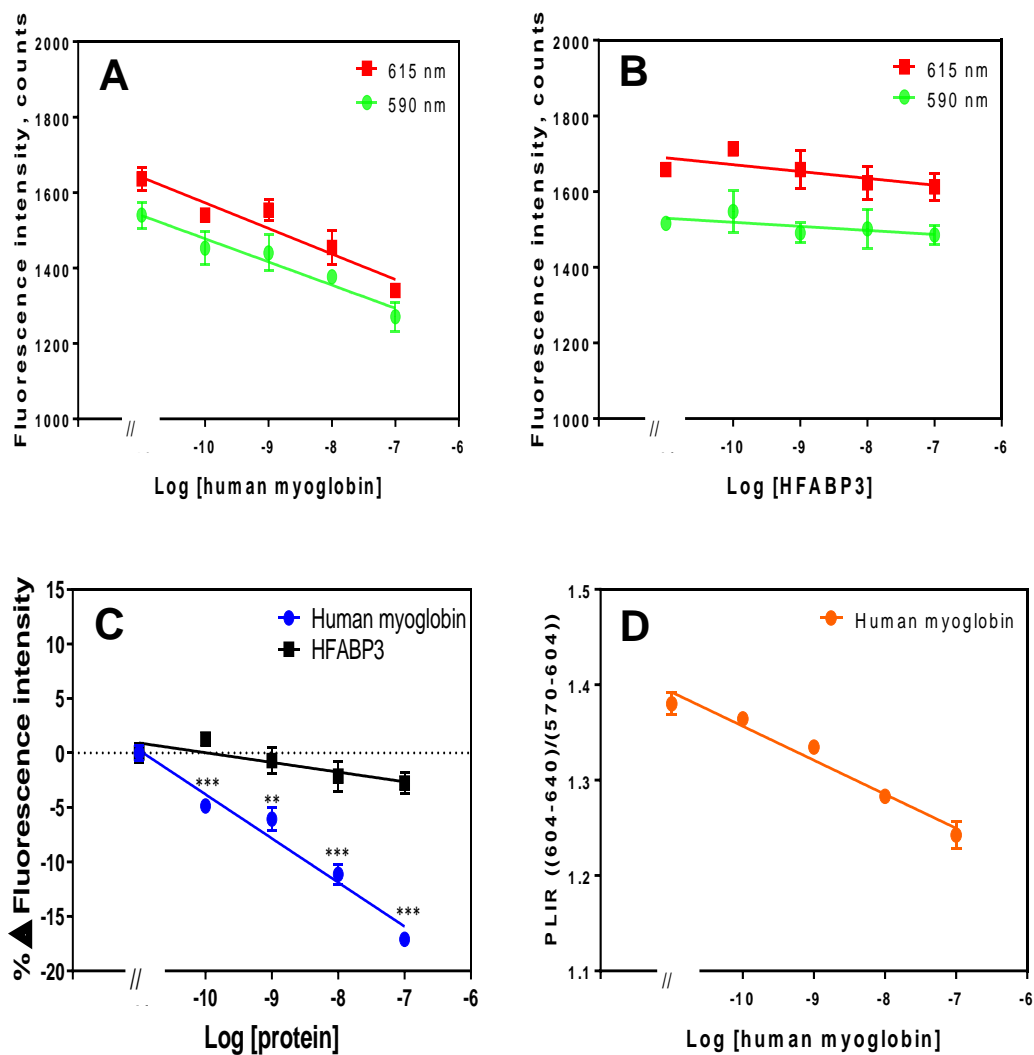


Figure 4.16 Fluorescence quenching of maleimido-mono-amide-DOTA modified anti-human myoglobin Affimer. (A), fluorescence intensity spectra of Eu^{3+} chelated by maleimido-mono-amide-DOTA modified anti-human myoglobin Affimer; (B), fluorescence intensity spectra of the same complex after HFABP3 added; (C), percentage change in fluorescence intensity; (D), photoluminescence intensity ratio, $\lambda_{\text{ex}} = 395 \text{ nm}$. Data are means \pm SEM ($n = 6$). Some error bars are smaller than data points (*, ** and *** indicate significance with p -value $< .05$, $.01$, and $.001$ respectively of the specific analyte (human myoglobin) compared to the control (HFABP3) data).

4.4.5 Fluorescence intensity of Eu³⁺ chelated PMDA modified anti- human myoglobin Affimer complex in human serum

The fluorescence spectrum of Eu³⁺ chelated by PMDA- modified anti-human myoglobin Affimer was investigated in 1, 2.5 and 5% (v/v) human serum samples. The Eu³⁺ complex was tested against different concentrations of human myoglobin in presence of human serum. The fluorescence intensity peaks in 1% (v/v) human serum were measured and plotted as shown in **Figure 4.17**. The fluorescence intensity of the Eu³⁺ complex changed substantially with increasing concentration of human myoglobin. The fluorescence intensities for the Eu³⁺ complex with different concentrations of human myoglobin are shown in **Figure 4.17 A**. The data show that the Eu³⁺ complex specifically binds to human myoglobin allowing significant fluorescence quenching of Eu³⁺. Importantly, there was no significant change in the fluorescence intensity when the control protein HFABP3 was added (**Figure 4.17 B**). The percentage change in fluorescence intensity in the Eu³⁺ complex modified with human myoglobin Affimer showed a $\sim 2.88 \pm 0.59$ % difference at a concentration of 100 fM of the analyte ($P < .05$) and $\sim 15.60 \pm 0.65$ % difference at 100 nM ($P < .005$). The PLIR result for the Eu³⁺ complex modified with human myoglobin was > 1 at 1.78-1.6.

In 2.5 % (v/v) human serum, the percentage change in fluorescence intensity showed a smaller, $\sim 4.68 \pm 0.99$ % difference at a concentration of 100 pM of the analyte ($P < .05$) and $\sim 10.85 \pm 1.62$ % difference at 100 nM ($P < .005$) while the PLIR value decreased to > 1 at 1.2-1.18 (**Figure 4.18**). However, when using the same complex in 5 % (v/v) human serum there was no significant fluorescence quenching observed most likely due to non-specific binding to other proteins in the human serum (**Figure 4.19**).

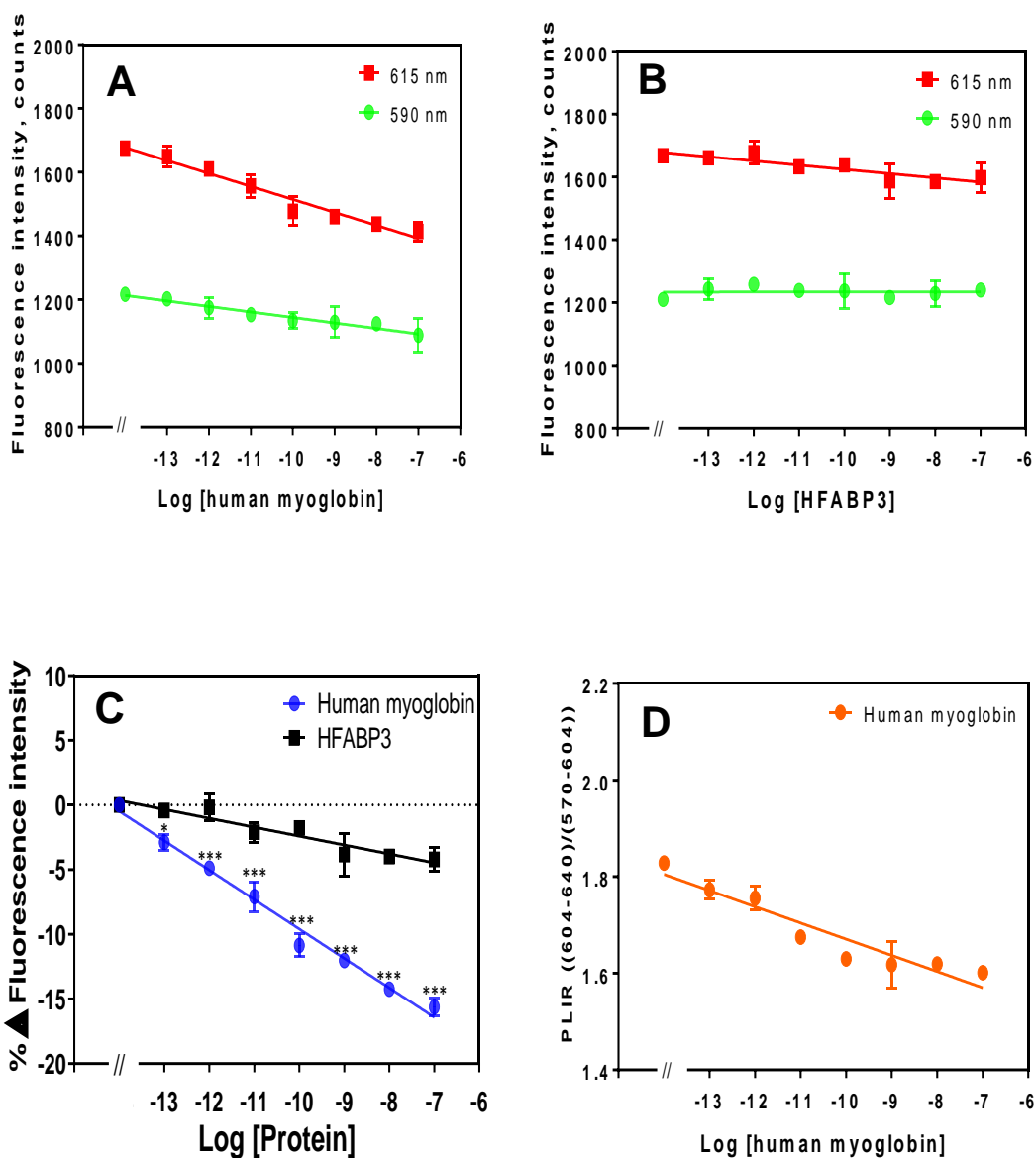


Figure 4.17 Fluorescence intensity spectra of Eu^{3+} chelated by PMDA modified anti-human myoglobin Affimer complex in 1% (v/v) human serum. Fluorescence was measured at 590 and 615 nm with $\lambda_{\text{ex}} = 395$ nm. (A), fluorescence intensity spectra of Eu^{3+} chelated PMDA modified anti-human myoglobin Affimer; (B), fluorescence intensity spectra of the same complex after HFABP3 added; (C), percentage change in fluorescence intensity; (D), photoluminescence intensity ratio. Data are means \pm SEM ($n = 6$). Some error bars are smaller than data points (*, ** and *** indicate significance with p -value $< .05$, $.01$, and $.001$ respectively of the specific analyte (human myoglobin) compared to the control (HFABP3) data).

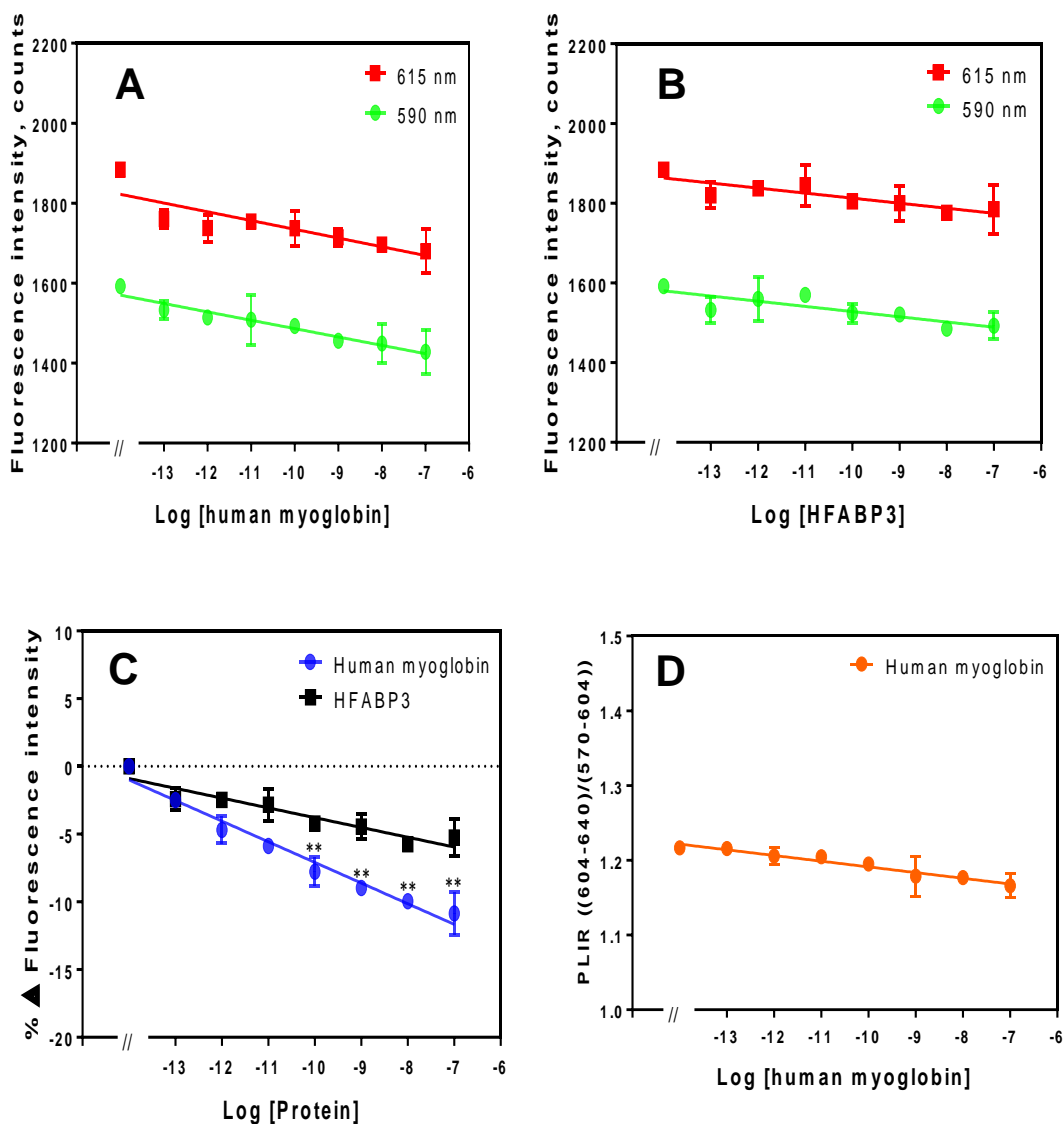


Figure 4.18 Fluorescence intensity spectra of Eu^{3+} chelated by PMDA modified anti- human myoglobin Affimer complex in 2.5 % (v/v) human serum. Fluorescence was measured at 590 and 615 nm with $\lambda_{ex}=395$ nm. (A), fluorescence intensity spectra of Eu^{3+} chelated PMDA modified anti- human myoglobin Affimer; (B), fluorescence intensity spectra of the same complex after HFABP3 added; (C), percentage change in fluorescence intensity; (D), photoluminescence intensity ratio. Data are means \pm SEM (n= 6). Some error bars are smaller than data points (*, ** and *** indicate significance with p -value < .05, .01, and .001 respectively of the specific analyte (human myoglobin) compared to the control (HFAPB3) data).

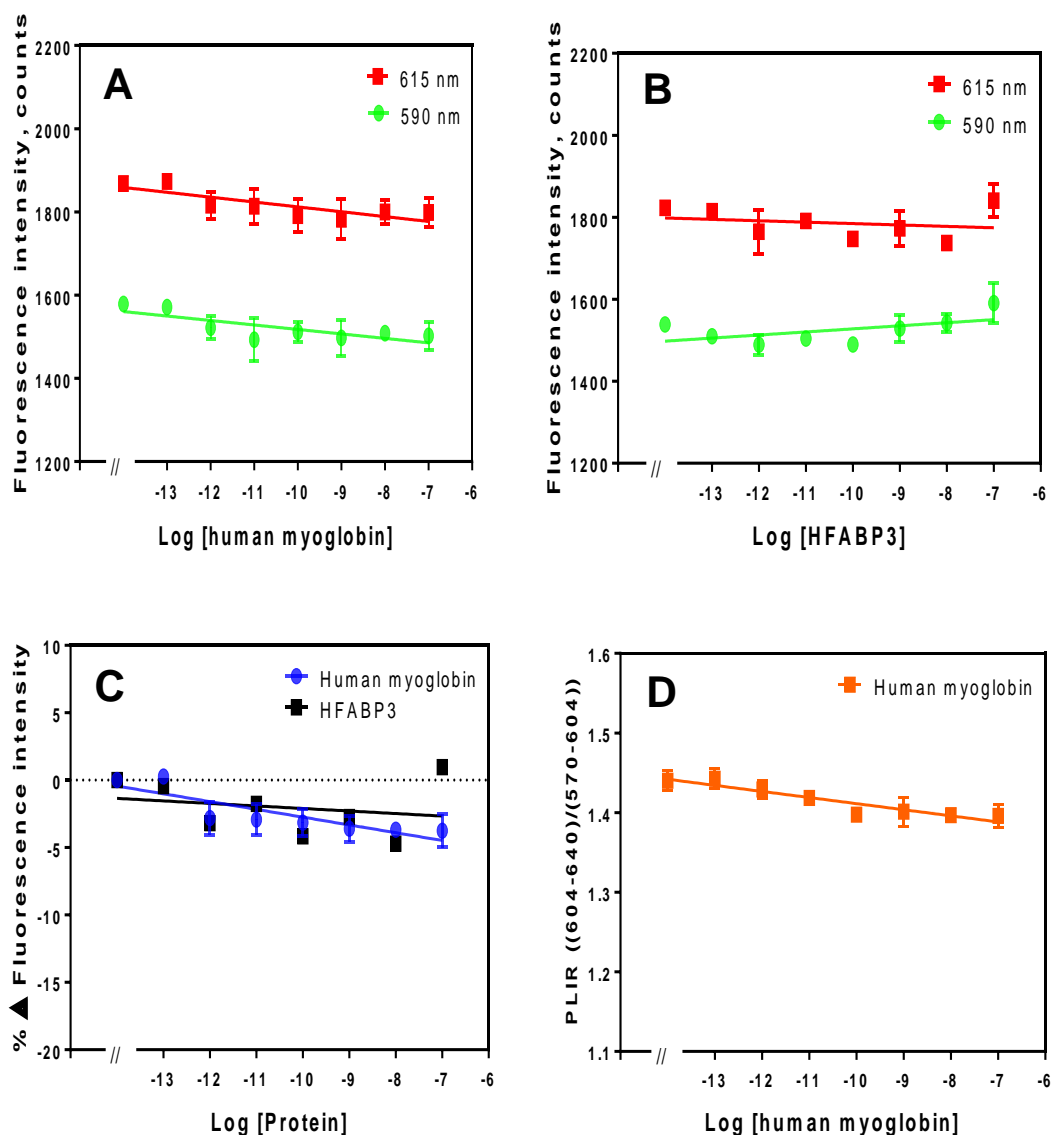


Figure 4.19 Fluorescence intensity spectra of Eu^{3+} chelated by PMDA modified anti-human myoglobin Affimer complex in 5% (v/v) human serum. Fluorescence was measured at 590 and 615 nm with $\lambda_{\text{ex}} = 395$ nm. (A), fluorescence intensity spectra of Eu^{3+} chelated PMDA modified anti-human myoglobin Affimer; (B), fluorescence intensity spectra of the same complex after HFABP3 added; (C), percentage change in fluorescence intensity; (D), photoluminescence intensity ratio. Data are means \pm SEM ($n = 6$). Some error bars are smaller than data points.

4.4.6 Fluorescence intensity of Eu³⁺ chelated PMDA modified anti- GFAP Affimer complex in 1, 2.5 and 5 % (v/v) human serum

The biomarker, GFAP, is elevated after ischemic stroke. It is distinct from myoglobin and has a larger Mr (17 KDa for myoglobin vs 55 KDa for GFAP) was also selected to test the Eu³⁺ complex specificity. In a similar manner, the fluorescence spectra of Eu³⁺ chelated by PMDA- modified anti- GFAP Affimer was investigated in 1, 2.5 and 5 % (v/v) human serum samples as shown in **Figure 4.20 to 4.22**. The results show that the fluorescence intensity of Eu³⁺ complex changed significantly with increasing concentration of GFAP indicating specific Eu³⁺ complex binding to the analyte and hence fluorescence quenching of Eu³⁺. The fluorescence intensity of the complex showed insignificant non-specific binding when incubated with the control protein HFABP3. The percentage change in fluorescence intensity in the targeted Eu³⁺ complex in 1 % (v/v) human serum showed a $\sim 2.22 \pm 0.85$ % difference at a concentration of 100 fM of the analyte ($P < .005$) and $\sim 10.82 \pm 1.08$ % difference at 100 nM ($P < .001$). The PLIR results for the same Eu³⁺ complex also remained > 1 at 1.39-1.25 (**Figure 4.20**). When tested in 2.5 % (v/v) human serum, the percentage change was $\sim 1.14 \pm 0.77$ % at a concentration of 100 pM of the analyte ($P < .05$) and $\sim 7.81 \pm 1.08$ % difference at 100 nM ($P < .005$) with the PLIR value being > 1 at 1.2-1.18 (**Figure 4.21**). There was no fluorescence quenching observed when using the Eu³⁺ complex in 5 % (v/v) human serum (**Figure 4.22**).

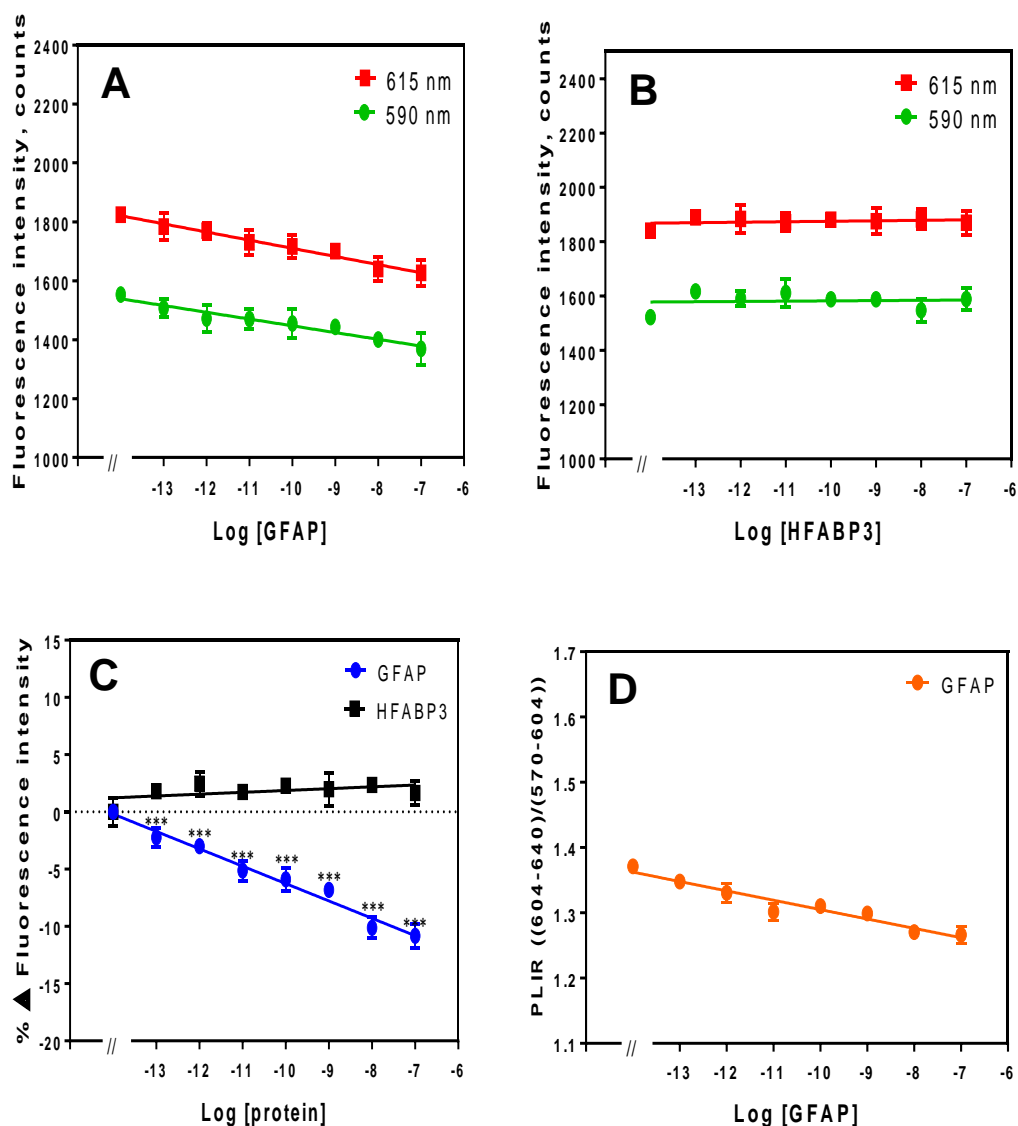


Figure 4.20 Fluorescence intensity spectra of Eu^{3+} chelated by PMDA modified GFAP Affimer complex in 1 % (v/v) human serum. Fluorescence was measured at 590 and 615 nm with $\lambda_{\text{ex}} = 395$ nm. (A), fluorescence intensity spectra of Eu^{3+} chelated PMDA modified GFAP Affimer; (B), fluorescence intensity spectra of the same complex after HFABP3 added; (C), percentage change in fluorescence intensity; (D), photoluminescence intensity ratio. Data are means \pm SEM ($n = 6$). Some error bars are smaller than data points (*, ** and *** indicate significance with p -value $< .05$, $.01$, and $.001$ respectively of the specific analyte (GFAP) compared to the control (HFABP3) data).

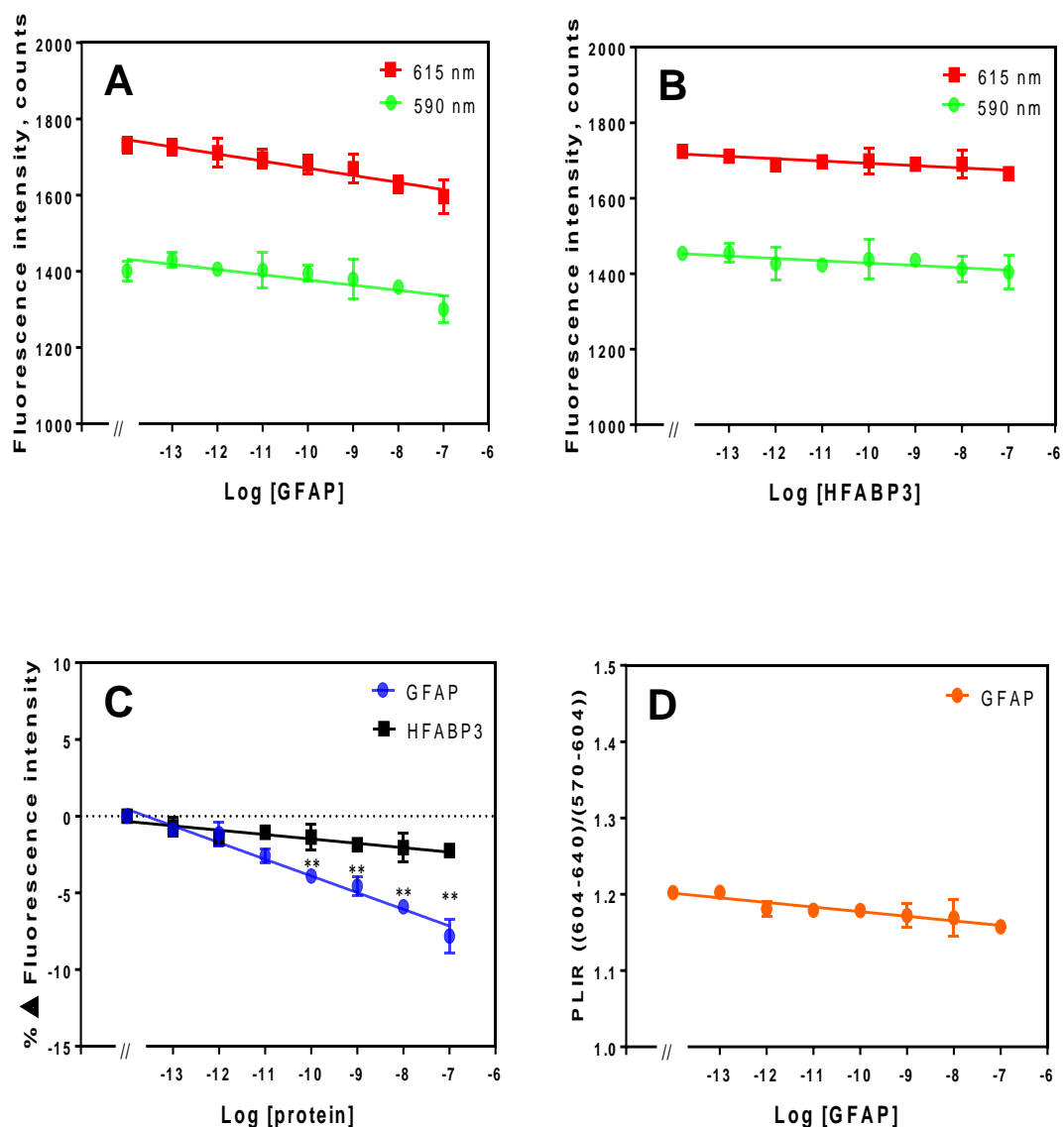


Figure 4.21 Fluorescence intensity spectra of Eu^{3+} chelated by PMDA modified GFAP Affimer complex in 2.5 % (v/v) human serum. Fluorescence was measured at 590 and 615 nm with $\lambda_{ex}= 395$ nm. (A), fluorescence intensity spectra of Eu^{3+} chelated PMDA modified GFAP Affimer; (B), fluorescence intensity spectra of the same complex after HFABP3 added; (C), percentage change in fluorescence intensity; (D), photoluminescence intensity ratio. Data are means \pm SEM (n= 6). Some error bars are smaller than data points (*, ** and *** indicate significance with p -value < .05, .01, and .001 respectively of the specific analyte (GFAP) compared to the control (HFAPB3) data).

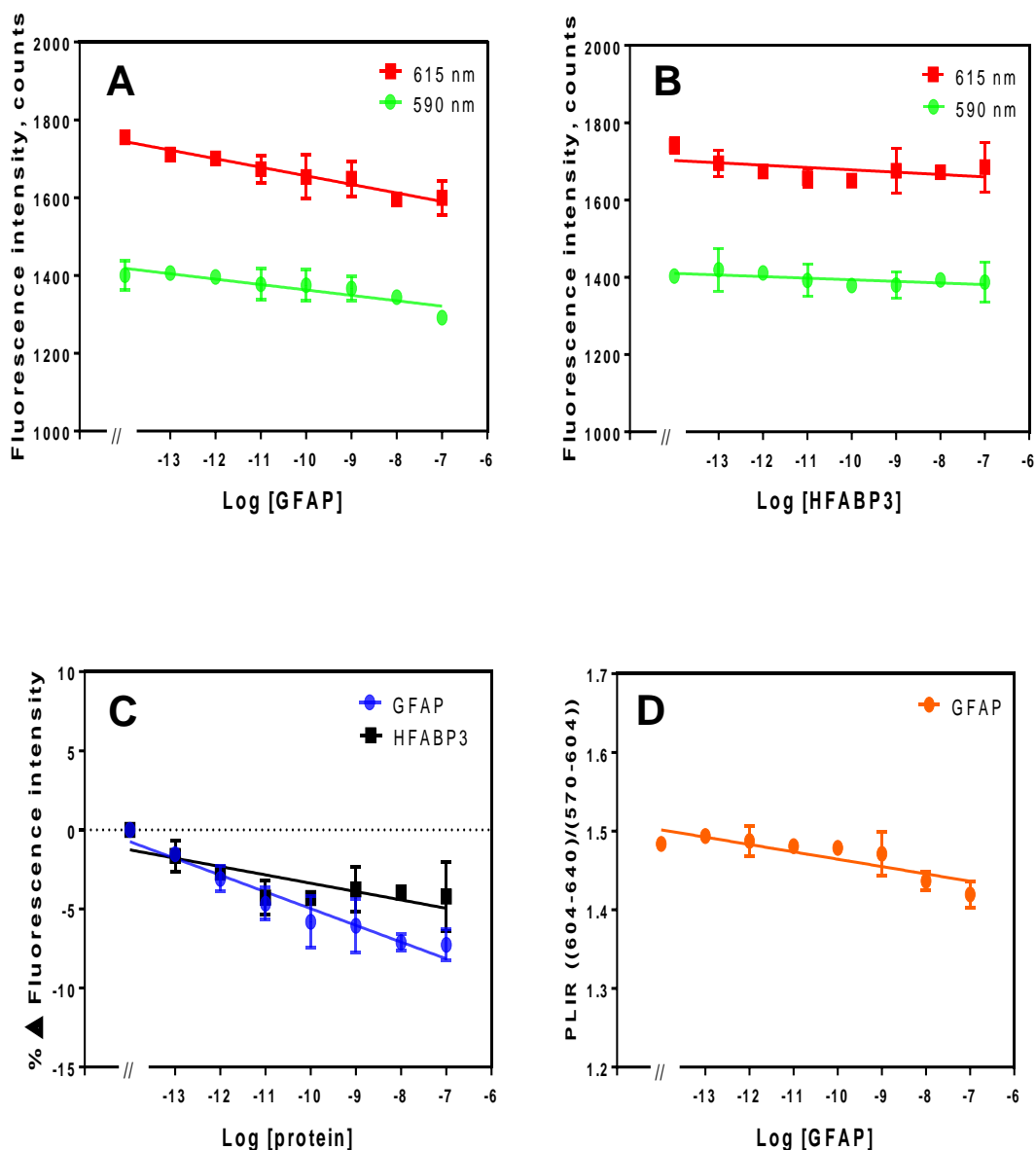


Figure 4.22 Fluorescence intensity spectra of Eu^{3+} chelated by PMDA modified GFAP Affimer complex in 5 % (v/v) human serum. Fluorescence was measured at 590 and 615 nm with $\lambda_{\text{ex}} = 395$ nm. (A), fluorescence intensity spectra of Eu^{3+} chelated PMDA modified GFAP Affimer; (B), fluorescence intensity spectra of the same complex after HFABP3 added; (C), percentage change in fluorescence intensity; (D), photoluminescence intensity ratio. Data are means \pm SEM ($n = 6$). Some error bars are smaller than data points.

4.5 Discussion

The data presented in this chapter are the first to suggest a specific Eu^{3+} complex for the purpose of optical biosensing of human analytes using an Affimer as a bioreceptor. Using a biochemical approach, whereby Affimer scaffold lysine residues were modified to introduce three carboxy groups able to effectively chelate the Eu^{3+} . After optimisation in PBS the system was tested in diluted human serum. A systematic approach was used to develop a robust system. The Eu^{3+} was excited at 395 nm while the emission wavelengths were 590 and 615 nm. The optimisation experiments with the Eu^{3+} complex revealed that 100 μM Eu^{3+} concentration chelated to PMDA modified Affimer in PBS buffer and allowed sensitive detection of targeted analytes based on fluorescence quenching. When the Eu^{3+} complex was tested in human serum the system was able to detect as low as 100 fM of the analyte's concentrations but the system would only tolerate up to 2.5 % (v/v) human serum. The percentage change in Eu^{3+} complex fluorescence when incubated with human myoglobin and GFAP confirmed the high sensitivity of the system at detecting different analytes. In the next chapter (**Chapter 5**) we show that other, much higher Mr biomarker protein can also be measured.

The challenge in developing a lanthanide complex for biosensing against a specific analyte is to produce a stable detection system with reliable binding properties between the bioreceptor on the complex and the target analyte. Eu^{3+} complexes were reported to be used as luminescent probes sensing H_2S , triplet oxygen, H_2O_2 and nitric oxide (Pershagen et al., 2012, Szijjártó et al., 2013, Peng and Xian, 2014, Tropiano and Faulkner, 2014, Thorson et al., 2015). A common theme between all these Eu^{3+} complexes was the activation of an irreversible

transformation of the ligand. The Eu^{3+} complex detection mechanism of the target analyte was based on Eu^{3+} emission enhancement. Although, all of the complexes allowed an efficient change in fluorescence response, the systems were of limited use. The main disadvantage of the systems was irreversibility. Accordingly, the design of such a system was useless for the purpose of our application where an accurate measurement of analyte concentration is important.

Other interesting designs are probes for amino acids and protein detection (Pazos et al., 2008, Hirayama et al., 2009, Jiang et al., 2010, Tsukube et al., 2010, Wang et al., 2011, Terai et al., 2012a, Zhang et al., 2012a, Terai et al., 2012b) , although selective detection of specific amino acids is very challenging because they share the same amine and carboxylic acid functional groups, Shinoda's group (2014) were successful at establishing a combinatorial library to enhance lanthanide emission for selected amino acids. The library consisted of four different lanthanides (Eu^{3+} , Tb^{3+} , Nd^{3+} , Yb^{3+}), seven N- heteroaromatics and seven amino acid substrates to obtain 196 combinations (Wang et al., 2014). Nonetheless, the responsive fluorescence of the complex was dependent primarily on the ligands employed and again did not allow specific concentration measurement. It would be almost impossible to detect analyte concentration using this system. The introduction of a protein targeting group to the ligand as an antenna enhanced luminescent lanthanide complexes for specific sensing of specific proteins. Guo's group (2011), reported a Tb^{3+} complex with metronidazole as ligand, as the luminescent sensor for human serum albumin (HAS) (Wang et al., 2011). They reported an increased emission intensity of Tb^{3+} upon addition of HAS. To date, there are no reports in the literature that describes a lanthanide complex system which allows specific analyte sensing and

concentration measurements simultaneously. Our Eu^{3+} complex system appears to be the first to achieve this. The ligand in our system consists of PMDA modified lysine- NH_2 groups acting as chelators on an Affimer. Our hypothesis was that conjugating the ligand to the Affimer would aid establishing rapid and reliable system while the detection specificity would be enhanced via the bioreceptor recognition. Design of the experiments allowed appropriate use of control Affimer- Eu^{3+} complex and not just Eu^{3+} complex. This is a feature that allowed the quantification of fluorescence quenching to enable statistical comparison.

4.5.1 The selection criteria of the chelator ligand for the Eu^{3+} complex system

Considering the four different Eu^{3+} chelating structures, the choice of chelating group was dictated by its ability to chelate Eu^{3+} efficiently and link to the Affimer in a stable reaction. Four different chelators were investigated for this purpose, all of which are classified as type 1 complex system. Different linkage strategies were employed in order to ensure correct analyte binding site orientation on the Affimer in attempt to increase the sensitivity of the system.

PMDA is chelator that has two acid anhydride groups. After reaction of one anhydride with a lysine- NH_2 group, creating a peptide bond and a pendant – COO^- group, it is most likely that the second anhydride is hydrolysed to create two more – COO^- . Although, this yields 3x – COO^- to chelate the Eu^{3+} . The modification strategy was designed based on protocols from other groups (Hassani, 2012, Dixon and Perham, 1968). Our results are in keeping with their findings confirming the linkage strategy between PMDA and the Affimer and

PMDA chelation of the COO^- created with Eu^{3+} . PMDA was the smallest and cheapest chelator amongst others tested.

Maleimido-mono-amide-DOTA is a bifunctional molecule as it can chelate lanthanide ions via carboxylic groups while the maleimide moiety readily reacts covalently with thiol groups on either protein scaffolds or cell membrane (Bodenmiller et al., 2012). Affimers contain a single cysteine at the C-terminus so it is worth investigation as to whether modification via this functional group would enhance the binding sensitivity of the Affimer to the analytes. The data using the maleimido-mono-amide-DOTA as chelator for Eu^{3+} complex were comparable to those observed when using the PMDA. Both systems met the criteria for analyte detection but maleimido-mono-amide-DOTA is much more expensive at around six times the cost of PMDA. In addition, utilising the cysteine as a conjugation site requires TCEP reduction free the thiol functional group on the Affimer before modification with maleimido-mono-amide-DOTA.

A large number of DOTA-NHS-ester molecules have been synthesised, some of which are used in clinical application for the treatment of Non-Hodgkin's lymphoma (VF Massicano et al., 2016). Lysines are the main sites for conjugation, but others have also reported conjugation using the thiol groups of cysteine residues with DOTA maleimide derivatives under mild neutral conditions (Lewis and Shively, 1998, Li et al., 2002). Our results demonstrated non-specific binding by the control Affimers which rendered the targeted Eu^{3+} complex unsuitable.

P-SCN-Bn-DTPA has been previously used as a metal chelator in the development of receptor binding assays. Zhang *et al* (2012) reported that they were able to design Eu^{3+} complex chelated to P-SCN-Bn-DTPA to insulin-like

peptide 3 protein (Zhang et al., 2012b). They were able to establish a cell-based receptor -binding assay for screening of novel relaxin family peptide receptor 2 (RXFP2) agonist or antagonists. In our experiment, we observed a non-specific binding in the control Affimer, a feature that was not reported by Zhang et al (2012). However, their experiments were carried out using a cell-based binding assay in a 96 well plate while ours was in diluted human serum. Further optimisation steps would be warranted in order to investigate the non-specific binding results and how to overcome this problem.

Chapter five:

**Time resolved fluorescence
assay using Affimer chelated
Eu³⁺**

Chapter 5

Time resolved fluorescence assay using Affimer chelated Eu³⁺

5.1 Introduction

Bioanalytical assays for the measurement of protein biomarkers should be highly sensitive and specific. Measurements are often carried out with the sample medium, such as plasma or urine and constitute the most common clinical diagnostic tests. When a new assay is translated from analytical laboratory to a point-of-care setting, low cost, ease of use and rapid turnaround time are important factors. Some biomarkers are present in very low concentrations and therefore, enhancement of assay sensitivity can offer an advantage. The existing point of care investigations using fluorescence microplate readers are characterised as being sensitive, high-speed and high-throughput. Although these studies have aided in better understanding of biomolecular (Zhou et al., 1997, Sundberg, 2000, Marx et al., 2001) and cellular processes and continue to serve as the gold standard diagnostic tool, they are not without limitations. Batch to batch variability and assay time are the main shortcomings in standard techniques such as ELISA which requires multiple processing steps.

Exploitation of the long-lived fluorescence of lanthanide complexes can offer a potential solution to existing assays. Their long lived fluorescence enables removal of short lived background fluorescence and therefore improves signal to noise (Szkop et al., 2019, Saha and Imran, 2019). As a result using time-gated

acquisition of signals allows better sensitivity and wider dynamic range of sensing. Considering the promising results that our Eu^{3+} -Affimer based complex showed thus far, we decided to investigate time resolved assays for rapid analysis of biomarkers using plate reader, which also allows for multiple replicates and therefore better statistics than fluorimeter.

5.2 Aims

The aims for this chapter were to:

- I. Characterise Eu^{3+} complex fluorescence integration time.
- II. Investigate the fluorescence intensity measurements of the Eu^{3+} complex with different analytes using the plate reader.
- III. Investigate the size effect of the biomarker targets on the fluorescence intensity measurements of the Eu^{3+} complex.
- IV. Assess the effect of anti-coagulant chelators (EDTA and citrate) on the sensitivity of the Eu^{3+} complex to the biomarkers of C-reactive protein.

5.3 Integration time optimisation of Eu³⁺ complex

The fluorescence spectrum of Eu³⁺ complex was investigated using a time-resolved fluorescence microplate reader. The principle of time resolved fluorescence measurements are shown in **Figure 5.1**. For a start, the initial delay time 20 μ s was chosen to remove the short-lived background fluorescence and only the Eu³⁺ fluorescence remains. The length of the measurement (integration time) was optimised to explore the optimal time for the sensitivity of the Eu³⁺ complex. All previous optimisation steps of the Eu³⁺ complex was applied in similar manner before the integration time was considered. The integration time is the duration over which the fluorescence signal is collected as shown in **Figure 5.2**, 6 different integration times were tested; 10, 15, 20, 25, 50 and 60 μ s. At 10 μ s, 15 μ s and 20 μ s integration times, the percentage quenching seen of Eu³⁺-PMDA- anti- GFAP Affimer complex was comparable with a dose dependent effect of the GFAP concentration. The most significant percentage change in fluorescence counts of the complex was observed at the 50 μ s integration time with $\sim 8.24 \pm 1.22$ % change in fluorescence counts at 100 nM of GFAP concentration when compared to control. The maximum reading that can be obtained using the plate reader was 65000 counts and so when integration time was increased beyond 50 μ s, the system saturated at this value. Accordingly, 50 μ s integration time was chosen to be the optimum integration time.

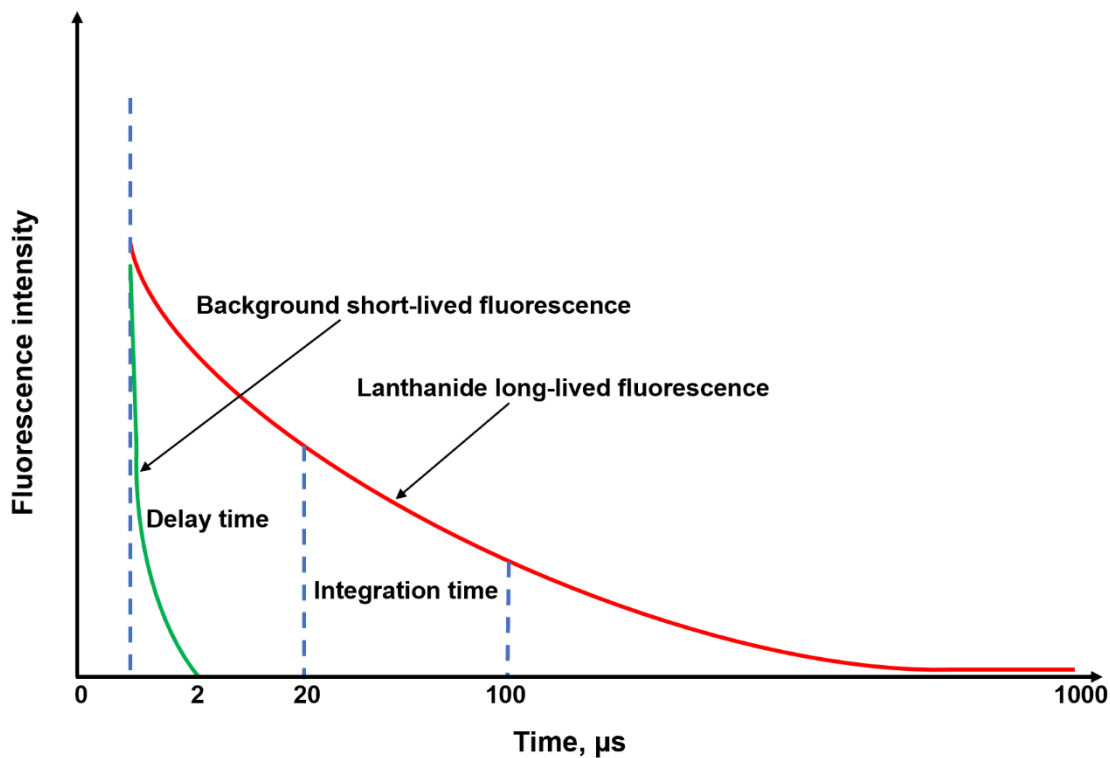


Figure 5.1 The principle of time resolved fluorescence measurements of chelated Eu^{+3} by modified Affimer complex. The short-lived background fluorescence (green line) decays after several ns - 2 μs to a negligible level. The lanthanide long-lived fluorescence (red line) is collected after 20 μs in the gate time.

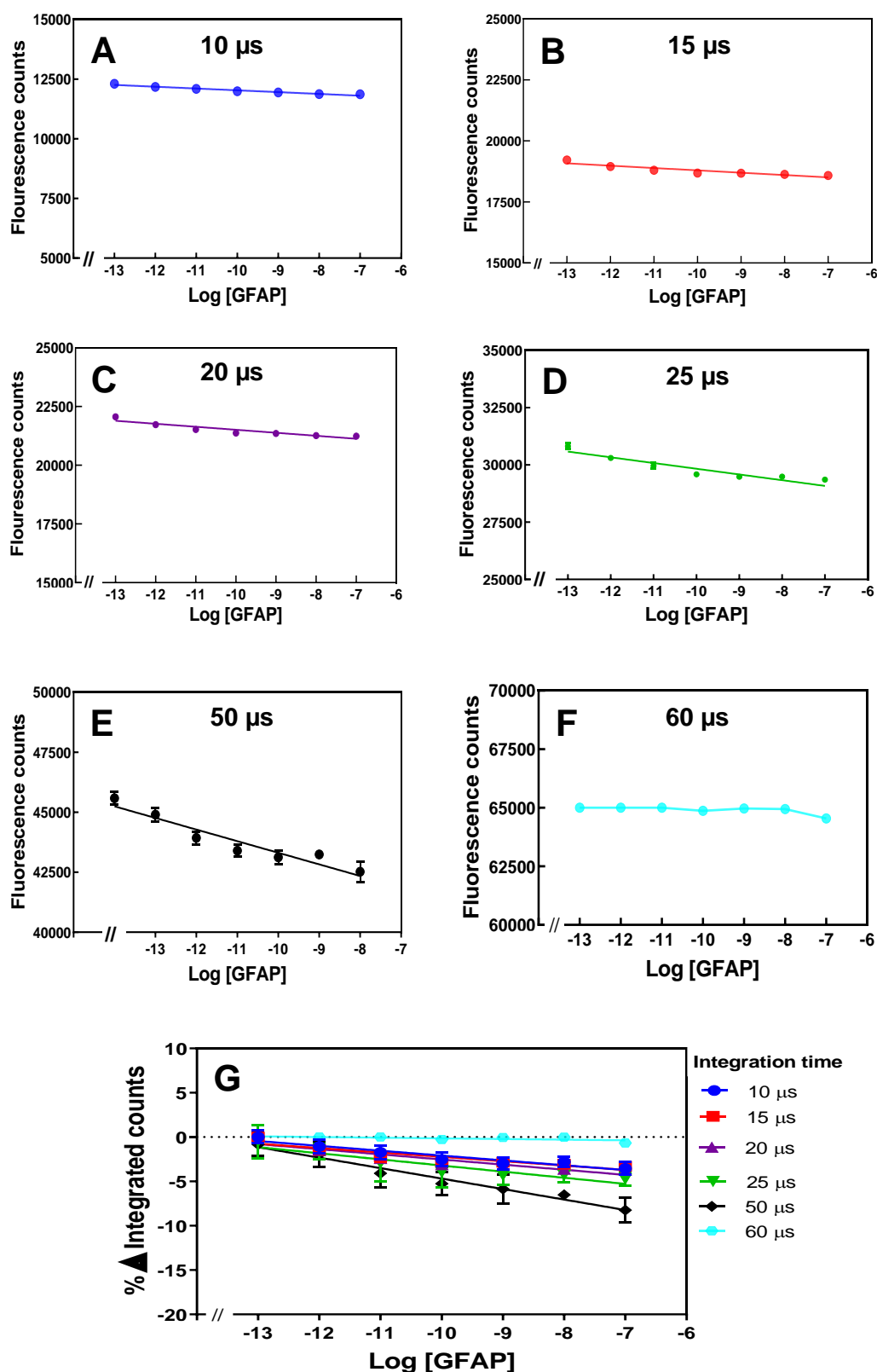


Figure 5.2 Integration times for PMDA modified anti- GFAP Affimer Eu^{3+} complex. Five different integration times were selected to measure the fluorescence counts of the Eu^{3+} complex: (A), 10 μs ; (B), 15 μs ; (C), 20 μs ; (D), 25 μs ; (E), 50 μs ; (D), 60 μs and (G), represents the percentage change of fluorescence counts of the six integration times against increasing dose of GFAP, (mean \pm SEM, n= 3).

5.4 Time resolved fluorescence assay of PMDA modified anti-human myoglobin Affimer and - GFAP Affimer chelated Eu^{3+}

The time resolved fluorescence of PMDA modified anti- human myoglobin and anti- GFAP Affimer Affimer- Eu^{3+} complexes were then investigated using optimised microplate reader protocol (**Table 5.1**). The percentage change in fluorescence count was presented in normalised data analysis.

In Eu^{3+} chelated by PMDA modified anti- human myoglobin Affimer and anti- GFAP Affimer complexes (**Figure 5.3** and **Figure 5.5**; respectively), substantial fluorescence quenching was observed with a similar pattern that was presented in **Chapter 4**. The percentage change in fluorescence counts of the Eu^{3+} complexes were measured in PBS (**Figure 5.3, 5.5**) and 1 % (v/v) human serum (**Figure 5.4, 5.6**). The quenching of fluorescence measured using plate reader was directly proportional to increasing concentration of the respective analytes from 100 fM to 100 nM and was in keeping with the trend observed previously using a fluorimeter (**Chapter 4, Figure 4.6**). A similar trend was seen in measurements made in 1% (v/v) human serum, although the percentage change observed here was slightly less (4-6 %, $P < .001$) than that observed using a cuvette and fluorimeter (10-15 %, $P < .001$; (**Chapter 4**)).

The plate reader data appears to be promising but further validation studies were warranted to test the applicability on other analytes.

Table 5.1 Fluostar Optima control settings.

Sample	Plate mode settings	Optical settings
No. of replicate: 3	No. of cycles: 8	Excitation: 395 nm
Replicate reads/ well: 8	No. of flashes per well: 200 (maximum)	Emission: 520- 640 Gain: 2000 (maximum) Integration start: 20 μ s Integration time: 50 μ s

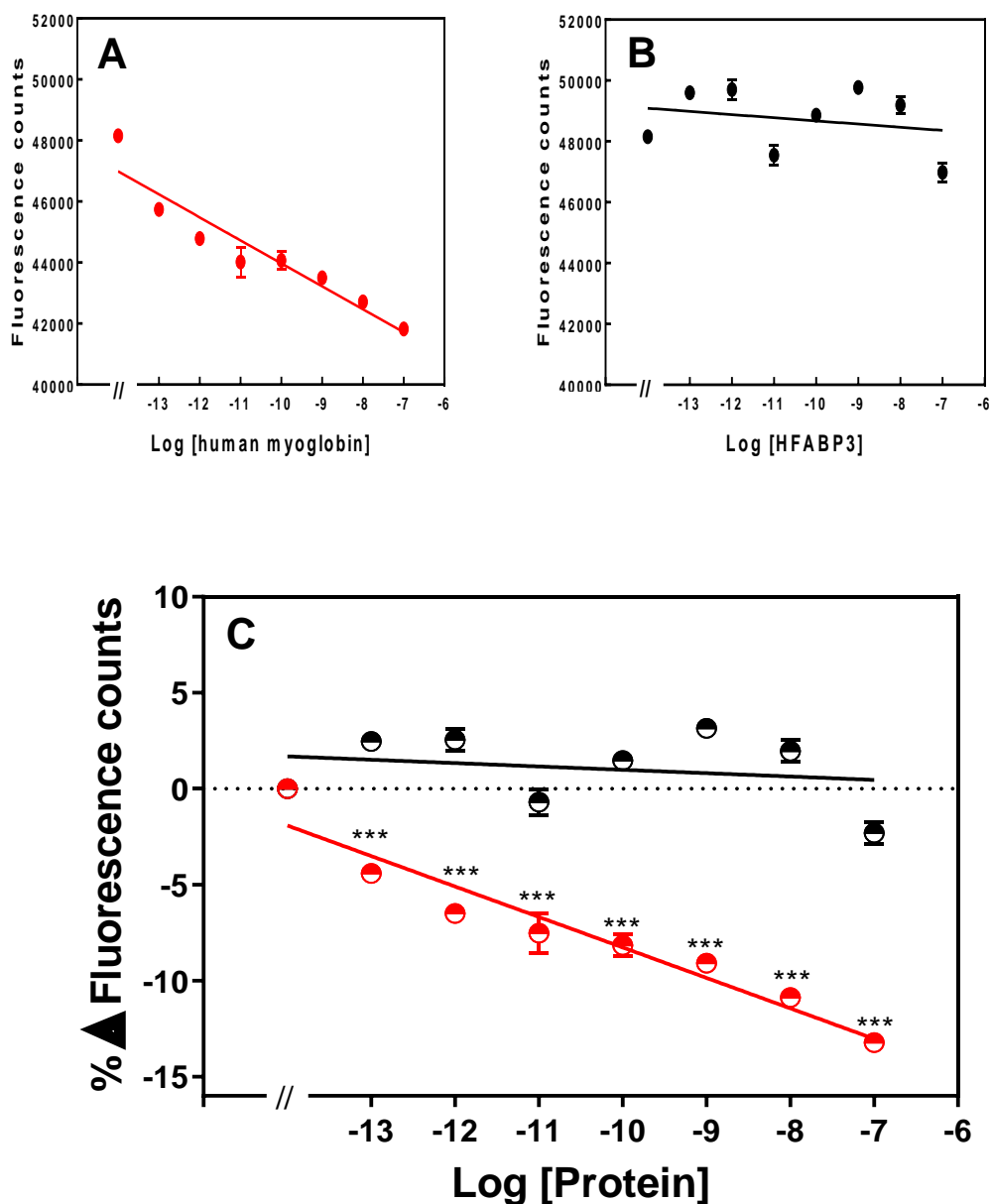


Figure 5.3 Time resolved fluorescence of Eu^{3+} complex in PBS. (A), time resolved fluorescence counts of Eu^{3+} chelated by PMDA modified anti- human myoglobin Affimer in PBS, pH 7.4; (B), control, time resolved fluorescence with the same complex with HFABP3 added; (C), percentage change in fluorescence counts. Symbols denote: (●), human myoglobin ;(●), HFABP3. Some error bars are smaller than data points (*, ** and *** indicate significance with p-value < .05, .01, and .001 respectively of the specific analyte (human myoglobin) compared to the control (HFABP3) data). Data are means \pm SEM (n= 3).

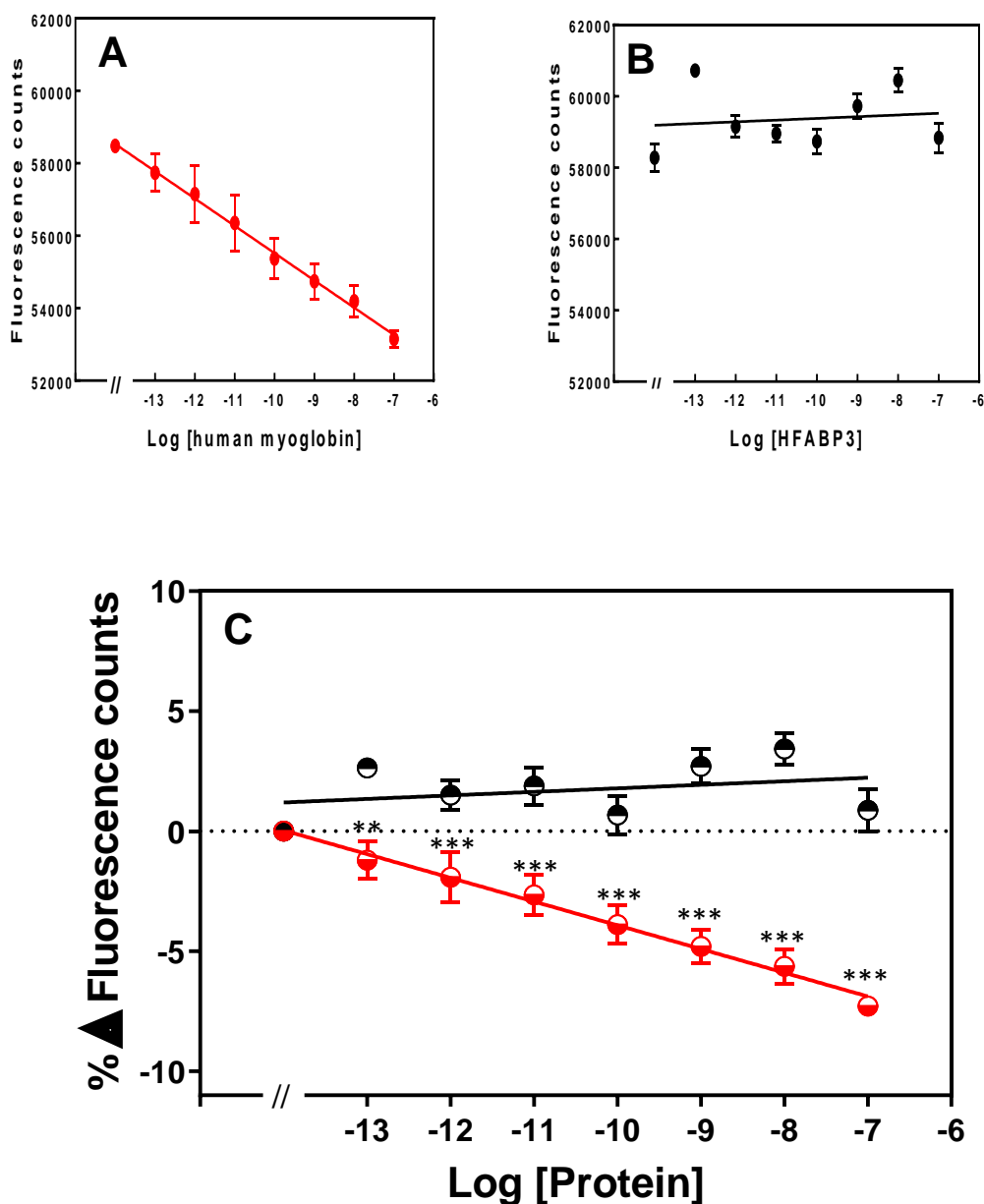


Figure 5.4 Time resolved fluorescence of Eu^{3+} complex in 1% (v/v) human serum. (A), time resolved fluorescence counts of Eu^{3+} chelated by PMDA modified anti- human myoglobin Affimer; (B), control, time resolved fluorescence with the same complex with HFABP3 added; (C), percentage change in fluorescence. Symbols denote: (●), human myoglobin ;(●), HFABP3. Some error bars are smaller than data points (*, ** and *** indicate significance with p-value < .05, .01, and .001 respectively of the specific analyte (human myoglobin) compared to the control (HFABP3) data). Data are means \pm SEM (n= 3).

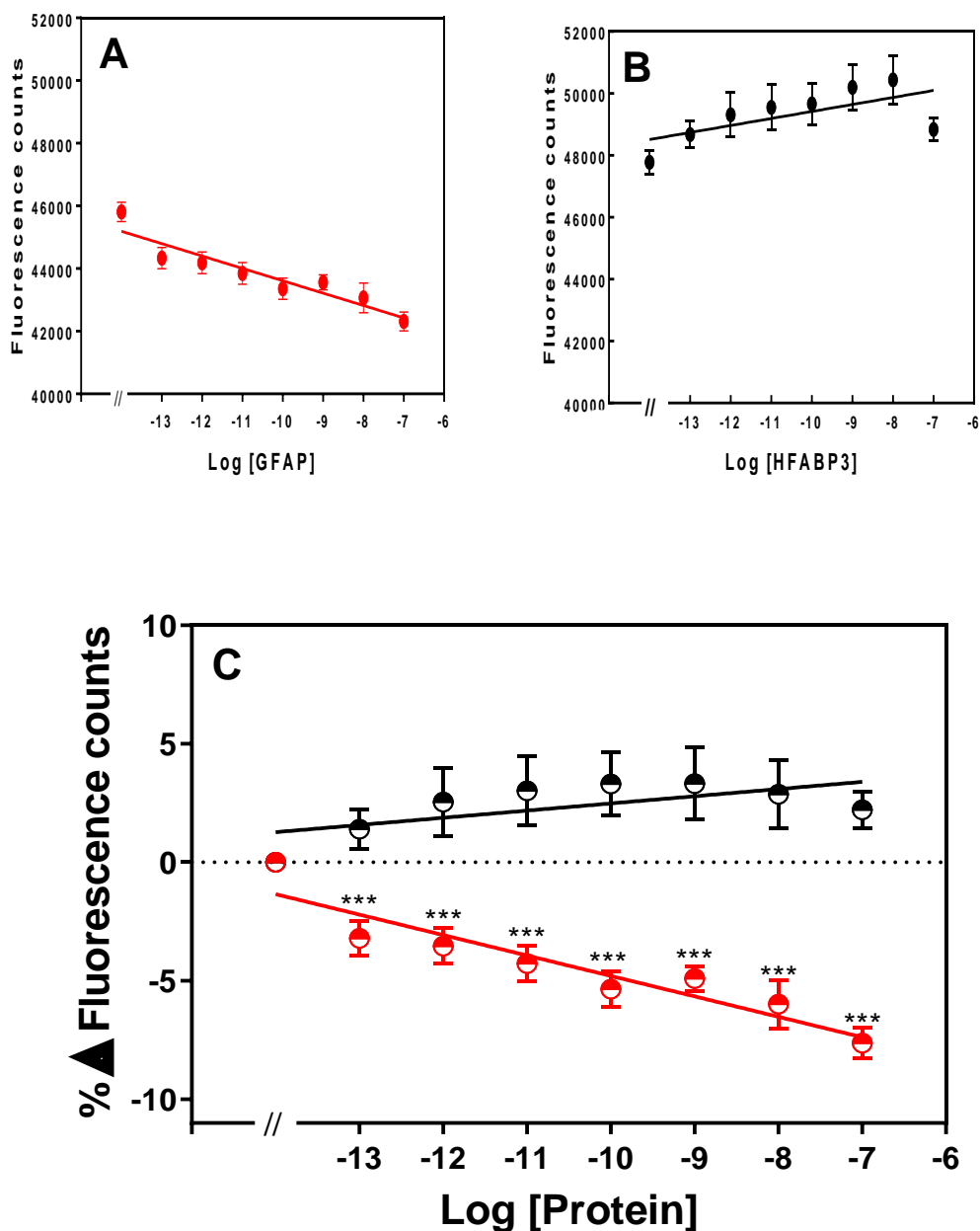


Figure 5.5 Time resolved fluorescence of Eu^{3+} complex in PBS. (A), time resolved fluorescence counts of Eu^{3+} chelated by PMDA modified anti- GFAP Affimer in PBS, pH 7.4; (B), control, time resolved fluorescence with the same complex with HFABP3 added; (C), percentage change in fluorescence. Symbols denote: (●), GFAP ; (●), HFABP3. Some error bars are smaller than data points (*, ** and *** indicate significance with p-value < .05, .01, and .001 respectively of the specific analyte (GFAP) compared to the control (HFABP3) data). Data are means \pm SEM (n= 3).

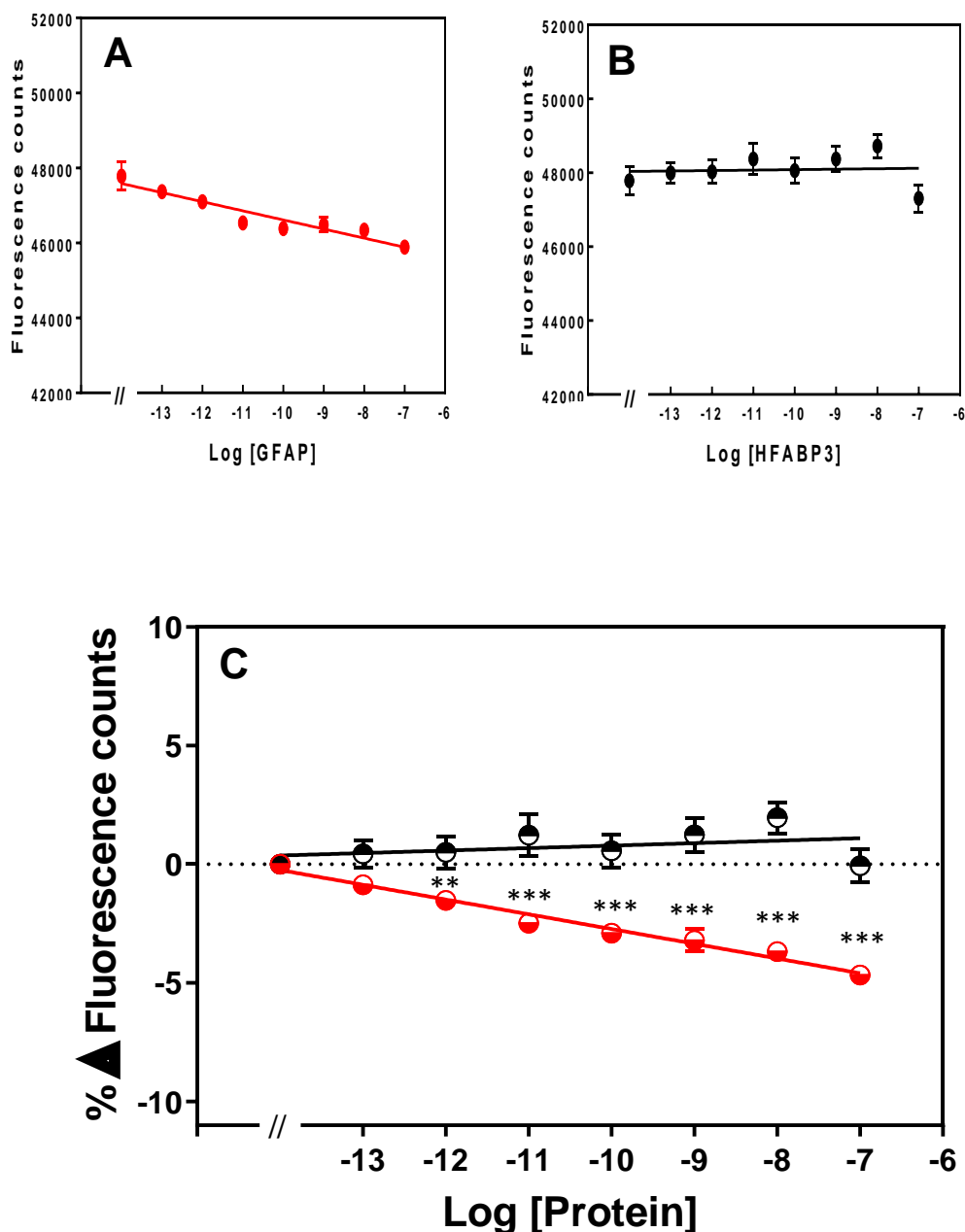


Figure 5.6 Time resolved fluorescence of Eu^{3+} complex in 1% (v/v) human serum. (A), time resolved fluorescence counts of Eu^{3+} chelated by PMDA modified anti- GFAP Affimer; (B), control, time resolved fluorescence with the same complex with HFABP3 added; (C), percentage change in fluorescence. Symbols denote: (●), GFAP; (○), HFABP3. Some error bars are smaller than data points (*, ** and *** indicate significance with p-value < .05, .01, and .001 respectively of the specific analyte (GFAP) compared to the control (HFABP3) data). Data are means \pm SEM (n= 3).

5.5 Time resolved fluorescence of Eu^{3+} chelated by PMDA modified anti- CRP and CEA Affimers

Here, we aimed to investigate the applicability of the Eu^{3+} complex time resolved fluorescence assay using biomarkers protein CRP and CEA which are substantially larger than myoglobin and GFAP; CRP is 119 KDa whilst CEA is approximately 200 KDa. The time resolved fluorescence count was measured in 1 % (v/v) human serum. **Figure 5.7** and **5.8** are plot showing the change in fluorescence of the Eu^{3+} complexes directed against CRP or CEA respectively. The data show a significant percentage change in fluorescence with increasing dose of the respective biomarkers when compared to control, HFABP3 ($P < .001$; 1 pM-100 nM). The percentage change in time resolved fluorescence counts of Eu^{3+} chelated by PMDA modified anti- CRP Affimer was $\sim 3.10 \pm 0.42$ % at a concentration of 100 pM of the analyte ($P < .001$) and $\sim 10.61 \pm 0.24$ % difference at 100 nM ($P < .001$) in 1 % (v/v) human serum (**Figure 5.7**). The percentage change in time resolved fluorescence counts of Eu^{3+} chelated by PMDA modified anti- CEA Affimer was $\sim 4.79 \pm 0.54$ % at a concentration of 100 pM of the analyte ($P < .001$) and $\sim 17.05 \pm 0.15$ % difference at 100 nM ($P < .001$) in 1 % (v/v) human serum as show in **Figure 5.8**.

Interestingly, with the percentage change observed against CRP and CEA (**Figure 5.7** and **Figure 5.8**), the fluorescence quenching was far more greater (10-17 %, $P < .0001$) as compared to GFAP and human myoglobin. The data suggested that the size of the biomarker may have a substantial effect on quenching of the Eu^{3+} complex fluorescence and further investigation into the size effect was needed.

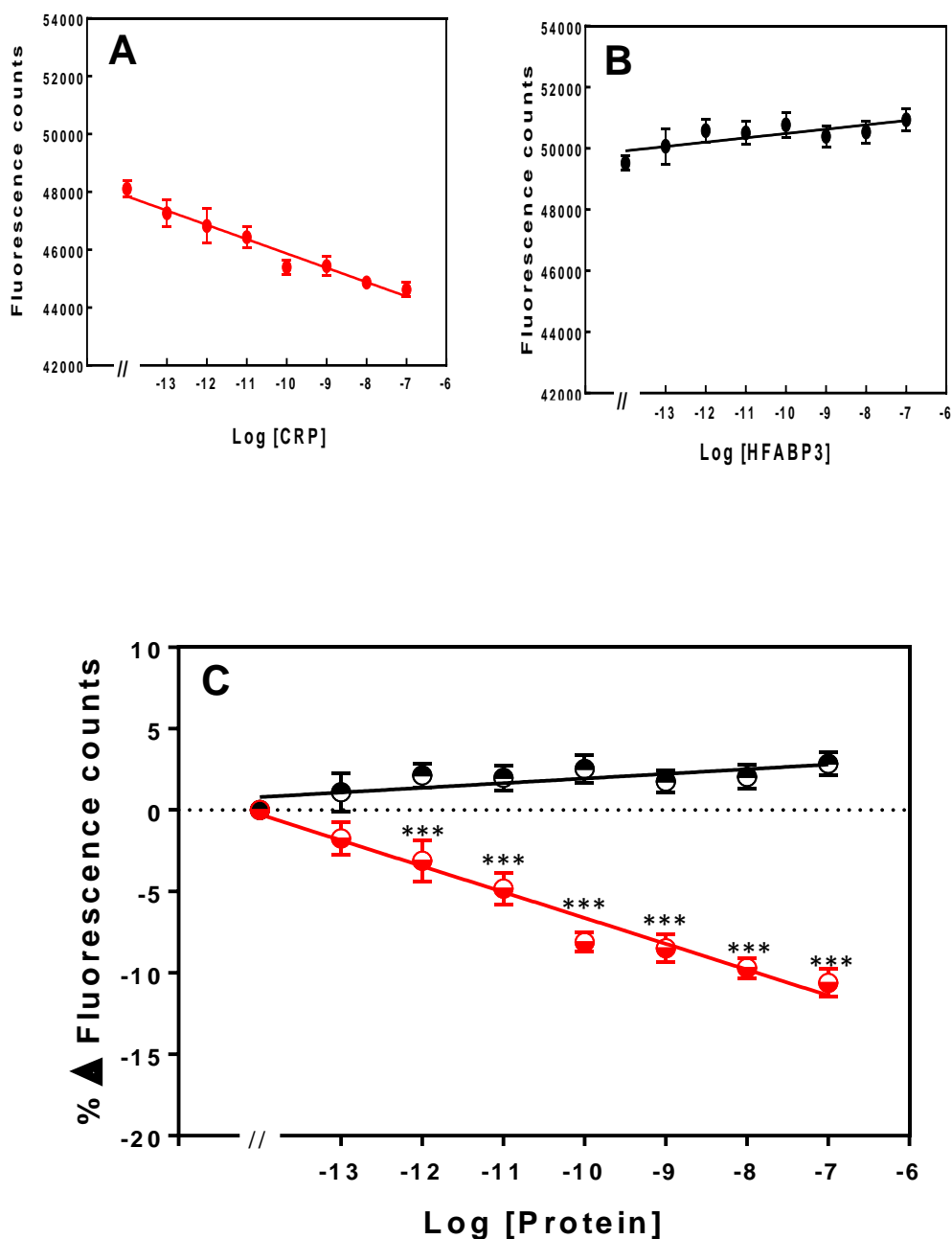


Figure 5.7 Time resolved fluorescence of Eu^{3+} complexes in 1% (v/v) human serum. (A), time resolved fluorescence counts of Eu^{3+} chelated by PMDA modified anti- CRP Affimer; (B), control, time resolved fluorescence with the same complex with HFABP3 added; (C), percentage change in fluorescence. Fluorescence was integrated over 50 s. Symbols denote: (\bullet), CRP ;(\blacktriangle), HFABP3. Some error bars are smaller than data points (*, ** and *** indicate significance with p-value < .05, .01, and .001 respectively of the specific analyte (CRP) compared to the control (HFABP3) data). Data are means \pm SEM (n= 3).

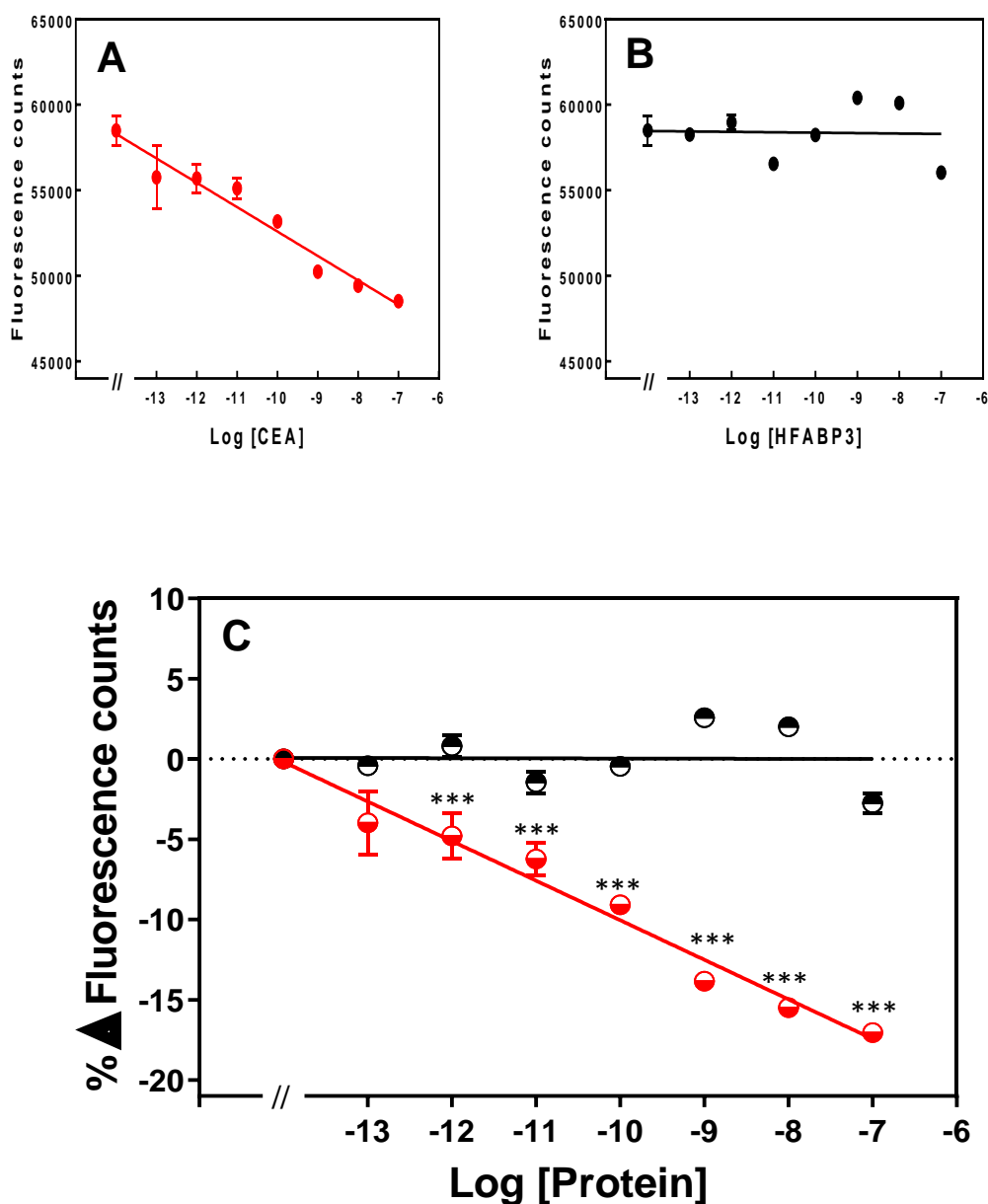


Figure 5.8 Time resolved fluorescence of Eu^{3+} complexes in 1% (v/v) human serum. (A), time resolved fluorescence counts of Eu^{3+} chelated by PMDA modified anti-CEA Affimer; (B), control, time resolved fluorescence with the same complex with HFABP3 added; (C), percentage change in fluorescence. Fluorescence was integrated over 50 s. Symbols denote: (●), CEA; (●), HFABP3. Some error bars are smaller than data points (*, ** and *** indicate significance with p-value < .05, .01, and .001 respectively of the specific analyte (CEA) compared to the control (HFABP3) data). Data are means \pm SEM (n= 3).

5.6 Time resolved fluorescence assay with Eu^{3+} complex and monoclonal/ polyclonal antibody as sandwich assay

Time resolved fluorescence of the Eu^{3+} complex was further investigated to ascertain the size effect of the biomarker on the detection sensitivity. In order to increase the size of the biomarker, we performed a sandwich assay where the biomarker was bound by the Eu^{3+} -Affimer complex and by an IgG simultaneously. The fluorescence quenching observed for the Eu^{3+} complex against GFAP with added monoclonal and polyclonal anti-GFAP IgG is shown in **Figure 5.9**. There was no significant difference in fluorescence quenching when comparing the Eu^{3+} - anti- GFAP Affimer complex plus monoclonal antibody, but significant fluorescence quenching (~ 5 %) was detected when polyclonal anti- GFAP IgG was added. This may be due to the anti- GFAP Affimer and mAb recognizing the same epitope.

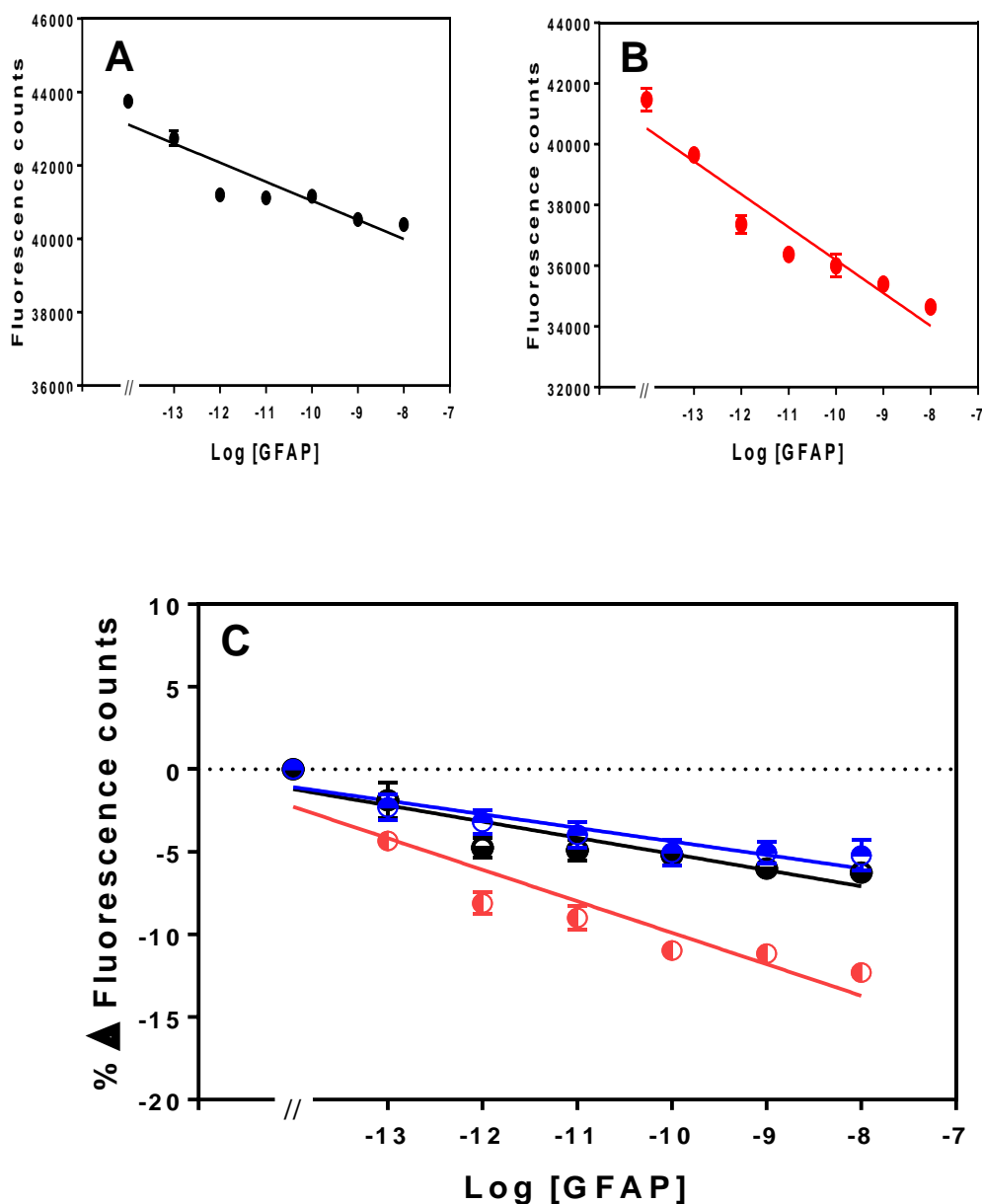


Figure 5.9 Time resolved fluorescence assay with Eu^{+3} complex and mAb/pAb as sandwich assay in 1% (v/v) human serum. (A), time resolved fluorescence counts of Eu^{+3} chelated by PMDA modified anti- GFAP Affimer and monoclonal anti- GFAP IgG; (B), time resolved fluorescence counts of Eu^{+3} chelated by PMDA modified anti- GFAP Affimer and polyclonal anti- GFAP IgG; (C), percentage change in fluorescence. Symbols denote: (\bullet), GFAP ;(\circ), GFAP + mAb;(\ominus), GFAP + pAb. Some error bars are smaller than data points (*, ** and *** indicate significance with p-value < .05, .01, and .001 respectively of the specific analyte (GFAP) compared to the control (HFAPB3) data). Data are means \pm SEM (n= 3).

Time resolved fluorescence assay of Eu^{3+} complex and polyclonal antibody (sandwich assay) for the biomarkers of CEA, CRP and human myoglobin were also tested to ascertain the size effect on the percentage change in fluorescence quenching of the Eu^{3+} complex. It is clearly obvious that the bigger the analyte the higher the percentage change in fluorescence quenching (**Table 5.2**).

Table 5.2 Showing the percentage quench in fluorescence counts of the chelated Eu^{3+} to PMDA modified Affimers in PBS + 1 % (v/v) human serum.

Biomarker	Molecular weight (KDa)	Δ % fluorescence counts of biomarker	Δ % fluorescence counts of biomarker + polyclonal Ab
Myoglobin	17	7.44 \pm 1.17	17.25 \pm 2.37
CRP	119	10.05 \pm 2.46	22.08 \pm 0.85
CEA	200	17.05 \pm 1.50	36.31 \pm 6.24

Δ % fluorescence counts of chelated Eu^{3+} by PMDA modified human myoglobin, CRP and CEA Affimers were measured at 100 nM concentration of biomarker. Data are means \pm SEM (n= 3).

5.7 Effect of chelating agents on plate based time resolved fluorescence assay

When considering the applicability of the Eu^{3+} complex for clinical use, attention has to be paid to the fact that blood samples are typically collected in tubes which contains EDTA or citrate, as anti-coagulant. If our complex was to be used for testing human blood samples, we should investigate the EDTA and citrate would be confounding factors for any readings generated using the Eu^{3+} complex. Here, we investigated the effect of the EDTA and citrate chelators on the Eu^{3+} complex sensitivity. When adding EDTA and citrate to the human serum, no significant fluorescence quenching of the Eu^{3+} chelated anti- CRP Affimer complex was seen (**Figure 5.10**). A likely explanation for the negative results is that the concentration of EDTA and citrate (10 μM) is 10x the concentration of the modified Affimer (1 μM), so the EDTA and citrate compete with the Affimer and hence chelate the Eu^{3+} in the human serum. Accordingly, our assay is applicable to human serum but not plasma or other biofluids where chelators are present.

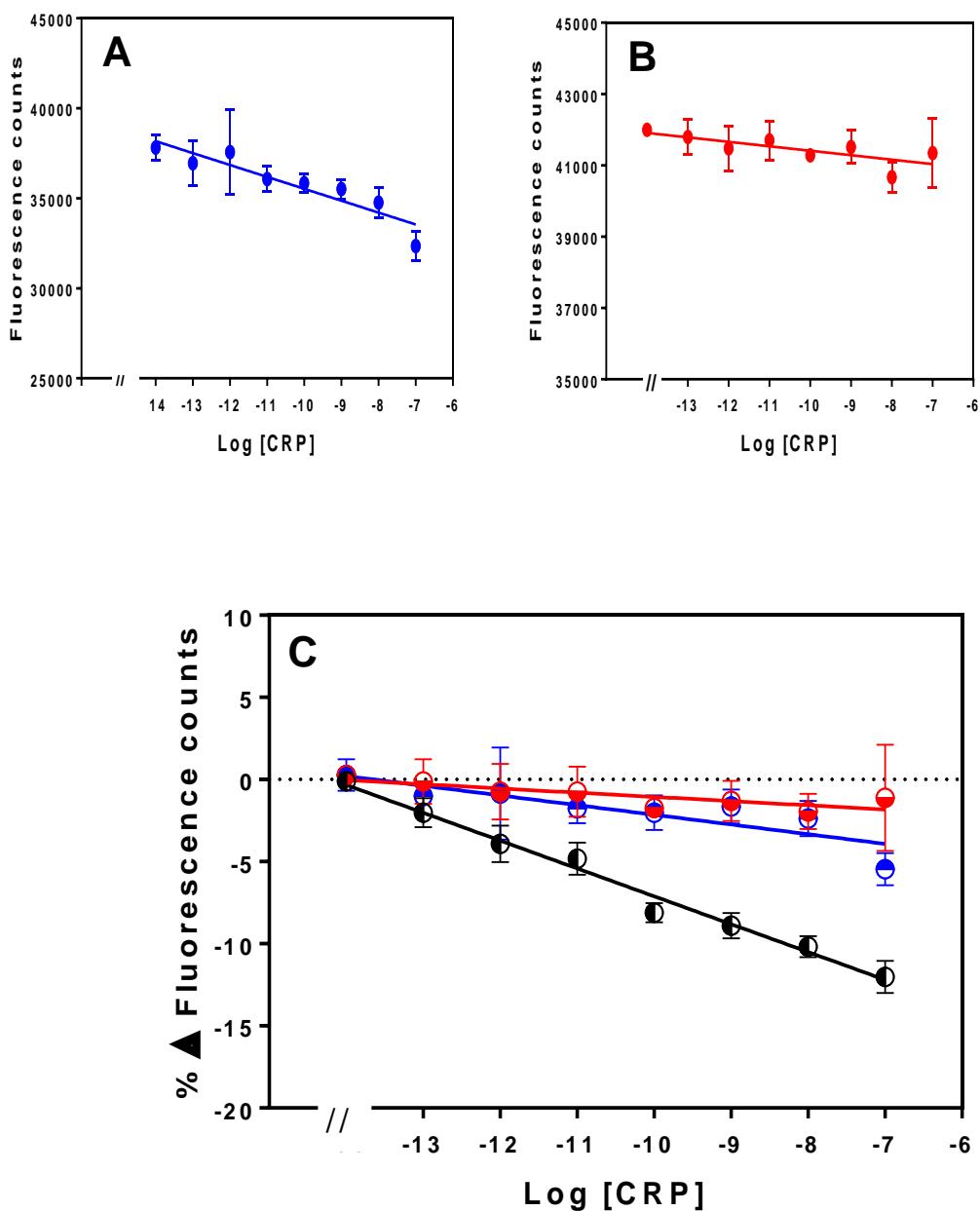


Figure 5.10 Time resolved fluorescence assay with Eu^{+3} complex and EDTA/citrate in 1% (v/v) human serum. (A), time resolved fluorescence counts of Eu^{+3} chelated by PMDA modified anti- CRP Affimer and EDTA; (B), time resolved fluorescence counts of Eu^{+3} chelated by PMDA modified anti- CRP Affimer and citrate; (C), percentage change in fluorescence counts. Symbols denote: (●), time resolved fluorescence counts of Eu^{+3} chelated by PMDA modified anti- CRP Affimer; (●), time resolved fluorescence counts of Eu^{+3} chelated by PMDA modified anti- CRP Affimer + EDTA; (●), time resolved fluorescence counts of Eu^{+3} chelated by PMDA modified anti- CRP Affimer + citrate. Some error bars are smaller than data points. Data are means \pm SEM (n= 3).

5.8 Isothermal titration calorimetry of Eu^{3+} -Affimer complex

We conducted preliminary experiments using isothermal titration calorimetry (ITC) to determine the Gibbs energy (ΔG), enthalpy (ΔH), entropy (ΔS), stoichiometry (n), and the association rate constant (k_a) associated with interaction between Eu^{3+} and PMDA modified anti-human myoglobin Affimer. The titrations were performed by adding 2 μl of 300 μM Eu^{3+} solution into calorimeter sample cell containing 500 μl of 3 μM modified anti- human myoglobin Affimer modified by PMDA, whereas the reference cell was loaded with PBS buffer. ITC data were recorded and as shown in **Figure 5.11**. The positive values of ΔH suggested the interaction between Eu^{3+} and PMDA modified anti- human myoglobin Affimer was an endothermic process. The n value (6.6) indicated that the binding interaction was with approximately six to seven binding sites of Eu^{3+} to PMDA modified anti- human myoglobin Affimer. Since there are 11 lysine residues then a maximum of eleven $\times 3$ $-\text{COO}^-$ could be created if all lysine were modified individually. But some lysine are quite close to others, so we probably have lysine- lysine crosslinking by PMDA which will yield 2 \times $-\text{COO}^-$ from 2 \times lysine (**Figure 5.12**).

In addition, the binding affinity constant k_D (5 μM) suggested that the binding of Eu^{3+} and PMDA modified Affimer was of modest affinity (Velázquez-Campoy et al., 2004). The ITC results warrant further optimisation and replication before these observations are fully confirmed. Other attempts to measure Eu^{3+} - Affimer interaction, e.g. by SPR, MS-MS and other approaches were largely unsuccessful.

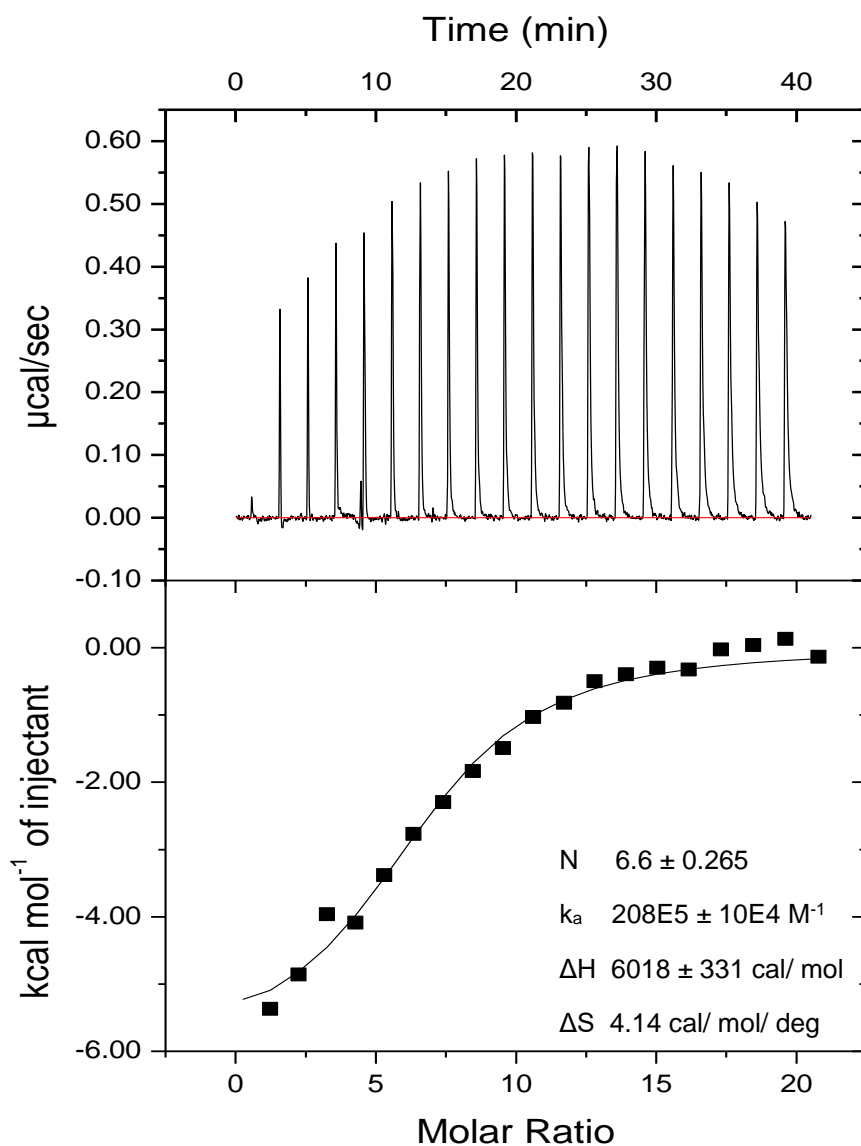


Figure 5.11 ITC data of the interaction between Eu^{3+} and PMDA modified anti-human myoglobin Affimer. (A), shows the sequential titration data of Eu^{3+} into PMDA modified anti-human myoglobin Affimer solution in PBS buffer; (B), the integrated heat data of the titration against the molar ratio of Eu^{3+} / PMDA modified anti-human myoglobin Affimer. The solid black line shows the fitted curve according to 6.6:1 site binding model.

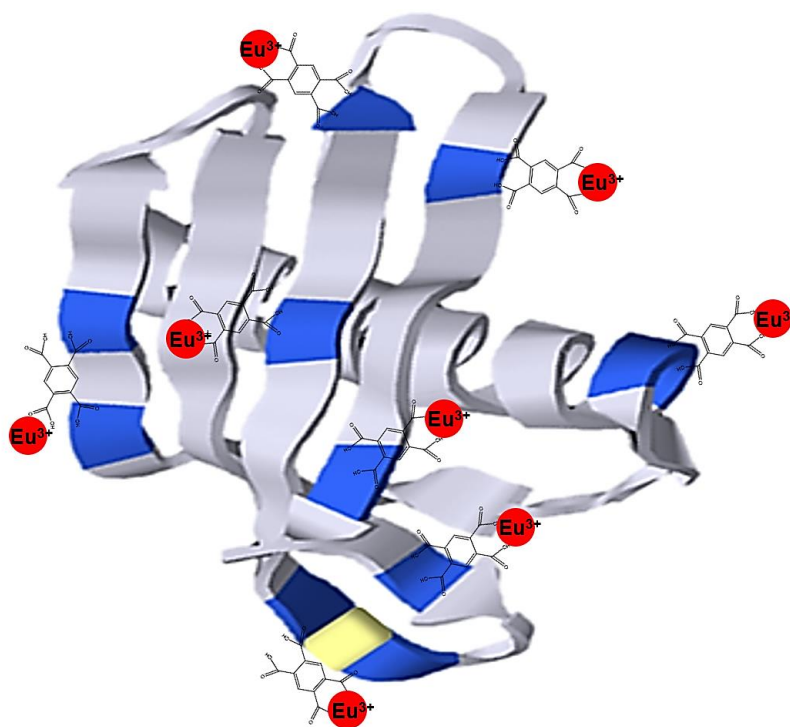


Figure 5.12 Affimer modified with PMDA chelated Eu^{3+} structure. The structure of a typical Affimer is shown. The blue colour represents the 11 lysine residues at the surface of the Affimer scaffold whilst the C-terminal cysteine coloured yellow (pdp. 4N6T). the red colour represents the Eu^{3+} .

5.9 Discussion

In this chapter, we present the results of the fluorescence measurements on Eu^{3+} chelated by PMDA modified Affimers against GFAP, human myoglobin, CRP and CEA using the plate reader as light energy source. We identified the optimum integration time for the Eu^{3+} complex to be 50 s which showed 8 % change in fluorescence counts at 10 nM of GFAP. Of clinical interest, the plate reader data showed that the Eu^{3+} complex allowed specific detection of the targeted analytes in as low as 100 fM concentration. Although the assay will only tolerate 1-2 % (v/v) human serum, and so the real limit of detection (LOD) is around 100 fold higher, ~ 10 pM which is higher than the clinical cut-off of the tested biomarker (**Table 5.3**). Importantly, the fluorescence quenching readings obtained from the plate reader were comparable to those observed when using the fluorimeter as reported in **Chapter 4**.

Table 5.3 Showing the clinical cut-off range of the biomarkers (myoglobin, GFAP, CRP and CEA) and their limit of detection range using Eu^{3+} based biosensor.

Biomarker	Eu^{3+} -based	Eu^{3+} -based Affimer +	Clinical cut-off range
	Affimer biosensor	pAb biosensor	
	LOD	LOD	
Myoglobin	10 pM- 10 μ M	10 pM- 10 μ M	> 60 pM
GFAP	100 pM- 10 μ M	10 pM- 10 μ M	> 30 pM
CRP	100 pM- 10 μ M	10 pM- 10 μ M	> 40 nM
CEA	100 pM- 10 μ M	10 pM- 10 μ M	> 25 pM

Although the measurement of the fluorescence quenching using the plate reader appeared to be slightly less sensitive when compared to the fluorimeter, the functionality of the plate reader allows many data replicates. This feature is essential for application in healthcare laboratories where large number of samples can be analysed simultaneously. When the biomarker was sandwiched between polyclonal antibody and Eu^{3+} - Affimer complex, the fluorescence quenching was further enhanced suggesting that the size of the analyte contributes substantially to the fluorescence quenching observed as shown in **(Table 5.2)**.

A lanthanide chelate based time-resolved fluorescence assay has been investigated by others and proved to be a successful for a wide range of areas such as diagnostics, detection assays, microbes and biomarker discovery. Such a luminescent lanthanide complexes provide long-lasting fluorescence ranging from microseconds to milliseconds. The design of our Eu^{3+} complex experimental setting takes advantage of the above features and rely on the presence of the analyte to cause the quenching.

Ethylenediaminetetraacetate (EDTA) is a hexadentate ligand that contains four carboxylic acid groups and two amine groups (Flora and Pachauri, 2010). It is able to chelate calcium and other metal ions (Banfi et al., 2007). The above features are exploited to prevent coagulation *in vitro* where binding to calcium, EDTA can prevent blood clotting and allows for whole blood analysis. EDTA is also used as a spray-coated to human blood sample collection tubes, at a concentration of 1-10 μM (Aldrich, 2019). Sodium citrate is another anticoagulant commonly used in blood collection tubes, with a 3.2 % buffered sodium citrate solution (Scientific, 2019) and again works by chelating calcium ions. The effects of EDTA and citrate on the chelated Eu^{3+} complex was studied in this Chapter

and demonstrated that they interfere with the time-resolved fluorescence reading. This represents a potential challenge to the clinical application of Eu^{3+} complex unless the assay is carried out on human serum rather than plasma; although a potential solution to this limitation may be to use microfluidic sample handling; this will be discussed further in the discussion Chapter next.

Chapter six: Discussion

Chapter 6

Discussion

6.1 General discussion

Point-of-care (POC) devices are becoming important in addressing the clinical needs for rapid diagnosis of certain medical conditions. In life-threatening conditions such as heart attacks and strokes, highly sensitive and rapid acquisition of results can offer a substantial improvement in the management of these conditions and the overall patient's care (Price et al., 2004). POC devices can also be applied to medical screening and potentially reduce the pressure on emergency departments. Improvements in commercially available POC devices has become one of the main priorities for researchers, physicians and medical device companies. With day to day advancements in biosensors technologies, we are more the likely to see a significant shift towards early diagnosis and improve cure rate of many diseases (Regan et al., 2018).

The overall aim of this project was to develop a novel biosensor platform to aid detecting protein biomarkers that are well known to be elevated in certain pathological conditions. A real-time optical biosensor for quantification of a range of protein biomarkers in human serum samples would be an ideal replacement for traditional methods in clinical laboratories provided that the new biosensor is rapid and accurate. Although the primary two were for biomarkers of vascular disease, we did show the general of applicability of our assay, and successfully

measured markers of inflammation/ bacterial infection (CRP) and of colorectal cancer (CEA).

To achieve this goal, we have developed and optimised a Eu^{3+} -chelated Affimer-based biosensor that allowed specific detection of target proteins in human serum. The project was divided into a number of distinct steps that progressed to achieve successful outcomes *in vitro*. The steps included Affimer purification followed by characterisation using biochemical and biophysical techniques, then Affimer functionalisation in order to chelate the Eu^{3+} and finally optimisation of the Eu^{3+} -Affimer complex in steady state and time-resolved fluorescence assays. The technical aspects, limitations and challenges that were faced during this project will be addressed in this Chapter alongside future prospects and recommendations.

6.2 Factors affecting Eu^{3+} -based biosensor performance

The fabrication of a highly sensitive and specific optical biosensor is governed by multiple factors which play fundamental roles in the sensor's performance. The fabrication of the Eu^{3+} -complex in this thesis progressed through many optimisation steps to achieve successful protein detection. The choice of lanthanide ion is important and Eu^{3+} was a good fit for purpose. Eu^{3+} was selected as the lanthanide used due to its long decay time and well-defined fluorescence intensity when compared to other lanthanide (Jiang et al., 2010). These characteristics of Eu^{3+} fluorescence complexes facilitate use of time-resolved fluorescence, in which background fluorescent emission can be removed by time gating the fluorescence collection (Mundoma and Greenbaum, 2003, Yuan et al., 1998, Xu et al., 1992). Recently Llorent-Martínez et al. (2019)

showed Eu^{3+} could be used to evaluate and quantify ascorbic acid in pharmaceuticals and biological fluids. The quenching effect produced by ascorbic acid on the time-resolved fluorescence signal of Eu^{3+} was tested in pharmaceutical preparations, human serum and human urine. The data were 100 % comparable to reference methods for detection and quantification of ascorbic acid and required no sample treatment except dilution (Llorent-Martínez et al., 2019). These findings suggest that Eu^{3+} based time resolved fluorescence assay is effective and specific and can be used to detect human biomarkers in different bodily solutions.

In our study, the purified Affimers were characterised for binding specificity and affinity using ELISA, immunoprecipitation (pull down) assays and SPR. The results suggested that the anti- human myoglobin and anti- GFAP Affimers showed specific binding features to human myoglobin and GFAP respectively. Importantly, when Eu^{3+} was chelated by PMDA-modified Affimers the complexes showed excellent capability at detecting the target protein in diluted human serum; anti- CEA or anti- CRP Affimers allowed specific detection of their target proteins. These results suggested that the optimised Eu^{3+} complex can be utilised for the detection of wide range of protein biomarkers provided that a specific Affimer is available. We also showed that Affimer modified with chelators via lysine or cysteine did not affect the binding specificity to target protein as long as an Affimer clone which lacked lysine in either binding loop was selected.

Several reports in the literature describe alternative bioreceptors to antibodies for the development of biosensors. Nucleic acid aptamers are becoming popular candidates due to their thermal stability, ease of modification and low-cost production (Lakhin et al., 2013, Ku et al., 2015). They are single-stranded oligonucleotides that can selectively bind to target analytes with similar

qualities to antibodies. For example, Yang et al (2018) fabricated an electrochemiluminescence (ECL) biosensor for the detection of troponin I using both aptamer and antibody (Yang et al., 2018). The aptamers were used to capture troponin I, while the biotinylated antibodies were conjugated with ruthenium complex-labelled streptavidin allowing an ECL detection. The biosensor had an LOD of 0.79 ng/L and a detection range of 1–10 ng/L. Others used peptides and aptamers as the bioreceptor to create a super-sandwich ECL biosensor for signal amplification (Liu et al., 2017). Other synthetic binding proteins such as affibodies and thioredoxin (Ferrigno, 2016) could have been alternative bioreceptors for this project but Affimer were the preferred choice since they were readily available.

The bioreceptor element of our system was essential and the specificity of the Eu^{3+} complex was dependent upon the ability of the Affimer to bind to the target analyte. Two analytes, human myoglobin and GFAP, were selected initially for detection using Affimer-based Eu^{3+} complex. Therefore, my first aim of the project was to assess the binding specificity of anti- human myoglobin and anti-GFAP Affimers to their target analytes. Affimers against human myoglobin and GFAP proteins were selected and subcloned into a *pET11 (a)* vector for protein production. Affimers that contained lysine in the binding loops were excluded from further analysis in order to ensure that only lysines on the Affimer scaffold were modified by PMDA. A single cysteine residue was also introduced at the C-terminus of the Affimer scaffold to be used for other modifications. This site offers advantageous control of the orientation of Affimers when used in other detection and imaging assays. For example, others have shown successful conjugation of Affimer utilising cysteine in biosensors and targeted nanoparticles (Zhurauski et al., 2018). Our system did not require strict Affimer orientation because the

Affimer- Eu^{3+} complex is essentially a homogenous liquid phase assay. However, when immobilisation of the bioreceptor is required, specific strategies are carefully considered to increase the bioreceptor immobilisation efficiency which is heavily reliant on the bioreceptor orientation. Specialised site-specific orientation strategies are available for bioreceptors immobilisation (Mohamad et al., 2015).

6.3 Detection range of anti- human myoglobin and anti- GFAP Affimer based biosensors in comparison to other assays

Considering our ultimate aim for developing a sensitive and accurate optical biosensor for detection of human biomarkers, we also compare the biosensor detection range to other reference methods. An additional important criterion for comparison would be the time taken between loading the biomarker sample into the assay and obtaining results for detection. The detection response time is a key parameter for successful commercialisation of any new biosensor and for some applications may be critical in some situation such as for heart attack or stroke biomarkers. The sensitivity and detection range of optimised anti-human myoglobin and anti- GFAP Affimer based Eu^{3+} complex in this study with the kinetic binding analysis from SPR (**Chapter 3, Section 3.3.3**) and a commercial human myoglobin and GFAP ELISA kits were compared. Results from each detection methods including the detection range and response time are presented in **Figure 6.1**. The Affimer-based Eu^{3+} complexes showed wider detection range (100 fM – 100 nM) when compared to other assays. The sensitivity and detection range of ELISA and SPR followed in decreasing order. Importantly, the response time for the Affimer-based Eu^{3+} complexes was substantially shorter at 30 min (including calibration curve) when compared to ELISA (120- 180 min) and SPR (6- 24 hr). Collectively, the Affimer-based Eu^{3+} complexes biosensor showed the most sensitive detection range and shortest response time. The advantage of our assay is that it is inexpensive (compared to SPR) and requires only a single reagent addition (as compared to ELISA). It also shows comparable or superior sensitivity.

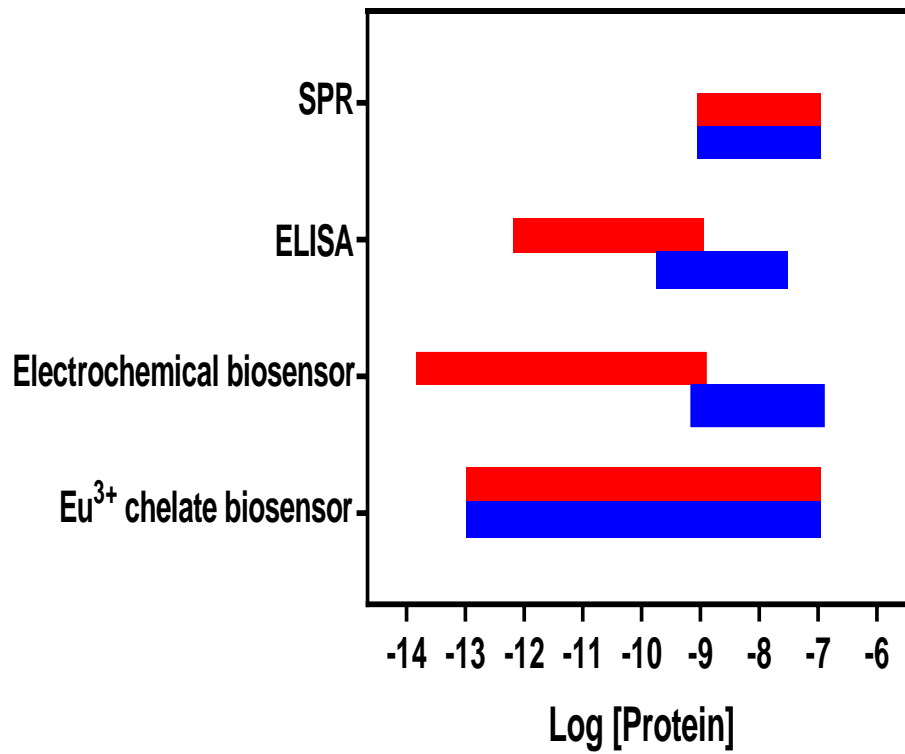


Figure 6.1 Comparison between Eu³⁺ chelates biosensor and other biosensor assays. Bar chart showing the detection range of anti- GFAP (■) and anti- human myoglobin (■) Affimer based Eu³⁺ chelates biosensor compared to commercial ELISA and SPR assay.

6.4 Future work and opportunities

The next step in testing the sensitivity of the Affimer-based Eu^{3+} complex would be on human samples obtained from patients who have sustained heart attacks or strokes. This would be a real point of care test which would also allow direct comparison with standard detection methods. Investigations into the nature of Affimer-analyte interactions would aid further optimisation steps of the biosensor. Measurement of the binding energetics between PMDA modified Affimer and Eu^{3+} would help in understanding the mechanism of the binding interaction between the heavy metal and protein and the number of Eu^{3+} to Affimer binding ratio.

The future of lanthanide complexes as optical biosensors is promising and offers an excellent solution to the limitations of the existing biosensors. The number of publications in the field of lanthanide- based biosensors has increased significantly in the past decade suggesting a healthy pipeline for translation from bench to clinic and commercialisation (Sayyadi et al., 2016, Zhang et al., 2012a, Huang et al., 2011). This technology could be ideal for early diagnosis of cardiovascular events and strokes and fabrication of sensitive biosensors should be tailored towards the feasibility of these techniques for point of care integration.

The range of commercially available bioreceptors for biosensor fabrication is also expanding rapidly although each bioreceptor has its own inherent advantages which make it suitable for a particular application. When considering the wide range of biosensors described in the literature for protein biomarker detection, several limitations prevent clinical implementation. The capability to effectively detect biomarkers directly in human serum in a timely manner is the main challenge. Our Affimer- based Eu^{3+} -complex was only tested in diluted

human serum conditions. A potential solution to this problem would be to immobilise the Eu^{3+} complex onto magnetic beads *before* the human serum samples are spiked with the Eu^{3+} complex. Magnetic beads are likely to allow washing of the off-target proteins from the complex human serum and then Eu^{3+} could be added (**Figure 6.2**).

Finally, rapid growth in the field of biosensors fabrication is quickly emerging on other areas such as cancer diagnostics. The Eu^{3+} complex detection methods can be applied to the field of cancer diagnosis to detect tumour biomarker proteins in blood, urine or faecal samples provided that a specific Affimer is developed against the target protein. Lanthanide- based biosensors hold great promise for future diagnostic and medical translation.

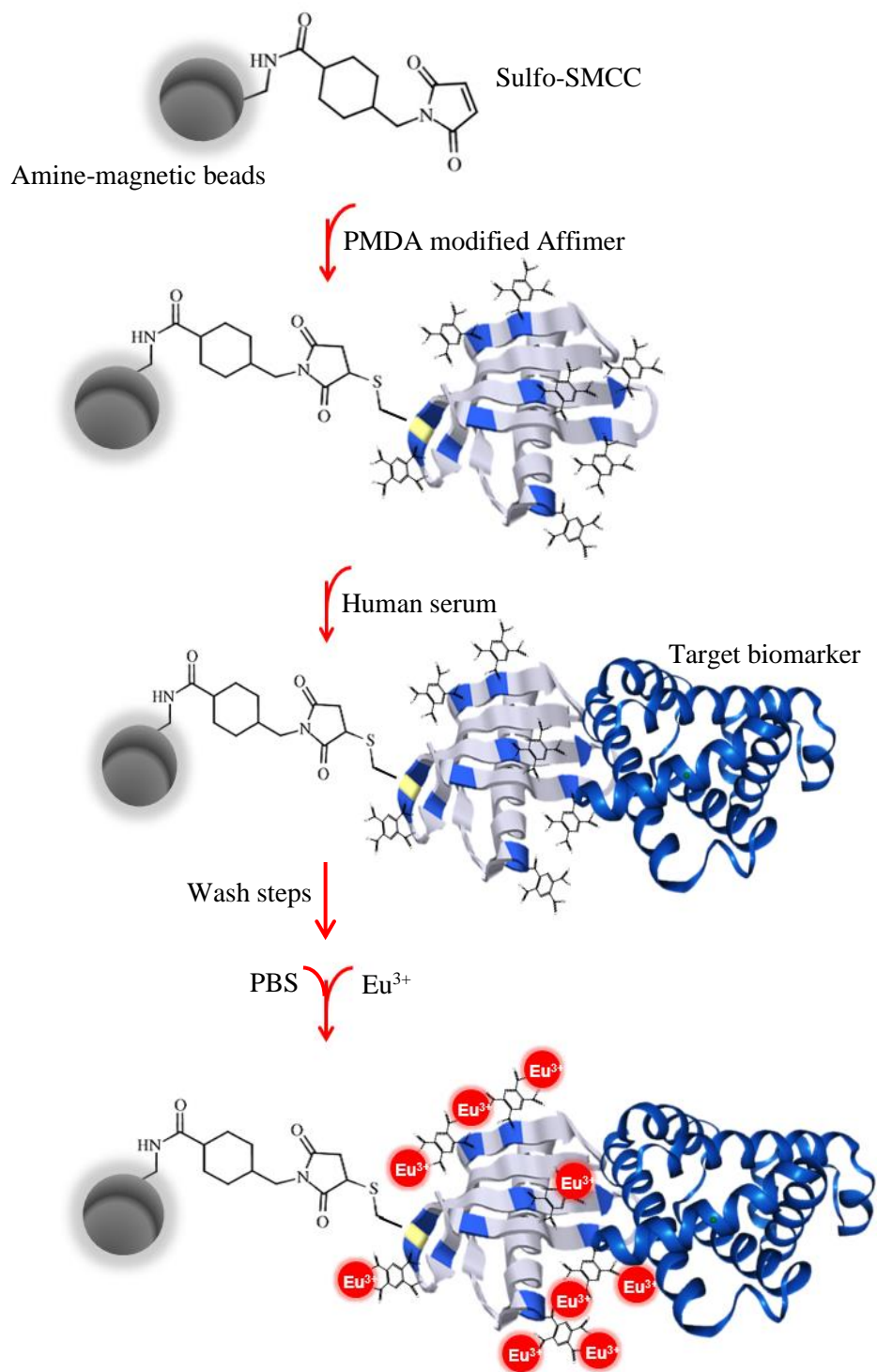


Figure 6.2 Schematic showing the reaction steps for Eu^{3+} chelated by PMDA modified Affimer onto amine-magnetic beads in human serum. First the cysteine-SH containing Affimer is reacted with the maleimide groups of Sulfo-SMCC attached to the amine-magnetic beads. Following by adding human serum and then removing the excess of non-target protein by washing. Finally, Eu^{3+} is chelated by PMDA modified Affimer.

References

- ADAMS, J. W. & IBERALL, E. R. 1949. *Bibliography of the Geology and Mineralogy of the Rare Earths and Scandium to 1971*, US Department of the Interior, Geological Survey; Washington, DC.
- AHMED, A., RUSHWORTH, J. V., HIRST, N. A. & MILLNER, P. A. 2014. Biosensors for whole-cell bacterial detection. *Clinical microbiology reviews*, 27, 631-646.
- AHMED, A., RUSHWORTH, J. V., WRIGHT, J. D. & MILLNER, P. A. 2013. Novel impedimetric immunosensor for detection of pathogenic bacteria *Streptococcus pyogenes* in human saliva. *Analytical chemistry*, 85, 12118-12125.
- AHMED, F. E., WILEY, J. E., WEIDNER, D. A., BONNERUP, C. & MOTA, H. 2010. Surface plasmon resonance (SPR) spectrometry as a tool to analyze nucleic acid–protein interactions in crude cellular extracts. *Cancer Genomics-Proteomics*, 7, 303-309.
- AIME, S., BOTTA, M., PARKER, D. & WILLIAMS, J. G. 1996. Extent of hydration of octadentate lanthanide complexes incorporating phosphinate donors: Solution relaxometry and fluorescence studies. *Journal of the Chemical Society, Dalton Transactions*, 17-23.
- AIZAWA, H., KUROSAWA, S., OGAWA, K.-I., YOSHIMOTO, M., MIYAKE, J. & TANAKA, H. 2001. Conventional diagnosis of C-reactive protein in serum using latex piezoelectric immunoassay. *Sensors and Actuators B: Chemical*, 76, 173-176.
- ALDRICH, S. 2019. Sigma Aldrich. *Online*. Disponível Em: *Www. Sigmaaldrich. Com*. [Acesso Em 28 Ago. 2017].

- ALPHA, B., LEHN, J. M. & MATHIS, G. 1987. Energy transfer fluorescence of europium (III) and terbium (III) cryptates of macrobicyclic polypyridine ligands. *Angewandte Chemie International Edition in English*, 26, 266-267.
- ANCEL, L., NIEDŹWIECKA, A., LEBRUN, C., GATEAU, C. & DELANGLE, P. 2013. Rational design of lanthanide binding peptides. *Comptes Rendus Chimie*, 16, 515-523.
- ARMELAO, L., QUICI, S., BARIGELLETI, F., ACCORSI, G., BOTTARO, G., CAVAZZINI, M. & TONDELLO, E. 2010. Design of luminescent lanthanide complexes: From molecules to highly efficient photo-emitting materials. *Coordination Chemistry Reviews*, 254, 487-505.
- ARNOUX, B., DUCRUIX, A. & PRANGÉ, T. 2002. Anisotropic behaviour of the C-terminal Kunitz-type domain of the $\alpha 3$ chain of human type VI collagen at atomic resolution (0.9 Å). *Acta Crystallographica Section D: Biological Crystallography*, 58, 1252-1254.
- ARYA, S. K., PUI, T. S., WONG, C. C., KUMAR, S. & RAHMAN, A. R. A. 2013. Effects of the electrode size and modification protocol on a label-free electrochemical biosensor. *Langmuir*, 29, 6770-6777.
- ATKINS, P. W. & DE PAULA, J. 1998. Physical Chemistry, Oxford University Press. Oxford, 5, 1007.
- AVNIR, D., KAUFMAN, V. R. & REISFELD, R. 1985. Organic fluorescent dyes trapped in silica and silica-titania thin films by the sol-gel method. Photophysical, film and cage properties. *Journal of Non-Crystalline Solids*, 74, 395-406.
- AVNIR, D., LEVY, D. & REISFELD, R. 1984. The nature of the silica cage as reflected by spectral changes and enhanced photostability of trapped rhodamine 6G. *The Journal of Physical Chemistry*, 88, 5956-5959.

- BAKER, M. 2015. Reproducibility crisis: Blame it on the antibodies. *Nature News*, 521, 274-276.
- BALA, A. & GÓRSKI, Ł. 2018. Peptide nucleic acid as a selective recognition element for electrochemical determination of Hg²⁺. *Bioelectrochemistry*, 119, 189-195.
- BALLOU, B., LAGERHOLM, B. C., ERNST, L. A., BRUCHEZ, M. P. & WAGGONER, A. S. 2003. Noninvasive Imaging of Quantum Dots in Mice. *Bioconjugate Chemistry*, 15, 79-86.
- BANFI, G., SALVAGNO, G. L. & LIPPI, G. 2007. The role of ethylenediamine tetraacetic acid (EDTA) as in vitro anticoagulant for diagnostic purposes. *Clinical Chemical Laboratory Medicine*, 45, 565-576.
- BARTLETT, P. N. 2008. *Bioelectrochemistry: fundamentals, experimental techniques and applications*, John Wiley & Sons.
- BARTON, A. C., COLLYER, S. D., DAVIS, F., GARIFALLOU, G.-Z., TSEKENIS, G., TULLY, E., O'KENNEDY, R., GIBSON, T., MILLNER, P. A. & HIGSON, S. P. 2009. Labelless AC impedimetric antibody-based sensors with pg ml⁻¹ sensitivities for point-of-care biomedical applications. *Biosensors and Bioelectronics*, 24, 1090-1095.
- BAUER, H., BLANC, J. & ROSS, D. L. 1964. Octacoordinate chelates of lanthanides. Two series of compounds. *Journal of the American Chemical Society*, 86, 5125-5131.
- BEDFORD, R., TIEDE, C., HUGHES, R., CURD, A., MCPHERSON, M., PECKHAM, M. & TOMLINSON, D. C. 2017. Alternative reagents to antibodies in imaging applications. *Biophysical reviews*, 9, 299-308.

- BEKIARI, V. & LIANOS, P. 1998. Strongly Luminescent Poly (ethylene glycol)-2, 2'-bipyridine Lanthanide Ion Complexes. *Advanced Materials*, 10, 1455-1458.
- BERG, J. M. & SHI, Y. 1996. The galvanization of biology: a growing appreciation for the roles of zinc. *Science*, 271, 1081-1085.
- BERTI, L., D'AGOSTINO, P. S., BOENEMAN, K. & MEDINTZ, I. L. 2009. Improved peptidyl linkers for self-assembly of semiconductor quantum dot bioconjugates. *Nano Research*, 2, 121-129.
- BINNEMANS, K. 2015. Interpretation of europium (III) spectra. *Coordination Chemistry Reviews*, 295, 1-45.
- BINZ, H. K. & PLÜCKTHUN, A. 2005. Engineered proteins as specific binding reagents. *Current opinion in biotechnology*, 16, 459-469.
- BJERNER, J., LEBEDIN, Y., BELLANGER, L., KUROKI, M., SHIVELY, J. E., VARAAS, T., NUSTAD, K., HAMMARSTRÖM, S. & BØRMER, O. P. 2002. Protein epitopes in carcinoembryonic antigen. *Tumor biology*, 23, 249-262.
- BLASSE, G., DIRKSEN, G., SABBATINI, N. & PERATHONER, S. 1987. Photophysics of Ce³⁺ cryptates. *Inorganica chimica acta*, 133, 167-173.
- BODENMILLER, B., ZUNDER, E. R., FINCK, R., CHEN, T. J., SAVIG, E. S., BRUGGNER, R. V., SIMONDS, E. F., BENDALL, S. C., SACHS, K. & KRUTZIK, P. O. 2012. Multiplexed mass cytometry profiling of cellular states perturbed by small-molecule regulators. *Nature biotechnology*, 30, 858-867
- BONNET, C. S. & GUNNLAUGSSON, T. 2009. Lanthanide macrocyclic quinolyl conjugates as luminescent molecular switches and logic gate functions using HO⁻ and O₂ as inputs. *New Journal of Chemistry*, 33, 1025-1030.

- BRADBURY, A. & PLÜCKTHUN, A. 2015. Reproducibility: Standardize antibodies used in research. *Nature News*, 518, 27-29.
- BRIENT-LITZLER, E., PLÜCKTHUN, A. & BEDOUELLE, H. 2010. Knowledge-based design of reagentless fluorescent biosensors from a designed ankyrin repeat protein. *Protein Engineering, Design & Selection*, 23, 229-241.
- BÜNZLI, J.-C. G. 2006. Lanthanide-containing luminescent molecular edifices. *Journal of alloys and compounds*, 408, 934-944.
- BÜNZLI, J.-C. G. 2010. Lanthanide fluorescence for biomedical analyses and imaging. *Chemical reviews*, 110, 2729-2755.
- BÜNZLI, J.-C. G., CHAUVIN, A.-S., KIM, H. K., DEITERS, E. & ELISEEVA, S. V. 2010. Lanthanide fluorescence efficiency in eight- and nine-coordinate complexes: Role of the radiative lifetime. *Coordination Chemistry Reviews*, 254, 2623-2633.
- BÜNZLI, J.-C. G., COMBY, S., CHAUVIN, A.-S. & VANDEVYVER, C. D. 2007. New opportunities for lanthanide luminescence. *Journal of rare earths*, 25, 257-274.
- BÜNZLI, J.-C. G. & IHRINGER, F. 1996. Photophysical properties of lanthanide dinuclear complexes with p-nitro-calix [8] arene. *Inorganica chimica acta*, 246, 195-205.
- BÜNZLI, J.-C. G. & PIGUET, C. 2005. Taking advantage of luminescent lanthanide ions. *Chemical Society Reviews*, 34, 1048-1077.
- BURDETTE, S. C. & LIPPARD, S. J. 2003. Meeting of the minds: metalloneurochemistry. *Proceedings of the National Academy of Sciences*, 100, 3605-3610.

- CASA, E., KUROSAWA, C., KUROSAWA, S., AIZAWA, H., PARK, J.-W. & SUZUKI, H. 2006. Immunosensor using surface plasmon resonance for C-reactive protein detection. *Electrochemistry*, 74, 153-155.
- CHAMBERS, J. P., ARULANANDAM, B. P., MATTA, L. L., WEIS, A. & VALDES, J. J. 2008. Biosensor recognition elements. Texas Univ at San Antonio Dept of Biology. 10, 1–12.
- CHAMES, P., VAN REGENMORTEL, M., WEISS, E. & BATY, D. 2009. Therapeutic antibodies: successes, limitations and hopes for the future. *British journal of pharmacology*, 157, 220-233.
- CHAPLIN, D. D. 2010. Overview of the immune response. *Journal of Allergy and Clinical Immunology*, 125, S3-S23.
- CHAUBEY, A. & MALHOTRA, B. 2002. Mediated biosensors. *Biosensors and Bioelectronics*, 17, 441-456.
- CHO, M., LIM, K. & WOO, K. 2010. Facile synthesis and optical properties of colloidal silica microspheres encapsulating a quantum dot layer. *Chemical Communications*, 46, 5584-5586.
- CIUBOTARU, I., POTEMPA, L. A. & WANDER, R. C. 2005. Production of modified C-reactive protein in U937-derived macrophages. *Experimental Biology and Medicine*, 230, 762-770.
- CLARK JR, L. C. & LYONS, C. 1962. Electrode systems for continuous monitoring in cardiovascular surgery. *Annals of the New York Academy of sciences*, 102, 29-45.
- DAMBORSKÝ, P., ŠVITEL, J. & KATRLÍK, J. 2016. Optical biosensors. *Essays in biochemistry*, 60, 91-100.

- DARBANDI, M., URBAN, G. & KRÜGER, M. 2010. A facile synthesis method to silica coated CdSe/ZnS nanocomposites with tuneable size and optical properties. *Journal of Colloid and Interface Science*, 351, 30-34.
- DARMOSTUK, M., RIMPELOVA, S., GBELCOVA, H. & RUMML, T. 2015. Current approaches in SELEX: An update to aptamer selection technology. *Biotechnology advances*, 33, 1141-1161.
- DASARI, S. & PATRA, A. K. 2015. Luminescent europium and terbium complexes of dipyridoquinoxaline and dipyridophenazine ligands as photosensitizing antennae: structures and biological perspectives. *Dalton Transactions*, 44, 19844-19855.
- DAY, R. N. & DAVIDSON, M. W. 2012. Fluorescent proteins for FRET microscopy: monitoring protein interactions in living cells. *Bioessays*, 34, 341-350.
- DE LEÓN-RODRÍGUEZ, L. M. & KOVACS, Z. 2007. The synthesis and chelation chemistry of DOTA-peptide conjugates. *Bioconjugate chemistry*, 19, 391-402.
- DE PICCIOTTO, S., DICKSON, P. M., TRAXLMAYR, M. W., MARQUES, B. S., SOCHER, E., ZHAO, S., CHEUNG, S., KIEFER, J. D., WAND, A. J. & GRIFFITH, L. G. 2016. Design Principles for SuCESsFul Biosensors: Specific Fluorophore/Analyte Binding and Minimization of Fluorophore/Scaffold Interactions. *Journal of molecular biology*, 428, 4228-4241.
- DE SA, G., NUNES, L., WANG, Z.-M. & CHOPPIN, G. 1993. Synthesis, characterization, spectroscopic and photophysical studies of ternary complexes of Eu (III) with 3-aminopyrazine-2-carboxylic acid (HL) and

- heterobiaryl ligands (2, 2'-bipyridine and 1, 10-phenanthroline). *Journal of alloys and compounds*, 196, 17-23.
- DEFFAR, K., SHI, H., LI, L., WANG, X. & ZHU, X. 2009. Nanobodies-the new concept in antibody engineering. *African Journal of Biotechnology*, 8, 2645-2652.
- DEKA, J., KUHLMANN, J. & MÜLLER, O. 1998. A domain within the tumor suppressor protein APC shows very similar biochemical properties as the microtubule-associated protein tau. *European Journal of Biochemistry*, 253, 591-597.
- DIXON, H. & PERHAM, R. 1968. Reversible blocking of amino groups with citraconic anhydride. *Biochemical Journal*, 109, 312-314.
- DIXON, M. C. 2008. Quartz crystal microbalance with dissipation monitoring: enabling real-time characterization of biological materials and their interactions. *Journal of biomolecular techniques: JBT*, 19, 151-158.
- DOI, N. & YANAGAWA, H. 1999. Design of generic biosensors based on green fluorescent proteins with allosteric sites by directed evolution. *FEBS letters*, 453, 305-307.
- DONG, H., DU, S.-R., ZHENG, X.-Y., LYU, G.-M., SUN, L.-D., LI, L.-D., ZHANG, P.-Z., ZHANG, C. & YAN, C.-H. 2015. Lanthanide nanoparticles: from design toward bioimaging and therapy. *Chemical reviews*, 115, 10725-10815.
- EBERSBACH, H., FIEDLER, E., SCHEUERMANN, T., FIEDLER, M., STUBBS, M. T., REIMANN, C., PROETZEL, G., RUDOLPH, R. & FIEDLER, U. 2007. Affilin—novel binding molecules based on human γ -B-crystallin, an all β -sheet protein. *Journal of molecular biology*, 372, 172-185.

- ELISEEVA, S. V. & BÜNZLI, J.-C. G. 2010. Lanthanide fluorescence for functional materials and bio-sciences. *Chemical Society Reviews*, 39, 189-227.
- EYRING, L. 1979. The binary rare earth oxides. *Handbook on the physics and chemistry of rare earths*, 3, 337-399.
- EYRING, L., GSCHNEIDNER, K. A. & LANDER, G. H. 2002. *Handbook on the physics and chemistry of rare earths*, Elsevier.
- FAULKNER, S., POPE, S. J. & BURTON-PYE, B. P. 2005. Lanthanide complexes for fluorescence imaging applications. *Applied Spectroscopy Reviews*, 40, 1-31.
- FEILMEIER, B. J., ISEMINER, G., SCHROEDER, D., WEBBER, H. & PHILLIPS, G. J. 2000. Green fluorescent protein functions as a reporter for protein localization in *Escherichia coli*. *Journal of bacteriology*, 182, 4068-4076.
- FERRIGNO, P. K. 2016. Non-antibody protein-based biosensors. *Essays in biochemistry*, 60, 19-25.
- FLEETWOOD, F., KLINT, S., HANZE, M., GUNNERIUSON, E., FREJD, F. Y., STÅHL, S. & LÖFBLUM, J. 2014. Simultaneous targeting of two ligand-binding sites on VEGFR2 using biparatopic Affibody molecules results in dramatically improved affinity. *Scientific reports*, 4, 7518.
- FLORA, S. J. & PACHAURI, V. 2010. Chelation in metal intoxication. *International journal of environmental research and public health*, 7, 2745-2788.
- FREY, S. & GONG, M. 1994. DeW. Horrocks, W., Jr. *Inorg. Chem*, 33, 3229.
- FRIEDMAN, M., LINDSTRÖM, S., EKERLJUNG, L., ANDERSSON-SVAHN, H., CARLSSON, J., BRISMAR, H., GEDDA, L., FREJD, F. Y. & STÅHL, S. 2009. Engineering and characterization of a bispecific HER2x EGFR-

- binding affibody molecule. *Biotechnology and applied biochemistry*, 54, 121-131.
- GAO, X. H., CUI, Y. Y., LEVENSON, R. M., CHUNG, L. W. K. & NIE, S. M. 2004. In vivo cancer targeting and imaging with semiconductor quantum dots. *Nature Biotechnology*, 22, 969-976.
- GONÇALVES E SILVA, F. R., MALTA, O. L., REINHARD, C., GÜDEL, H.-U., FIGUET, C., MOSER, J. E. & BÜNZLI, J.-C. G. 2002. Visible and near-infrared fluorescence of lanthanide-containing dimetallic triple-stranded helicates: energy transfer mechanisms in the SmIII and YbIII molecular edifices. *The Journal of Physical Chemistry A*, 106, 1670-1677.
- GREENBAUM, D., COLANGELO, C., WILLIAMS, K. & GERSTEIN, M. 2003. Comparing protein abundance and mRNA expression levels on a genomic scale. *Genome biology*, 4, 117.
- GUNNLAUGSSON, T., LEONARD, J. P., SÉNÉCHAL, K. & HARTE, A. J. 2003. pH responsive Eu (III)- phenanthroline supramolecular conjugate: novel "Off- On- Off" luminescent signaling in the physiological pH range. *Journal of the American Chemical Society*, 125, 12062-12063.
- HAMZEH-MIVEHROUD, M., ALIZADEH, A. A., MORRIS, M. B., CHURCH, W. B. & DASTMALCHI, S. 2013. Phage display as a technology delivering on the promise of peptide drug discovery. *Drug discovery today*, 18, 1144-1157.
- HANAOKA, K., KIKUCHI, K., KOJIMA, H., URANO, Y. & NAGANO, T. 2003. Selective detection of zinc ions with novel luminescent lanthanide probes. *Angewandte Chemie International Edition*, 42, 2996-2999.
- HANAOKA, K., KIKUCHI, K., KOJIMA, H., URANO, Y. & NAGANO, T. 2004. Development of a zinc ion-selective luminescent lanthanide chemosensor

- for biological applications. *Journal of the American Chemical Society*, 126, 12470-12476.
- HASSANI, L. 2012. The effect of chemical modification with pyromellitic anhydride on structure, function, and thermal stability of horseradish peroxidase. *Applied biochemistry and biotechnology*, 167, 489-497.
- HATAKEYAMA, K., WAKABAYASHI-NAKAO, K., OHSHIMA, K., SAKURA, N., YAMAGUCHI, K. & MOCHIZUKI, T. 2013. Novel protein isoforms of carcinoembryonic antigen are secreted from pancreatic, gastric and colorectal cancer cells. *BMC research notes*, 6, 381.
- HAURUM, J. S. 2006. Recombinant polyclonal antibodies: the next generation of antibody therapeutics? *Drug discovery today*, 11, 655-660.
- HELMA, J., CARDOSO, M. C., MUYLDERMANS, S. & LEONHARDT, H. 2015. Nanobodies and recombinant binders in cell biology. *J Cell Biol*, 209, 633-644.
- HEMMILÁ, I. & MUKKALA, V.-M. 2001. Time-resolution in fluorometry technologies, labels, and applications in bioanalytical assays. *Critical reviews in clinical laboratory sciences*, 38, 441-519.
- HENNESSEY, H., AFARA, N., OMANOVIC, S. & PADJEN, A. L. 2009. Electrochemical investigations of the interaction of C-reactive protein (CRP) with a CRP antibody chemically immobilized on a gold surface. *Analytica chimica acta*, 643, 45-53.
- HEY, T., FIEDLER, E., RUDOLPH, R. & FIEDLER, M. 2005. Artificial, non-antibody binding proteins for pharmaceutical and industrial applications. *TRENDS in Biotechnology*, 23, 514-522.
- HIRAYAMA, T., TAKI, M., KODAN, A., KATO, H. & YAMAMOTO, Y. 2009. Selective labeling of tag-fused protein by tryptophan-sensitized

fluorescence of a terbium complex. *Chemical Communications*, 3196-3198.

HIRST, N. A. 2014. *Development of biosensors for early detection of anastomotic leak and sepsis*. University of Leeds.

HUANG, D.-W., NIU, C.-G., ZENG, G.-M. & RUAN, M. 2011. Time-resolved fluorescence biosensor for adenosine detection based on home-made europium complexes. *Biosensors and Bioelectronics*, 29, 178-183.

HUGHES, D. J., TIEDE, C., PENSWICK, N., AH-SAN TANG, A., TRINH, C. H., MANDAL, U., ZAJAC, K. Z., GAULE, T., HOWELL, G. & EDWARDS, T. A. 2017. Generation of specific inhibitors of SUMO-1–and SUMO-2/3–mediated protein-protein interactions using Affimer (Adhiron) technology. *Sci. Signal.*, 10, eaaj2005.

HULKO, M., HOSPACH, I., KRASTEVA, N. & NELLES, G. 2011. Cytochrome C biosensor—A model for gas sensing. *Sensors*, 11, 5968-5980.

ILKHANI, H., SARPARAST, M., NOORI, A., BATHAIE, S. Z. & MOUSAVI, M. F. 2015. Electrochemical aptamer/antibody based sandwich immunosensor for the detection of EGFR, a cancer biomarker, using gold nanoparticles as a signaling probe. *Biosensors and Bioelectronics*, 74, 491-497.

IUPAC-IUB, C. O. B. N. 1971. Abbreviations and symbols for nucleic acids, polynucleotides and their constituents. *Biochimica et biophysica acta. Nucleic acids and protein synthesis.*, 247, 1-12.

IZUMI, H., TORIGOE, T., ISHIGUCHI, H., URAMOTO, H., YOSHIDA, Y., TANABE, M., ISE, T., MURAKAMI, T., YOSHIDA, T. & NOMOTO, M. 2003. Cellular pH regulators: potentially promising molecular targets for cancer chemotherapy. *Cancer treatment reviews*, 29, 541-549.

- JACKSON, Z. 2017. *Production of a novel Affimer based biosensor for the detection of porcine reproductive and respiratory syndrome virus nucleocapsid protein*. University of Leeds.
- JIANG, L., WU, J., WANG, G., YE, Z., ZHANG, W., JIN, D., YUAN, J. & PIPER, J. 2010. Development of a visible-light-sensitized europium complex for time-resolved fluorometric application. *Analytical chemistry*, 82, 2529-2535.
- KHALED, Y. S., AMMORI, B. J. & ELKORD, E. 2013. Myeloid-derived suppressor cells in cancer: recent progress and prospects. *Immunology and cell biology*, 91, 493-502.
- KIDO, J. & OKAMOTO, Y. 2002. Organo lanthanide metal complexes for electroluminescent materials. *Chemical reviews*, 102, 2357-2368.
- KIM, J. Y., KIM, N. K., SOHN, S. K., KIM, Y. W., KIM, K. J. S., HUR, H., MIN, B. S. & CHO, C. H. 2009. Prognostic value of postoperative CEA clearance in rectal cancer patients with high preoperative CEA levels. *Annals of surgical oncology*, 16, 2771-2778.
- KIRBY, A. F. & RICHARDSON, F. 1983. Detailed analysis of the optical absorption and emission spectra of europium (3+) in the trigonal (C₃) Eu (DBM) 3. H₂O system. *The Journal of Physical Chemistry*, 87, 2544-2556.
- KLINK, S. I. 2000. *Synthesis and photophysics of light-converting lanthanide complexes*, Ph. D. dissertation, Enschede, The Netherlands.
- KORNDÖRFER, I. P., SCHLEHUBER, S. & SKERRA, A. 2003. Structural mechanism of specific ligand recognition by a lipocalin tailored for the complexation of digoxigenin. *Journal of molecular biology*, 330, 385-396.
- KOUTSOUMPELI, E., TIEDE, C., MURRAY, J., TANG, A., BON, R. S., TOMLINSON, D. C. & JOHNSON, S. 2017. Antibody mimetics for the

detection of small organic compounds using a quartz crystal microbalance.

Analytical chemistry, 89, 3051-3058.

KU, T.-H., ZHANG, T., LUO, H., YEN, T. M., CHEN, P.-W., HAN, Y. & LO, Y.-H.

2015. Nucleic acid aptamers: An emerging tool for biotechnology and biomedical sensing. *Sensors*, 15, 16281-16313.

KUMMER, L., HSU, C.-W., DAGLIYAN, O., MACNEVIN, C., KAUFHOLZ, M.,

ZIMMERMANN, B., DOKHOLYAN, N. V., HAHN, K. M. & PLÜCKTHUN,

A. 2013. Knowledge-based design of a biosensor to quantify localized ERK activation in living cells. *Chemistry & biology*, 20, 847-856.

KURIKI, K., KOIKE, Y. & OKAMOTO, Y. 2002. Plastic optical fiber lasers and

amplifiers containing lanthanide complexes. *Chemical reviews*, 102, 2347-2356.

KYLE, H. F., WICKSON, K. F., STOTT, J., BURSLEM, G. M., BREEZE, A. L.,

TIEDE, C., TOMLINSON, D. C., WARRINER, S. L., NELSON, A. &

WILSON, A. J. 2015. Exploration of the HIF-1 α /p300 interface using peptide and Adhiron phage display technologies. *Molecular bioSystems*, 11, 2738-2749.

LAKHIN, A., TARANTUL, V. & GENING, L. 2013. Aptamers: problems, solutions

and prospects. *Acta Naturae (англоязычная версия)*, 5.

LAW, G.-L., PARKER, D., RICHARDSON, S. L. & WONG, K.-L. 2009. The

mechanism of quenching of the lanthanide excited state for optical probes using sensitised emission. *Dalton Transactions*, 8481-8484.

LEHN, J. M. 1978. Cryptates: the chemistry of macropolycyclic inclusion

complexes. *Accounts of chemical research*, 11, 49-57.

- LEI, J., GAO, G., FENG, J., JIN, Y., WANG, C., MAO, Q. & JIANG, J. 2015. Glial fibrillary acidic protein as a biomarker in severe traumatic brain injury patients: a prospective cohort study. *Critical Care*, 19, 362.
- LEWIS, M. R. & SHIVELY, J. E. 1998. Maleimidocysteineamido-DOTA derivatives: new reagents for radiometal chelate conjugation to antibody sulfhydryl groups undergo pH-dependent cleavage reactions. *Bioconjugate chemistry*, 9, 72-86.
- LI, C., LAW, G.-L. & WONG, W.-T. 2004. Luminescent Tb³⁺ complex with pendant crown ether showing dual-component recognition of H⁺ and K⁺ at multiple pH windows. *Organic letters*, 6, 4841-4844.
- LI, H., LAN, R., CHAN, C.-F., JIANG, L., DAI, L., KWONG, D. W., LAM, M. H.-W. & WONG, K.-L. 2015. Real-time in situ monitoring via europium emission of the photo-release of antitumor cisplatin from a Eu–Pt complex. *Chemical Communications*, 51, 14022-14025.
- LI, L., TSAI, S.-W., ANDERSON, A.-L., KEIRE, D. A., RAUBITSCHKEK, A. A. & SHIVELY, J. E. 2002. Vinyl sulfone bifunctional derivatives of DOTA allow sulfhydryl-or amino-directed coupling to antibodies. Conjugates retain immunoreactivity and have similar biodistributions. *Bioconjugate chemistry*, 13, 110-115.
- LIS, S. 2002. Fluorescencespectroscopy of lanthanide (III) ions in solution. *Journal of alloys and compounds*, 341, 45-50.
- LIS, S., ELBANOWSKI, M., MAKOWSKA, B. & HNATEJKO, Z. 2002. Energy transfer in solution of lanthanide complexes. *Journal of Photochemistry and Photobiology A: Chemistry*, 150, 233-247.

- LIU, D., TANG, K., LIU, W., SU, C., YAN, X., TAN, M. & TANG, Y. 2010. A novel luminescent chemosensor for detecting Hg²⁺ based on the pendant benzo crown ether terbium complex. *Dalton Transactions*, 39, 9763-9765.
- LIU, J. T., CHEN, C. J., IKOMA, T., YOSHIOKA, T., CROSS, J. S., CHANG, S.-J., TSAI, J.-Z. & TANAKA, J. 2011. Surface plasmon resonance biosensor with high anti-fouling ability for the detection of cardiac marker troponin T. *Analytica chimica acta*, 703, 80-86.
- LIU, M., YE, Z., XIN, C. & YUAN, J. 2013a. Development of a ratiometric time-resolved fluorescence sensor for pH based on lanthanide complexes. *Analytica chimica acta*, 761, 149-156.
- LIU, X., LIU, H., LI, M., QI, H., GAO, Q. & ZHANG, C. 2017. Highly sensitive Electrochemifluorescence assay for cardiac troponin I and adenosine triphosphate by using Supersandwich amplification and bifunctional aptamer. *Chemelectrochem*, 4, 1708-1713.
- LIU, Z., HE, W. & GUO, Z. 2013b. Metal coordination in photoluminescent sensing. *Chemical Society Reviews*, 42, 1568-1600.
- LLORENT-MARTÍNEZ, E., SOLER-GALLARDO, M., FERNÁNDEZ-POYATOS, M. & RUIZ-MEDINA, A. 2019. Determination of Ascorbic Acid in Pharmaceuticals and Biological Fluids by the Quenching of Europium Luminescence. *Analytical Letters*, 1-10.
- LORENZ, W. & SCHULZE, K. 1975. Application of transform-impedance spectrometry. *Journal of Electroanalytical Chemistry*, 65, 141-153.
- LUDWIG, R., MATSUMOTO, H., TAKESHITA, M., UEDA, K. & SHINKAI, S. 1995. Study on monolayers of metal complexes of calixarenes and their fluorescence properties. *Supramolecular Chemistry*, 4, 319-327.

- MAHATNIRUNKUL, T. 2017. *One-step gold nanoparticle size-shift assay using synthetic binding proteins and dynamic light scattering*. University of Leeds.
- MALON, A., VIGASSY, T., BAKKER, E. & PRETSCH, E. 2006. Potentiometry at trace levels in confined samples: ion-selective electrodes with subfemtomole detection limits. *Journal of the American Chemical Society*, 128, 8154-8155.
- MARVIN, J. S. & HELLINGA, H. W. 1998. Engineering biosensors by introducing fluorescent allosteric signal transducers: construction of a novel glucose sensor. *Journal of the American Chemical Society*, 120, 7-11.
- MARX, M.-C., WOOD, M. & JARVIS, S. 2001. A microplate fluorimetric assay for the study of enzyme diversity in soils. *Soil biology and biochemistry*, 33, 1633-1640.
- MATSUMOTO, K. 2010. Time-resolved fluorescence microscopy and microarray using europium chelate labels.
- MCGILL, I. 2000. Rare earth elements. *Ullmann's encyclopedia of industrial chemistry*.
- MEHRVAR, M. & ABDI, M. 2004. Recent developments, characteristics, and potential applications of electrochemical biosensors. *Analytical sciences*, 20, 1113-1126.
- MEHRVAR, M., BIS, C., SCHARER, J. M., MOO-YOUNG, M. & LUONG, J. H. 2000. Fiber-optic biosensors-trends and advances. *Analytical sciences*, 16, 677-692.
- MEJRI, M., BACCAR, H., BALDRICH, E., DEL CAMPO, F., HELALI, S., KTARI, T., SIMONIAN, A., AOUNI, M. & ABDELGHANI, A. 2010. Impedance biosensing using phages for bacteria detection: Generation of dual signals

- as the clue for in-chip assay confirmation. *Biosensors and Bioelectronics*, 26, 1261-1267.
- MELANSON, S. F., LEWANDROWSKI, E. L., JANUZZI, J. L. & LEWANDROWSKI, K. B. 2004. Reevaluation of myoglobin for acute chest pain evaluation: would false-positive results on "first-draw" specimens lead to increased hospital admissions? *American journal of clinical pathology*, 121, 804-808.
- MELBY, L. & ROSE, N. 1964. E. Abramson and JC Caris. *J. A rn. chem. Soc*, 86, 5117.
- MELBY, L., ROSE, N., ABRAMSON, E. & CARIS, J. 1964. Synthesis and fluorescence of some trivalent lanthanide complexes. *Journal of the American Chemical Society*, 86, 5117-5125.
- MICHALET, X., PINAUD, F. F., BENTOLILA, L. A., TSAY, J. M., DOOSE, S., LI, J. J., SUNDARESAN, G., WU, A. M., GAMBHIR, S. S. & WEISS, S. 2005. Quantum dots for live cells, in vivo imaging, and diagnostics. *Science*, 307, 538-544.
- MICHEL, M. A., SWATEK, K. N., HOSPENTHAL, M. K. & KOMANDER, D. 2017. Ubiquitin linkage-specific affimers reveal insights into K6-linked ubiquitin signaling. *Molecular cell*, 68, 233-246. e5.
- MILLNER, P., CAYGILL, R., CONROY, D. & SHAHIDAN, M. 2012. Impedance interrogated affinity biosensors for medical applications: novel targets and mechanistic studies. *Biosensors for medical applications*. Elsevier.
- MIRANDA, F. F., BRIENT-LITZLER, E., ZIDANE, N., PECORARI, F. & BEDOUELLE, H. 2011. Reagentless fluorescent biosensors from artificial families of antigen binding proteins. *Biosensors and Bioelectronics*, 26, 4184-4190.

- MOHAMAD, N. R., MARZUKI, N. H. C., BUANG, N. A., HUYOP, F. & WAHAB, R. A. 2015. An overview of technologies for immobilization of enzymes and surface analysis techniques for immobilized enzymes. *Biotechnology & Biotechnological Equipment*, 29, 205-220.
- MOORE, E. G., SAMUEL, A. P. & RAYMOND, K. N. 2009. From antenna to assay: lessons learned in lanthanide luminescence. *Accounts of chemical research*, 42, 542-552.
- MUNDOMA, C. & GREENBAUM, N. L. 2003. Binding of europium (III) ions to RNA stem loops: role of the primary hydration sphere in complex formation. *Biopolymers: Original Research on Biomolecules*, 69, 100-109.
- NAESSENS, M., LECLERC, J. C. & TRAN-MINH, C. 2000. Fiber optic biosensor using *Chlorella vulgaris* for determination of toxic compounds. *Ecotoxicology and Environmental Safety*, 46, 181-185.
- NI, X., CASTANARES, M., MUKHERJEE, A. & LUPOLD, S. E. 2011. Nucleic acid aptamers: clinical applications and promising new horizons. *Current medicinal chemistry*, 18, 4206-4214.
- NISHIOKA, T., FUKUI, K. & MATSUMOTO, K. 2007. Lanthanide chelates as luminescent labels in biomedical analyses. *Handbook on the physics and chemistry of rare earths*, 37, 171-216.
- O'KENNEDY, R., FITZGERALD, S. & MURPHY, C. 2017. Don't blame it all on antibodies—The need for exhaustive characterisation, appropriate handling, and addressing the issues that affect specificity. *TrAC Trends in Analytical Chemistry*, 89, 53-59.
- ORMÖ, M., CUBITT, A. B., KALLIO, K., GROSS, L. A., TSIEN, R. Y. & REMINGTON, S. J. 1996. Crystal structure of the *Aequorea victoria* green fluorescent protein. *Science*, 273, 1392-1395.

- PAL, R. & PARKER, D. 2007. A single component ratiometric pH probe with long wavelength excitation of europium emission. *Chemical Communications*, 474-476.
- PARK, K. S. 2018. Nucleic acid aptamer-based methods for diagnosis of infections. *Biosensors and Bioelectronics*, 102, 179-188.
- PARKER, D., SENANAYAKE, P. K. & WILLIAMS, J. G. 1998. Luminescent sensors for pH, pO₂, halide and hydroxide ions using phenanthridine as a photosensitiser in macrocyclic europium and terbium complexes. *Journal of the Chemical Society, Perkin Transactions 2*, 2129-2140.
- PARKER, D. & WILLIAMS, J. G. 1996. Getting excited about lanthanide complexation chemistry. *Journal of the Chemical Society, Dalton Transactions*, 3613-3628.
- PAZOS, E., TORRECILLA, D., VÁZQUEZ LÓPEZ, M., CASTEDO, L., MASCARENAS, J. L., VIDAL, A. & VÁZQUEZ, M. E. 2008. Cyclin A probes by means of intermolecular sensitization of terbium-chelating peptides. *Journal of the American Chemical Society*, 130, 9652-9653.
- PELLEY, J. L., DAAR, A. S. & SANER, M. A. 2009. State of Academic Knowledge on Toxicity and Biological Fate of Quantum Dots. *Toxicological Sciences*, 112, 276-296.
- PENAS, C., MASCAREÑAS, J. L. & VÁZQUEZ, M. E. 2016. Coupling the folding of a β -hairpin with chelation-enhanced fluorescence of Tb (III) and Eu (III) ions for specific sensing of a viral RNA. *Chemical science*, 7, 2674-2678.
- PENG, B. & XIAN, M. 2014. Fluorescent probes for hydrogen sulfide detection. *Asian Journal of Organic Chemistry*, 3, 914-924.

- PERSHAGEN, E., NORDHOLM, J. & BORBAS, K. E. 2012. Luminescent lanthanide complexes with analyte-triggered antenna formation. *Journal of the American Chemical Society*, 134, 9832-9835.
- PIHLASALO, S., DEGUCHI, T., VIRTAMO, M., JACOBINO, J., CHARY, K., LÓPEZ-PICÓN, F. R., BRUNHOFER-BOLZER, G., HUTTUNEN, R., FALLARERO, A. & VUORELA, P. 2017. Luminometric Nanoparticle-Based Assay for High Sensitivity Detection of β -Amyloid Aggregation. *Analytical chemistry*, 89, 2398-2404.
- PIRES, G., COSTA, I., BRITO, H., FAUSTINO, W. & TEOTONIO, E. 2016. Luminescent and magnetic materials with a high content of Eu 3+-EDTA complexes. *Dalton Transactions*, 45, 10960-10968.
- POLLOK, B. A. & HEIM, R. 1999. Using GFP in FRET-based applications. *Trends in cell biology*, 9, 57-60.
- PONSEL, D., NEUGEBAUER, J., LADETZKI-BAEHS, K. & TISSOT, K. 2011. High affinity, developability and functional size: the holy grail of combinatorial antibody library generation. *Molecules*, 16, 3675-3700.
- PRASHER, D. C., ECKENRODE, V. K., WARD, W. W., PRENDERGAST, F. G. & CORMIER, M. J. 1992. Primary structure of the *Aequorea victoria* green-fluorescent protein. *Gene*, 111, 229-233.
- PRICE, C. P., JOHN, A. S. & HICKS, J. M. 2004. *Point-of-care testing*, AACC Press Washington, DC.
- RAINA, M., SHARMA, R., DEACON, S. E., TIEDE, C., TOMLINSON, D., DAVIES, A., MCPHERSON, M. & WÄLTI, C. 2015. Antibody mimetic receptor proteins for label-free biosensors. *Analyst*, 140, 803-810.
- RAJAPAKSE, H. E., GAHLAUT, N., MOHANDESSI, S., YU, D., TURNER, J. R. & MILLER, L. W. 2010. Time-resolved fluorescence resonance energy

- transfer imaging of protein–protein interactions in living cells. *Proceedings of the National Academy of Sciences*, 107, 13582-13587.
- RANJAN, R., ESIMBEKOVA, E. N. & KRATASYUK, V. A. 2017. Rapid biosensing tools for cancer biomarkers. *Biosensors and Bioelectronics*, 87, 918-930.
- RAVALLI, A., DOS SANTOS, G. P., FERRONI, M., FAGLIA, G., YAMANAKA, H. & MARRAZZA, G. 2013. New label free CA125 detection based on gold nanostructured screen-printed electrode. *Sensors and Actuators B: Chemical*, 179, 194-200.
- RAVINDRA, N. M., PRODAN, C., FNU, S., PADRONI, I. & SIKHA, S. K. 2007. Advances in the manufacturing, types, and applications of biosensors. *Jom*, 59, 37-43.
- REGAN, B., O'KENNEDY, R. & COLLINS, D. 2018. Point-of-Care Compatibility of Ultra-Sensitive Detection Techniques for the Cardiac Biomarker Troponin I—Challenges and Potential Value. *Biosensors*, 8, 114.
- REISFELD, R. 1990. Spectroscopy and applications of molecules in glasses. *Journal of Non-Crystalline Solids*, 121, 254-266.
- REISFELD, R. 2002. Fluorescent dyes in sol-gel glasses. *Journal of Fluorescence*, 12, 317-325.
- REN, C., KOBEISSY, F., ALAWIEH, A., LI, N., LI, N., ZIBARA, K., ZOLTEWICZ, S., GUINGAB-CAGMAT, J., LARNER, S. F. & DING, Y. 2016. Assessment of serum UCH-L1 and GFAP in acute stroke patients. *Scientific reports*, 6, 24588.
- RESCH-GENGER, U. 2008. *Standardization and quality assurance in fluorescence measurements II: bioanalytical and biomedical applications*, Springer Science & Business Media.

- REYES, R., CREMONA, M., TEOTONIO, E., BRITO, H. & MALTA, O. 2004. Voltage color tunable OLED with (Sm, Eu)- β -diketonate complex blend. *Chemical physics letters*, 396, 54-58.
- RICHARDS, D. A., MARUANI, A. & CHUDASAMA, V. 2017. Antibody fragments as nanoparticle targeting ligands: a step in the right direction. *Chemical science*, 8, 63-77.
- RICHARDSON, J., HILL, A., LUXTON, R. & HAWKINS, P. 2001. A novel measuring system for the determination of paramagnetic particle labels for use in magneto-immunoassays. *Biosensors and Bioelectronics*, 16, 1127-1132.
- ROBINSON, J. I., BAXTER, E. W., OWEN, R. L., THOMSEN, M., TOMLINSON, D. C., WATERHOUSE, M. P., WIN, S. J., NETTLESHIP, J. E., TIEDE, C. & FOSTER, R. J. 2018. Affimer proteins inhibit immune complex binding to Fc γ RIIIa with high specificity through competitive and allosteric modes of action. *Proceedings of the National Academy of Sciences*, 115, E72-E81.
- ROMER, T., LEONHARDT, H. & ROTHBAUER, U. 2011. Engineering antibodies and proteins for molecular in vivo imaging. *Current opinion in biotechnology*, 22, 882-887.
- RONKAINEN, N. J., HALSALL, H. B. & HEINEMAN, W. R. 2010. Electrochemical biosensors. *Chemical Society Reviews*, 39, 1747-1763.
- RUSHWORTH, J. V. & HIRST, N. A. 2013. *Impedimetric biosensors for medical applications: current progress and challenges*, Momentum Press.
- SAHA, S. & IMRAN, I. B. 2019. A sensitive lanthanide label array method for rapid fingerprint analysis of plant polyphenols based on time-resolved luminescence. *Analytical Methods*, 11, 5044-5054.

- Sambrook, J. & Russell, D.W. 2001. *Molecular Cloning: A Laboratory Manual*. 3rd Edition, Page A1.3. *CSHL Press Cold Spring Harbor*. New York.
- SANTOSH, B. & YADAVA, P. K. 2014. Nucleic acid aptamers: research tools in disease diagnostics and therapeutics. *BioMed research international*, 2014.
- SAYYADI, N., JUSTINIANO, I., CONNALLY, R. E., ZHANG, R., SHI, B., KAUTTO, L., EVEREST-DASS, A. V., YUAN, J., WALSH, B. J. & JIN, D. 2016. Sensitive time-gated immunofluorescence detection of prostate cancer cells using a TEGylated europium ligand. *Analytical chemistry*, 88, 9564-9571.
- SCIENTIFIC, T. F. 2019. Guidelines for Maintaining Cultured Cells. *Dostupno na adresi: <https://www.thermofisher.com/hr/en/home/references/gibco-cell-culturebasics/cell-culture-protocols/maintaining-cultured-cells.html>*. Datum pristupa, 20.
- SHAMSUDDIN, S. H. B. 2018. *Biosensors for detection of colorectal cancer*. University of Leeds.
- SHARMA, R., DEACON, S. E., NOWAK, D., GEORGE, S., SZYMONIK, M., TANG, A., TOMLINSON, D., DAVIES, A., MCPHERSON, M. & WÄLTI, C. 2016a. Label-free electrochemical impedance biosensor to detect human interleukin-8 in serum with sub-pg/ml sensitivity. *Biosensors and Bioelectronics*, 80, 607-613.
- SHARMA, S., BYRNE, H. & O'KENNEDY, R. J. 2016b. Antibodies and antibody-derived analytical biosensors. *Essays in biochemistry*, 60, 9-18.
- SHIMOMURA, O. 2008. Nobel Lecture: Discovery of Green Fluorescent Protein, GFP. *Nobel Prize*. Disponível em < <http://www.nobelprize>.

org/nobel_prizes/chemistry/laureates/2008/shimomura_lecture. pd>

Acesso em, 15.

- SHUVAEV, S., STARCK, M. & PARKER, D. 2017. Responsive, Water-Soluble Europium (III) Luminescent Probes. *Chemistry—A European Journal*, 23, 9974-9989.
- SILACCI, M., BAENZIGER-TOBLER, N., LEMBKE, W., ZHA, W., BATEY, S., BERTSCHINGER, J. & GRABULOVSKI, D. 2014. Linker length matters, Fynomer-Fc fusion with an optimized linker displaying picomolar IL-17A inhibition potency. *Journal of Biological Chemistry*, 289, 14392-14398.
- SILVERMAN, J., LU, Q., BAKKER, A., TO, W., DUGUAY, A., ALBA, B. M., SMITH, R., RIVAS, A., LI, P. & LE, H. 2005. Multivalent avimer proteins evolved by exon shuffling of a family of human receptor domains. *Nature biotechnology*, 23, 1556-1561.
- SIMON, S., ROY, D. & SCHINDLER, M. 1994. Intracellular pH and the control of multidrug resistance. *Proceedings of the National Academy of Sciences*, 91, 1128-1132.
- SINGH, K., BANERJEE, S. & PATRA, A. K. 2015. Photocytotoxic luminescent lanthanide complexes of DTPA–bisamide using quinoline as photosensitizer. *RSC Advances*, 5, 107503-107513.
- SLOOFF, L., POLMAN, A., KLINK, S., GRAVE, L., VAN VEGGEL, F. & HOFSTRAAT, J. 2001. Concentration effects in the photodegradation of lissamine-functionalized neodymium complexes in polymer waveguides. *JOSA B*, 18, 1690-1694.
- SMITH, D. G., MCMAHON, B. K., PAL, R. & PARKER, D. 2012. Live cell imaging of lysosomal pH changes with pH responsive ratiometric lanthanide probes. *Chemical Communications*, 48, 8520-8522.

- SONG, K.-M., LEE, S. & BAN, C. 2012. Aptamers and their biological applications. *Sensors*, 12, 612-631.
- SPROSTON, N. R. & ASHWORTH, J. J. 2018. Role of C-reactive protein at sites of inflammation and infection. *Frontiers in immunology*, 9, 754.
- STADLER, L. K. J., HOFFMANN, T., TOMLINSON, D. C., SONG, Q., LEE, T., BUSBY, M., NYATHI, Y., GENDRA, E., TIEDE, C. & FLANAGAN, K. 2011. Structure– function studies of an engineered scaffold protein derived from Stefin A. II: Development and applications of the SQT variant. *Protein Engineering, Design & Selection*, 24, 751-763.
- STEIN, G. & WÜRZBERG, E. 1975. Energy gap law in the solvent isotope effect on radiationless transitions of rare earth ions. *The Journal of Chemical Physics*, 62, 208-213.
- SUNDBERG, S. A. 2000. High-throughput and ultra-high-throughput screening: solution-and cell-based approaches. *Current opinion in biotechnology*, 11, 47-53.
- SUNI, I. I. 2008. Impedance methods for electrochemical sensors using nanomaterials. *TrAC Trends in Analytical Chemistry*, 27, 604-611.
- SZÍJJÁRTÓ, C., PERSHAGEN, E., ILCHENKO, N. O. & BORBAS, K. E. 2013. A Versatile Long-Wavelength-Absorbing Scaffold for Eu-Based Responsive Probes. *Chemistry–A European Journal*, 19, 3099-3109.
- SZKOP, M., BRYGOŁA, K., JANCZEWSKA, M. & CIACH, T. 2019. A simple time-resolved fluorescence assay for quantitative determination of DOTA chelator. *Analytical biochemistry*, 584, 113384.
- TAKALO, H., HEMMILÄ, I., SUTELA, T. & LATVA, M. 1996a. Synthesis and fluorescence of novel Eu III complexing agents and labels with 4-(phenylethynyl) pyridine subunits. *Helv. Chim. Acta*, 79, 789-802.

- TAKALO, H., HEMMILÄ, I., SUTELA, T. & LATVA, M. 1996b. Synthesis and Fluorescence of Novel Eu(III) Complexing Agents and Labels with 4-(Phenylethynyl) pyridine Subunits. *Helvetica chimica acta*, 79, 789-802.
- TAN, H., ZHANG, Y. & CHEN, Y. 2011. Detection of mercury ions (Hg²⁺) in urine using a terbium chelate fluorescent probe. *Sensors and Actuators B: Chemical*, 156, 120-125.
- TERAI, T., ITO, H., KIKUCHI, K. & NAGANO, T. 2012a. Salicylic-Acid Derivatives as Antennae for Ratiometric Luminescent Probes Based on Lanthanide Complexes. *Chemistry—A European Journal*, 18, 7377-7381.
- TERAI, T., KIKUCHI, K., URANO, Y., KOJIMA, H. & NAGANO, T. 2012b. A long-lived luminescent probe to sensitively detect arylamine N-acetyltransferase (NAT) activity of cells. *Chemical Communications*, 48, 2234-2236.
- THANGSUNAN, P. 2018. *Affimer-based impedimetric biosensors: the new analytical platform for biorecognition applications*. University of Leeds.
- THIBON, A. & PIERRE, V. C. 2009. Principles of responsive lanthanide-based luminescent probes for cellular imaging. *Analytical and bioanalytical chemistry*, 394, 107-120.
- THORSON, M. K., UNG, P., LEAVER, F. M., CORBIN, T. S., TUCK, K. L., GRAHAM, B. & BARRIOS, A. M. 2015. Lanthanide complexes as luminogenic probes to measure sulfide levels in industrial samples. *Analytica chimica acta*, 896, 160-165.
- TIEDE, C., BEDFORD, R., HESELTINE, S. J., SMITH, G., WIJETUNGA, I., ROSS, R., ALQALLAF, D., ROBERTS, A. P., BALLS, A. & CURD, A. 2017. Affimer proteins are versatile and renewable affinity reagents. *Elife*, 6, e24903.

- TIEDE, C., TANG, A. A., DEACON, S. E., MANDAL, U., NETTLESHIP, J. E., OWEN, R. L., GEORGE, S. E., HARRISON, D. J., OWENS, R. J. & TOMLINSON, D. C. 2014. Adhiron: a stable and versatile peptide display scaffold for molecular recognition applications. *Protein Engineering, Design and Selection*, 27, 145-155.
- TROPIANO, M. & FAULKNER, S. 2014. A lanthanide based sensor for the time-gated detection of hydrogen sulfide. *Chemical Communications*, 50, 4696-4698.
- TSARYUK, V., LEGENDZIEWICZ, J., PUNTUS, L., ZOLIN, V. & SOKOLNICKI, J. 2000. Optical spectroscopy of the adducts of europium tris (dipivaloylmethanate) with derivatives of 1, 10-phenanthroline. *Journal of alloys and compounds*, 300, 464-470.
- TSUKUBE, H., NODA, Y. & SHINODA, S. 2010. Poly (arginine)-Selective Coprecipitation Properties of Self-Assembling Apoferritin and Its Tb³⁺ Complex: A New Luminescent Biotool for Sensing of Poly (arginine) and Its Protein Conjugates. *Chemistry—A European Journal*, 16, 4273-4278.
- TWEEDIE, M., SUBRAMANIAN, R., LEMOINE, P., CRAIG, I., MCADAMS, E., MCLAUGHLIN, J., MACCRAITH, B. & KENT, N. Fabrication of impedimetric sensors for label-free point-of-care immunoassay cardiac marker systems, with passive microfluidic delivery. 2006 International Conference of the IEEE Engineering in Medicine and Biology Society, 2006. IEEE, 4610-4614.
- VAN EMON, J. M., CHUANG, J. C., DILL, K. & XIONG, G. 2008. Immunoassays and biosensors. *Analysis of pesticides in food and environmental samples*. CRC Press.

- VASHIST, S. K. & VASHIST, P. 2011. Recent advances in quartz crystal microbalance-based sensors. *Journal of Sensors*, 2011.
- VELÁZQUEZ-CAMPOY, A., OHTAKA, H., NEZAMI, A., MUZAMMIL, S. & FREIRE, E. 2004. Isothermal titration calorimetry. *Current protocols in cell biology*, 23, 17.8. 1-17.8. 24.
- VF MASSICANO, A., B PUJATTI, P., F ALCARDE, L., F SUZUKI, M., J SPENCER, P. & B ARAÚJO, E. 2016. Development and biological studies of; ¹⁷⁷Lu-DOTA-rituximab for the treatment of Non-Hodgkin's lymphoma. *Current radiopharmaceuticals*, 9, 54-63.
- VIGUIER, R. F. & HULME, A. N. 2006. A sensitized europium complex generated by micromolar concentrations of copper (I): toward the detection of copper (I) in biology. *Journal of the American Chemical Society*, 128, 11370-11371.
- WANG, H., MENG, A. M., LI, S. H. & ZHOU, X. L. 2017a. A nanobody targeting carcinoembryonic antigen as a promising molecular probe for non-small cell lung cancer. *Molecular medicine reports*, 16, 625-630.
- WANG, J. 2001. Glucose biosensors: 40 years of advances and challenges. *Electroanalysis: An International Journal Devoted to Fundamental and Practical Aspects of Electroanalysis*, 13, 983-988.
- WANG, W., GUO, Y., TIEDE, C., CHEN, S., KOPYTYNSKI, M., KONG, Y., KULAK, A., TOMLINSON, D., CHEN, R. & MCPHERSON, M. 2017b. Ultraefficient cap-exchange protocol to compact biofunctional quantum dots for sensitive ratiometric biosensing and cell imaging. *ACS applied materials & interfaces*, 9, 15232-15244.
- WANG, X., CHANG, H., XIE, J., ZHAO, B., LIU, B., XU, S., PEI, W., REN, N., HUANG, L. & HUANG, W. 2014. Recent developments in lanthanide-

- based luminescent probes. *Coordination Chemistry Reviews*, 273, 201-212.
- WANG, X., WANG, X., WANG, Y. & GUO, Z. 2011. Terbium (III) complex as a luminescent sensor for human serum albumin in aqueous solution. *Chemical Communications*, 47, 8127-8129.
- WATSON, A., WU, X. Y. & BRUCHEZ, M. 2003. Lighting up cells with quantum dots. *Biotechniques*, 34, 296-303.
- WEGNER, K. D. & HILDEBRANDT, N. 2015. Quantum dots: bright and versatile in vitro and in vivo fluorescence imaging biosensors. *Chemical Society Reviews*, 44, 4792-4834.
- WEN, W., HUANG, J.-Y., BAO, T., ZHOU, J., XIA, H.-X., ZHANG, X.-H., WANG, S.-F. & ZHAO, Y.-D. 2016. Increased electrocatalyzed performance through hairpin oligonucleotide aptamer-functionalized gold nanorods labels and graphene-streptavidin nanomatrix: Highly selective and sensitive electrochemical biosensor of carcinoembryonic antigen. *Biosensors and Bioelectronics*, 83, 142-148.
- WERNER, R. G. 2004. Economic aspects of commercial manufacture of biopharmaceuticals. *Journal of Biotechnology*, 113, 171-182.
- WERTS, M. H., HOFSTRAAT, J. W., GEURTS, F. A. & VERHOEVEN, J. W. 1997. Fluorescein and eosin as sensitizing chromophores in near-infrared luminescent ytterbium (III), neodymium (III) and erbium (III) chelates. *Chemical physics letters*, 276, 196-201.
- WHITE, S., SZEWCZYK, J. W., TURNER, J. M., BAIRD, E. E. & DERVAN, P. B. 1998. Recognition of the four Watson–Crick base pairs in the DNA minor groove by synthetic ligands. *Nature*, 391, 468-471.

- WU, B., JIANG, R., WANG, Q., HUANG, J., YANG, X., WANG, K., LI, W., CHEN, N. & LI, Q. 2016. Detection of C-reactive protein using nanoparticle-enhanced surface plasmon resonance using an aptamer-antibody sandwich assay. *Chemical Communications*, 52, 3568-3571.
- WU, X. Y., LIU, H. J., LIU, J. Q., HALEY, K. N., TREADWAY, J. A., LARSON, J. P., GE, N. F., PEALE, F. & BRUCHEZ, M. P. 2003. Immunofluorescent labeling of cancer marker Her2 and other cellular targets with semiconductor quantum dots. *Nature Biotechnology*, 21, 41-46.
- XU, Y.-Y., HEMMILÄ, I. A. & LÖVGREN, T. N.-E. 1992. Co-fluorescence effect in time-resolved fluoroimmunoassays. A review. *Analyst*, 117, 1061-1069.
- XUE, X., WANG, B., DU, W., ZHANG, C., SONG, Y., CAI, Y., CEN, D., WANG, L., XIONG, Y. & JIANG, P. 2016. Generation of affibody molecules specific for HPV16 E7 recognition. *Oncotarget*, 7, 73995-74005.
- YANG, L., MAO, H., WANG, Y. A., CAO, Z., PENG, X., WANG, X., DUAN, H., NI, C., YUAN, Q., ADAMS, G., SMITH, M. Q., WOOD, W. C., GAO, X. & NIE, S. 2009. Single Chain Epidermal Growth Factor Receptor Antibody Conjugated Nanoparticles for in vivo Tumor Targeting and Imaging. *Small*, 5, 235-243.
- YANG, X., ZHAO, Y., SUN, L., QI, H., GAO, Q. & ZHANG, C. 2018. Electrogenerated chemifluorescence biosensor array for the detection of multiple AMI biomarkers. *Sensors and Actuators B: Chemical*, 257, 60-67.
- YAO, H., ZHANG, Y., XIAO, F., XIA, Z. & RAO, J. 2007. Quantum dot/biofluorescence resonance energy transfer based highly sensitive detection of proteases. *Angewandte Chemie International Edition*, 46, 4346-4349.

- YEH, C.-H., SU, K.-F. & LIN, Y.-C. 2016. Development of an impedimetric immunobiosensor for measurement of carcinoembryonic antigen. *Sensors and Actuators A: Physical*, 241, 203-211.
- YEN, W., SHIONOYA, S. & YAMAMOTO, H. 2007. Phosphor Handbook CRC Press. Boca Raton.
- YILMAZ, A., MEMON, S. & YILMAZ, M. 1999. Synthesis and binding properties of calix [4] arene telomers. *Journal of Polymer Science Part A: Polymer Chemistry*, 37, 4351-4355.
- YUAN, J., MATSUMOTO, K. & KIMURA, H. 1998. A new tetradentate β -diketonate–europium chelate that can be covalently bound to proteins for time-resolved fluoroimmunoassay. *Analytical chemistry*, 70, 596-601.
- YUAN, J., WANG, G., MAJIMA, K. & MATSUMOTO, K. 2001. Synthesis of a terbium fluorescent chelate and its application to time-resolved fluoroimmunoassay. *Analytical chemistry*, 73, 1869-1876.
- ZELENSKY, A. N. & GREASY, J. E. 2005. The C-type lectin-like domain superfamily. *The FEBS journal*, 272, 6179-6217.
- ZHANG, L., WANG, Y., YE, Z., JIN, D. & YUAN, J. 2012a. New class of tetradentate β -diketonate-europium complexes that can be covalently bound to proteins for time-gated fluorometric application. *Bioconjugate chemistry*, 23, 1244-1251.
- ZHANG, W.-J., GAO, X.-J., LIU, Y.-L., SHAO, X.-X. & GUO, Z.-Y. 2012b. Design, recombinant preparation and europium-labeling of a fully active easily-labeled INSL3 analog for receptor-binding assays. *Process biochemistry*, 47, 1856-1860.
- ZHAO, Q., LI, F. & HUANG, C. 2010. Phosphorescent chemosensors based on heavy-metal complexes. *Chemical Society Reviews*, 39, 3007-3030.

- ZHOU, M., DIWU, Z., PANCHUK-VOLOSHINA, N. & HAUGLAND, R. P. 1997. A stable nonfluorescent derivative of resorufin for the fluorometric determination of trace hydrogen peroxide: applications in detecting the activity of phagocyte NADPH oxidase and other oxidases. *Analytical biochemistry*, 253, 162-168.
- ZHURAUSKI, P., ARYA, S. K., JOLLY, P., TIEDE, C., TOMLINSON, D. C., FERRIGNO, P. K. & ESTRELA, P. 2018. Sensitive and selective Affimer-functionalised interdigitated electrode-based capacitive biosensor for Her4 protein tumour biomarker detection. *Biosensors and Bioelectronics*, 108, 1-8.
- ZWIER, J. M., BAZIN, H., LAMARQUE, L. & MATHIS, G. R. 2014. Luminescent lanthanide cryptates: from the bench to the bedside. *Inorganic chemistry*, 53, 1854-1866.